FACULDADE DE ENGENHARIA DA UNIVERSIDADE DO PORTO



Interaction Studies Between Biocompatible Polymers and Amyloid-β Peptides

Ana Isabel Lopes Coelho de Mascarenhas Saraiva

Thesis submitted to the University of Porto for a Ph.D.degree in Chemical and Biological Engineering

Porto, 2009

To my Family...

....

Eles não sabem, nem sonham,
que o sonho comanda a vida.
Que sempre que um homem sonha
o mundo pula e avança
como bola colorida
entre as mãos de uma criança.

António Gedeão (1906–1997) *in* "Pedra filosofal"
MOVIMENTO PERPÉTUO (1956)

Resumo

A ocorrência de doenças resultantes de alterações estruturais e "misfolding" (enrolamento incorrecto) de péptidos e proteínas tornou o estudo do "folding" (enrolamento) de proteínas uma área de investigação importante, tendo já sido identificadas mais de 20 doenças causadas pela deposição de amilóide. Entre elas encontra-se a Doença de Alzheimer (DA), que é considerada a causa mais comum de demência na terceira idade. A DA é caracterizada pela acumulação extracelular de placas senis, aparecimento de "tangles" (emaranhados) neurofibrilares intracelulares e perda neuronal. O péptido β-amilóide (Aβ) é o componente fibrilar maioritário das placas neuríticas nos cérebros com DA e está relacionado com a patogénese da doença. As isoformas mais comuns deste péptido possuem 40 e 42 resíduos de comprimento e, embora sob condições normais o Aβ40 seja mais abundante, o Aβ42 é a forma predominante nas placas, sendo também aquela que apresenta neurotoxicidade mais elevada. Recentemente, oligómeros solúveis que precedem a formação de fibras foram propostos como as principais espécies neurotóxicas que contribuem para a neurodegeneração e demência. É aceite que o Aβ solúvel, em "random coil" (desestruturado) ou em hélice-α, exerce funções no sistema nervoso central. O "misfolding" do Aβ numa estrutura rica em folhas-β com tendência para formar agregados induz neurotoxicidade.

As interfaces, e especialmente a interface constituída pelas membranas lipídicas, promovem o "misfolding" do Aβ e a sua oligomerização. Esta tese teve como objectivo estudar a interacção do Aβ com superfícies planas e com nanopartículas (superfícies curvas, NPs), com a finalidade de elucidar qual a influência das interfaces no comportamento do Aβ.

O Aβ tem carácter anfifílico, e por isso as interacções hidrofóbicas e electrostáticas são ambas muito importantes na determinação da estrutura deste péptido e na sua retenção ao nível membranar. As superfícies sólidas adsorbentes constituem modelos apropriados para estudar de uma forma independente as diferentes interacções possíveis. Várias técnicas, tais como microbalança de cristal de quartzo com monitorização da dissipação (MCQ-D), microscopia de força atómica e espectroscopia de infravermelho com reflecção total atenuada foram utilizadas para avaliar o comportamento do Aβ em superfícies planas, que incluiram bicamadas lipídicas suportadas (BLSs). Os péptidos Aβ adsorbem fracamente às superficies hidrofílicas, apresentando no entanto uma elevada afinidade para superfícies hidrofóbicas e rugosas que promovem agregação. No que diz respeito a superfícies carregadas, o Aβ tem maior afinidade para superfícies com carga positiva verificando-se após adsorção, um aumento do conteúdo de folhas-β. Medições

com MCQ-D sugerem que, quando comparadas com monómeros, os oligómeros são espécies viscoelásticas que achatam em contacto com superfícies sólidas. Quando ocorre agregação, o Aβ40 forma agregados amorfos com uma estrutura rica em folhas-β enquanto o Aβ42, no mesmo intervalo de tempo, fibrila. Esta pode ser uma razão para a citotoxicidade mais elevada atribuída ao Aβ42. Ao contrário dos monómeros e das fibras, os oligómeros de Aβ interagem fortemente com as BLSs neutras. O colesterol, que é considerado um factor de risco para o desenvolvimento da DA, conhecido por aumentar a rigidez das membranas, diminui a inserção do péptido nas bicamadas zwitteriónicas. No entanto, os domínios rígidos actuam como moldes capazes de aumentar localmente a concentração de Aβ e induzir oligomerização. A importância das interacções hidrofóbicas na agregação do Aβ foi confirmada com os resultados descritos.

Considerando as NPs, a hipótese inicial era que a oligomerização e a citotoxicidade podiam ser reprimidas por NPs fluoradas que induzem uma conversão "random coil" → hélice-α no Aβ40 e inibem a fibrilogénese, enquanto os seus análogos hidrogenados conduzem à formação de folhas-β e agregação. Através das técnicas de dicroísmo circular (DC), calorimetria de titulação isotérmica, *imuno-dot blot* e electroforese em gel de poliacrilamida tratado com SDS demonstra-se que as NPs fluoradas e hidrogenadas apresentam diferentes capacidades para modificar a conformação do Aβ e influenciar a oligomerização. As NPs fluoradas, que promovem um aumento do conteúdo de hélices-α dos péptidos Aβ, exercem um efeito anti-oligomérico enquanto os análogos hidrogenados não. Os ensaios de citotoxicidade indicam que a conversão conformacional do péptido numa estrutura secundária rica em hélices-α também exibe actividade antiapoptótica, aumentando a viabilidade de células tratadas com espécies oligoméricas. Com a finalidade de testar a influência do potencial zeta das NPs na estrutura do péptido, NPs sem átomos de flúor mas com elevadas densidades de carga foram sintetizadas por sulfonação e sulfatação de poliestireno, o que conduziu à formação de microgéis e latexes. Ambas as estruturas poliméricas foram capazes de influenciar a conformação do Aβ, mas neste caso para um estado desestruturado e, ainda, de reverter a fibrilação como demonstrado por DC. A oligomerização foi retardada e a citotoxicidade reduzida. O balanço adequado entre porções hidrofílicas que conferem solubilidade e cadeias hidrofóbicas para explorar as interacções intermoleculares responsáveis pelo *assembly* do Aβ parece ser uma característica essencial das NPs que conseguem evitar os efeitos indesejáveis citados acima.

Abstract

The occurrence of diseases that result from the structural transformation and misfolding of peptides and proteins has made the study of protein folding an important research field and more than 20 diseases have been identified which are caused by the deposition of amyloid. Amongst them is Alzheimer´s Disease (AD), considered the most common cause of dementia in elderly. The AD is characterized by extracellular accumulation of senile plaques, intracellular appearance of neurofibrillary tangles and neuronal loss. The amyloid-β peptide (Aβ) is a major fibrillar component of neuritic plaques in AD brains and is related to the pathogenesis of the disease. The most common isoforms are 40 and 42 residues long and, although under normal conditions Aβ40 is more abundant, usually Aβ42 is the predominant form found in plaques presenting enhanced neurotoxicity. Soluble oligomers that precede fibril formation have been proposed as the main neurotoxic species contributing to neurodegeneration and dementia. It is accepted that soluble unordered or α-helical Aβ exerts physiological functions in the central nervous system. Misfolding of Aβ to a β-sheet enriched structure prone to aggregation leads to neurotoxicity.

Interfaces, in particular the lipid membrane interface, promote Aβ misfolding and oligomerization. With the aim of elucidating the role of interfaces on Aβ behaviour, interaction studies of Aβ with planar surfaces and with nanoparticles (highly curved surfaces, NPs) were performed.

Aβ is amphipatic, so hydrophobic and electrostatic interactions are very important in determining the structure of Aβ peptides and its retention in the membrane. Solid sorbent surfaces are suitable model systems to study the different interactions independently. Several techniques such as quartz crystal microbalance with dissipation monitoring (QCM-D), atomic force microscopy and attenuated total reflection infrared spectroscopy were employed in this thesis for the investigation of the behaviour of Aβ on planar surfaces, which included supported lipid bilayers (SLBs). It was found that Aβ peptides adsorb weakly onto hydrophilic surfaces whereas the affinity is high for hydrophobic and rough surfaces that promote aggregation. Considering charges, Aβ prefers positively charged surfaces and upon adsorption the β-sheet content increases. QCM-D measurements suggested that, when compared to monomers, the oligomers are viscoelastic species which flatten when in contact with a solid surface. When aggregation occurs, Aβ40 forms amorphous aggregates with β-sheet enriched structure whereas in the same time interval Aβ42 fibrillates. This might be a reason for the increased cytotoxicity attributed to Aβ42. Aβ oligomers

interact strongly with neutral SLBs, while monomers and fibrils do not. Cholesterol, a risk factor of AD and known for increasing the membrane stiffness, diminishes the insertion of the peptide in zwitterionic bilayers. Nevertheless, the rigid domains act as templates able to increase locally Aβ concentration and to drive oligomerization. The importance of hydrophobic interactions in Aβ aggregation was confirmed with the above results.

Considering NPs, the starting hypothesis was that oligomerization and cytotoxicity could be repressed by fluorinated NPs that were shown to induce random coil → α-helix conversion of Aβ40 and to inhibit fibrillogenesis, while their hydrogenated analogues lead to β-sheet formation and aggregation. It is shown here that fluorinated and hydrogenated NPs with different ability to change Aβ conformation influence Aβ oligomerization as assessed by circular dichroism (CD), isothermal titration calorimetry, immuno-dot blot and SDS polyacrylamide gel electrophoresis. Fluorinated NPs, which promote an increase in α-helical content of Aβ peptides, exert an anti-oligomeric effect while hydrogenated analogues do not. Cytotoxicity assays confirmed the hypothesis indicating that the conformational conversion of the peptide into a α-helical enriched secondary structure has also antiapoptotic activity, increasing the viability of cells treated with oligomeric species. In order to test the influence of the zeta potential of the NPs on the peptide structure, NPs without fluorine atoms but with high charge densities were synthesized by sulfonation and sulfation of polystyrene, which lead to the formation of microgels and latexes. Both polymeric nanostructures were able to affect the conformation of Aβ, but in this case to an unordered state and, moreover, to revert fibrillation as shown by CD. Oligomerization was delayed and cytotoxicity reduced as well. The proper balance between hydrophilic moieties that allow solubility and hydrophobic chains to exploit the intermolecular interactions of Aβ assembly seem to be an essential feature of the NPs that succeeded to avoid the above mentioned undesirable effects.

Résumé

L'apparition de maladies résultant d'une transformation structurale et du "misfolding" (repliement) de peptides et protéines ont suscité l'intérêt de nombreux chercheurs et ainsi, plus de 20 maladies causées par la déposition de plaques amyloïdes ont été identifiées grâce à l'étude de la conformation des protéines. Parmi les différentes maladies neurodégénératives identifiées, la maladie d'Alzheimer (AD) est considérée comme la cause la plus commune de démence chez les personnes âgées. L'AD est une maladie caractérisée par une accumulation extracellulaire de plaques séniles, l'apparition de neurofibrilles enchevêtrées et une perte neuronale. Le peptide appelé amyloïde-β (Aβ) est le composant fibrillaire majeur des plaques formées dans le cerveau des patients atteint de la maladie. L'isoforme la plus commune est formée de 40 à 42 acides aminés; dans des conditions standards, la forme Aβ40 est la plus abondante; la forme Aβ42 est généralement prédominante dans les plaques présentant une neurotoxocité accrue. Il a été proposé que les oligomères solubles, à l'origine de la formation de fibrilles, sont les espèces les plus neurotoxiques contribuant à la neurodégénérescence et à la démence. De plus, il a été admis que le peptide Aβ soluble, de conformation α-helicoidale ou non-organisée (pelote statique non périodique), exerce des fonctions physiologiques sur le système nerveux central. Le repliement de Aβ en structure enrichie en feuillet-β conduit ainsi à l'agrégation de ces peptides, dès lors neurotoxiques.

Les interfaces, en particulier les interfaces membranaires lipidiques, conduisent au repliement de Aβ et à l'oligomérisation. Dans le but d'élucider le rôle des interfaces sur le comportement de Aβ, des études portant sur l'interaction de Aβ avec des surfaces planes ainsi qu'avec des nanoparticules (surface de grande courbature, NPs) ont été menées.

Aβ est une molécule amphipathique, ou les interactions hydrophobes et électrostatiques jouent donc un rôle important dans la structure des peptides Aβ et leur rétention dans la membrane. Les surfaces solides sorbantes sont des systèmes modèles adéquats pour étudier les différentes interactions indépendamment. Plusieurs techniques telles que la microbalance à quartz avec enregistrement de dissipation (QCM-D), la microscopie à force atomique et la spectroscopie infrarouge à réflexion totale atténuée ont été employées au cours de ces travaux de thèse afin d'élucider le comportement de Aβ sur des surfaces planes, incluant l'étude sur bicouche lipidique (SBLs). Ainsi, il a été remarqué que le peptide Aβ absorbe faiblement sur des surfaces hydrophiles alors que son importante affinité pour des surfaces hydrophobes et rugueuses conduit à son

agrégation. Concernant les charges, Aβ est attiré par les surfaces chargées positivement et après son adsorption, la proportion de feuillet-β augmente. Les mesures QCM-D montrent par ailleurs que, comparés aux monomères, les oligomères sont des espèces plus viscoélastiques qui s'aplanissent au contact de surfaces solides. Lorsque le phénomène d'agrégation se produit, Aβ40 forme des agrégats amorphes et possède une structure enrichie en feuillet-β alors que Aβ42 forme des fibrilles. Ce pourrait être la raison de la cytotoxicité plus importante attribuée au Aβ42. Les oligomères Aβ interagissent fortement avec les SBLs neutres, contrairement aux monomères et aux fibrilles. Le cholestérol, facteur de risque de l'AD et connu pour augmenter la rigidité des membranes, diminue l'insertion de peptide dans des bicouches zwitterioniques. Néanmoins, les domaines rigides agissent comme des empreintes permettant d'augmenter localement la concentration en Aβ et conduisant ainsi à l'oligomérisation. L'importance des interactions hydrophobes dans les phénomènes d'agrégation de Aβ a donc été confirmée grâce à ces résultats.

Concernant les NPs, l'hypothèse initiale était que l'oligomérisation et la cytotoxicité pourraient être inhibées par des NPs fluorées par induction d'une conversion structurale du peptide Aβ40 de pelote statique non périodique à α-hélices, et par inhibition de la fibrillogénèse. Au contraire, les NPs hydrogénées conduiraient à la formation de feuillet-β et à l'agrégation. Il a été démontré au cours de cette thèse, notamment grâce à des techniques de dichroïsme circulaire (CD), titration calorimétrique isotherme, *immuno-dot blot*, et électrophorèse sur gel de polyacrilamide SDS que les NPs fluorées et hydrogénées influencent l'oligomérisation de Aβ. Les NPs fluorées, qui conduisent à l'enrichissement en structures α-hélicoïdale des peptides Aβ, exercent un effet anti-oligomérique, contrairement à leurs analogues hydrogénées. Les tests de cytotoxicité ont confirmés les hypothèses, démontrant ainsi que la conversion du peptide en structure secondaire enrichie en α-hélices présente une activité anti-apoptotique, augmentant ainsi la viabilité des cellules traitées avec les espèces oligomériques. Afin d'étudier l'influence du zeta potentiel des NPs sur la structures des peptides, des NPs non-fluorées mais avec une grande densité de charges ont été synthétisées par sulfonation et sulfation du polystyrène, ce qui a conduit à la formation de microgels et de latex. Ces deux nano-structures polymériques affectent la conformation de Aβ conduisant à une structure non-organisée et sont également capable d'inhiber la fibrillation (démontré par CD). De plus, l'oligomérisation est retardée et la cytotoxicité réduite. La balance entre les parties hydrophiles augmentant la solubilité, et les chaines hydrophobes permettant les interactions intermoléculaires au sein des agrégats Aβ est une caractéristique essentielle des NPs pour réussir à refreiner les effets indésirables précédemment cités.

Zusammenfassung

Krankheiten, die aufgrund von Strukturumwandlungen und falschen Proteinfaltungen auftreten, haben die Untersuchung von Proteinfaltungen zu einem wichtigen Forschungsgebiet gemacht. Mehr als 20 Krankheiten, die mit Amyloidablagerungen verbunden sind, wurden bereits identifiziert. Unter diesen ist die Alzheimer-Krankheit (AK) die häufigste Ursache für Demenz bei älteren Menschen. Die AK ist charakterisiert durch die extrazelluläre Akkumulation von senilen Plaques, das intrazelluläre Auftreten von neurofribrillären Tangles und neuronalen Verlust. Das Amyloid-β Peptid (Aβ) ist die Hauptkomponente von neuritischen Plaques in AK Gehirnen und gehört zur Pathagonese der Krankheit. Die verbreitetsten Isoformen sind 40 und 42 Reste lang und, obwohl unter normalen Bedingungen Aβ40 häufiger ist, ist Aβ42 die dominierende Form in Plaques, die erhöhte Neurotoxizität zeigen. Lösliche Oligomere, die der Fibrillenbildung vorangehen, wurden als die wesentlichsten neurotoxischen Spezies erkannt, die zu Neurodegeneration und Demenz führen. Es ist allgemein anerkannt, dass lösliche unstrukturierte oder α-helikale Aβ physiologische Funktionen im zentralen Nervensystem ausüben. Falsche Faltung von Aβ zu an β-Faltblatt reichen Strukturen, die zur Aggregation neigen, führt zur Neurotoxizität.

Grenzflächen, besonders die Lipidmembranoberflächen, begünstigen die falsche Faltung von Aβ und die Oligomerisation. Mit der Absicht, die Rolle von Grenzflächen aufzuklären, wurden Wechselwirkungen von Aβ mit planaren Oberflächen und Nanopartikeln (stark gekrümmte Oberflächen, NPs) untersucht.

Aβ ist amphipathisch, so dass hydrophobe und elektrostatische Wechselwirkungen für die Bestimmung der Struktur der Aβ Peptide und deren Verbleib in der Membran sehr wichtig sind. Feste Oberflächen sind geeignete Modellsysteme, um die verschiedenen Wechselwirkungen getrennt zu untersuchen. Verschiedene Techniken wie die Quarz Mikrowaage mit Dissipationsmessung (QCM-D), die Rasterkraftmikroskopie und die Infrarotspektroskopie in abgeschwächter Totalreflektion wurden in dieser Arbeit für die Untersuchung des Verhaltens von Aβ auf planaren Oberflächen einschließlich der gestützten Lipiddoppelschichten (SLBs) eingesetzt. Es wurde gefunden, dass die Aβ Peptide auf hydrophilen Oberflächen nur schwach adsorbieren wogegen die Affinität für hydrophobe und raue Oberflächen sehr groß ist, wobei die Aggregation gefördert wird. Bezüglich Ladungen wurde gefunden, dass Aβ positiv geladene Oberflächen bevorzugt und die Adsorption den Gehalt an β–Faltblatt erhöht. QCM-D Messungen zeigen, dass die Oligomere im Vergleich mit den Monomeren viskoelastische Spezies sind, die sich im Kontakt

mit festen Oberflächen abflachen. Wenn Aggregation einsetzt, dann bildet Aβ40 amorphe Aggregate mit an β–Faltblatt reichen Strukturen, wohingegen im gleichen Zeitintervall Aβ42 Fibrillen bildet. Das kann der Grund für die erhöhte Zytotoxizität von Aβ42 sein. Aβ Oligomere wechselwirkung stark mit neutralen SLBs während Monomere und Fibrillen das nicht machen. Cholesterol, das als Risikofaktor der AK dafür bekannt, dass es die Membransteifigkeit erhöht, schwächt den Einbau des Peptids in zwitterionische Doppelschichten ab. Dennoch agieren die steifen Domänen als Template, die die Konzentration von Aβ lokal erhöhen und damit Oligomerisation fördern. Die Bedeutung hydrophober Wechselwirkungen im Aggregationsprozess von Aβ wurde durch die obigen Ergebnisse bestätigt.

Die Starthypothese für die Experimente mit Nanopartikeln (NPs) war die Beobachtung, dass Oligomerisation und Zytotoxizität durch fluorierte NPs unterdrückt werden konnte, da diese zu einer Umwandlung von ungeordnet zu α-helikal bei Aβ40 führen und die Fibrillenbildung hemmen. Die hydrierten Analoga führen dagegen zur Bildung von β-Faltblatt und Aggregation. Hier wird gezeigt, dass fluorierte und hydrierte NPs mit ihren unterschiedlichen Fähigkeiten, die Konformation von Aβ zu verändern, die Oligomerisation von Aβ beeinflussen, was durch Zirkulardichroismus (CD), isotherme Titrationskalorimetrie, Immuno-Dot-Blot und SDS Polyacrylamid-Gelelektrophorese. Fluorierte NPs fördern den Gehalt an α-Helix in Aβ Peptiden und haben eine anti-oligomere Wirkung während die hydrierten Analoga das nicht machen. Zytotoxizitäts-Prüfungen bestätigten die Anfangshypothese indem sie zeigten, dass die Umwandlung zu α-helikal reichen Sekundärstrukturen auch anti-apoptotische Aktivität hat, wobei die Lebensfähigkeit von Zellen, die mit oligomeren Spezies behandelt wurden, erhöht ist. Um den Einfluss des Zeta-Potentials der NPs auf die Peptid-Struktur zu prüfen, wurden NPs ohne Fluor aber mit hoher Ladungsdichte durch Sulfonierung und Sulfatierung synthetisiert, die zur Bildung von Mikrogelen und Latizes. Beide polymeren Nanostrukturen sind in der Lage, die Konformation von Aβ zu beeinflussen, wobei ungeordnete Strukturen entstehen, und die Fibrillenbildung umzukehren, wie durch CD Messungen gezeigt werden konnte. Oligomerisation wurde verzögert und die Zytotoxizität reduziert. Die richtige Balance zwischen hydrophilen Resten, die die Löslichkeit befördern, und hydrophoben Ketten, die intermolekulare Wechselwirkungen mit Aβ Aggregaten aufweisen, scheint das entscheidende Merkmal der NPs zu sein, um ungewünschte Effekte zu vermeiden.

Table of Contents

List of Abbreviations ix

1. Introduction 1

2. Background 3

2.1. Protein Folding, Misfolding and Aggregation 3
2.1.1. The Mistery of Protein Folding 3
2.1.2. From Sequence to Structure 6
2.1.3. Protein Secondary Structure 10
2.1.4. Protein Tertiary and Quaternary Structure 16
2.1.5. Protein Folding in the Cell 18
2.1.6. Protein Misfolding and Disease 21

2.2. Amyloidosis 26
2.2.1. Structural Features of Amyloid Fibrils 27
2.2.2. Amyloid Fibril Formation 28
2.2.3. Pathogenesis of Amyloid Deposition 31

2.3. Alzheimer´s Disease 33
2.3.1. Histopathology of AD 33
2.3.2. The Amyloid Cascade Hypothesis 34
2.3.3. Metabolism of Aβ and AD 35
2.3.4. Aβ Oligomerization and Fibrillation 40
2.3.5. Mechanisms of Aβ Toxicity 44
1.3.5.1. Membrane Effects 45
1.3.5.2. Metals 45
1.3.5.3. Oxidative Stress 46
1.3.5.4. Calcium Homeostasis 47
1.3.5.5. Apoptosis 49
1.3.5.6. Inflammation 50
2.3.6. Therapeutic Strategies for AD 50

3. Aβ Adsorption on Planar Surfaces 55

3.1. Introduction 55

3.2. Materials and Methods 56
3.2.1. Materials 56
3.2.1.1. Amyloid β-Peptides 56
2.2.1.2. Lipids 57
3.2.2. Instrumentation and Methodologies 59
2.2.2.1. Quartz Crystal Microbalance 59
2.2.2.2. Atomic Force Microscopy 62
2.2.2.3. Attenuated Total Reflection Infrared Spectroscopy 64
3.2.3. Surfaces 70
2.2.3.1. Hydrophilic vs Hydrophobic Surfaces 70
2.2.3.2. Positively vs Negatively Charged Surfaces 70
2.2.3.3. Supported Lipid Bilayers 72

3.3. Results 75
3.3.1. Adsorption of Aβ Peptides on Hydrophilic vs Hydrophobic Surfaces 75
3.3.2. Adsorption of Aβ Peptides on Positively vs Negatively Charged Surfaces 77
3.3.3. Interaction of Aβ Peptides with Supported Lipid Bilayers 83
3.4. Discussion and Conclusions 91
4. Controlling Aβ Oligomerization with Nanoparticles 105
4.1. Introduction 105
4.2. Materials and Methods 108
4.2.1. Synthesis of Fluorinated NPs 108
4.2.2. Synthesis and Characterization of Sulfonated ans Sulfated NPs 108
4.2.2.1. Polymerization in Microemulsion leading to Microgels 109
4.2.2.2. Heterophase Polymerization with Reactive Surfactants 112
4.2.3. Instrumentation and Methodologies 114
4.2.3.1. Circular Dichroism 114
4.2.3.2. Isothermal Titration Calorimetry 120
4.2.3.3. Thioflavine T Fluorescence Assay 123
4.2.3.4. Immuno-Dot Blot Assay 124
4.2.3.5. SDS Polyacrylamide Gel Electrophoresis 125
4.2.3.6. Cell culture and evaluation of toxicity 127
4.3. Results 131
4.3.1. Fluorinated vs Hydrogenated NPs 131
4.3.2.1. Effect on Aβ Secondary Structure and Aggregation 131
4.3.2.2. Energetics of the Interactions 135
4.3.2.3. Effect on Aβ Oligomer Formation 136
4.3.2.4. Effect on Aβ-induced Cytotoxicity 140
4.3.2. Sulfonated and Sulfated NPs 143
4.3.2.1. Nanoparticles Synthesis 143
4.3.2.2. Effect on Aβ Secondary Structure and Aggregation 146
4.3.2.3. Effect on Aβ Oligomer Formation 148
4.3.2.4. Effect on Aβ-induced Cytotoxicity 151
4.4. Discussion and Conclusions 153
5. Concluding Remarks 161
Properties and conventions associated with the standard amino acids 165
References 167
List of Figures 181
List of Tables 187
Acknowledgements 189
Legal Regulations 193

List of Abbreviations

Aβ	Amyloid β-peptide
AD	Alzheimer´s disease
ADDL	Aβ-derived diffusible ligands
ADP	Adenosine diphosphate
AFM	Atomic force microscopy
AIBN	Azobis(isobutyronitril)
AICD	APP intracellular domain
AMC	7-Amino-4-methylcoumarin
Ac-DEVDAMC	Acetyl-Asp-Glu-Val-Asp-7-amido-4-methylcoumarin
α1-AT	α1-Antitrypsin
APG2019	1-(Allyloxy polyalkoxy)-3-phenyloxy propyl polyethylene glycolethersulphate
APP	Amyloid precursor protein
APS	Ammonium Peroxodisulfate
ATP	Adenosine triphosphate
ATR	Attenuated total reflection
BBB	Blood-brain-barrier
BSA	Bovine serum albumin
CHC	Central hydrophobic cluster
CD	Circular dichroism
CFTR	Cystic fibrosis transmembrane conductance regulator
CJD	Creutzfeldt-Jakob disease
CMC	Critical micellar concentration
CNS	Central nervous system
CR	Congo red
CSF	Cerebrospinal fluid
CTMA	Cetyltrimethylammonium chloride
D	Dissipation factor
DLS	Dynamic light scattering
D_h	Hydrodynamic diameter
m-DIB	m-Diisopropenylbenzene
DMPC	Dimyristoylphosphatidylcholine

DMSO	Dimethyl sulfoxide
DMTAP	1,2-Dimyristoyl trimethylammonium-propane
DNA	Deoxyribonucleic acid
DPPC	Dipalmitoylphosphatidylcholine
EBSS	Earle's balanced salt solutions
ECL	Enhanced chemiluminescence
Egg PC	Egg-yolk L-α-Phosphatidylcholine
Egg PG	Egg-yolk L-α-Phosphatidyl-DL-glycerol
EM	Electron microscopy
ER	Endoplasmic reticulum
FBS	Fetal bovine serum
FTIR	Fourier transform infrared spectroscopy
GM1	GalBeta1-3GalNAcBeta1-4(NeuAcAlpha2-3)GalBeta1-4GlcBeta1-1'-Cer
GTP	Guanosine triphosphate
HFIP	1,1,1,3,3,3-Hexafluoro-2-propanol
4HNE	4-Hydroxynonenal
IAPP	Islet amyloid polypeptide
IDE	Insulin-degrading enzyme
IG	Immunoglobulin
IL	Interleukin
IR	Infrared spectroscopy
IRE	Internal reflection element
ITC	Isothermal titration calorimetry
KLH	Keyhole limpet hemocyanin
LbL	Layer-by-layer
LMW	Low molecular weight
LTP	Long-term potentiation
MALDI-TOF	Matrix-assisted laser desorption/ionization time-of-flight
MEM	Minimum essential media
MLV	Multilamellar vesicle
mRNA	Messenger ribonucleic acid
MRW	Mean residue weight
MTT	(3-(4,5-Dimethylthiazol-2-yl)-2,5-diphenyltetrazolium bromide)
NEAA	Non-essential amino acids

NMR	Nuclear magnetic resonance
NOS	Nitric oxide synthase
NP	Nanoparticle
NSAIDs	Non-steroidal anti-inflammatory drugs
NTF	Neurofibrillary tangles
OR	Optical rotation
ORD	Optical rotatory dispersion
PAH	Poly(allylamine hydrochloride)
PBS	Phosphate buffered saline
PC	Phosphatidylcholine
PD	Parkinson's disease
PEGA	Poly(ethylene glycol)-azo
PEI	Poly(ethylenimine)
PG	Phosphatidylglycerol
pI	Isoelectric point
PSS	Poly(sodium 4-styrenesulfonate)
QCM-D	Quartz crystal microbalance with dissipation monitoring
ROS	Reactive oxygen species
SDS	Sodium dodecyl sulfate
SDS-PAGE	Sodium dodecyl sulfate-polyacrylamide gel electrophoresis
SLB	Supported lipid bilayer
S/N	Signal to noise
SOD	Superoxide dismutase
STM	Scanning tunneling microscopy
SUV	Small unilamellar vesicle
TBS-T	Tris-buffered saline supplemented with 0.05% Tween
TEM	Transmission electron microscopy
TFE	Trifluoroethanol
THF	Thioflavine T
ThT	Tumor necrosis factor
TNF	Tetrahydrofuran
TSM	Thickness shear mode
UV	Ultraviolet
WT	Wild type

1. Introduction

Protein folding is a structural transition from the inactive linear sequence of amino acids into the biologically active three-dimensional form of the molecule, the native structure. The failure to reach or maintain the correct folded structure can lead to pathological conditions referred to as protein misfolding diseases. Although Alzheimer's disease (AD), cystic fibrosis, mad cow disease and many forms of cancer seem to be unrelated in symptoms and characteristics of the proteins involved, some common features underlying the origin of these diseases have emerged in recent years. The prevalence of such pathological states increases with ageing, probably due to a decline in the cellular control and repair mechanisms, but mutations may disturb the scenario, leading to early-onset disease. The largest group of misfolding diseases is characterized by the appearance of highly organized β-structured proteinaceous fibrillar aggregates known as amyloid fibrils. Amyloid diseases comprise an important class of human pathologies, including AD, Parkinson´s disease (PD), spongiform encephalopathies, type II diabetes mellitus and systemic amyloidosis.

AD, a neurodegenerative disorder of the elderly, is the most prevalent form of dementia. The cognitive decline associated with AD drastically affects the social and behavioural skills of people living with this disease. Clinically, AD is characterized by a progressive decline in cognition, and histopathologically by the presence of senile plaques and neurofibrillary tangles in the brain, and the degeneration of basal forebrain cholinergic neurons. In the past two decades, evidences from genetic and animal models have established a causative role of the amyloid β-peptide (Aβ) in the disease. In AD brains, the peptide is found in a fibrillar form organized in a β-sheet structure, being the main constituent of the plaque deposits. Aβ is a 4kDa amphiphilic peptide of 39 to 43 amino acid residues long, derived from the amyloid precursor protein (APP) by sequential action of two aspartyl proteases called β- and γ-secretases. The accumulation of Aβ in the brain, which may result from overproducion due to APP mismetabolism, or/and a failure in Aβ clearance, is central in the pathogenesis of AD.

Soluble oligomers that precede fibril formation have been proposed as the main neurotoxic species contributing to neurodegeneration and dementia. Moreover, oligomers have been implicated in other amyloid-associated neurodegenerative diseases, such as PD and Huntington´s disease, thus suggesting that oligomeric species formed early in the aggregation process may be a common pathogenic mediator. Membrane permeabilization by oligomers may initiate a common group of downstream pathologic processes, including intracellular calcium dyshomeostasis,

production of reactive oxygen species (ROS), altered signaling pathways, and mitochondrial dysfunction that represent key effectors of cellular dysfunction and cell death.

The major obstacle in managing AD and designing a rationale for therapeutic approaches is the incomplete understanding of the pathogenesis of the disease, and the drugs used today provide only symptomatic treatment. In order to overcome AD, it is necessary to lower the Aβ levels in the brain, and several therapeutic strategies such as inhibition of production, promotion of degradation, inhibition of aggregation, and clearance of deposits have been proposed. A coherent pharmacological approach for preventing Aβ oligomerization would be to find compounds able to specifically stabilize the initial conformations and/or destabilize the β-sheet conformation in order to inhibit oligomerization. The targeting of small Aβ oligomers seems to be a good place to start the search of therapeutic approaches to improve AD treatment. An overview of the main concepts related to the unsolved problem of protein folding and to the pathogenic processes arising from it, with emphasis on AD, is presented in Chapter 2.

This thesis foccuses on studies of the interaction of Aβ peptides with planar surfaces and nanoparticles (NPs). The overall aim was to understand Aβ assembly and counteract it in order to avoid aggregation. In particular, studies were performed to: (i) elucidate, using planar sorbent surfaces, the role of hydrophobic and electrostatic interactions on Aβ behaviour (Chapter 3); and (ii) investigate the possibility to induce and stabilize an α-helical/unordered structure of the peptide through NPs in order to avoid oligomerization and cytotoxicity (Chapter 4). Such studies may represent an important step towards a detailed understanding of the initial stages of aggregation and hence assist in smart drug design of inhibitors and development of therapeutic strategies against AD as briefly summarized in Chapter 5.

2. Background

2.1. Protein Folding, Misfolding and Aggregation

The term protein derives from the Greek πρώτειος (proteios), meaning "first" or "foremost". Proteins carry out many vital cellular functions determined by their precise three-dimensional structures (the native conformations). The manner in which a newly synthesized chain of amino acids transforms itself into a perfectly folded protein depends both on the intrinsic properties of the amino acid sequence and on multiple contributing influences from the crowded cellular milieu. Folding and unfolding are crucial ways of regulating biological activity and targeting proteins to different cellular locations. Understanding how proteins fold has long been a major goal and can be of great therapeutic value since aggregation of misfolded proteins that escape the cellular quality-control mechanisms is a common feature of a wide range of highly debilitating and increasingly prevalent diseases.

2.1.1. The Mystery of Protein Folding

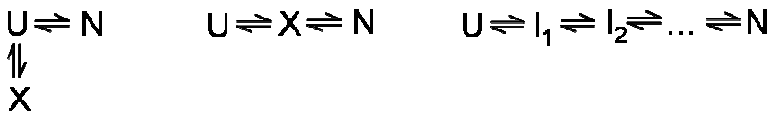
Alzheimer´s disease. Mad Cow disease. Cystic fibrosis. An inherited form of emphysema. Even many cancers. Recent discoveries show that all these apparently unrelated diseases result from protein misfolding. What is exactly the phenomenon of protein folding? Other than water, proteins are the most abundant molecules in biology, being fundamental components of all living cells. Hemoglobin that carries oxygen to tissues, insulin that signals our bodies to store excess sugar, antibodies that fight infection, actin and myosin that allow muscles to contract, and collagen that makes up tendons and ligaments (and even much of bones) - all are proteins.

Relatively simple monomeric subunits provide the key to the structure of the thousands of different proteins. All proteins, whether from the most ancient lines of bacteria or from the most complex forms of life, are constructed from the same ubiquitous set of 20 amino acids that are covalently linked. Each protein begins as a polypeptide, which is translated from a sequence of messenger ribonucleic acid (mRNA) as a linear chain of amino acids that lacks a three-dimensional structure. Each amino acid in the chain has certain chemical features given by their side-chain (hydrophilic, hydrophobic, electrically charged, for instance). The interior of a cell is an

extraordinarily complex environment in which proteins and other macromolecules are present at a concentration of 300–400 $mg \cdot mL^{-1}$ [1]. It is now known that within the cells of living organisms there are several auxiliary factors that assist in the folding process, including folding catalysts and molecular chaperones [2]. These factors enable polypeptide chains to fold efficiently in the complex and crowded milieu of the cell but do not determine their native structures; the latter are fully encoded by the amino acid sequences. The question of how proteins find their unique native states simply from the information contained within this code is at the heart of molecular biology and the mechanism by which a protein could, in principle, fold to a specific structure was until very recently shrouded in mystery.

The landmark studies of Anfinsen showed that ribonuclease could be refolded after denaturation while preserving enzyme activity, thereby suggesting that all the information required by protein to adopt its final conformation is encoded in its primary structure [3, 4]. This finding led Anfinsen to put forward the thermodynamic hypothesis of protein folding: the polypeptide chain spontaneously folds into the conformation corresponding to the minimum Gibbs free energy level under a given set of environmental conditions, in a "path independent" way. The question, then, became to understand how a polypeptide folds in a time-scale compatible with biologically relevant processes. Cyrus Levinthal, in 1969, noted that due to the huge number of degrees of freedom in an unfolded polypeptide chain, the molecule has an astronomical number of possible conformations [5]. If the protein is to attain its correct folding by sequentially trying all possible conformations, it would require a time longer than the age of the universe to arrive at its correct native conformation, even if sampling occurs at a very fast rate (nanosecond or picosecond). Levinthal suggested that a protein is guided through intermediates into the native state, following a specific "folding pathway". So an alternative view was proposed, according to which protein folding could be under kinetic, rather than thermodynamic control, with the final folded state of a protein being the state reached faster (i.e., for which lower activation barriers need to be overcome) and not necessarily the most stable amongst all possible conformations. These two lines of argument have led to the ''Levinthal paradox'': How could folding be pathway dependent and pathway independent at the same time? Levinthal framed the puzzle as if the two goals – achieving the global minimum and doing so quickly – were mutually exclusive, and his argument led to a search for folding pathways.

The modern era of folding experiments began soon after Levinthal´s pivotal argument leading to three of the most important classical models of protein folding [6], included in the "Classical View" of the kinetics of this process. They are (i) the off-pathway of the reaction scheme (1), (ii) the on-pathway model (2) and (iii), the sequential model (3):



(1) (2) (3)

where U represents the fully unfolded denaturated state, N the native state, and X or I represent intermediate states between those of U and N. According to the classical view, folding proceeds via a single defined pathway, as observed in simple chemical reactions.

A so-called "New View" [7] of the kinetics of protein folding has emerged in the last two decades, resulting from a combination of advances in experimental methods that are more informative at the atomic level (e.g. nuclear magnetic resonance (NMR)), from statistical mechanical view of protein structure and dynamics and extensive simulation studies of protein folding. The new models use the language of "folding tunnels" and "energy landscapes". According to this view, folding is a stochastic search of the many conformations accessible to a polypeptide chain on funnel-shape landscapes. An energy landscape is the free energy of each conformation as a function of the degrees of freedom, such as the dihedral bond angles along the peptide backbone (discussed later in more detail). The vertical axis of the funnel (Figure 2.1) represents the "internal free energy" of a given chain configuration (everything except the conformational entropy): the sum of hydrogen bonds, ion-pairs, torsion angle energies, hydrophobic and solvation free energies, and so on, for a chain in a particular conformation. It is dependent on external conditions such as temperature or solvent. The many lateral axes represent the conformational coordinates. Each conformation is represented by a point on the multidimensional energy surface. Conformations that are similar geometrically are close on the energy landscape. Energy landscapes can have different features, hills correspond to high energy conformations (for example burying polar groups in hydrophobic cores) and valleys are configurations that are more favorable than others nearby. The kinetic process of folding or unfolding can be seen as rolling a ball on this energy surface (Figure 2.1). The distinction between a pathway and a funnel is that whereas a pathway is a one-dimensional route through configuration space, a funnel describes the reduction of the conformational space accessible to the polypeptide chain as the native state is approached.

The high degree of disorder of the polypeptide chain is reduced as folding progresses, as the more favorable enthalpy associated with stable native-like interactions can offset the decreasing entropy as the structure becomes more ordered. Thus, the main difference between the theories of protein folding lies in the fact that the "new view" allows some species to escape from a pre-programmed pathway (i.e., there might be multiple ways down the funnel).

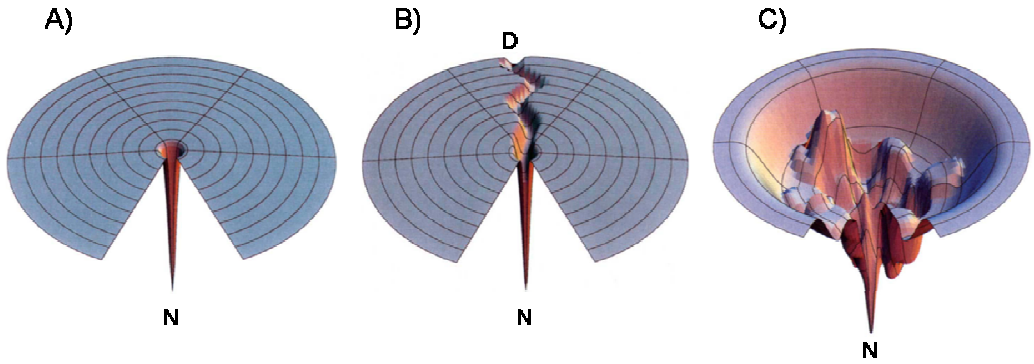


Figure 2.1. Protein folding energy landscapes. N represents the native conformation. The vertical axis of a funnel represents the "internal free energy" of a given chain configuration. The many lateral axes represent the conformational coordinates. A): the Levinthal "golf-course" landscape where the chain searches for N randomly, on a level playing field of energies. B): the "pathway solution" that leads from a denaturated conformation D to N, allowing a more directed and faster conformational searching than in A. C): the "new view", according to which folding is a stochastic process on a funnel-shape landscape (*adapted from* [6]).

2.1.2. From Sequence to Structure

Protein stability is intimately related with protein folding – proteins have to be folded into their final active state (and maintain it) to be stable. The Gibbs free energy, *G*, is given by the equation

$$G = H - TS \qquad (2.1)$$

where *H* represents the enthalpy, *T* is the temperature and *S* the entropy. For a protein of 150 amino acid residues the Δ*G* of folding is usually between -5 to -15 kcal·mol^{-1} [8]. This value results from the balance between two large and opposing contributions, the stabilizing energy originating from favorable interactions upon folding and the unfavorable entropic contribution resulting from the limitation of the conformational space available to the polypeptide chain. This Δ*G* is comparable to the energy of a few hydrogen bonds, even though a protein may have hundreds of hydrogen bonds. Thus, proteins are only marginally stable. The major stabilizing forces are hydrogen bonding and the hydrophobic effect [9].

The hydrophobic interaction has an entropic nature and gives the main thermodynamic contribution to protein folding [9]. Water molecules cannot form hydrogen bonds with non-polar side chains of amino acid residues; thus, water molecules form ice-like "cages" around these side chains, resulting in a loss of entropy if these side chains are solvent exposed. The clustering or burying of hydrophobic side chains into the interior of the protein in "hydrophobic cores" reduces

this entropic loss (fewer water molecules in a ice-like state) (Figure 2.2). This can be energetically quite favorable; the burial of a single -CH_2- group has a ΔG of about -1 kcal·mol^{-1} (close to the energy of a hydrogen bond). So the hydrophobic forces are responsible for the initial stage in protein folding, the hydrophobic collapse, which gives rise to the molten globule state. There are several evidences supporting the importance of the hydrophobic effect on protein folding. First, non polar solvents denaturate proteins [10]. According to a hydrophobic mechanism, the non polar solvent reduces the free energy of the unfolded state by solvating the exposed non polar amino acid residues. Second, a large number of crystal structures of proteins have become available and they show that a predominant feature of globular protein structures is the sequestration of non polar residues into a core where they largely avoid contact with water [11]. Third, protein stability is affected by different salt species (particularly at high salt concentrations) in the same rank as lyotropic series (Hofmeister), and this is generally taken as empirical evidence for hydrophobic interactions.

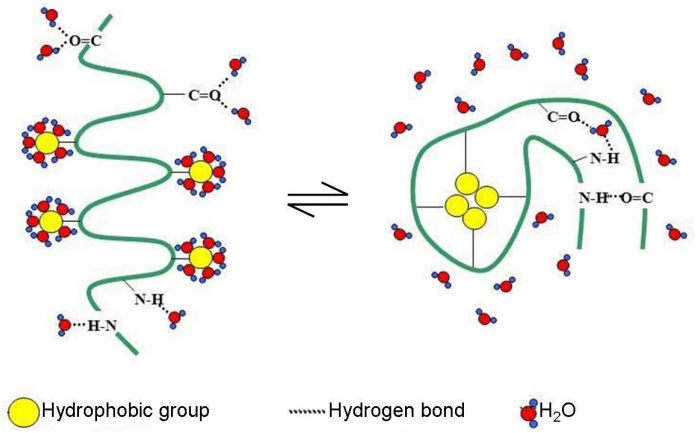


Figure 2.2. Schematic illustrating the formation of a hydrogen bond and a hydrophobic bond during the folding of a protein (*adapted from* [9]).

Hydrogen bonds are weaker than covalent bonds but play a very important role in determining the native state of protein structure. They require a hydrogen bond donor with high electronegativity and a hydrogen bond acceptor with the same property (called pillar atoms) that "share" the hydrogen atom. Within the protein backbone, these are usually between N—H and C=O (amide hydrogen and the carbonyl oxygen). Their average length (defined as the distance between the pillar atoms) is 2.5 - 3.5 Å, most are about 2.8 Å. The energy of the hydrogen bond depends on the distance between the two pillar atoms and on their properties but usually ΔG is -1 to -5 kcal·mol^{-1}. When analyzing crystallographic and NMR structural data, the presence of a

hydrogen bond can be suggested when the distance between two appropriate atoms is lower than the sum of the van der Waals radii of the atoms and the hydrogen [12].

Although there is a tendency for hydrophobic residues to be in the interior of the protein, and polar ones on the surface, there are a lot of polar parts in the interior, mostly the main chain groups. They interact with each other by forming hydrogen bonds, and therefore give rise to the appearance of secondary structure elements (discussed in the next section).

Van der Waals interactions are often found between non polar molecules, and hydrophobic side chains of proteins. They play a major role in the last stages of protein folding since the interior of a protein has many side chains very close to each other. Crystal structures reveal that the interior of proteins is packed at the same density as solids, implying that a high number of close contacts are made in the correctly folded form of the protein. The total van der Waals interactions of a protein molecule could therefore sum to hundreds of $kJ \cdot mol^{-1}$.

The ionic force leads to a high change in enthalpy. However, the enthalpy change, when forming a salt bridge is proportional to the inverse of the relative dielectric constant of the medium according to Coulomb´s law (Equation 2.2); thus, on the surface of the protein is proportional to the dielectric constant of water, and inside of the protein to the dielectric constant of hydrophobic side chains.

$$E = \frac{q_1 q_2}{4\pi\varepsilon r} \qquad (2.2)$$

where E is the energy of the interaction, q_1 and q_2 are the charges, ε is the dielectric constant of the medium and r is the distance between charges q_1 and q_2. As ε is higher in case of water than in case of the hydrophobic interior of the protein, one could think that the major part of salt bridges would occur in the interior. But for a protein molecule, the majority of charged groups are at the surface, where they are solvated and neutralized by counterions. Occasionally, there are ion pairs buried in the protein interior that can contribute to stabilization of folding. Nevertheless, one must take into account not only the enthalpy changes, but the entropy changes as well. If a salt bridge is formed in the interior of a protein the entropy decreases, which works against the high negative enthalpy change. The ionic interaction is an entropy force, as well as the hydrophobic forces.

The role of ionic interactions in the native structure of proteins is very important. However, they are mainly established in the last stages of protein folding, when an appropriate position of the charged, interacting amino acid residues is reached; then, the conformational variability of the local structure is constrained, and so the entropy decrease is not so high. It should also be noticed

that charged amino acids are important for folding also because they destabilize misfolded states through repulsion between similar charges or by desolvation of charged groups that become buried in the interior in an incorrectly folded state.

Although covalent bonds are mostly associated with the primary structure of proteins, they influence the tertiary structure in some special aspects. These cases are disulfide bonds, and Pro residues. The disulfide bridge is formed between two Cys residues in a redox reaction. As the cytoplasm possesses a reducing environment, there is no intracytoplasmic protein with disulfide bonds. But in the oxidizing external environment of the cell stable proteins are needed. That is why a lot of, if not all extracellular proteins have disulfide bridges. The *in vivo* control during disulfide formation is a natural consequence of protein folding, as the Cys residues can be in proximity to each other to interact in the last stage of folding, when the overall structure of the protein is more or less near the native conformation. This way the positions of disulfide bridges are more or less constrained by the thermodynamics of the folding (as the formation of disulfides decreases the entropy, only in the last stage can they form).

If we compare the contribution of different forces to the native protein stability, we can see that most of the stability comes from hydrophobic forces, then from van der Waals interactions and hydrogen bonds, and the ionic interactions and disulfide bonds are coming last.

Last but not least the loss of conformational entropy has to be taken into account. The conformational entropy is the entropy associated with the physical arrangement of a polymer chain that assumes a compact or globular state in solution. A polypeptide chain is larger when unfolded if compared to the more compact folded state, characterized by much more restricted conformational space, and this contributes to destabilization [13]. This conformational entropy change on folding to a defined state (entropy calculated from the probability that a state could be reached by chance alone), called ΔS_{conf} is quite large and is given by

$$\Delta S_{conf} = R \ln N \qquad (2.3)$$

where R is the gas constant and N is the estimated probability of the folded state.

In proteins, backbone dihedral angles and side chain rotamers are commonly used to define the degrees of freedom. In particular, the conformational entropy of the amino acid side chains in a protein is thought to be a major contributor to the energetic stabilization of the denatured state and thus a barrier to protein folding [13]. The limited conformational range of Pro residues lowers the conformational entropy of the denatured state and thus increases the energy difference between denatured and native states. A correlation has been observed between the thermostability

of a protein and its Pro residue content [14]. It has been suggested that conformational entropy may be a guiding force in the formation of protein secondary structure [15].

2.1.3. Protein Secondary Structure

Although proteins are linear polymers, the structures of most proteins are not the random coils found for synthetic non-natural polymers. Several types of secondary structure are particularly stable and occur widely contributing significantly to the stabilization of the overall protein fold. Using fundamental chemical principles and a few experimental observations, Linus Pauling[1] and Robert Corey predicted the existence of α-helical and β conformations in 1951, several years before the first complete protein structure was elucidated [16]. In April of 1951, readers of the *Proceedings of the National Academy of Sciences of the U.S.A.* had a surprise of big proportions: seven studies from the same authors, all on the subject of protein structure. The papers extended prior research and were grouped together for maximum attention, since the authors probably realized the bombshell they had dropped on the scientific world. Knowledge of the inner workings of proteins would be the key to understanding biology at the molecular level.

L-amino acids represent the vast majority of amino acids found in proteins. The sequence of amino acids that form a polypeptide is called the primary structure. In a polypeptide, adjacent amino acids are linked by amide bonds (peptide bond) from the carboxylic acid group (-COOH) of amino acid *i* to the amino group ($-NH_2$) of *i + 1*. The peptide bond is more commonly found in a trans conformation. Due to the presence of a partial double bond at the C_i—N_{i+1}, the peptide bond is inflexible; flexibility for rotation is placed around the Cα (carbon atom connected to the R group of the amino acid residues). Hence, the atoms O=C_i—N_{i+1}—H are fixed on the same plane, known as the peptide plane (Figure 2.3 A). Each residue *i* in the sequence is described by two backbone dihedral angles (also known as torsion angles): ψ, angle between the planes (N_i, $C\alpha_i$, C_i) and (H, N_i, $C\alpha_i$), and Φ, angle between the planes (N_i, $C\alpha_i$, C_i) and ($C\alpha_i$, C_i, O). The whole plane may rotate around the N—Cα bond (Φ angle) or C—Cα bond (ψ angle). In a peptide, combinations of ψ and Φ angles are restricted to certain regions due to unfavorable orbital overlap that precludes some

[1] As a curiosity, Pauling is one of a small number of individuals to have been awarded more than one Nobel Prize (in 1954, Pauling was awarded the Nobel Prize in Chemistry for research with X-ray crystallography and modeling in crystal and protein structures and, in 1962, was awarded the Nobel Peace Prize for his campaign against above ground nuclear testing), one of only two people to receive them in different fields (the other was Marie Curie) and the only person in that group to have been awarded each of his prizes without sharing it with another recipient.

combinations of ψ and Φ. A plot of their distribution is called the Ramachandran plot [17] and shows the sterical favored angles in the "ψ - Φ space" (Figure 2.3 B).

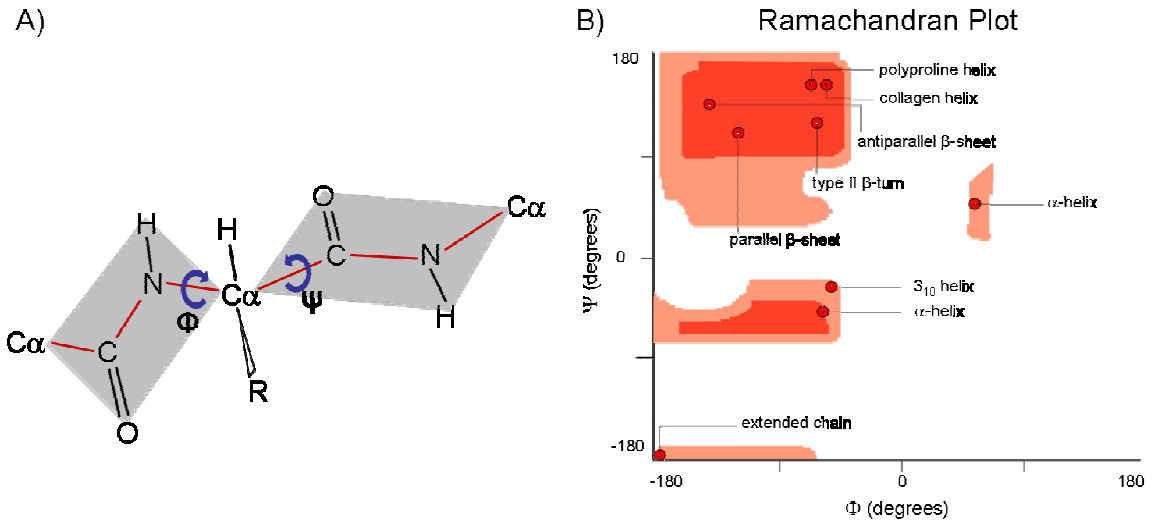


Figure 2.3. A) Peptide bonds and dihedral angles. The grey areas correspond to peptide planes and the red line formed by the repeating —Cα—C—N—Cα— is the backbone of the polypeptide chain. Only the bonds around Cα can rotate, defined by the ψ and Φ angles; the C—N single bonds of planar peptide groups are rigid. B) Ramachandran plot. Common protein secondary structure elements are marked at the positions of their average ψ and Φ values. Shown in red are the combinations of the backbone torsion angles ψ and Φ that are "allowed" because they do not result in steric interference (assuming that atoms are hard spheres). The salmon regions are allowed if some relaxation of steric hindrance is permitted. The isolated pink α-helical region on the right is actually for a left-handed helix, which is only rarely observed in short segments in proteins.

There are arrangements of backbone geometries in which the ψ and Φ angles of the backbone repeat in a regular pattern. These regular segments form the elements of the secondary structure of proteins and are stabilized by the presence of hydrogen bonds. Three general types of secondary structure elements have been defined: i) (right handed) helices, a very stable element where backbone hydrogen bonds are formed between oxygen of residue i and nitrogen of residue *i* + 4 (α-helix); ii) turns, where the direction of the chain is reversed and backbone hydrogen bonds are formed between facing residues, and iii) β-sheets, where backbone hydrogen bonds are formed between extended segments of the chain not necessarily close in the primary sequence that may run either in the same (parallel) or reverse (anti-parallel) direction. Each of these structures will be discussed more in detail.

The α-helix is the most common secondary structural element in a folded polypeptide chain, possibly because they are generated by hydrogen bonding between C=O and N—H groups close together in the sequence. It is a right- or left-handed coiled conformation, in which every backbone N—H_i group donates a hydrogen bond to the backbone C=O_{i+4} group of the amino acid four

residues earlier (i+4 → i hydrogen bonding). Usually in proteins, the amino acids are arranged in a right-handed helical structure because all the amino acids except Gly in proteins have the L-configuration and steric constraints favor the right-handed helix. Each amino acid corresponds to a 100° turn in the helix (i.e., the helix has 3.6 residues per turn), and a rise per residue of 1.5 Å along the helical axis. So the distance per turn is 5.4 nm (3.6×1.5 Å). Residues in α-helices typically adopt backbone (Φ, ψ) dihedral angles around (-60°, -45 to -50°). Consequently, α-helical dihedral angles generally fall on a diagonal stripe on the Ramachandran plot (Figure 2.3 B), ranging from (-90°, -15°) to (-35°, -70°). Similar structures include the 3_{10} helix (i+3 → i hydrogen bonding) and the π-helix (i+5 → i hydrogen bonding). These alternative helices are relatively rare, although the 3_{10} helix is often found at the ends of α-helices, "closing" them. Transient helices (sometimes called δ-helices) have also been reported as intermediates in molecular dynamics simulations of α-helical folding.

The α-helix is tightly packed; there is almost no free space within the helix. The amino-acid side chains are on the outside of the helix, and point roughly towards the N-terminus. This directionality is sometimes used in preliminary, low-resolution electron-density maps to determine the direction of the protein backbone. In many α-helices, polar and hydrophobic residues are distributed 3-4 residues apart in the sequence to produce a helix with one hydrophilic face and one hydrophobic face, known as amphipathic α-helix. Helices with this character often occur on the surfaces of proteins, with the polar face in contact with water, or at interfaces. A helix has an overall dipole moment caused by all the individual dipoles from the carbonyl groups of the peptide bond pointing along the helix axis (Figure 2.4). This can lead to destabilization of the helix through entropic effects. As a result, α-helices are often capped at the N-terminus end by a negatively charged amino acid, such as glutamic acid, in order to neutralize this helix dipole. Less common (and less effective) is C-terminal capping with a positively charged amino acid, such as Lys. The N-terminal positive charge is commonly used to bind negatively charged ligands such as phosphate groups, which is especially effective because the backbone amides can serve as hydrogen bond donors.

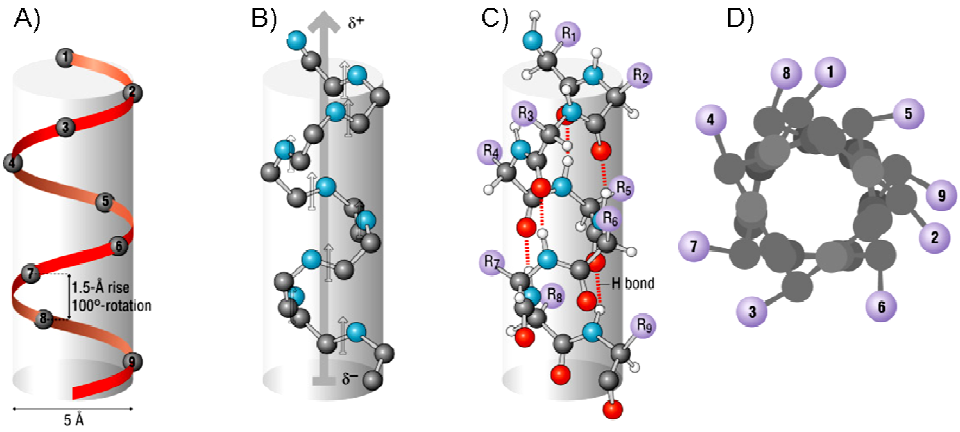


Figure 2.4. The α-helix. The chain path with average helical parameters is indicated showing A) the Cα only, B) the backbone fold with peptide dipoles and C) the full structure with backbone hydrogen bonds in red. The protein chain runs downwards, i.e., its N-terminus is at the top and its C-terminus at the bottom of the figure. Note that the sidechains point slightly upwards, i.e., towards the N-terminus. D) Top view (from the N-terminal end) along the axis of an idealized α-helical polypeptide. Side chains (1-9) project outward from the helical axis at 100° intervals.

Not all the polypeptides can form a stable α-helix. The residues Ala, Glu and Leu have tendency to be involved in α-helices. There are five different kinds of constraints that affect the stability of an α-helix: (i) the electrostatic repulsion (or attraction) between amino acid residues with charged R groups, (ii) the bulkiness of adjacent R groups, (iii) the interactions between amino acid side chains spaced three (or four) residues apart, (iv) the occurrence of Pro residues, and (v) the interaction between amino acids at the ends of the helix and the electric dipole inherent to this structure.

The backbone hydrogen bonds of α-helices are generally considered slightly weaker than those found in β-sheets, and are readily attacked by water molecules. However, in more hydrophobic environments such as the plasma membrane, or in the presence of co-solvents such as TFE, peptides readily adopt stable α-helical structure.

The β-sheet is the second form of regular secondary structure in proteins consisting of β strands connected laterally by three or more hydrogen bonds, forming a generally twisted pleated sheet. A β-strand is a stretch of amino acid residues, typically 5–10 amino acids long, whose peptide backbones are almost fully extended. The association of β-sheets has been implicated in the formation of protein aggregates and fibrils observed in many human diseases, notably the amyloidosis.

The majority of β-strands are arranged adjacent to other strands and form an extensive hydrogen bond network with their neighbors in which the N—H groups in the backbone of one

strand establish hydrogen bonds with the C=O groups in the backbone of the adjacent strands. So, in contrast to the α-helix, the β-strands involve hydrogen bonds between backbone groups from residues distant from each other in the linear sequence. Adjacent strands in a β-sheet are aligned so that their Cα atoms are adjacent and their side chains point in the same direction. The side chains point outwards from the folds of the pleats, roughly perpendicularly to the plane of the sheet; successive residues point outwards on alternating faces of the sheet. The "pleated" appearance of β-strands arises from tetrahedral chemical bonding at the Cα atom that causes the distance between $C\alpha_i$ and $C\alpha_{i+2}$ to be approximately 6 Å, rather than the 7.6 Å (2 × 3.8 Å) expected from two fully extended peptide bonds (distance between residues 3.8 Å). The energetically preferred dihedral angles (Φ, ψ) of (–135°, 125°) (broadly, the upper left region of the Ramachandran plot, see Figure 2.3) diverge somewhat from the fully extended conformation (φ, ψ) = (–180°, 180°). The "sideways" distance between adjacent Cα atoms in hydrogen-bonded β-strands is roughly 5 Å.

Usually β-strands are represented in protein topology diagrams by an arrow pointing toward the C-terminus. Adjacent β-strands can form hydrogen bonds in antiparallel, parallel, or mixed arrangements (Figure 2.5). In an antiparallel arrangement, the successive β-strands alternate directions so that the N-terminus of one strand is adjacent to the C-terminus of the next. This is the arrangement that produces the strongest inter-strand stability because it allows the inter-strand hydrogen bonds between carbonyls and amines to be planar. The peptide backbone dihedral angles (φ, ψ) are about (–140°, 135°) in antiparallel sheets. In a parallel arrangement, all of the N-termini of successive strands are oriented in the same direction; this orientation is slightly less stable because it introduces non planarity in the inter-strand hydrogen bonding pattern. The dihedral angles (φ, ψ) are about (–120°, 115°) in parallel sheets. Parallel sheets are always buried and small parallel sheets almost never occur. Antiparallel sheets by contrast are frequently exposed to the aqueous environment on one face. β-strands usually have a pronounced right-handed twist due to steric effects arising from the L- amino acid configuration. Parallel strands are less twisted than antiparallel ones. The effect of strand twist is that sheets consisting of several long strands are themselves twisted.

Large aromatic residues (Tyr, Phe and Trp) and β-branched amino acids (Thr, Val, Ile) are favored to be found in β-strands since they can be accomodated more easily in a β structure than in a tightly coiled α-helix. Interestingly, different types of residues (such as Pro) are likely to be found in the edge of β-sheets, presumably to avoid the "edge-to-edge" association between proteins that might lead to aggregation and amyloid formation.

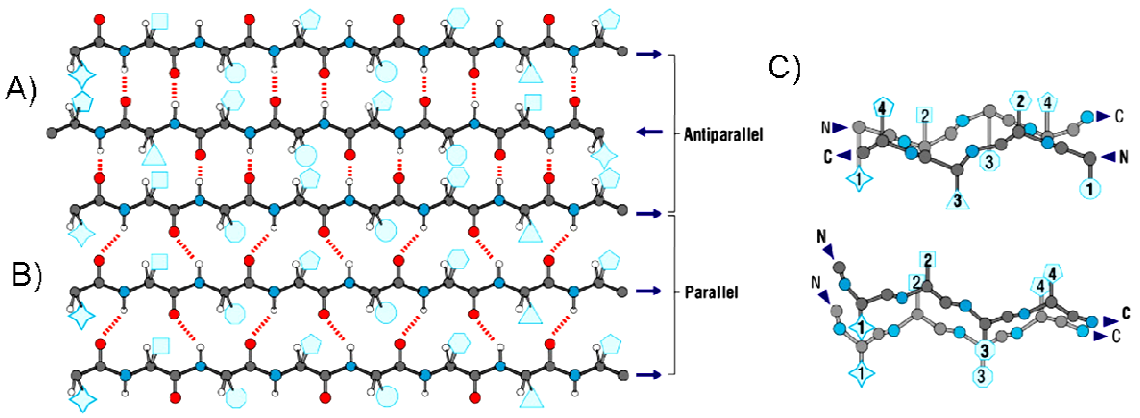


Figure 2.5. The structure of the β-sheet. On the left is shown a mixed β-sheet, containing both antiparallel A) and parallel B) segments. Oxygen atoms are colored red and nitrogen atoms colored blue and hydrogen bonding patterns are represented by red dotted lines (more linear in the antiparallel sheet). On the right C), are edge-on views of antiparallel (top) and parallel sheets (bottom), showing the corrugated appearance. Consecutive side chains (numbered) point from alternate faces of both types of sheet.

According to the most common definition, a turn is defined by the close approach of two Cα atoms (< 7 Å), when the corresponding residues are not involved in a regular secondary structure element such as an α-helix or β-sheet. Turns are the simplest secondary structural element and are grouped by their hydrogen bonding and by their backbone dihedral angles. At the level of hydrogen bonds, the nomenclature is similar to that of helices. A β-turn (most common form, Figure 2.6) is characterized by hydrogen bond in which the donor and acceptor residues are separated by three residues ($i \rightarrow i\pm3$ hydrogen bonding). A γ-turn is characterized by $i \rightarrow i\pm2$ hydrogen bonding, an α-turn is characterized by $i \rightarrow i\pm4$ hydrogen bonding and a π-turn is characterized by $i \rightarrow i\pm5$ hydrogen bonding. Finally, ω-loop is a general term for a longer loop with no internal hydrogen bonding. There is not need of a well-formed hydrogen bond. Thus, it is more correct to define a β-turn by the close approach of Cα atoms of residues separated by three peptide bonds, and so on. Within each hydrogen-bonding type, turns may be classified by their backbone dihedral angles. A turn can be converted into its inverse turn by changing the sign on all of its dihedral angles (the inverse turn is not a true mirror image since the chirality of the Cα atoms is maintained). The classical and inverse β-turns are usually distinguished with a prime, e.g., type I and type II β-turns. A hairpin is a special case of a turn, in which the direction of the protein backbone reverses and the flanking secondary structure elements interact. For example, a β-hairpin connects two hydrogen-bonded, antiparallel β-strands.

Water molecules can donate and accept hydrogen bonds in the C=O and N—H groups not involved in hydrogen binding with other backbone atoms. Therefore, turns are found on the surface

of folded proteins, where they are in contact with the aqueous environment. The tight geometry of the turn means that some residues, such as Gly (small and flexible) and Pro (peptide bonds involving the imino nitrogen readily assume a cis configuration), are found more commonly in turns than others.

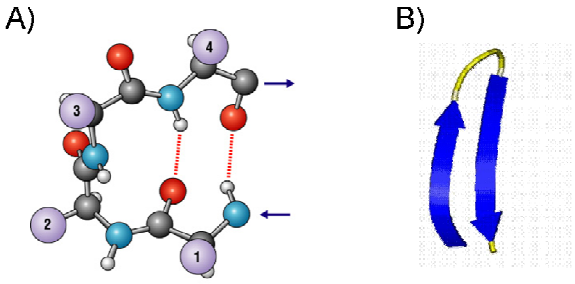


Figure 2.6 A) Typical β-turn. Schematic diagram showing the backbone hydrogen bonds that stabilize the reversal of the chain direction. 1, 2, 3 and 4 are side chains. B) Typical representation of a β-hairpin.

Some amino acids are accommodated in the different types of secondary structure better than others, i.e., they have conformational preferences. Yet it is generally easier to identify helical stretches in sequences that to identify regions of β structure even thought the prediction of a protein structure is a hard task. The environment in which a protein is synthesized and allowed to fold are significant determinants of its final shape and are usually not directly taken into account by current prediction methods.

2.1.4. Protein Tertiary and Quaternary Structure

Globular proteins are compact structures. The three-dimensional arrangement of all atoms is referred as the tertiary structure of the protein. Amino acids that are far apart in the polypeptide sequence and reside in different types of secondary structure may interact when the protein is folded. The breakthrough in understanding globular protein folding came from x-ray diffraction studies of myoglobin carried out by John Kendrew in the 1950s [18]. With the elucidation of the tertiary structures of hundreds of other globular proteins, it became clear that different amino acid sequences and different tertiary structures reflect differences in function.

Each protein has a distinct structure adapted for its particular biological function. But there are some important properties that are common: (i) compact folding, (ii) hydrophobic amino acid side chains oriented towards the interior and (iii) hydrophilic side chains on the surface. These specific structures are stabilized by interactions described earlier. Close packing of atoms maximizes both

the probability that these interactions will occur and their strength, helping to guide the interaction of regions of given secondary structure. Because the tertiary structure is not regular, it is hard to describe it simply. One way to characterize a tertiary structure is by the topological arrangement of the various secondary structure elements as they pack together (called structural motifs), since some patterns occur repeatedly in proteins that differ in biological function and amino acid sequence (some examples in Figure 2.7).

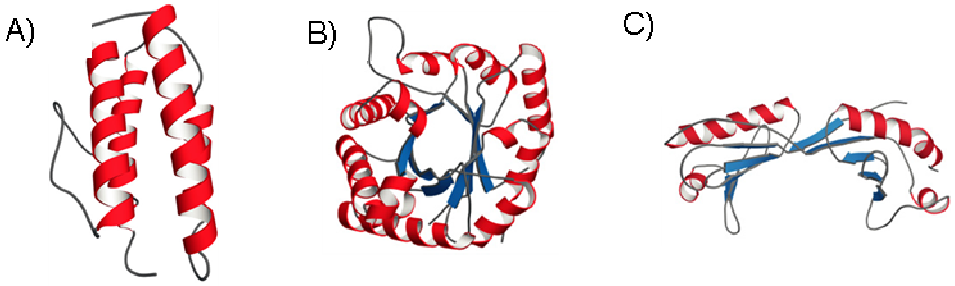


Figure 2.7. Examples of some common structural motifs in proteins. A) Four-helix bundle (Myohemerythrin); B) α/β Barrel (Triose phosphate isomerase); C) α/β with saddle (TATA-binding protein).

Like referred to before, the most important proof that the tertiary structure of a globular protein is determined by its amino acid sequence came from experiments showing that denaturation of some proteins is reversible [3]. However, prions defy this concept; the same primary structure can give rise to different secondary and tertiary structures. The study of homologous proteins has strengthened this conclusion. In a series of homologous proteins from different species (e.g cytochrome *c*) the amino acid residues at certain positions of the sequence are invariant, whereas at other positions they may vary. Many of the invariant residues of homologous proteins appear to occur at critical points along the polypeptide chain. Some are found at or near bends, others at cross-linking points between loops such as Cys residues involved in disulfide bonds.

One effect of the tertiary structure is to create a complex surface topography that enables a protein to interact specifically either with small molecules or with other macromolecules, with which it may have regions of complementary topology and charge. These recognition sites are often formed from the stretches of amino acids joining secondary structure elements. Helical segments and β-strands are often connected by tight turns, but more often there are long stretches of amino acids in between secondary structural elements that do not adopt regular backbone conformations. Such loops are found at the surface of proteins and typically stick out to the solvent. Consequently

they provide convenient sites for protein recognition, ligand binding and membrane interaction. Moreover, although the native tertiary structure is thermodynamically very stable, it should not be regarded as absolutely rigid. Globular proteins have a certain amount of flexibility in their backbones and undergo short-range internal fluctuations. Many proteins also undergo small conformational changes in the course of their biological function (many times associated with the binding of a ligand). The individual secondary structure elements in a protein pack together in part to bury the hydrophobic side chains, forming a compact molecule with very little empty space in the interior as discussed. Although the density of atoms in the hydrophobic core of a folded protein is high, the packing is not perfect. There are many cavities that range in size from subatomic packing defects to ones large enough to accommodate several water molecules. If the cavity walls are lined with hydrophobic side chains, the cavity is usually found to contain no ordered water, but more commonly there are some polar groups lining the cavity and these interact with buried water molecules that fill the space.

Some proteins contain two or more separate polypeptide chains, which may be identical or different in structure. Protein assemblies composed of more than one polypeptide chain are called oligomers and the individual chains of which they are made are termed monomers or subunits. Oligomers containing two, three, four, five, six or even more subunits are known as dimers, trimers, tetramers, pentamers, hexamers, and so on. Much the commonest of these are dimers. The arrangement of proteins and protein subunits in three-dimensional complexes constitutes the quaternary structure. The interactions between subunits are stabilized by the same forces that stabilize tertiary structure and are tight and specific. The macromolecular assemblies form spontaneously when the right amounts of the appropriate components are present. Large assemblies sometimes reflect complex functions and one obvious example is the complicated structure of ribosomes which carry out protein synthesis.

2.1.5. Protein Folding in the Cell

In a cell, proteins are synthesized on ribosomes from the genetic information encoded in the cellular DNA. Most proteins can be unfolded and refolded in dilute solution, demonstrating that the primary structure contains all the information necessary to specify the folded state. However, the interior of a cell is not a dilute solution [1].

In vivo, protein folding can in principle begin whilst a nascent chain is still attached to the ribosome, and there is evidence that some proteins do fold at least partially in such a co-

translational manner [19]. Other proteins are known to undergo the major part of their folding in the cytoplasm after release from the ribosome, or to fold in specific compartments such as the endoplasmatic reticulum (ER) following translocation through membranes [20]. During folding, partially folded proteins expose hydrophobic regions, which could lead to nonproductive associations and protein aggregation. The aggregation problem is exacerbated by the fact that stable folding of a protein domain cannot occur until the entire domain is synthesized. Ensuring accuracy in protein folding is crucial for maintaining proper cellular functions.

A diverse and ubiquitous class of proteins, known as molecular chaperones, has evolved to assist the folding of newly synthesized proteins [2]. Chaperones have many cellular functions such as modulation of protein conformation and activity, disaggregation and refolding of proteins after cellular stress (e.g., temperature or osmotic pressure) and translocation of proteins across membranes; they are present in all cell types and cellular compartments. These proteins were originally discovered because they are produced in increased quantities in response to raised temperatures: this is why many chaperones are named Hsp (heat-shock protein) followed by a number denoting molecular weight [21]. While small monomeric proteins are able to fold in the absence of chaperones *in vivo*, chaperones are critically important for the folding of medium- to large-sized multidomain proteins.

Many chaperones are protein machines that operate through conformational changes brought about by binding and hydrolysis of ATP. Chaperones function by binding transiently to exposed hydrophobic surfaces in unfolded or misfolded proteins in a manner that is regulated by conformational changes in the substrate-binding domain of the chaperone. ATP binding to the ATP-binding domain induces a conformational change that allows the chaperone to bind to its target, while hydrolysis of the ATP to ADP by the chaperone ATPase leads to its release. Replacement of the ADP by ATP starts the cycle again. These controlled cycles of binding and release allow the unfolded polypeptide repeated opportunities to achieve proper folding without the risk of aggregation.

Some chaperones interact with nascent chains as they emerge from the ribosome, whereas others are involved in guiding later stages of the folding process [20, 22]. Chaperones serve protein folding in multiple ways: one is by acting as a cage to prevent aggregation while folding takes place; another is to accelerate the folding process by helping proteins out of their kinetic traps – that is, some chaperones can actively undo an already formed but incorrect structure; thirdly, some chaperones actively disassemble and unfold of proteins for subsequent degradation. Molecular chaperones often work in tandem to ensure that the various stages in the folding of such systems are all completed efficiently. Molecular chaperones do not themselves increase the rate of

individual steps in protein folding; rather, they increase the efficiency of the overall process by reducing the probability of competing reactions. However, there are several classes of folding catalyst not usually classified as chaperones that accelerate potentially slow steps in the folding process. The most important are peptidylprolyl isomerases, which increase the rate of cis–trans isomerization of peptide bonds involving Pro residues, and protein disulphide isomerases, which enhance the rate of formation and reorganization of disulphide bonds [23].

Many of the details of the functions of molecular chaperones have been determined from studies of their effects on folding *in vitro*. The best characterized of the chaperones studied in this manner is the bacterial complex involving GroEL, a member of the family of chaperonins (Hsp60 in eukaryotes), and its co-chaperone GroES. Many aspects of the sophisticated mechanism through which this coupled system functions are now well understood [20, 22]. Of particular interest is that GroEL, and other members of this class of molecular chaperone, contains a cavity in which incompletely folded polypeptide chains can enter and undergo the final steps in the formation of their native structures while sequestered and protected from the outside world [24]. Chaperones are found in all cellular compartments in which protein synthesis and folding reactions occur. In bacteria, the folding of approximately 30% of all proteins is affected in mutant cells in which GroEL is defective. In eukaryotes, Hsp70 can be isolated bound to 15–20% of newly synthesized proteins.

Despite these factors, given the complexity and stochastic nature of the folding process, it would be remarkable if misfolding never occurred. In eukaryotic systems, many of the proteins that are synthesized in a cell are destined for secretion to the extracellular environment. These proteins are translocated into the ER, where folding takes place before secretion through the Golgi apparatus. The ER contains a wide range of molecular chaperones and folding catalysts, and in addition the proteins that fold here must satisfy a "quality-control" check before being exported (Figure 2.8) [25].

Such a process is particularly important because there seem to be few molecular chaperones outside the cell, although one (clusterin), at least, has been discovered [26]. This quality-control mechanism involves a remarkable series of glycosylation and deglycosylation reactions that enables correctly folded proteins to be distinguished from misfolded ones [25]. The importance of these regulatory systems is underlined by recent experiments that suggest that a large fraction of all polypeptide chains synthesized in a cell fail to pass this test and are targeted for degradation. Like the "heat shock response" in the cytoplasm, the "unfolded protein response" in the ER is also stimulated (upregulated) during stress and, is strongly linked to the avoidance of misfolding diseases [27].

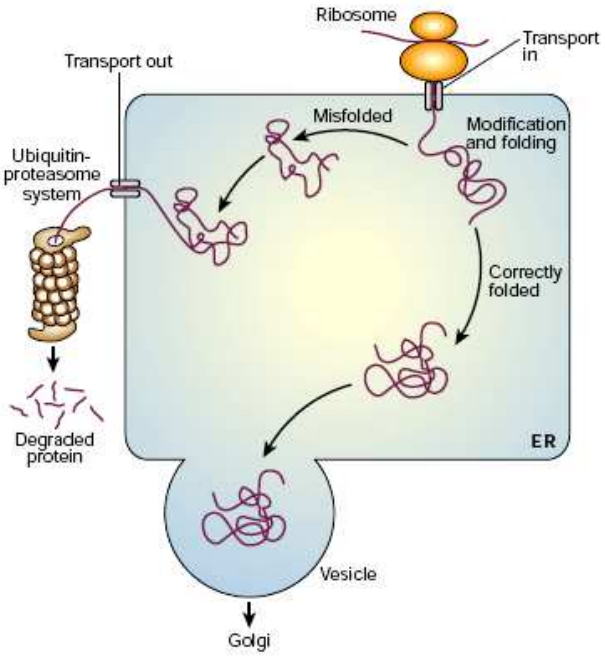


Figure 2.8. Regulation of protein folding in the ER. Most newly synthesized proteins are translocated into the ER, where they fold into their three-dimensional structures. Correctly folded proteins are then transported to the Golgi complex and delivered to the extracellular environment. However, incorrectly folded proteins are detected by a quality-control mechanism and sent along another pathway (the unfolded protein response) in which they are ubiquitinated and then degraded in the cytoplasm by proteasomes (*from* [28]).

2.1.6. Protein Misfolding and Disease

In parallel with our improved understanding of protein folding, recent years have also witnessed a growing interest in the "protein misfolding problem". What is protein misfolding? In a very interesting review by Dobson [29], he states:

"The term "protein folding" is universally accepted to refer to the process that results in the acquisition of the native structure from a completely or partially unfolded state. I use the term "misfolding" to describe processes that result in a protein acquiring a sufficient number of persistent non-native interactions to affect its overall architecture and/or its properties in a biologically significant manner. Thus a monomeric intermediate populated during the normal folding process of a protein will not usually be described as misfolded, even though it may have some non-native contacts between its residues. If a monomeric protein were to find its way into a compact stable structure with a non-native topology, however, such a species would be described as misfolded, as its architecture (and almost invariably its biological) would be demonstrably distinct from that of the native state. The aggregation process that leads to a peptide or protein to

form an amyloid fibril will universally be described on this definition as "misfolding", as the interactions that determine the structure and properties of such fibrils are distinct from those that determine the structure and properties of the biologically active forms of the molecules concerned."

Failure to reach or maintain the correct folded structure can have serious consequences, and a broad range of debilitating human diseases arises from the failure of a specific peptide or protein to adopt, or remain in, its native functional conformational state. Even if, following translation, a protein successfully attains its biologically active state, this often does not mean the end-point of its folding/unfolding life. Many proteins go through cycles of unfolding and refolding due to a variety of factors that include transport across a membrane, cellular secretion, or exposure to stress conditions. Also these diseases are often associated with ageing, perhaps reflecting a general decline in cellular repair systems, but some of them are prevalent in young individuals. As a result, the chance for a protein to misfold is relatively high. These pathological conditions are generally referred to as protein misfolding (or protein conformational) diseases. They include pathological states in which impairment in the folding efficiency of a given protein results in a reduction in the quantity of the protein that is available to play its normal role [30]. This reduction can arise as the result of one of several posttranslational processes, such as an increased probability of degradation via the quality control system of the ER, as occurs in cystic fibrosis and α1-antitrypsin (α1-AT) deficiency, or the improper trafficking of a protein, as seen in early-onset emphysema [30]. Many of the pathological features of the protein misfolding diseases, and the characteristics of the proteins with which they are associated, appear at first sight to be quite diverse. Despite this diversity, it is increasingly evident from the experimental data emerging from a wide range of studies that there are some, perhaps many, common features in the underlying physicochemical and biochemical origins of the various disorders.

The largest group of misfolding diseases, however, is associated with the conversion of specific peptides or proteins from their soluble functional states ultimately into highly organized fibrillar aggregates. These structures are generally described as amyloid fibrils or plaques when they accumulate extracellularly, whereas the term "intracellular inclusions" has been suggested as more appropriate when fibrils morphologically and structurally related to extracellular amyloid form inside the cell (Table 2.1).

The native conformation of a protein usually has little tendency to aggregate because interactions within the protein fold render the majority of hydrophobic and main chain amide and carbonyl groups capable of forming strong hydrogen bonds inaccessible to intermolecular interactions. In the denaturated state, however, there is an exposure of these regions of the

polypeptide chain and so there is an opportunity for intermolecular interactions to take place. Going back to the "new view" of the protein folding previously described and to Figure 2.1, some of the routes in the funnel can lead to a low energy valley that, although still higher than the native state in free energy level, persistently traps the protein in a non-native conformation. Protein-protein interactions in this non-native conformation may lead to protein aggregation and amyloid formation [30].

According to Figure 2.9, therapeutic intervention can occur in the form of drugs that reduce the production of a certain protein, drugs that increase the rate of clearance of misfolded/aggregated proteins, and drugs that increase the native-state stability or increase the kinetic barrier to misfolding/aggregation [31].

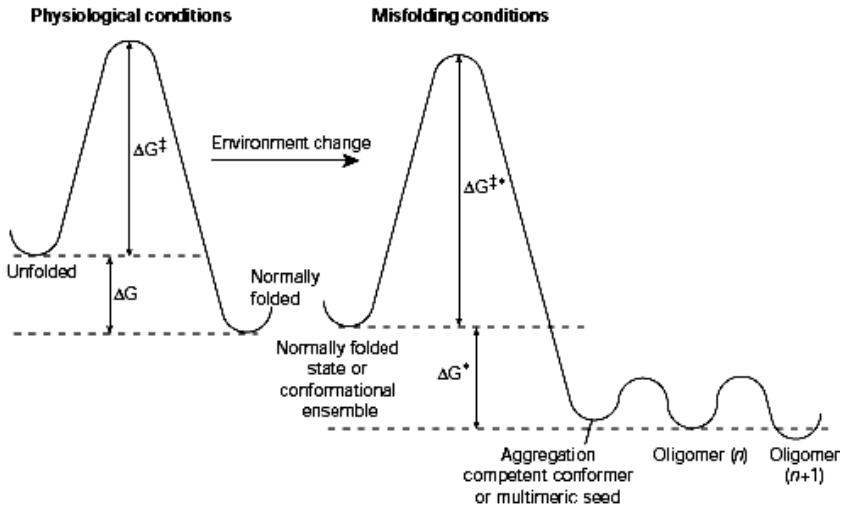


Figure 2.9. Free-energy diagram showing to what extent a given sequence under native conditions prefers a normally folded conformation. The difference in free energy (ΔG) between the native state and the unfolded conformations (unfolded state) dictates the relative population of each state. The free energy of activation ($\Delta G^{\ddagger}$) governs how fast one conformation will convert to another. Under denaturing conditions, a misfolded aggregation-prone conformation can be preferred to the folded native state as a consequence of the interplay between sequence and environment (*from* [31]).

Table 2.1. Human diseases associated with formation of extracellular amyloid deposits or intracellular inclusions with amyloid-like characteristics [30].

Disease	Aggregating protein / peptide	Number of residues	Native structure
Neurodegenerative diseases			
Alzheimer's disease[c]	Amyloid β peptide (Aβ)	40 or 42[f]	Unfolded
Spongiform encephalopathies[c,e]	Prion protein or fragments	253	Unfolded (residues 1–120) α-helical (residues 121–230)
Parkinson's disease[c]	α-Synuclein	140	Unfolded
Dementia with Lewy bodies[c]	α-Synuclein	140	Unfolded
Frontotemporal dementia with Parkinsonism[c]	Tau	352–441[f]	Unfolded
Amyotrophic lateral sclerosis[c]	Superoxide dismutase	153	All-β, Ig like
Huntington's disease[d]	Huntingtin with polyQ expansion	3144[g]	Largely natively unfolded
Spinocerebellar ataxias[d]	Ataxins with polyQ expansion	816[g,h]	All-β, AXH domain (residues 562–694); rest are unknown
Spinocerebellar ataxia 17[d]	TATA box-binding protein with polyQ expansion	339[g]	α+β, TBP like (residues 159-339); unknown (residues 1–158)
Spinal and bulbar muscular atrophy[d]	Androgen receptor with polyQ expansion	919[g]	All-α, nuclear receptor ligand-binding domain (residues 669-919); rest are unknown
Hereditary dentatorubral pallidoluysian atrophy[d]	Atrophin-1 with polyQ expansion	1185[g]	Unknown
Familial British dementia[d]	ABri	23	Unfolded
Familial Danish dementia[d]	ADan	23	Unfolded
Nonneuropathic systemic amyloidosis			
AL amyloidosis[c]	Immunoglobulin light chains or fragments	~90[f]	All-β, Ig like
AA amyloidosis[c]	Fragments of serum amyloid A protein	76–104[f]	All-α, unknown fold
Familial Mediterranean fever[c]	Fragments of serum amyloid A protein	76–104[f]	All-α, unknown fold
Senile systemic amyloidosis[c]	Wild-type transthyretin	127	All-β, prealbumin like
Familial amyloidotic polyneuropathy[d]	Mutants of transthyretin	127	All-β, prealbumin like
Hemodialysis-related amyloidosis[c]	β2-microglobulin	99	All-β, Ig like
ApoAI amyloidosis[d]	N-terminal fragments of apolipoprotein AI	80–93[f]	Natively unfolded
ApoAII amyloidosis[d]	N-terminal fragments of apolipoprotein AII	98[i]	Unknown
ApoAIV amyloidosis[c]	N-terminal fragments of apolipoprotein AIV	~70	Unknown
Finnish hereditary amyloidosis[d]	Fragments of gelsolin	71	Natively unfolded

Lysozyme amyloidosis[d]	Mutants of lysozyme	130	α+β, lysozyme fold
Fibrinogen amyloidosis[d]	Variants of fibrinogen α-chain	27–81[f]	Unknown
Icelandic hereditary cerebral amyloid angiopathy[d]	Mutant of cystatin C	120	α+β, cystatin like
Nonneuropathic localized diseases			
Type II diabetes[c]	Amylin, also called IAPP	37	Unfolded
Medullary carcinoma of the thyroid[c]	Calcitonin	32	Unfolded
Atrial amyloidosis[c]	Atrial natriuretic factor	28	Unfolded
Hereditary cerebral haemorrhage with amyloidosis[d]	Mutants of Aβ	40 or 42[f]	Unfolded
Pituitary prolactinoma	Prolactin	199	All-α, 4-helical cytokines
Injection-localized amyloidosis[c]	Insulin	21 + 30[j]	All-α, insulin like
Aortic medial amyloidosis[c]	Medin	50[k]	Unknown
Hereditary lattice corneal dystrophy[d]	C-terminal fragments of kerato-epithelin	50–200[f]	Unknown
Corneal amylodosis associated with trichiasis[c]	Lactoferrin	692	α+β, periplasmic-binding protein like II
Cataract[c]	γ-Crystallins	Variable	All-β, γ-crystallin like
Calcifying epithelial odontogenic tumors[c]	Unknown	~46	Unknown
Pulmonary alveolar proteinosis[d]	Lung surfactant protein C	35	Unknown
Inclusion-body myositis[c]	Aβ	40 or 42[f]	Unfolded
Cutaneous lichen amyloidosis[c]	Keratins	Variable	Unknown

[a]Data refer to the number of residues of the processed polypeptide chains that deposit into aggregates, not of the precursor proteins.

[b]According to Structural Classification Of Proteins (SCOP), these are the structural class and fold of the native states of the processed peptides or proteins that deposit into aggregates prior to aggregation.

[c]Predominantly sporadic, although in some cases hereditary forms associated with specific mutations are well documented.

[d]Predominantly hereditary, although in some cases sporadic forms are documented.

[e]Five percent of the cases are transmitted (e.g., iatrogenic).

[f]Fragments of various lengths are generated and have been reported to be present in *ex vivo* fibrils.

[g]Lengths shown refer to the normal sequences with nonpathogenic traits of polyQ.

[h]Length shown is for ataxin-1.

[i]The pathogenic mutation converts the stop codon into a Gly codon, extending the 77-residue protein by 21 additional residues.

[j]Human insulin consists of two chains (A and B, with 21 and 30 residues, respectively) covalently linked by disulfide bridges.

[k]Medin is the 245–294 fragment of human lactadherin.

2.2. Amyloidosis

In 1838, Mathias Schleiden (a German botanist) associated the term amyloid to the normal amylaceous constituent of plants. In 1854, Rudolf Virchow used the term amyloid to describe abnormal extracellular material seen in the liver during autopsy that reacted with iodine and sulfuric acid, which, at the time, was a marker for starch; thus, the term amyloid or starchlike [32]. 70 years after Virchow's description, Divry and colleagues recognized that the amyloid deposits showed green birefringence when stained with Congo red (CR) and viewed under polarized light [33]. This observation remains the *sine qua non* of the diagnosis of amyloidosis. In 1959, with the use of electron microscopy (EM), Cohen and Calkins first recognized that all forms of amyloidosis have a nonbranching fibrillar structure and the proteinaceous nature of this material was established [34]. Identification of the actual chemical composition of the plaques was only achieved in 1984, when Glenner and Wong isolated a 4 kDa peptide currently known as Aβ from AD brains [35].

The pathology of more than 40 human degenerative diseases is associated with the deposition of amyloid. Collectively referred to as protein deposition diseases, these include various sporadic (e.g. AD and PD), familial, and transmissible degenerative disorders (e.g. spongiform encephalopathies such as Creutzfeldt-Jakob disease (CJD)), many of which affect, amongst other tissues and organs, the brain and the central nervous system (CNS).

Amyloidosis can be defined as any pathological state associated with the formation of extracellular amyloid deposits with no clinical or pathological evidence of disease in the absence of such deposits. In local amyloidosis, the amyloid is restricted to a particular organ or tissue. In systemic amyloidosis, deposits can be present in any or all of the viscera, connective tissue and blood vessel walls. The diseases can be broadly grouped into neurodegenerative conditions, in which aggregation occurs in the nervous system, non-neuropathic localized amyloidosis, in which aggregation occurs in a single type of tissue other than the brain and non-neuropathic systemic amyloidosis, in which aggregation occurs in multiple tissues [30] (Table 2.1). In neurodegenerative diseases, the quantities of aggregates involved can be almost undetectable, whereas in some systemic diseases literally kilograms of protein can be found in one or more organs [36]. Some of these conditions, such as AD and PD, are predominantly sporadic, although hereditary forms are well documented. Other conditions, such as the lysozyme and fibrinogen amyloidosis, arise from specific mutations and are hereditary. In addition to sporadic (85%) and hereditary (10%) forms, spongiform encephalopathies (prion diseases) can also be transmissible (5%) in humans as well as in other mammals [30, 37].

2.2.1. Structural Features of Amyloid Fibrils

Despite large differences in the size, native structure and function of amyloidogenic proteins, all amyloid fibrils are of indeterminate length (usually < 200 nm), unbranched, with a diameter of 70 to 120 Å [38]. Early x-ray diffraction examinations of amyloid fibrils gave simple patterns with 4.7 to 4.8 Å meridional reflections and 10 Å equatorial reflections, arising from the molecular spacings present within the regularly repeating, ordered structural elements of the fibrils [39]. They are characteristic of a cross-β structure in which the polypeptide chain is organized in β-sheets arranged parallel to the fibril axis with their constituent β-strands perpendicular to the fibril axis (Figure 2.10). *Ex vivo* fibrils cannot be crystallized, and there is no high-resolution structure of natural amyloid fibrils, but biophysical methods such as solid state NMR are now yielding much more detailed molecular structures of amyloid fibrils created *in vitro* [40].

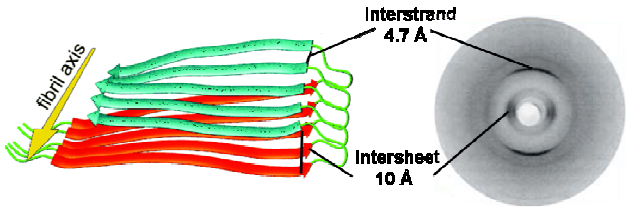


Figure 2.10. X-ray diffraction signature of amyloid fibrils with the sharp meridional main chain spacing (4.7 Å) and the diffuse equatorial side reflection (*adapted from* [50]).

Fibrils can be imaged *in vitro* using transmission electron microscopy (TEM) and atomic force microscopy (AFM) (Figure 2.11 A). These techniques reveal that the fibrils usually consist of a number (typically 2–6) of protofilaments (Figure 2.11 D), each about 2–5 nm in diameter [41]. These protofilaments twist together to form ropelike fibrils that are typically 7–13 nm wide [38, 41]. Sunde *et* al. have proposed a molecular model of the common core protofilament structure of amyloid fibrils (Figure 2.11 C). A number of β-sheets make up the protofilament structure. These sheets run parallel to the axis of the protofilament, with their component β-strands perpendicular to the fibril axis. With normal twisting of the β-strands, the β-sheets twist around a common helical axis that coincides with the axis of the protofilament, giving a helical repeat of 115.5 Å containing 24 β-strands [38].

The fibrils have the ability to bind specific dyes such as thioflavin T (ThT) and CR [42]. Amyloid binds the dye CR and exhibits red-green birefringence when viewed in cross-polarized light (Figure

2.11 B). ThT is a benzothiazole dye that exhibits enhanced fluorescence upon binding to amyloid fibrils and is commonly used to diagnose amyloid fibrils, both *ex vivo* and *in vitro* [43].

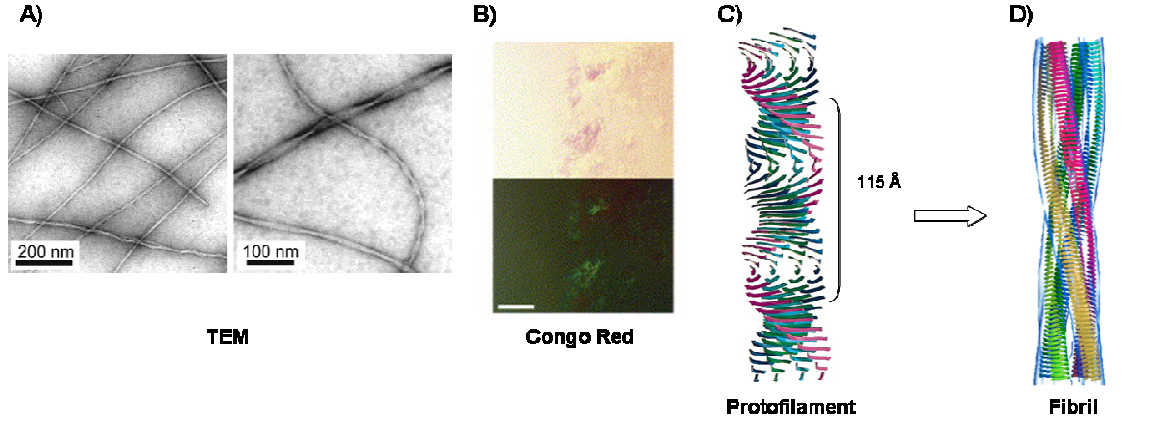


Figure 2.11. Amyloid fibrils and protofilaments. A) TEM images of Aβ40 fibrils [44]. B) Polarized microscopy images of fibrils stained with Congo red: top, bright field; bottom, dark field. The scale bar represents 100 μm [45]. C) Molecular model of a protofilament [38]. D) Model of insulin fibril with 4 protofilaments colored differently [46].

2.2.2. Amyloid Fibril Formation

Each amyloid disease involves predominantly the aggregation of a specific protein, although a range of other components including additional proteins and carbohydrates are incorporated into the deposits when they form *in vivo*. In many cases, molecular chaperones have been found associated with amyloid deposits, although the reason for this remains to be established [47]. The conversion of the structure of the native protein into a predominantly antiparallel β-sheet secondary structure is a pathological process closely related to physiological protein folding. Since the folding is reversible, a folded protein, when required or when subjected to stress (that causes disruptions of hydrogen bonding and hydrophobic interactions between some side chains), partially unfolds to its intermediately folded state(s), a process that can be exacerbated by mutations [48, 49].

When a protein enters the off-folding pathway, it can go into two different routes by which aggregation may occur, formation of disordered and amorphous aggregates or ordered amyloid fibrils. The route depends on the rate of unfolding and aggregation, the amino acid sequence and the nature of the formed species. A disordered aggregation mechanism results from the rapid unfolding and subsequent aggregation of intermediately folded proteins, in which individual monomers add to the growing clump of aggregated protein through a random process. This leads

to the formation of amorphous aggregates which eventually become so large that they form an insoluble precipitate. However, under normal circumstances in the cell, amorphous aggregation is often not of major concern because the cell has machinery and mechanisms (such as tagging of the protein with ubiquitin) to detect their formation and to dispose them into the proteasomal mechanism before they precipitate [48].

In contrast to the formation of amorphous aggregates, aggregation may occur more slowly through a highly ordered, nucleation-dependent mechanism in which partially folded forms of the protein associate to form a stable nucleus [49, 50]. This nucleus then acts as a template to sequester other intermediates to add to the growing thread of aggregated protein forming the protofibrils (that should not be confused with the protofilaments that are the constituent units of mature fibrils). The sequential addition of partially folded intermediates to the ends of the chain leads to the formation of a highly structured and insoluble amyloid fibril. The time course of the conversion of a peptide or protein into its fibrillar form typically includes (Figure 2.12):

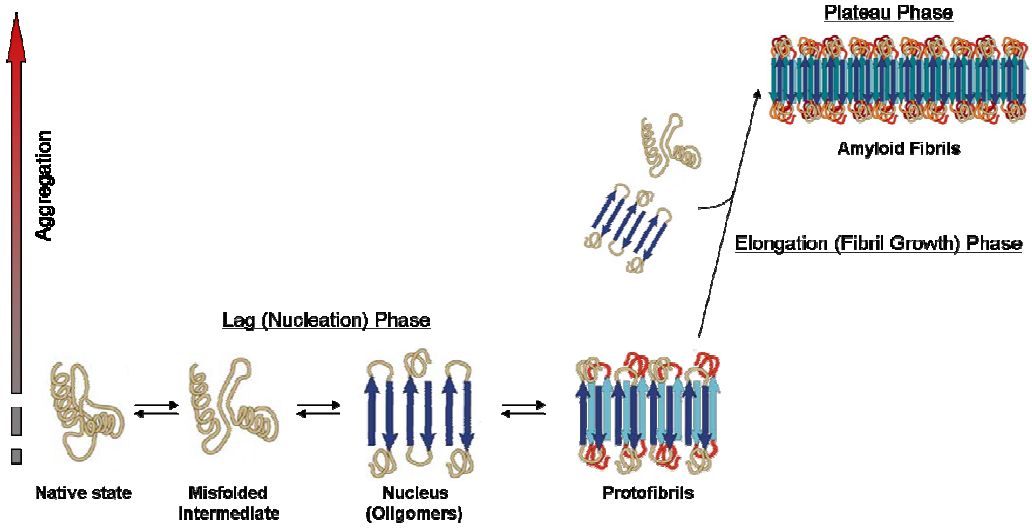


Figure 2.12. Representation of the amyloid forming pathway.

1. Lag phase: important event in which unfolding occurs and a variety of oligomers form, including β-sheet-rich species that provide nuclei for the formation of mature fibrils; the formation of this nucleus is a thermodynamically unfavorable process, and therefore the rate-limiting in the overall process of fibril formation.
2. Elongation phase: once a nucleus is formed, fibril growth is thought to proceed exponentially by addition of either monomers or oligomers to the growing nucleus.
3. Plateau phase: steady state when maximum fibril growth has been reached.

As with many other processes dependent on a nucleation step, including crystallization, addition of preformed fibrillar species to a sample of a protein under aggregation conditions ("seeding") causes the lag phase to be shortened and ultimately abolished when the rate of the aggregation process is no longer limited by the need for nucleation [51].

Although evolution has shaped the protein folding funnel (via changes in the amino acid sequence and the introduction of chaperones, for example) such that partially folded states which are prone to aggregate are only transiently formed, alterations to the protein sequence or a decrease in the effectiveness of the cellular protective mechanisms can dramatically affect the energy landscape, switching from a kinetically favored native, functional state towards the globally most stable structure, the amyloid fibril (Figure 2.13) [49].

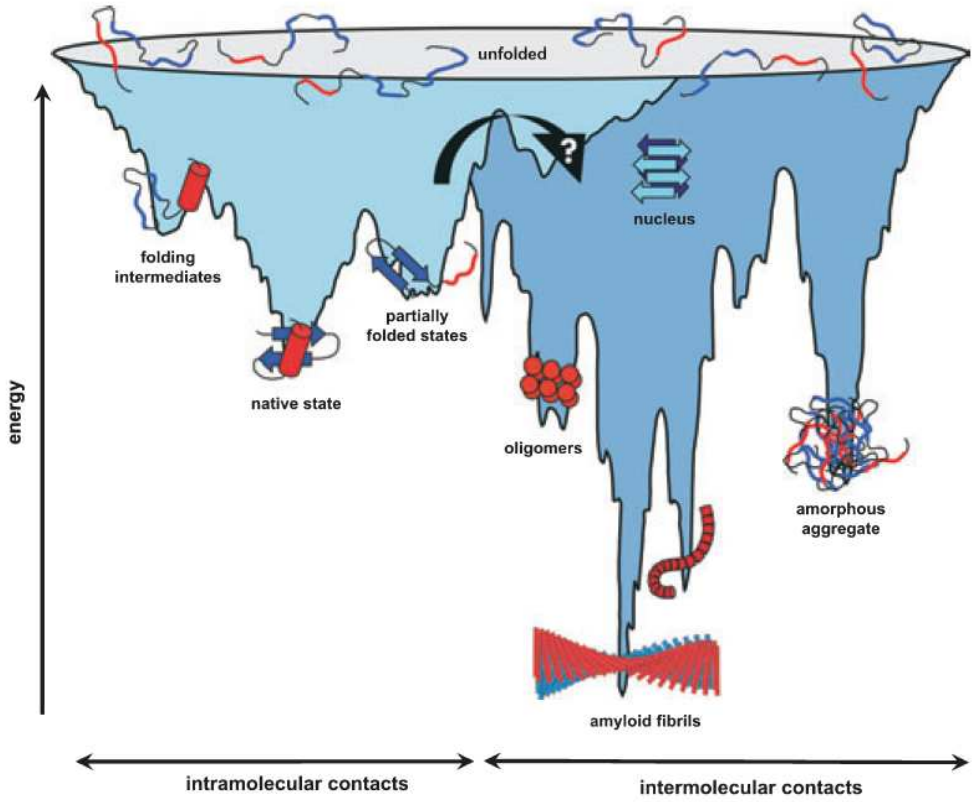


Figure 2.13. A schematic energy landscape for protein folding and aggregation. The surface shows the multitude of conformations 'funneling' towards the native state via intramolecular contact formation, or towards the formation of amyloid fibrils via intermolecular contacts (*from* [49]).

In recent years, a number of proteins that are not related to disease have been shown to form amyloid fibrils *in vitro* and it has been suggested that all proteins will form amyloid if exposed to the appropriate conditions [52, 53]. The generic fibrillar form of proteins can be regarded as dominated by hydrogen bonding between the amide and the carbonyl groups of the main chain,

rather than by specific interactions of the side chains that dictate the structure of globular functional proteins. Even though the ability to form amyloid fibrils seems to be generic, the propensity to do so under given circumstances can vary markedly between different sequences.

One important determinant of the aggregation of an unfolded polypeptide chain is the hydrophobicity of the side chains. Amino acid substitutions within regions of the sequence that play a crucial role in the behaviour of the whole sequence can reduce (or increase) the aggregation propensity of a sequence when they decrease (or increase) the hydrophobicity at the site of mutation [54, 55]. Another key factor in protein aggregation are charged residues, acting as structural gatekeepers by means of repulsive forces [56]. In addition to charge and hydrophobicity, a low propensity to form α-helical structure and a high propensity to form β-sheet structure are also likely to be important factors encouraging amyloid formation [57, 58]. In certain proteins as gelsolin, partial unfolding caused by mutation makes the protein susceptible to the attack of proteases, providing highly amyloidogenic polypeptides [59]. Another important facet of this topic is that chemical modifications, for example those induced by physiologically formed metabolites [60, 61], or interactions with small molecules or metal ions [62] may play a much more important role in the aggregation process than might be imagined, e.g., by perturbing the thermodynamics or kinetics sufficiently to alter the details of the resulting amyloid structure.

2.2.3 Pathogenesis of Amyloid Deposition

The presence of highly organized and stable fibrillar deposits in the organs of patients suffering from protein deposition diseases led initially to the postulate that this material is the causative agent of the various disorders. The deposition of large amounts of fibrillar material can subvert the tissue architecture and consequently cause organ dysfunction. Amyloid fibrils can also cause organ dysfunction by interacting with local receptors [63].

However, more recent findings have raised the possibility that precursors of amyloid fibrils, such as low molecular weight oligomers and/or structured protofibrils, are the real pathogenic species, at least in neuropathic diseases. It is increasingly evident that prefibrillar aggregates from several peptides and proteins can either be toxic to cells or perturb their function. In Aβ and transthyretin amyloidosis, soluble oligomeric intermediates of fibril assembly are cytotoxic *in vitro* [64-66] and *in vivo* [67]. Soluble fibril precursors are likely to mediate cellular toxicity through a mechanism that causes oxidative stress and activates the apoptotic pathway. According to this

hypothesis, mature fibrils are inactive protainaceous reservoirs in equilibrium with the smaller, putatively toxic assemblies [68].

Oligomer-mediated cytotoxicity is a key issue in neuropathic protein deposition diseases, although the question arises as to whether a similar mechanism is central in the pathogenesis of non neuropathic diseases. Systemic amyloidosis are often associated with accumulation of large quantities (kilograms in some cases) of amyloid deposits in the affected tissues and organs [50]. Undoubtedly, the impairment and disruption of tissue architecture, caused by these deposits in vital organs, are major features of these diseases and could well be the most important factors in the pathogenesis of at least some of these non neuropathic degenerative conditions. Patients can have mechanical problems in carrying out even routine everyday tasks [37, 50]. Examples include difficulties in swallowing when amyloid accumulation occurs in the tongue and in moving because of extreme pain when amyloid accumulation occurs in joints. The elucidation of the mechanism of tissue damage by amyloid fibril proteins is undoubtedly an important issue in therapeutic approaches, although the optimum strategy must be to prevent aggregation or even production of the amyloidogenic protein before it can generate any potential damaging deposits [30].

2.3. Alzheimer's Disease

Alzheimer´s Disease (AD) is the most common cause of dementia in the elderly, affecting more than 20 million people worldwide. The risk of AD dramatically increases in individuals beyond the age of 70 and it is predicted that the incidence of AD will increase threefold within the next 50 years (http://www.alz.org). AD was first described by the Bavarian psychiatrist Alois Alzheimer in 1907 [69]. The patient was a woman in her early 50s. At the time it was believed to be a rare presenile disorder and not the most common cause of senile dementia.

2.3.1. Histopathology of AD

The initial symptom of AD is typically impaired short term memory. Also language and spatial orientation can be affected at an early stage of the disease. *Post mortem* neuropathological examinations of AD patients brains reveal histopathological lesions in the brain and blood vessels, senile plaques and neurofibrillary tangles (NTF) (Figure 2.14), which still to this day are referred to as the pathological hallmarks of AD [69]. These plaques are abundant in the medial temporal lobe and cortical areas of the brain, as well as dead neurons. NTF´s are twisted helical cytoskeletons and contain fibrillar aggregates of the microtubule-associated protein tau that exhibit hyperphosphorylation and oxidative modifications [70, 71]. It is generally believed that Aβ precedes tau in the pathogenesis, i.e., Aβ causes the tau pathology [72].

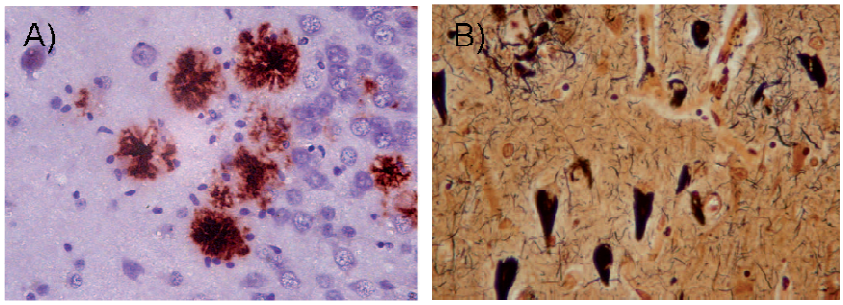


Figure 2.14. Histopathological lesions in AD. A) Senile plaques; B) Neurofibrillary tangles.

Because there can be other causes of memory loss, definitive diagnosis of AD requires *post mortem* examination of the brain, which must contain sufficient numbers of plaques and tangles to qualify as affected by AD [73, 74]. Brain regions involved in learning and memory processes,

including the temporal and frontal lobes, exhibit severe atrophy in AD patients as the result of degeneration of synapses and death of neurons (Figure 2.15) [75]. However, the best correlate of cognitive impairment appears to be loss of synapses, not cell death per se [76].

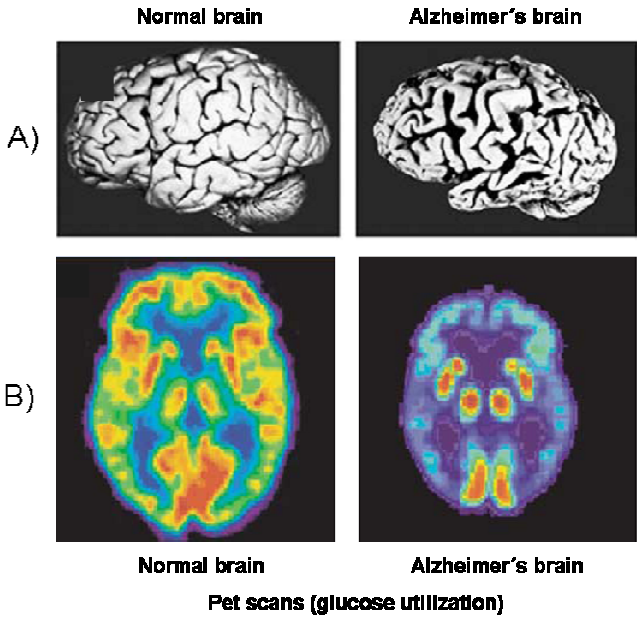


Figure 2.15. Alzheimer's disease results in shrinkage of brain regions involved in learning and memory which is correlated with major reductions in cellular energy metabolism in living patients. A) Compared with the brain of a healthy person, the brain of an Alzheimer's disease patient exhibits marked shrinkage of gyri in the temporal lobe (lower part of the brain) and frontal lobes (left part of the brain). B) Positron emission tomography (Pet) images showing glucose uptake (red and yellow indicate high levels of glucose uptake) in a living healthy person and a normal control subject. The Alzheimer's patient exhibits large decreases in energy metabolism in the frontal cortex (top of brain) and temporal lobes (sides of the brain) (*from* [75]).

2.3.2. The Amyloid Cascade Hypothesis

A large body of evidence from genetic and animal models has established a causative role of Aβ in the disease [35, 77-80]. In 1984, Glenner, a pioneer of amyloid studies, first isolated the previously undescribed protein that forms amyloid fibrils in Alzheimer's disease, expanding interest in amyloid by linking it to one of the commonest and most important human diseases [35]. He named this protein β-protein, reflecting his earlier original discovery of the cross β core structure of amyloid fibrils. The Alzheimer's deposits soon came to be called β-amyloid, the protein itself amyloid-β, and its precursor the amyloid precursor protein (APP). In AD brains, the peptide is found in a fibrillar form organized in a β-sheet structure, being the main constituent of the plaque deposits, extracellular deposits of fibrils and amorphous aggregates of Aβ [81]. The amyloid

cascade hypothesis was formulated almost 20 years ago and states that amyloid deposition of the Aβ peptide drives neurofibrillary tangle formation and various toxic events, which finally cause AD [77]. It has been the leading hypothesis in the field, but over the years it has also been challenged. Even though the hypothesis is built around Aβ as the central mediator of AD pathology, some modifications have been proposed in recent years. This is due to the emerging evidence for the pathological role of soluble oligomeric Aβ [64, 65, 67], preceding plaque formation, and the role of intracellular Aβ [82], and will be discussed more in detail below.

Another hypothesis has been postulated to explain the molecular mechanism of AD, the cholinergic hypothesis. The cholinergic hypothesis is supported by many studies, showing that a dysfunctional cholinergic system is sufficient to produce memory deficit in animal models that are analogous to Alzheimer's dementia [83]. Brains from AD patients show degeneration of cholinergic neurons of the basal forebrain [84]. A marked decline in cholinergic markers, choline acetyltransferase and acetyl cholinesterase has been reported in the cerebral cortex of AD brain [85]. Although cholinergic deficits cannot fully account for the overall neuropathological features observed in AD, it represents a significant part of AD etiology.

2.3.3. Metabolism of Aβ and AD

Aβ is a 4 kDa amphiphilic peptide of 39 to 43 amino acid residues long, generated by specific endoproteolytic cleavages of the APP, a ubiquitous glycosylated transmembrane protein [86], encoded by a gene localized in chromosome 21. Aβ is present at very low concentrations ($<10^{-8}$ M) in biological fluids and its physiological role is unknown [87].

APP is an integral membrane protein with a single membrane-spanning domain, a large extracellular glycosylated N-terminus and a shorter cytoplasmatic C-terminus. The Aβ sequence is located at the cell surface (or on the lumenal side of ER and Golgi membranes), with part of the peptide embedded in the membrane. APP is produced in several different isoforms ranging in size from 695 to 770 amino acids, and the shorter APP695 is the most abundant form in brain [88].

Enzyme activities involved in cleavage of APP at the α-, β- and γ-secretase sites have been identified. Several zinc metalloproteinases and the aspartyl protease BACE2 can cleave the APP at the α-secretase site, releasing secreted APPα from the cell surface and leaves an 83-amino-acid carboxy-terminal APP fragment (C83), avoiding the generation of intact Aβ (Figure 2.16 A) [89]. Physiological roles for sAPPα are supported by data showing that sAPPα is released from presynaptic terminals in response to electrical activity. sAPPα regulates neuronal excitability and

enhances synaptic plasticity, learning and memory, possibly by activating a cell surface receptor that modulates the activity of potassium channels and/or activating a transcription factor [75].

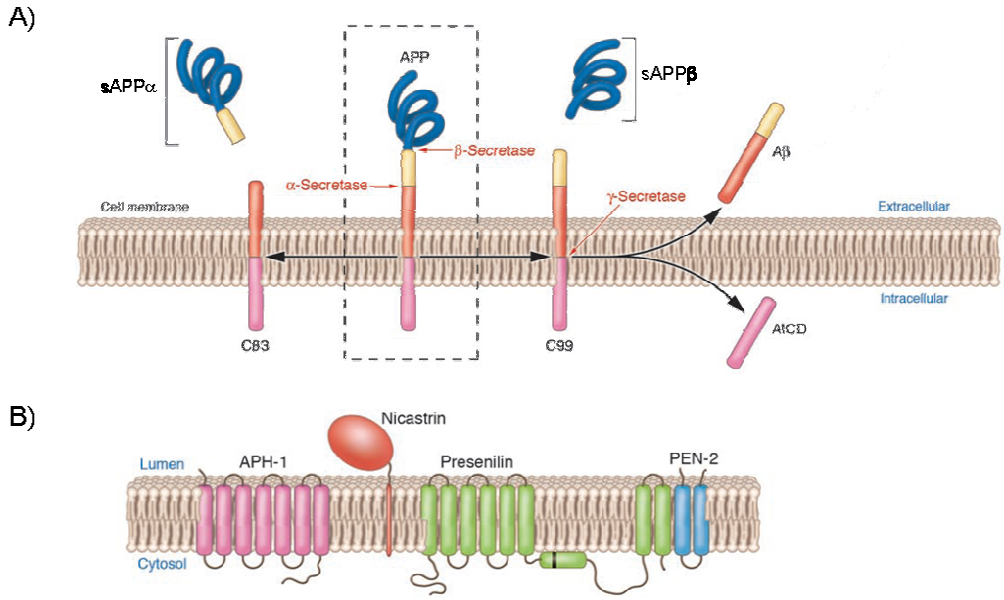


Figure 2.16. Proteolytic processing of APP. A) APP processing and Aβ accumulation. Mature APP (inside dashed box) is metabolized by 2 competing pathways, the α-secretase pathway that generates sAPPα and C83 (left) and the β-secretase pathway that generates sAPPβ and C99 (right). All carboxyterminal fragments (C83, C99) are substrates to γ-secretase, generating the AICD and the secreted peptides. B) Topology of the 4 components that comprise the γ-secretase complex. (*adapted from* [94]).

Amyloidogenic processing of APP involves sequential cleavages by β-secretase and γ-secretase at the N and C termini of Aβ, respectively (Figure 2.16 A). BACE1 (β-site APP-cleaving enzyme 1), a transmembranar aspartyl protease, is the major neuronal β-secretase and cleaves APP in the N-terminus, releasing secreted APPβ and the 99-amino-acid C-terminal fragment of APP (C99) [90]. γ-secretase, which cleaves APP within a transmembrane region, involves four essential subunits: presenilin-1 (PS1) or -2 (PS2), nicastrin, APH-1 and PEN-2 (Figure 2.16 B) [91]. γ-Secretase cleaves at multiple sites within the transmembrane domain of APP, generating Aβ peptides ranging in length from 38 to 43 residues [92]. Nearly 90% of secreted Aβ ends in residue 40, whereas Aβ42 accounts for less than 10% of secreted Aβ. Familial AD-linked mutations in APP just away from the C terminus of the Aβ domain increase Aβ42 production. Intriguingly, familial AD-linked mutations in PS1 and PS2 influence γ-secretase cleavage by mechanisms that generally favor cleavage at position 42 relative to that at position 40, thus increasing the Aβ42/40 ratio [92]. Cleavage of C99 by γ-secretase releases an APP intracellular domain (AICD) that can be translocated to the nucleus where it may regulate gene expression, including the induction of apoptotic genes (Figure 2.17 A) [75].

Cleavage of APP/C99 by caspases produces a neurotoxic peptide (C31). The C99 generated by BACE1 cleavage can also be internalized and further processed by γ-secretase to produce Aβ40/42 in endocytic compartments. Evidences from a number of studies indicate that amyloidogenic processing occurs in cholesterol- and sphingolipid-enriched membrane raft microdomains of intracellular organelles [93].

The normal functions of APP are not fully understood, but increasing evidence suggests it has important biological activities that affect neuronal development and function [88, 93]. A number of functional domains have since been mapped to the extra- and intracellular regions of APP. APP is transported along axons to presynaptic terminals where it accumulates at relatively high levels, which can result in Aβ deposition at synapses. One possible function of full-length APP is as a cell surface receptor that transduces signals within the cell in response to an extracellular ligand. However, neither a ligand nor downstream signaling cascades for APP have been clearly established [88]. In all, a trophic role for APP has been perhaps the most consistently and arguably the best established function for the molecule and APP has been shown to stimulate neurite outgrowth from a variety of settings [93].

As described, in normal conditions of APP processing the most common isoforms are 40 and 42 residues long, named Aβ40 and Aβ42, which differ by the number of residues at the C-terminus (Figure 2.17). The N-terminus is rich in charged residues and there are two stretches of hydrophobic residues, (Leu17-Ala21) and (Ala30-Ala42) believed to be the key for oligomerization, separated by a region containing 2 acidic residues (Glu22 and Asp23) [95-97]. Within the naturally occurring alloforms, substitutions are usually in or nearby the central hydrophobic cluster (CHC). In each instance, disease has variation in onset, symptoms and degree of fibrillation [98, 99]. Despite the small structural difference between the two peptides, they display distinct clinical, biological and biophysical behaviour. Although under normal conditions of APP processing Aβ40 is about 10 times more abundant, usually Aβ42 is the predominant species found in neuritic plaques [100, 101]. More, Aβ42 has been shown to aggregate and form fibrils more rapidly than Aβ40 [102, 103] and to have enhanced neurotoxicity [104-106].

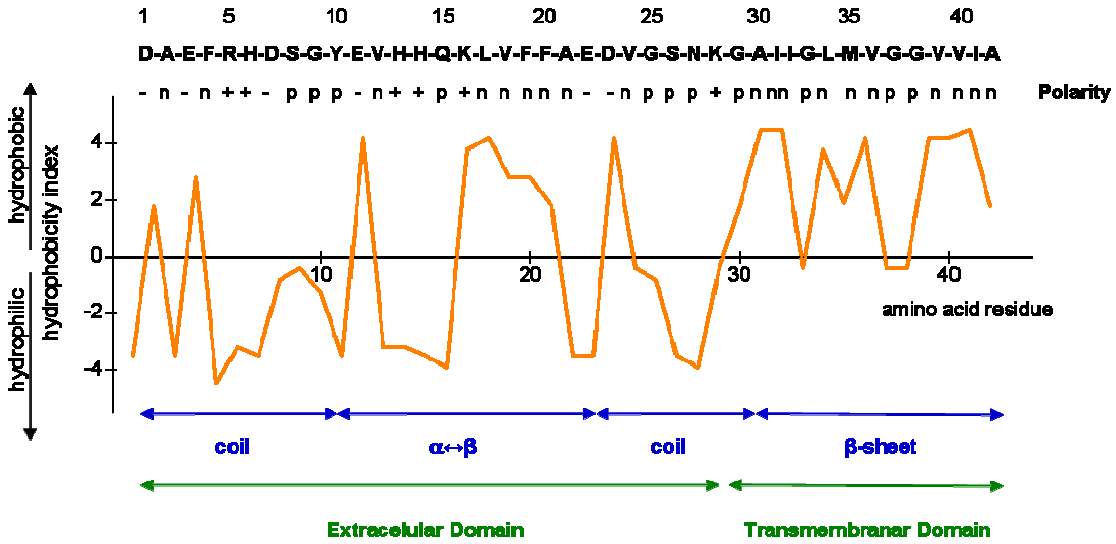


Figure 2.17. Primary sequence of Aβ42, polarity of its amino acid residues and secondary structures prediction [107]. The hydrophilic N-terminus is rich in charged residues and derives from the extracellular domain of APP, whereas the C-terminus is a transmembranar segment, essentially non polar and hydrophobic. The course of hydrophilic and hydrophobic nature within the sequence is shown by the plot of the hydrophobicity index according to Kyte and Doolittle [108] - more positive value indicate stronger hydrophobicity; hydrophilic amino acids have negative values. The polarity refers to pH 7 (n – non polar and p – polar).

The cause-and-effect relationship between Aβ accumulation and AD development has been strongly supported by the consistent increased Aβ (particularly Aβ42) production phenotypes of early-onset familial AD-causing gene mutations. Three genes are associated with early onset familial AD: APP, PS1 and PS2, observed in both *in vitro* and *in vivo* (Figure 2.18) [68, 70, 88, 109, 110]. Once the amino acid sequence of Aβ was determined, the gene encoding APP was cloned and localized to chromosome 21. DNA samples from pedigrees in which dominantly inherited AD occurred were then screened for mutations in APP, and several causative mutations were found. All mutations are located closely to the cleavage sites of either β-secretase or γ-secretase (Figure 2.18) [70]. All the APP mutations lead to the production of more Aβ42 or to a change in the aggregation properties of Aβ, thereby predisposing to the development of AD [80]. APP gene duplication alone also causes early-onset AD with cerebral amyloid angiopathy. This agrees with the finding of AD changes in individuals with Down syndrome (trisomy 21), in which the APP gene is triplicated [93]. Although mutations in APP gene are found only in rare cases of AD, they are important for providing definite evidence that APP and Aβ play a central role in AD pathogenesis. Subsequent linkage analysis identified a region of chromosome 14 as the locus of a mutation(s) responsible for inherited AD in several different pedigrees, and the PS1 gene was identified as the affected gene.

Mutations in a gene on chromosome 1 with high homology to PS1, now called PS2, were then shown to cause a few cases of inherited AD. PS1 mutations account for most of the reported familial AD (FAD) cases and generally lead to an onset of AD before the age of 50 [70]. In contrast to PS1 mutations, mutations in PS2 are relatively rare.

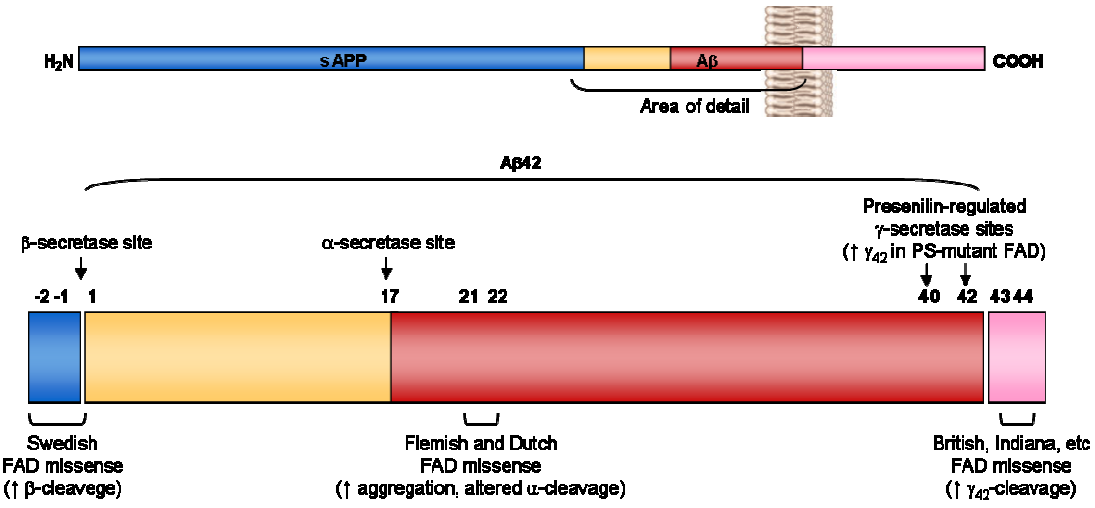


Figure 2.18. Structure of APP around the Aβ domain, secretase cleavage sites, and location of some familial AD missense mutations.

The steady-state Aβ levels in the brain are determined by the metabolic balance between anabolic and catabolic activities [87, 111, 112]. Subtle alterations in this metabolic balance over a long period of time could result in the appearance of pathogenic forms of Aβ, influencing both the pathological progression and the incidence of the disease. For instance, just a 1.5-fold increase in Aβ42, caused by most of the above mutations, results in aggressive pre-senile Aβ pathology [111]. Therefore, in order to overcome AD, it is necessary to lower the Aβ levels in the brain, and several therapeutic strategies, such as inhibition of production, promotion of degradation, inhibition of aggregation, and clearance of deposits, have been proposed [68, 113]. In sporadic AD brains, where the elevation of anabolic activity seems to be rarely observed, a reduction in the catabolic activity towards Aβ involving Aβ-degrading enzymes such as neprilysin has been a candidate cause for Aβ accumulation associated with late-onset AD development. Either the up-regulation of the catabolic activity or down-regulation of the anabolic activity should prevent or reduce Aβ deposition and thus be applicable to the prevention and therapy of AD (Figure 2.19) [68].

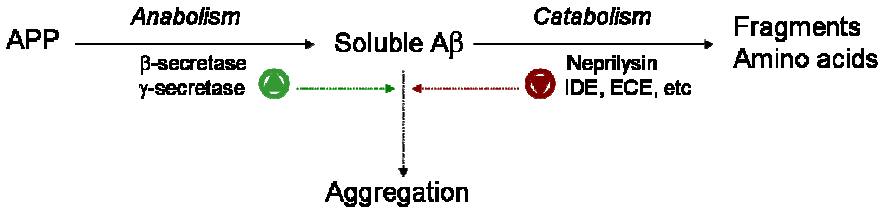


Figure 2.19. Metabolism of Aβ. Either the up-regulation of anabolism or the down-regulation of catabolism accelerates aggregation through increasing the steady-state levels of Aβ. IDE = insulin-degrading enzyme; ECE = endothelin-converting enzyme.

The vast majority of cases of AD are sporadic but molecular genetic analyses suggest that there are likely to be many genes that influence one's susceptibility to AD. The first such susceptibility gene identified was apolipoprotein E for which there are three alleles that encode three different isoforms of apolipoprotein E (ε2, ε3 and ε4). Individuals that produce the ε4 isoform are at increased risk of AD whereas the ε2 allele appears to be protective. The mechanism whereby ε4 promotes AD is not established, but there is evidence that ε4 enhances Aβ aggregation and reduces Aβ clearance. In addition, data suggest that ε4 might increase the risk of AD by enhancing amyloidogenic processing of APP [75]. As with other age-related diseases (cardiovascular disease, diabetes, cancers, and so on), there are likely to be behavioural, dietary and other environmental factors that may affect the risk of AD. However, this area of research has not yet matured to a point where clear recommendations can be made.

Although extracellular Aβ can cause neurotoxicity both *in vitro* and *in vivo* [64, 65, 67, 68], accumulating evidences support the view that intracellular Aβ triggers the initiation of AD [82, 114]. Although intracellular Aβ has been known to localize in compartmental cellular organelles such as ER, endosome, and lysosomal network, it has been observed in the cytoplasm of the brains of AD patients [82] as well as AD transgenic mouse [115]. Furthermore, it has been demonstrated that cytosolic Aβ can induce apoptosis in cultured neuron cells [114].

2.3.4. Aβ Oligomerization and Fibrillation

Early studies clearly demonstrated that aggregation of Aβ was essential for toxicity, but characterization of the assemblies that formed *in vitro* was limited, and it was assumed that since amyloid fibrils were detectable, these assemblies mediated the observed toxicity. Recent debate has focused on whether amyloid fibrils or soluble oligomers of Aβ are the main neurotoxic species that contribute to neurodegeneration and dementia [68, 116]. The most frequent objection is the weak

correlation between the number of amyloid deposits detected by neuropathological analysis of *post mortem* brains and the degree of cognitive impairment experienced by the patients in life [117]. Since soluble Aβ levels, both intracellular and extracellular, correlate better with the severity of AD than insoluble Aβ [118], there is growing evidence that one or more of the soluble oligomeric forms of Aβ may be a critical component in AD pathology rather than the insoluble fibrils. Here, the term "soluble Aβ" loosely any form of Aβ that is soluble in aqueous buffer and remains in solution following high speed centrifugation. High molecular-weight (oligomeric) soluble Aβ is greatly increased in AD brains as assessed by molecular sieving and centrifugation [119]. It has been shown that soluble oligomers of Aβ, but not monomers or insoluble fibrils, may be responsible for synaptic dysfunction in the brains of AD patients and in AD animal models. The so-called Aβ-derived diffusible ligands (ADDLs) [64] or protofibrils [65] cause subtle injury to cultured neurons. Injection in rats of Aβ oligomers can inhibit long-term potentiation (LTP) in the hippocampus, which is required for memory formation [67]. Measurements with two different oligomer-specific antibodies suggest increased levels of oligomer immunoreactivity in AD brain lysates compared to controls [120, 121].

Soluble oligomers have been implicated in other amyloid-associated neurodegenerative diseases, such as Parkinson´s disease [122] and Huntington´s disease [123], thus suggesting that oligomeric species formed early in the aggregation process may be a common mediator of the earliest symptoms of disease. It was suggested that these oligomeric structures induce toxicity through a mechanism related to the folded structure rather than sequence [106, 124]. Further evidence for related toxic structures was obtained when antibodies specific to Aβ oligomers were shown to inhibit toxicity not only of Aβ oligomers, but several other protein oligomers as well [120]. Some researchers even propose that plaques are inert end products, possibly protecting the brain from the toxic soluble Aβ species. As schematized in Figure 2.20, the hypothesis today states that increased Aβ production caused by mutation or other factors such as faulty Aβ clearance lead to Aβ oligomerization and deposition which eventually results in the pathogenic events associated with AD, such as neuronal/synaptic dysfunction, resulting in dementia.

Several *in vitro* formed Aβ oligomers have been described in the literature, with protofibrils and ADDLs being the best characterized. Aβ protofibrils have been described as curvy structures with a diameter of 4-10 nm, a length of up to 200 nm [125, 126] and a beaded appearance with a periodicity of 3-6 nm [127]. ADDLs are small soluble globular Aβ oligomers, ranging in size from trimers to 24-mers [128]. These oligomers have been detected in brain homogenates from AD patients, using an ADDL specific antibody [121]. The structural features of these oligomeric species are still not fully elucidated though.

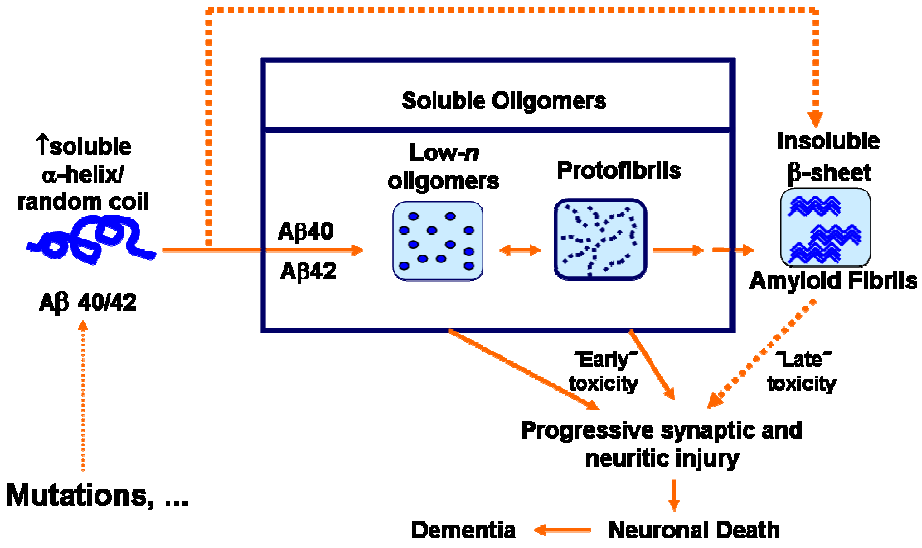


Figure 2.20. Mechanism of AD according to the updated amyloid hypothesis where oligomeric species of Aβ are the main neurotoxic species contributing to neurodegeneration and dementia.

Aβ assembly is an example of the general class of nucleation-dependent aggregation, comprising a slow nucleation step, producing a "lag phase" during assembly, followed by a rapid fibril elongation step (Figure 2.12). It has been demonstrated that the CHC in the Leu17-Ala21 region is essential for the aggregation of Aβ peptides [129-132]. A large number of studies suggest that a Asp23-Lys28 loop region connected to the CHC and the second hydrophobic domain in the C-terminus is involved in Aβ fibril growth. In structure-activity investigations on Aβ(25-35) and Aβ42, the turn in the Val24-Trp27 region and the second hydrophobic domain were reported to be necessary for aggregation [133]. Furthermore, circular dichroism (CD) and NMR (1H, 15N, and 13C) measurements showed that the oxidation of the Met35 side chain to methionine sulfoxide (Met35(O)) diminishes the tendency of both WT-Aβ40 and WT-Aβ42 to aggregate [134, 135]. These results explicitly indicate that these three distinct regions may be involved in the aggregation. Other NMR experiments show that Aβ oligomers are stabilized in the in-register parallel arrangement of the molecules, presumably with all hydrophobic C-terminus tails clustered together [132]. Moreover, Aβ oligomerization is highly pH dependent. Precipitation and amyloid formation are most efficient at pH 5, near the pI of the peptide [43]. Guo *et* al. have shown that formation of favorable charge-charge interactions is not essential for Aβ oligomerization, demonstrating that other classes of stabilizing interactions; namely, hydrophobic interactions and hydrogen bonds, are chiefly responsible for stabilizing Aβ oligomers relative to monomers [136]. These interactions must overcome the unfavorable entropy changes that accompany oligomerization [9].

Fundamental characteristics of the Aβ sequence, which displays β-extended chain structure propensity in the regions 17-21 and 31-36 even as a soluble monomer, might influence the aggregation [135]. Certain localized peptide regions are predisposed towards β-strand and bend-like structures and it has been proposed that monomeric Aβ exists in solution as a metastable loop-like structure in which each monomer contains an antiparallel β-sheet [103]. Tycko and co-workers proposed a structural model based on solid-state NMR of Aβ40 fibrils formed from solution [131, 137]. In this model, the protofilament contacts between β-sheet layers are side chain-side chain interactions along the hydrophobic faces created by side chains of the C-terminal segment and the CHC. The N-terminal residues are expected to be in random conformations. The core of the protofilament is hydrophobic with the exception of the oppositely charged side chains of Asp23 and Lys28, which form salt bridges [44]. There is a structural polymorphism in Aβ fibrils prepared under identical conditions (concentration, pH, ionic strength, buffer composition, and temperature). Agitation of an unseeded, initially monomeric Aβ40 solution during fibril growth produces the striated ribbon morphology, whereas quiescent conditions produce twisted morphologies (Figure 2.21).

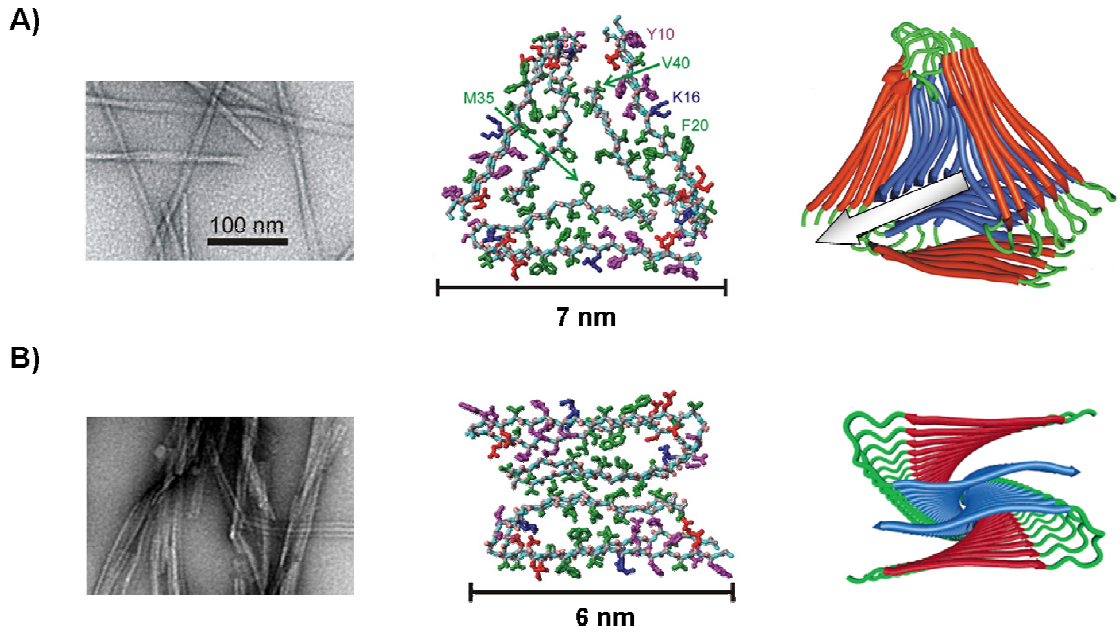


Figure 2.21. TEM and NMR based structural models of Aβ40 protofilaments. TEM images, ribbon representations and atomic representation where hydrophobic, polar, negatively-charged, and positively charged amino acid side chains are green, magenta, red, and blue, respectively; backbone nitrogen and carbonyl oxygen atoms are cyan and pink and unstructured N-terminal residues 1–8 are omitted (*adapted from* [131, 137]). A) Fibrils with twisted morphology. B) Fibrils with striated morphology.

The predominant morphology may be influenced by a variety of competing factors, including rates of spontaneous nucleation, fibril extension, and fibril fragmentation [137]. Agitation may influence both nucleation and fragmentation. Amyloid fibrils with twisted morphologies in negatively stained TEM images (similar to Figure 2.21 A) are formed by many other polypeptides, including amylin, insulin, and mammalian prion proteins. So the model may represent a general structural motif for a class of fibrils with similar morphologies.

2.3.5. Mechanisms of Aβ Toxicity

Aβ induces neurotoxic effects via extracellular and intracellular ways due to the ability to impair fundamental cellular processes. Studies based on the level of Ca^{2+} and cell death mechanism have suggested that the toxicity of misfolded and aggregated states of different proteins, such as Aβ peptide, proceeds through the modification of the same specific biochemical properties and such modification depends on the type of aggregates rather than on the specific amino acid sequences [124].

morphology.

What is the relationship between Aβ assembly and AD? Low-*n* Aβ oligomers appear to be particularly important because they are potent neurotoxins and are isolable from AD patients, and their concentrations correlate positively with neuropathology *in vivo*. There are several reports on Aβ dimers occurring *in vivo*. Schmechel *et* al. demonstrated for the first time that a biochemically defined assembly of Aβ into dimers probably represents the initial step in amyloidogenesis [138]. The presence of Aβ dimers in the cortex has been suggested to initiate the accumulation of Aβ in the human brain [139], and dimeric Aβ is proposed to initiate aggregation by accumulation in lipid rafts [140]. Nonfibrillar SDS-stable dimers have been characterized as neurotoxic derivatives [64] and selectively blocked hippocampal LTP in the absence of monomers, protofibrils, or fibrils [67]. Cleary et al. provided experimental evidence that defined molecular species of the Aβ interfere with cognitive function [141]. Aβ oligomers were remarkably potent at concentrations of amyloid-β monomer in the conditioned medium that are similar to those found in human cerebrospinal fluid (CSF). These effects are characterized by rapid onset, high potency and transiency. This demonstration that cognitive deficits are directly attributable to low amounts of naturally assembled Aβ oligomers indicates that trimers may be particularly active.

2.3.5.1. Membrane Effects

The most obvious target that is accessible to both the cytosolic and the extracellular compartments is the plasma membrane that forms the interface between the two compartments. It is naturally conceivable that Aβ interacts with membranes because it is an enzymatic product of a transmembrane protein, APP. Moreover, Aβ is an amphipatic peptide and structures as these can form micelles or interact with membranes directly. Membranes can affect soluble proteins and peptides through a variety of ways: electrostatic interactions between amino acids and charged headgroups, new partially folded or unfolded free energy minima at the surface, increased aggregation due to a faster diffusion over a 2D surface and a lower surface pH due to anionic lipid headgroups [142].

A growing body of evidence suggests that membrane permeabilization by oligomers may represent the common, primary mechanism of pathogenesis of amyloid related degenerative diseases [143]. Membrane insertion can perturb plasma membrane structure and function and it has been shown that Aβ40 inserts into membranes of hippocampal neurons from AD brains [144]. Aβ oligomers have also been shown to increase the conductance of lipid bilayers and living cell membranes by lowering the "dielectric barrier", possibly by increasing the membrane dielectric constant, introducing localized structural defects, or thinning the membrane (thereby facilitating charge translocation across the bilayer) [145]. These effects may be related to oligomer-induced release of membrane components, including cholesterol, phospholipids and monosialogangliosides, which in turn may lead to tau hyperphosphorylation and neurodegeneration [146]. Structured membrane reorganization may also occur, since Aβ40 forms cation-sensitive ion channels in neuronal plasma membranes and liposomes [144, 146]. It is worth to be aware that two general classes of Aβ/membrane interactions may occur: (i) non-receptor mediated as discussed above and (ii) specific receptor-mediated interactions.

2.3.5.2. Metals

Evidences exist that metals are involved in the pathogenesis of AD. Metals have been detected around amyloid plaques in AD brain, and it has been proposed that aggregation of Aβ is mediated by interaction with metals, in particular Zn, Cu and Fe [62]. Two distinct ways in which the metal ion can bind the peptide have been suggested, generically termed as inter- and intra-molecular modes [147]. Different structural models for each of the two binding modes have been proposed in which

different numbers of His residues are involved in the metal coordination. With a combination of complementary experimental techniques, the atomic structure around the metal binding site of Aβ peptides complexed with either Cu^{2+} or Zn^{2+} has been determined, and it has been observed that Cu^{2+} binds to three His, whereas Zn^{2+} is complexed to four His. Lacking a fourth His in the Aβ sequence, this geometrical arrangement leads to Zn^{2+} promoted inter-peptide aggregation [148]. These results are in agreement with the hypothesis that assigns different physiological roles to the two metals, with Zn favoring peptide aggregation.

2.3.5.3. Oxidative Stress

Oxidative stress is a major feature in the pathophysiology of AD and it occurs when generation of free radicals during normal metabolic processes in the cell overpowers the anti-oxidative defense system. Due to the presence of unpaired electrons, ROS are very unstable and highly reactive radicals. If not removed or neutralized, they react with lipids, proteins, and nucleic acids and damage cellular functions. Cells in the brains of AD patients exhibit abnormally high amounts of oxidatively modified proteins, lipids and DNA [149]. Several sources of oxidative stress have been proposed. Metals may also contribute to the oxidative insults observed in AD-affected brains. Aβ has a strong positive formal reduction potential and displays high affinity binding for Cu^{2+}, Zn^{2+} and Fe^{3+} ions [150]. Aβ/Cu(Fe) complexes are capable of generating ROS which mediate toxicity. The generated peroxide may degrade forming a highly reactive hydroxyl radical (ROS) via Fenton chemistry or a Haber-Weiss reaction as outlined below:

$$A\beta + M^{(n+1)+} \rightarrow A\beta^{\bullet} + M^{n+} \qquad \text{(reduction of the metal ion)}$$

$$M^{n+} + O_2 \rightarrow M^{n+1} + O_2^{-}$$

$$O_2^{-} + O_2^{-} + 2H^{+} \rightarrow H_2O_2 + O_2 \qquad \text{(production of } H_2O_2\text{)}$$

$$M^{n+} + H_2O_2 \rightarrow M^{(n+1)+} + OH^{\bullet} + OH^{-} \qquad \text{(Fenton chemistry)}$$

$$O_2^{-} + H_2O_2 \rightarrow OH^{\bullet} + OH^{-} + O_2 \qquad \text{(Haber-Weiss reaction)}$$

Aβ generation of ROS requires reduction of metal ions (Cu or Fe) thus inducing oxidation of another moiety. Mass spectrometry has shown that Cu^{2+} ions are able to oxygenate Aβ with the most likely candidate being the sulphur atom of Met35 [135, 146, 147, 150]. It has been proposed

that Met35 serves as a source of electrons for the reduction of $O_2 \rightarrow H_2O_2$ and brain tissue from AD patients contains deposits of oxidized Aβ [151].

When Aβ aggregation occurs at the cell membrane, membrane-associated oxidative stress results in lipid peroxidation and the subsequent generation of 4-hydroxynonenal (4HNE), a neurotoxic aldehyde that covalently modifies proteins on Cys, Lys and His residues (Figure 2.22). Some of the proteins oxidatively modified by this Aβ-induced oxidative stress include membrane transporters (ATPases, a glucose transporter and a glutamate transporter), receptors, GTP-binding proteins and ion channels. Oxidative modifications of tau by 4HNE and other reactive oxygen species can promote its aggregation and may thereby induce the formation of neurofibrillary tangles. By disturbing cellular ion homeostasis and energy metabolism, relatively low levels of membrane-associated oxidative stress can turn neurons vulnerable to excitotoxicity and apoptosis [75].

A relevant role is played by mitochondria where cell energy is produced. ROS are minor cytotoxic products of normal mitochondrial metabolism. Mitochondrial dysfunction has been linked directly to the aging process, the larger single risk factor for AD, and may lead to cell death. Exacerbation of age-related dysfunction by toxic Aβ assemblies may explain the linkage between both age and Aβ and AD [146]. Aβ oligomers may directly permeabilize the mitochondrial membrane, and the increase in energy demand to maintain ion homeostasis and membrane polarization may also be a source of mitochondrial stress (Figure 2.22). Mitochondrial oxidative stress resulting in impairment of the electron transport chain, increased production of superoxide anion radicals and decreased production of ATP. Superoxide is converted to H_2O_2 by the activity of superoxide dismutases (SOD), and superoxide can also interact with nitric oxide (NO) via nitric oxide synthase (NOS) to produce peroxynitrite ($ONOO^{\bullet}$). Interaction of H_2O_2 with Fe^{2+} or Cu^{+} generates the hydroxyl radical ($OH^{\bullet}$), a potent inducer of membrane-associated oxidative stress that contributes to the dysfunction of the ER (Figure 2.23) [75, 150]. Moreover, mitochondrial dysfunction may also feed back to upstream pathways that regulate the level of misfolded proteins because many chaperones and the proteasome system utilize ATP.

2.3.5.4. Calcium Homeostasis

Many signaling pathways are regulated directly or indirectly by intracellular Ca^{2+} levels or membrane depolarization, including pathways leading to up-regulation of autophagy and cell death. The inability of neurons to regulate calcium homeostasis is an aspect of AD pathogenesis

that appears to be intimately involved in the dysfunction and death of neurons. Extracellular applications of oligomers from several amyloidogenic proteins and peptides cause a rapid and large increase in cytosolic free calcium, whereas equivalent amounts of soluble monomer and fibrils have no detectable effect [124]. The Ca^{2+} influx is not blocked by cobalt, indicating that the effect is not due to activation of existing Ca^{2+} channels. Oligomer treatment of cells results in increased cytosolic Ca^{2+} in Ca^{2+}-free medium; this increase can be largely eliminated by pre-treatment to deplete ER calcium [124]. This suggests that external application of oligomers leads to liberation of Ca^{2+} from intracellular supplies.

Aβ may perturb calcium regulation by inducing oxidative stress, which impairs membrane calcium pumps and enhances calcium influx through voltage-dependent channels and ionotropic glutamate receptors (Figure 2.22). Other findings suggest that Aβ can promote Ca^{2+} influx by forming channels in membranes or by activating cell surface receptors coupled to calcium influx [152].

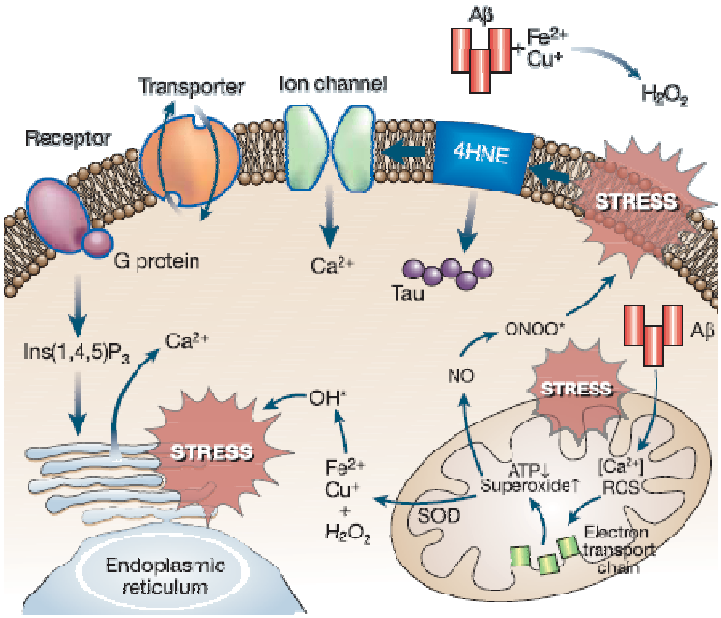


Figure 2.22. The neurotoxic action of Aβ involves generation of ROS and disruption of cellular calcium homeostasis. (*from* [75]).

2.3.5.5. Apoptosis

As mentioned earlier, the involved death pathway must have the ability to be induced both from the extracellular or the intracellular environment. Apoptosis is a well known cell death mechanism that answers to this request and neurodegeneration has been often associated with apoptosis. This mechanism controls the normal homeostasis of cell population in normal development and inflammation through programmed cell death involving changes in the cytoplasm, ER, mitochondria and nucleus. Failed control of cell number through apoptosis is common in cancer; on the contrary, excessive apoptosis is considered to play a role in different neurological disorders, including AD, stroke, and PD. Proteolytic enzymes of the caspase family play a central role in initiating and sustaining the event resulting in apoptotic cell death. In some forms of apoptosis, the extrinsic apoptotic pathway is initiated by activation of caspase-8 after death receptor ligation is presented on the cell membrane; in other instances, activation of the intrinsic apoptotic pathway is initiated by signalling molecules recruited by mitochondria that lead to cytochrome *c* release from mitochondrial matrix to cytoplasm and activation of caspase-9 [153]. Both these pathways are able to activate the executioner caspase-3 involved in the death process.

Apoptosis is a common final pathway of Aβ-induced neuronal dysfunction and it is particularly likely to occur following mitochondrial malfunction. Evidences suggest links between deposition of Aβ, oxidative stress, and apoptosis associated with AD [154] and Aβ has been shown to induce apoptosis in neurons, which may contribute to neuronal degeneration in AD [155]. Brain tissue from AD patients contains deposits of oxidized Aβ [151] and activated caspase-3 [156]. Apoptosis is considered a mechanism involved in neurodegenerative diseases, because it is selective at the individual cell level. In AD, neuronal loss is prominent in the cerebral cortex and limbic lobe, while different neuronal population is vulnerable in other neurodegenerative disease.

Some experimental studies suggest that Aβ can activate caspases through the extrinsic pathway, by binding of extracellular Aβ to receptors, while other studies suggest that the intrinsic pathway that involves ER or mitochondrial stress may be more relevant suggesting an intracellular role in neurodegeneration [157, 158]. Due to its structure, Aβ is able to bind a variety of biomolecules, including lipids, proteins, and proteoglycans. It has been suggested that Aβ secreted into the extracellular fluid never leaves the membrane lipid bilayer; fibrillation modifies its electric properties and alters ion channels which could allow lethal concentration of Ca^{2+} to enter into the cell and induce apoptosis [152]. Moreover, a subset of membrane proteins such as SEC-R (serpin-enzyme complex), integrins, RAGE (receptor for advanced glycosylation end-product), the α7nAChR (α7nicotinic acetylcholine receptor), the insulin receptor, and APP are able to bind monomeric

and/or fibrillar forms of Aβ. Perturbation of their functions could induce degenerative pathways [144]. Accumulation of Ca^{2+} in the matrix of mitochondria leads to an increase in ROS production, cytochrome *C* release and apoptosis [157]. Some mechanisms appear to contribute to apoptosis in response to ER stress (and release of Ca^{2+}) such as activation of ER-specific caspase-12 [159]. Another possibility is that intracellular Aβ may bind to alcohol dehydrogenase inside the mitochondria and activate apoptosis through stress and activation of caspase-9.

2.3.5.6. Inflammation

Inflammation is a response to eliminate the initial cause of cell injury such as necrotic cells that result from an original insult. If tissue health is not restored shortly, inflammation becomes chronic and continues to damage surrounding tissues. Chronic inflammation may also be a component of the core degenerative pathway as it is a pathological hallmark of AD [160]. Extracellular amyloid deposit in senile plaques activates a potentially pathological innate immune response in AD. Oligomerization of Aβ and deposition in the brain lead to microglial and astrocyte activation [161]. Microglia, astrocytes, and neurons are, indeed, responsible for the reaction activating inflammatory mediators such as cytokines and interleukines [162]. In turn, inflammatory mediators and stress conditions enhance APP production and its amyloidogenic processing to generate Aβ [163]. Practically, inflammatory response is at the same time the cause and effect of Aβ-induced toxicity and regulates soluble and insoluble amounts of Aβ.

2.3.6. Therapeutic Strategies for AD

There are currently no treatments available to cure AD. The drugs used today are only symptomatic treatments as they do not affect the actual disease process, only providing some improvement in memory and cognitive function. The existing therapeutics for AD are all cholinergic agents, specifically inhibitors of acetylcholinesterase, since AD causes substantial losses in cholinergic neurons [164]. These inhibitors increase the levels of acetylcholine to keep the remaining cholinergic neurons, but unfortunately this type of therapy does not stop the progressive loss of cholinergic neurons and eventually becomes ineffective. A better approach is the development of agents capable of affecting the molecules responsible for the neurodegeneration.

Understanding the relationships between pathological pathways has significant implications for therapeutic development. The progressive accumulation of Aβ aggregates is widely believed to

be fundamental to the initial development and progression of AD, but Aβ toxicity is a multifaceted phenomenon that may be induced by multiple assembly forms of Aβ and that triggers a cascade of biochemical events such as neurotoxicity, oxidative damage and inflammation. The main efforts in the development of treatment strategies for AD focus on the prevention of Aβ production, Aβ aggregation or downstream neurotoxic events (Figure 2.23).

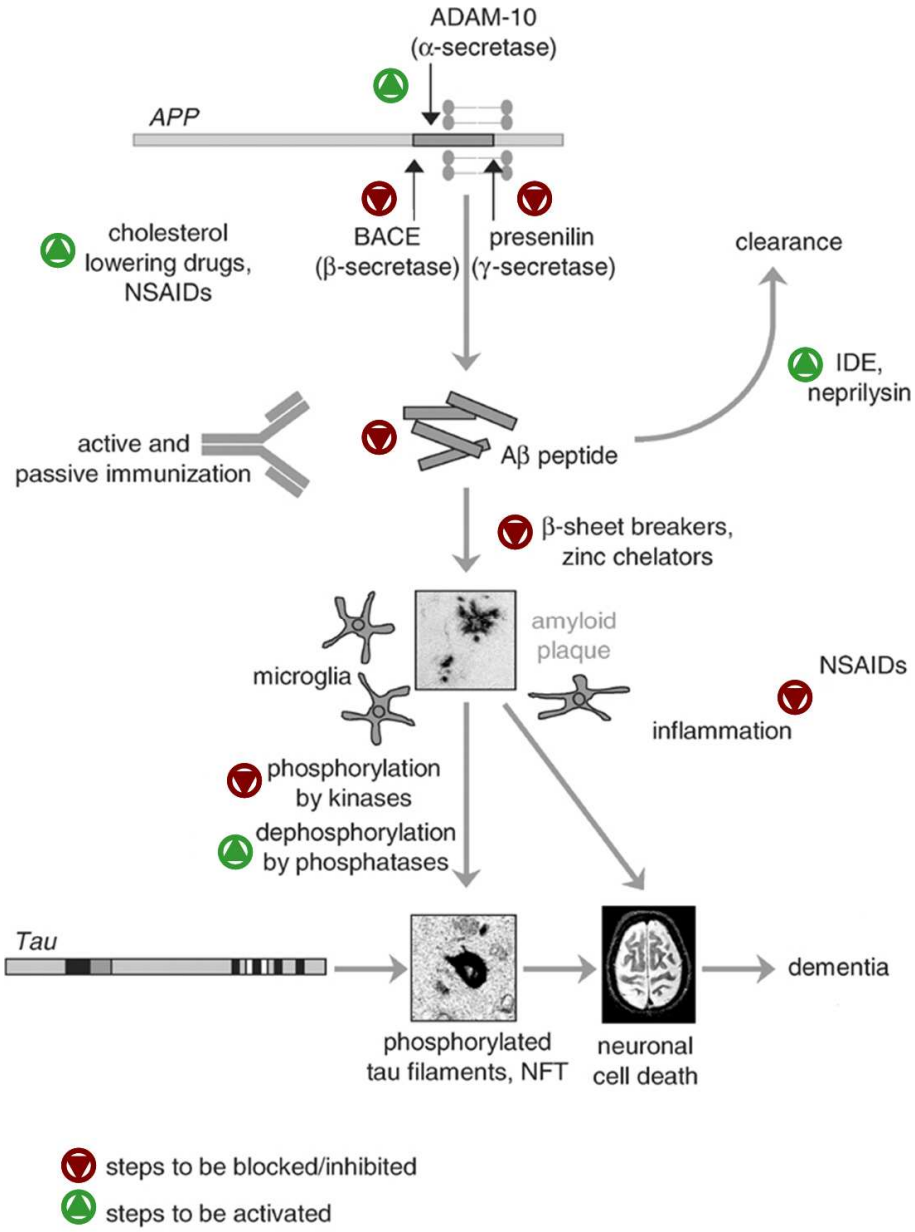


Figure 2.23. The amyloid cascade hypothesis suggests several possibilities of therapeutic intervention for disease modification in AD (*adapted from* [166]).

While information is lacking regarding the range of Aβ assemblies present in the human brain, therapeutic intervention should target the earliest stages of oligomerization, thus removing all potential Aβ toxins. At the moment, many therapeutic efforts have been concentrated on reducing or modulating Aβ production, including secretase inhibition and increase of Aβ clearance with amyloid vaccines, or blocking Aβ aggregation with different sources such as antibodies, breaker peptides, or small organic and natural molecules that selectively bind and inhibit Aβ aggregation, and fibril formation [165].

Decreasing the production of soluble Aβ seems to be particularly attractive since it might be possible to reduce Aβ concentration below the critical concentration needed for oligomerization by cell penetrating agents that reduce extracellular and/or intracellular monomer levels. Although no physiological function has been attributed to Aβ, severe or complete depletion of monomers could result in side effects. Substantial effort has gone into the development of inhibitors, activators and modulators of secretases in order to inhibit the accumulation of Aβ obtained by APP proteolysis. The two proteolytic activities involved in Aβ production, β- and γ-secretase, are attractive drug targets. A major problem in drug development arises from the finding that APP is not the only substrate of these secretases. For many years, γ-secretase attracted most of the attention because potent inhibitors could be easily identified but the identification of several substrates other than APP including the notch receptor that requires cleavage and is essential during embryonic development [167]. So it is unclear if potent γ-secretase inhibitors are therapeutically useful. However, certain non-steroidal anti-inflammatory drugs (NSAIDs) indirectly reduce oligomerization by modulation of γ-secretase activity. Such drugs decrease the formation of Aβ42 by shifting the γ-secretase cut by 4 N-terminal amino acid residues, and thus producing the smaller non aggregating Aβ38. Since these drugs do not block the γ-secretase activity *per se*, they do not show the side effects caused by lack of proper cleavage of Notch [168]. The finding that β-secretase-knockout mice are deficient in Aβ production, which was independently reported by three groups, was not unexpected, but it did provide *in vivo* validation of BACE1 as β-secretase, and it demonstrated that there is no compensatory mechanism for β-secretase cleavage in mice [167]. This is desirable for inhibitor development. Several β-secretase inhibitors are now available, and this seems to be a promising approach because mice lacking β-secretase do not have an overt phenoptype.

α-Secretase pathway stimulation leads to a reduction of the APP substrate that is available for Aβ formation, and it was demonstrated earlier that this pathway can be stimulated through cell-surface receptors [169]. However, it needs to be remembered that much more APP enters the α- than the β-secretase pathway, so the desired reduction in Aβ requires a marked change in the

metabolism of both APP and various other membrane proteins that are α-secretase substrates. The potential side effects of this approach are not known [167].

Instead of preventing Aβ aggregation, another approach involves up-regulation of enzymes involved in Aβ catabolism, such as insulin-degrading enzyme (IDE) and neprilysin. However, most Aβ fibrils can be largely resistant to proteolytic degradation, as reflected by their progressive accumulation in AD brains. It is unlikely that the catalytic centers of most enzymes that have been shown to degrade Aβ monomers can accommodate larger oligomers and fibrils [170]. IDE catabolizes natural Aβ monomers but not soluble dimers or trimers [171]. Among the proteases tested so far, only plasmin (a protease with a central role in fibrinolysis) and cathepsin B (a lysosomal cysteine proteinase) are capable of directly degrading Aβ oligomers and higher aggregates [172, 173].

The employment of small chemicals or natural molecules which bind and stabilize Aβ monomers preventing oligomerization and/or inhibit their binding to membranes, allowing the natural removal by the brain is also being investigated [174]. Only one of such agents has come to clinical trials [165]. Proteoglycans and their constituent glycosaminoglycans are associated with amyloid plaques from AD brain tissue and are thought to stabilize the aggregates making them more resistant to proteolysis, possibly by enhancing the nucleation phase [170], and Neurochem. Inc. has a compound, 3-amino-1-propanesulfonic acid Tramiprosate (Alzhemed^{TM}), a sulfated glycosaminoglycan mimetic designed to prevent Aβ binding to glycosaminoglycans [175].

Many *in vitro* inhibitors of Aβ aggregation have been identified, but no agent has come to clinical trials [176]. Recent animal studies using an *in vitro* inhibitor of Aβ fibrillogenesis, scyllo-cyclohexanehexol (AZD-103) have shown that its oral administration to APP transgenic mice caused an improvement in spatial reference memory and prevented the blocking of hippocampal LTP [165]. Inhibition of fibrillogenesis has been also studied using β-sheet breaker peptides [177], and a modified peptide with improved pharmacological properties was developed which showed a high rate of penetration across the brain-blood barrier (BBB) and the ability to reduce Aβ deposition in transgenic mice [178]. As Zn and Cu can form complexes with Aβ, another strategy involves lowering these metal levels. Zn/Cu ion chelation with the antibiotic clioquinol has been reported to lower amyloid load *in vivo* [179]. The cognition skills improvement was not significant but stratification by illness severity revealed a major effect of the treatment in the more severely affected group. However, only the less severely affected group exhibited a reduction in plasma Aβ42. Such chelators would also be expected to reduce oxidative stress in neurons.

One promising approach for preventing and treating AD is based upon stimulating the immune system to remove Aβ from the brain, either through active Aβ vaccination or passive

infusion of anti-Aβ monoclonal antibodies [170]. Unfortunately, active immunization of patients with anti Aβ antibodies that cross the BBB caused T-cell mediated, autoimmune meningoencephalitis inflammation in 6% of the trial participants [180].

Other therapeutic approaches being tested include anti-inflammatory agents as steroids that decline during normal ageing, such as oestrogen and testosterone [75]. Cholesterol-lowering statins as a potential treatment for AD are also suggested by retrospective epidemiology and it is intriguing that Apo ε4, the main risk factor for AD, is associated with increased plasma cholesterol [167]. Finally, the ability to identify individuals at risk for AD, based upon genetic (Apo ε4 genotype, for example) or environmental (overweight sedentary life style) factors will allow the application of more aggressive interventions in those individuals [75].

3. Aβ Adsorption on Planar Surfaces

3.1. Introduction

The adsorption of biological molecules at solid-liquid interfaces is growing in importance due to its application to a very broad range of fields. The interaction of proteins and peptides with solid surfaces is a fundamental phenomenon and is a key to several and novel applications for nanotechnology, biomaterials and biotechnological processes. So a deep understanding of the surface-induced adsorption behaviour of biologically relevant peptides and their molecular conformation at interfaces is essential. Fundamentally, the interaction of proteins or peptides and surfaces involves both protein binding and unfolding; these studies may therefore increase the knowledge of protein biophysics in general. The ultimate goal of such studies would be to measure, predict and understand the protein conformation, surface coverage, superstructure and kinetic details of the protein-surface interaction. *In vitro* studies show that interfaces and in particular the lipid membrane interface promote protein misfolding, while cytotoxicity studies show that one of the major effects of protein aggregates is an increase of the cell membrane permeability [143, 181].

There are several studies concerning the conformation and self-aggregation of Aβ peptides in a number of different environments, both in solution and at interfaces, but the misfolding mechanism is still an unsolved problem [182]. The peptides may be released to the aqueous environment as soluble monomers in nontoxic form and may be removed in healthy people or may aggregate in AD patients. A central hypothesis of the Aβ theory is that soluble unordered or α-helical Aβ might be considered as the "normal" conformation and exerts physiological functions in the CNS. In contrast, misfolding of Aβ to an "abnormal" β-sheet structure prone to aggregation leads to neurotoxicity. Due to the amphipathicity of the peptide, it may be retained in the membrane and hydrophobic and electrostatic interactions play important roles in determining the conformation and aggregation of Aβ peptides. Solid sorbent surfaces are suitable model systems to understand the roles of hydrophobic and electrostatic interactions in the conformation of the peptide at interfaces, and selecting appropriate solid surfaces, these interactions can be studied separately.

The investigation of the behaviour of Aβ peptides on solid planar surfaces, which include model lipid bilayers may represent an important step towards a detailed understanding of the

initial stages of aggregation and hence assist in drug design approaches that target inhibitors of amyloidogenesis.

3.2. Materials and Methods

3.2.1. Materials

3.2.1.1. Amyloid-β Peptides

Aβ peptides with purity higher than 95% were purchased from American Peptide Company (Sunnyvale, CA, U.S.A.) in lyophilized form and stored in desiccated containers at -20 °C until reconstitution. The molecular weights were checked by MALDI-TOF mass spectrometry (Figure 3.1) [183].

Prior to resuspension, each vial was allowed to equilibrate at room temperature for 30 min to avoid condensation upon opening of the vial. The first step in resuspending the lyophilized peptide was dissolution in cold HFIP to 1 $mg \cdot mL^{-1}$ followed by incubation at room temperature for at least 1 hour to establish monomerization. HFIP is a solvent that disrupts peptide-peptide interactions and facilitates the formation of α-helical structure [184]. HFIP was evaporated under a gentle stream of N_2 and the resulting clear film was again resuspended according to the conditions described for each assay.

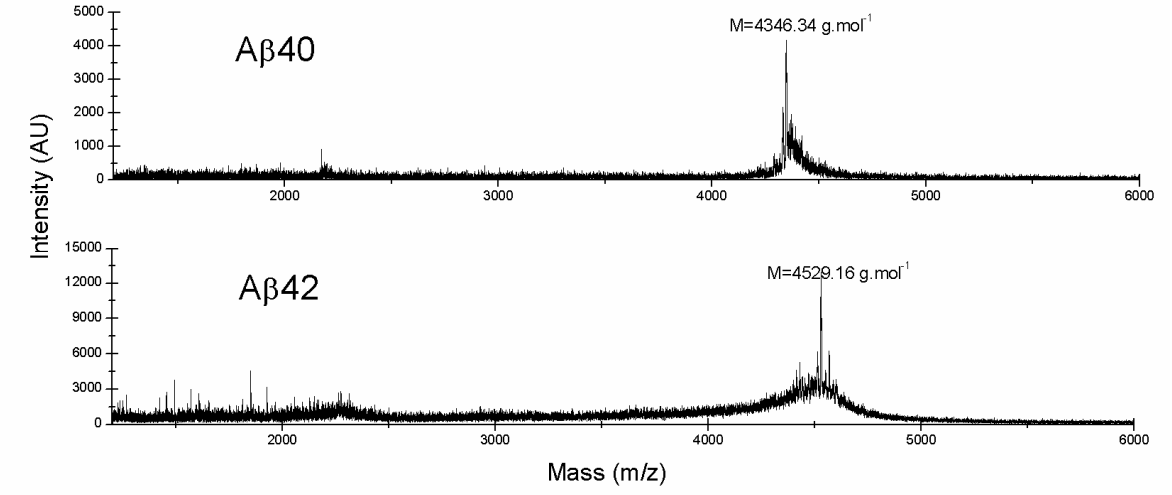


Figure 3.1. MALDI-TOF mass spectrometry profile of Aβ peptides.

3.2.1.2. Lipids

Phospholipids are the main component of naturally occurring bilayers, and phosphatidylcholine (PC) is the major membrane phospholipid in eukaryotic cells. Egg PC is one of the constituents of hens´eggs and it is often used in biomimetic membrane studies. Since this is a natural product, the composition may vary slightly but the average composition concerning fatty acids is rather constant and given in Table 3.1.

Table 3.1. Fatty acid content of egg PC.

Fatty Acid		Distribution (%)
Common Name	**Carbon skeleton***	
Palmitic	16:0	34
Palmitoleic	16:1(Δ^{9})	2
Stearic	18:0	11
Oleic	18:1(Δ^{9})	32
Linoleic	18:2($\Delta^{9,12}$)	18
Arachidonic	20:4($\Delta^{5,8,11,14}$)	3

* number of carbons:number and position of double bonds in the fatty acid chains

Egg phosphatidylglycerol (PG, sodium salt) from egg yolk lecithin is obtained from egg PC by the action of phospholipase D in the presence of the appropriate base (transphosphatidylation) so the fatty acid composition is identical to the one shown on Table 3.1.

Introducing DNA into eukaryotic cells is one of the recent major advances in molecular biology and there are several groups of cationic lipids for use in transfection systems. One example of nonviral delivery vectors are cationic liposomes characterized by a number of desired properties such as high efficiency and lack of toxicity [185]. 1,2-Dimyristoyl trimethylammonium-propane (DMTAP) is a synthetic molecule used for the preparation of such vesicles and is positively charged under physiological conditions. In this work it was used to confer a positive character to the egg PC bilayers.

Glycosphingolipids, although a minor component in most vertebrate tissues, constitute 5–10% of the total lipid mass in nerve cells [186]. Gangliosides, a class of glycosphingolipids ubiquitously present on the outer leaflet of plasma membranes, are closely associated with numerous membrane-mediated diseases. The monosialoganglioside GM1 is a member of the ganglio series that contain one sialic acid residue. GM1 plays important physiological roles and impacts neuronal plasticity and repair mechanisms, and the release of neurotrophins in the brain [187]. DMTAP and GM1 were purchased from Avanti Polar Lipids (Alabaster, Alabama, U.S.A).

Cholesterol is the most predominant sterol in the plasma membrane, and is related with numerous cellular roles such as lipid fluidity, receptor function and endocytosis. A healthy neuronal cell contains 25% cholesterol so this component is widely used for the preparation and study of artificial model membranes. Egg PC, egg PG and cholesterol were purchased from Sigma.

In an effort to use model fluid membranes we compared the formation of PC supported lipid bilayers (SLBs) on SiO_2 surfaces with and without the incorporation of other lipids/molecules that confer, e.g., a different charge or rigidity to the bilayers formed (Figure 3.2 and Table 3.2). The adsorption of Aβ peptides onto theses structures was examined.

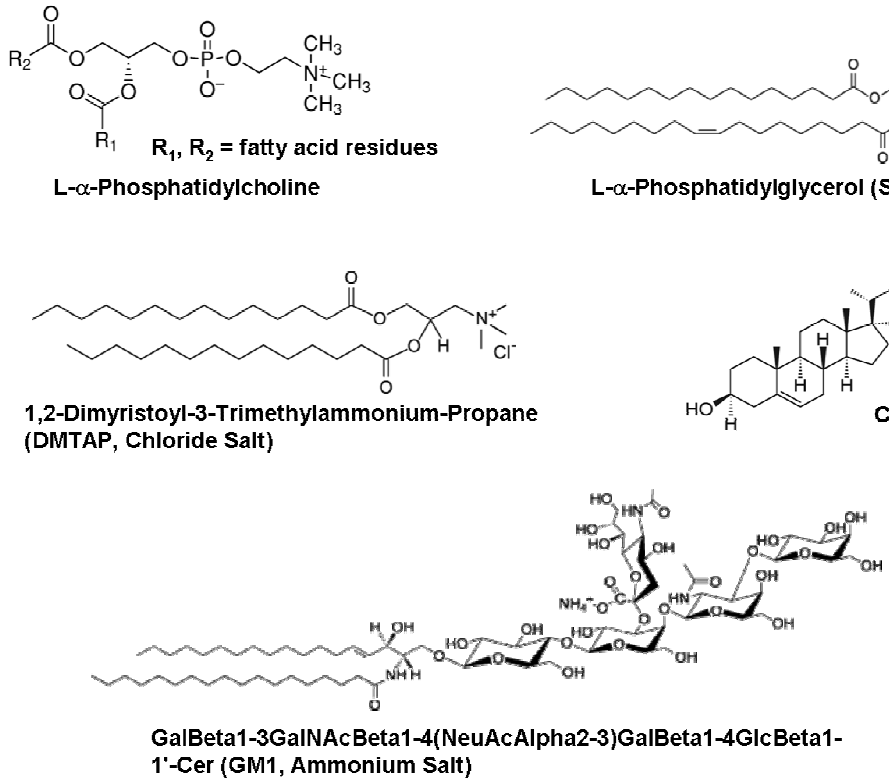


Figure 3.2. Chemical structures of the lipids and other substances used to prepare SLBs.

Table 3.2. Molecular weight of the molecules shown in Figure 2.2.

Substance	Molecular Weight ($g \cdot mol^{-1}$)
Egg PC	760.1
Egg PG	771.0
DMTAP	590.4
GM1	1,563.9
Cholesterol	386.6

3.2.2. Instrumentation and Methodologies

3.2.2.1. Quartz Crystal Microbalance

The Quartz Crystal Microbalance (QCM) is a high-resolution mass sensing technique, based upon the piezoelectric effect (ability of some materials to generate an electrical potential in response to mechanical stress). The QCM system is suitable for *in situ* measurements of peptide binding dynamics on model surfaces. The recent success of the QCM technique is related with the ability to sensitively measure mass changes on a variety of surfaces associated with liquid-solid interfacial phenomena (sensitivity is below 5 ng·cm^{-2} in liquid), as well as to characterize dissipative and viscoelastic behaviour of the mass deposited. Moreover, the measurements are in real time and there is no need of labeling. It has been described in detail by Rodahl in 1997 [188].

The sensing part is a thin piece of AT-cut metal coated quartz crystal [189]. AT-cut crystals are singularly rotated y-axis in which the top and bottom half move in opposite directions during oscillation, oscillating in thickness shear mode (TSM) at its very sharp resonant frequency. The TSM movement is in plane, lateral to the surface (Figure 3.3 A).

This crystal can, thanks to its piezoelectric properties and geometry be made to stably oscillate in TSM by application of an alternating current to the quartz crystal. The resonance frequency, *f*, depends on the total mass of the system. A mass adsorbed on the crystal surface, from, e.g., a solution, is normally detected as a decrease in the resonance frequency, Δ*f*. The QCM crystal can be driven at the fundamental frequency (5 MHz in this case) or at an overtone. At 15 MHz (i.e., the third overtone), a frequency shift of ~1 Hz corresponds to a mass change of ~6 ng·cm^{-2} according to the Sauerbrey equation (3.3). Sauerbrey proposed a simple physical model for the observed proportionality between added mass and induced *f* shift [190]. By defining the area density of the quartz as $m_q = t_q \rho_q$ where ρ_q and t_q are the density and thickness of the quartz plate, respectively he obtained

$$f = \frac{n v_q \rho_q}{2 m_q} \tag{3.1}$$

where *n* is the number of waves and v_q is the wave velocity in the plate. By differentiating,

$$df = -\frac{f}{m_q} dm_q \tag{3.2}$$

Assuming that for small mass changes the added film can be treated as an equivalent mass change of the quartz crystal itself. By making $d \rightarrow \Delta$,

$$\Delta f = -\frac{f}{m_q}\Delta m = -\frac{f}{t_q \rho_q}\Delta m = -\frac{n}{C}\Delta m \qquad (3.3)$$

where C (= 17.7 ng·cm^{-2}·Hz^{-1} at f = 5 MHz) is the mass sensitivity constant and n (= 1, 3, ...) is the overtone number. The Sauerbrey equation is applicable to thin, rigid and evenly distributed films. The damping (dissipation factor, D) of the oscillator represents the sum of all the energy losses in the system per oscillation cycle and is given by:

$$D = \frac{E_{dissipated}}{2\pi E_{stored}} \qquad (3.4)$$

Mathematically it is synchronous with the velocity of the object but with opposite direction. D provides qualitative and quantitative information about the viscolelastic properties (loss of oscillation energy). A rigid film perfectly follows the shear motion of the quartz crystal while a soft film dissipates the shear oscillation mainly through friction losses and the film does not move in phase with the crystal (Figure 3.3 B).

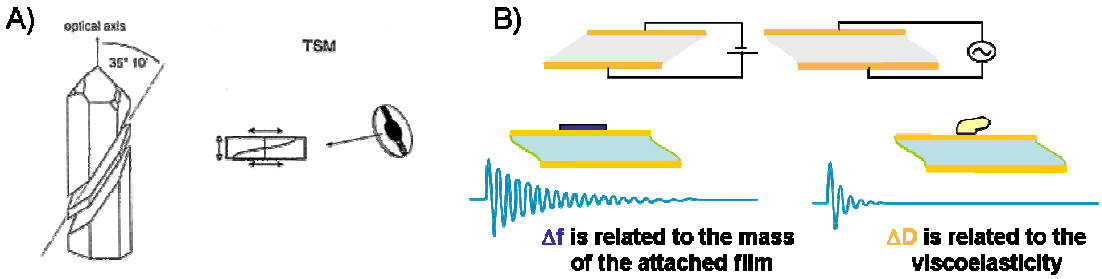


Figure 3.3. A) AT-cut of a quartz crystal from which the metal coated QCM quartz crystals are produced and a view of the TSM of oscillation (*adapted from* [188]). B) Δf is related with the mass adsorbed on the crystal surface; ΔD provides information about the viscolelastic properties of the adsorbed film.

In water, the sensing depth is limited to a region extending ~250 nm into the solution at the fundamental frequency (5 MHz). The amplitude of the sensor crystal oscillation, which sets the sensitivity, decreases from the center towards the edge. The higher the overtone number, the narrower the sensitive area. So the different overtones give information about the homogeneity of applied layers since the detection range decreases with increasing overtone number. Different f values for the overtones suggest vertical variations in film properties and the true mass will be

underestimated if only the Sauerbrey equation is used. *D* and the information from the different overtones allow theoretical modeling of the QCM response in order to characterize viscoelastic behaviour and one can determine the thickness of films outside the Sauerbrey region. This can be useful, for instance, when the thickness of the film increases and viscoelastic effects come to play. The adsorbed mass can be obtained by applying the Voight model to Δf and ΔD measured at (at least) two overtones as schematized in Figure 3.4 [191]. This yields the viscoelastic load on the crystal, that is, the Voight mass, including both adsorbed molecules and water. It should be noticed that a good fit requires films with homogeneous density, viscosity and/or shear modulus.

Adsorption measurements using the QCM technique provide information regarding the Aβ adsorption affinity for diverse surfaces as well as a direct comparison of the time scale for adsorption of the peptide film.

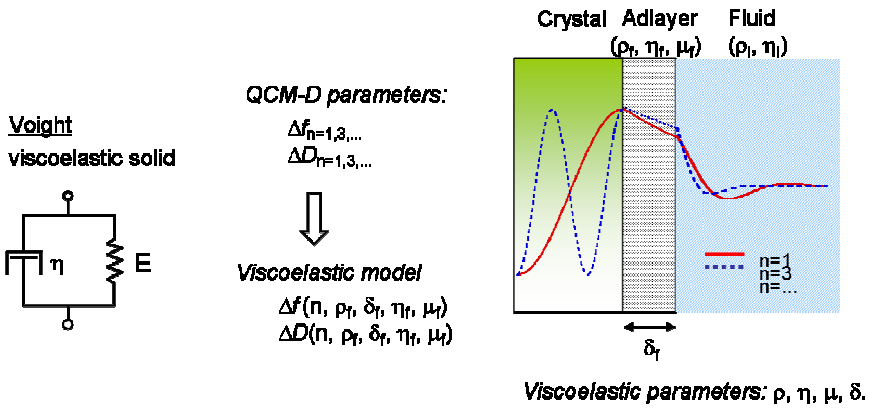


Figure 3.4. Application of the Voight model to Δf and ΔD measured at different overtones to characterize viscoelastic films adsorbed onto the QCM-D sensor crystal.

A Q-Sense E4 (Q-Sense, Gothenburg, Sweden) equipped with an axial flow chamber was used to conduct QCM-D measurements. In the thermally insulated fluid cell, the crystal is mounted horizontally and the exchange of the solutions is achieved perpendicularly to the crystal surface using a peristaltic pump (Ismatec SA, Switzerland). The fluid enters from a temperature-controlled loop before being introduced into the measurement cell. A Peltier element controls the temperature with an accuracy of ±0.05 °C. Data acquisition was performed with Q-Soft 301 (Q-Sense) and data interpretation with Q-Tool, also from Q-Sense. All data shown for the frequency shifts are normalized to the response of a 5MHz crystal and unless otherwise said, the curves correspond to the third overtone. In all QCM-D experiments, the cell was initially filled with buffer and rinsed several times until a stable baseline is established. When the baseline was stable, the buffer was exchanged for the solution to be studied and data were collected as a function of time

by recording the changes in *f* and *D*. Gold crystals (14 mm diameter) purchased from Q-Sense were cleaned before surface preparation using the following procedure: immersion in a 6:1:1 (vol/vol) solution of H_2O : NH_3(25%) : H_2O_2(30%) at 70 °C for 10 min followed by thorough rinsing with water and drying in a stream of N_2.

3.2.2.2. Atomic Force Microscopy

AFM is one of the most powerful tools for determining the surface topography of native biomolecules at subnanometer resolution [192]. Unlike X-ray crystallography and EM, the AFM allows biomolecules to be imaged not only under physiological conditions, but also while biological processes occur. Because of the high S/N ratio, the detailed topological information is not restricted to crystalline specimens.

AFM was a spin-off of scanning tunneling microscopy (STM) [193], intended to extend the possibilities of STM. The STM monitored electron tunneling, typically from one atom at the end of a probe to a conducting substrate. In 1986, Binnig, Quate and Gerber replaced the electron tunneling from a fine wire of the STM with the cantilever approach of AFM, which can analyze even insulating samples. Commercial instruments have been available since 1988, and since then there have been many developments and new modes of operation devised for AFM.

AFM imaging is fundamentally different from conventional microscopy: a sharp tip attached to a cantilever spring is scanned over the sample surface (Figure 3.5). Cantilever bending caused by the interaction force between sample and tip (usually in the range pN to nN) is detected by the deflection of a laser beam focused on the end of the cantilever. The sample is mounted on top of a piezoelectric scanner which scans in the *x* and *y* direction and adjusts the vertical distance between sample and tip according to the input from the detector feed back control, so that the cantilever deflection is constant.

There are two main AFM imaging modes. In contact mode (or static mode) the feedback loop between the laser detector and the piezo adjusts the vertical distance from tip to sample such that the cantilever is held at constant deflection, so a *z* value is associated to each *xy* pair. In the contact mode, molecules must be well adsorbed to the substrate to avoid being moved and/or damaged by the tip (Figure 3.6 A). In dynamic mode (Tapping Mode™, Digital Instruments/Veeco, CA), the feedback loop keeps the amplitude of an oscillating cantilever constant by correcting the vertical distance, and the tip touches the sample only at the bottom of the oscillation. This reduces lateral

forces on the molecules (Figure 3.6 B). One disadvantage of the tapping mode is the slightly lower resolution.

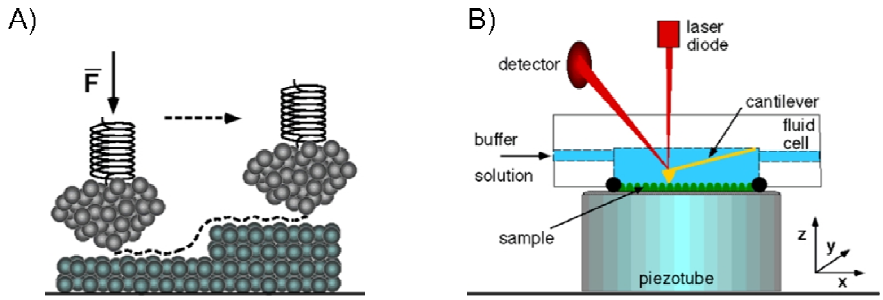


Figure 3.5. Principle of the AFM. A) A fine stylus is mounted on a cantilever spring and scanned over the surface. At sufficiently small forces the corrugations of the scanning lines represent the surface topography of the sample. B) The vertical deflection of the cantilever is detected by reflecting a laser beam onto a 2-segment photodiode. The photodiode signal is used to drive a servo system which controls the movement of the piezo *xyz*-translator. In this manner the applied force between the stylus and the sample can be kept constant within some tens of a pN. The imaging process can be performed in a liquid cell filled with buffer solution. This ensures that the biomolecules remain hydrated (*adapted from* [194]).

Using AFM, the systems can be imaged in solution allowing the samples to retain bulk properties while temporal changes are monitored. This is a distinctive characteristic of AFM regarding conventional imaging techniques of comparable resolution such as EM and it can be achieved using a fluid cell (as the one in Figure 3.5 B).

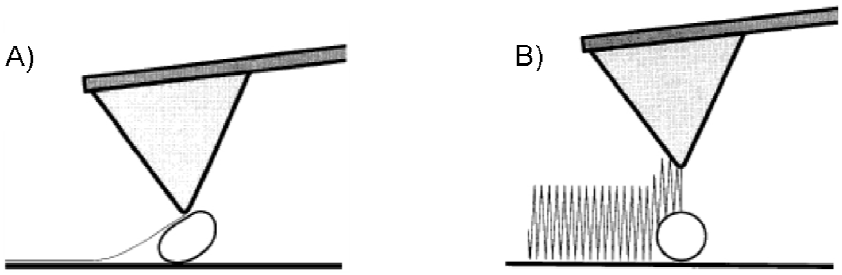


Figure 3.6. Comparison between the two AFM scanning types: A) contact mode and B) tapping mode (*adapted from* [191]).

AFM images were taken using a Nanoscope III AFM in Tapping Mode® (Veeco/Digital Instruments, Santa Barbara, CA). Arrow™ silicon tips (NanoWorld, Neuchâtel, Switzerland) with a resonance frequency of ~ 285 kHz and a spring constant of ~ 42 N/m were used. At least three regions of the surface were examined to verify if similar morphology existed throughout the sample. The images were analyzed using the Nanoscope V software from the AFM supplier. The results presented show height and amplitude images.

SLB formation was followed using a tapping-mode fluid cell (Veeco/Digital Instruments, Santa Barbara, CA) without O-ring. Aluminum coated silicon tips (Olympus, Tokyo, Japan) with a resonance frequency of ~ 300 kHz and a spring constant of ~ 42 N/m were used. The cell was washed with ethanol and ultrapure water and dried in a stream of N_2. SiO_2 wafers were attached to the magnetic plate with double tape and putted inside the fluid cell. The surface was covered with buffer, injected into the cell using a syringe. The AFM was equilibrated for some min before imaging. After, the buffer was exchanged for egg PC vesicles.

3.2.2.3. Attenuated Total Reflection Infrared Spectroscopy

A number of spectroscopic methods can reasonably estimate protein secondary structure content, such as Circular Dichroism (CD) spectroscopy, NMR spectroscopy and Infrared Spectroscopy (IR) (Table 3.3). Among them, IR spectroscopy, as a vibrational spectroscopy, constitutes one of the earliest experimental methods for estimating the secondary structure of peptides and proteins.

Table 3.3. Spectroscopic methods for probing protein structure [197].

Method	Structure	Advantages	Disadvantages
UV absorption	3ary	▪ inexpensive ▪ easy	very low resolution
CD	2ary (far UV) 3ary (near UV)	▪ easy ▪ 2ary structure ▪ effect of solvent composition	▪ low resolution ▪ interference by aromatic residues ▪ expensive
Fluorescence	3ary	▪ high sensitivity ▪ easy ▪ rel. inexpensive ▪ compactness and dynamics	limited to the study of semiburied aromatic residues
IR absorption	2ary	▪ easy ▪ rel. inexpensive ▪ applicable to solid samples	▪ water interference ▪ high protein concentration
Raman	2ary 3ary	▪ minimal interference by water ▪ applicable to solid samples	▪ slow ▪ not commonly available
NMR	2ary 3ary	▪ highest resolution ▪ protein dynamics	▪ expensive ▪ difficult ▪ high concentration ▪ limited to small proteins

The major types of molecular vibrations are stretching and bending. When the frequency of a specific vibration is equal to the frequency of the IR radiation directed on the molecule, the molecule absorbs the radiation [195, 196]. The transitions detected are those arising from vibration modes of bonds involving heteroatoms, since in this case the molecular dipole moment changes during the vibration. The approximate position of an IR absorption band is determined by the vibrating masses and the type of bond (single, double, triple), the exact position by electron withdrawing or donating effects of the intra- and intermolecular environment and by coupling with other vibrations.

The first IR spectrometers were dispersive spectrometers in which radiation from a broad band source passes through the sample and is dispersed by a monochromator into component frequencies. Fourier transform IR (FTIR) spectrometers have replaced dispersive instruments. Instead of viewing each component sequentially, all frequencies are examined simultaneously. The detector signal is related by a Fourier transformation to the measured spectrum via an interferometer. A second Fourier transform performed by a computer converts the measured interferogram back into a spectrum. The main advantage of Fourier transform spectrometers is the rapid data collection and high light intensity at the detector and in consequence the high S/N ratio.

IR spectroscopy on biological systems is usually performed in transmission mode. This means that the IR beam of the spectrometer is passed through the sample and, if the sample is homogeneous, it absorbs light according to the Beer-Lambert´s law

$$A = -\log\left(\frac{I}{I_0}\right) = c\varepsilon l \qquad (3.5)$$

where A is the absorbance, I and I_0 are the intensities of transmitted and incident light, respectively; c is the concentration of the absorbing substance, ε the molar extinction coefficient and l the pathlength.

Two important factors have to be considered in transmission IR of aqueous solutions of proteins. First, the vibrational extinction coefficients are generally very low, and relatively high protein concentrations have to be used. Second, IR absorption bands of liquid water overlap with several bands that are of interest in protein spectroscopy. Owing to the high IR absorption of water, IR samples are very thin, usually only a few µm optical pathlength. The water content in transmission samples is therefore quite low, which may in some cases constitute a major problem.

An alternative to transmission mode experiments is offered by the attenuated total reflection (ATR) technique. In a ATR experiment, the IR radiation is passed through an trapezoidal IR

transmitting crystal (also called an internal reflection element or IRE) with a high refractive index, e.g., germanium (Ge) or zinc selenide (ZnSe), allowing the radiation to be guided within the ATR element several times by total reflection (Figure 3.7 A) [198]. IR radiation is focused on and enters one of the faces of the IRE. If the angle θ at which the IR light hits the interface between the ATR crystal (the dense medium) and the air or solution (the rare medium), is greater than the critical angle calculated as

$$\theta_{critical} = \sin^{-1} \frac{\text{refractive index of rare medium}}{\text{refractive index of dense medium}} \qquad (3.6)$$

then the light will be totally internally reflected in the crystal.

By choosing the thickness and the length of the IRE, the total number of reflections N the light will undergo as it propagates down the crystal before emerging at the other end can be controlled according to

$$N = \left(\frac{\text{IRE length}}{\text{IRE thickness}} \right) \cot \theta \qquad (3.7)$$

At each internal reflection, the IR radiation actually penetrates a short distance (~1 μm) from the surface of the IRE into the sample (Figure 3.7 B). Thus, the obtained spectra are similar to those obtained from a very thin layer of the sample.

At each reflection, an evanescent wave with the same frequency as the incoming IR light is created in the rare medium that can penetrate to a depth d_p expressed by the equation:

$$d_p = \frac{\lambda}{2\pi n_1 \sqrt{(\sin^2 \theta - n_{21}^2)}} \qquad (3.8)$$

where λ is the wavelength of the light, n_1 is the refractive index of the ATR crystal (for Ge it is 4.0 and independent of λ), θ is the angle of incidence and, n_2 is the refractive index of the rare medium (sample) and $n_{21} = n_2/n_1$. The ATR method provides spectra for suface layers of a few micrometers without, in fact, cutting into them. The instruments have software programs designed to adjust the required penetration depth.

Most FTIR spectrometers work as single beam instruments, i.e., the measurement of a reference spectrum before or after the investigation of the sample is a prerequisite for the calculation of a spectrum. An ATR setup equipped with a flow-through cell enables the performance of *in situ* experiments changing sample conditions during measurement, e.g. by

adding of ligands, changing the pH or ion concentration. Consequently experiments may last for a long time and the spectrometer stability might become a problem, especially if a high resolution is required. A double beam or pseudo-double beam setup gets rid of most of these problems, if sample (S) and reference (R) are prepared at the same time and held under the same conditions during the experimental sequence. In this way, S and R are measured at the same time (double beam) or alternatively with short time intervals (pseudo-double beam), allowing comparison of S with R of the same age by an instrument in the same state of performance.

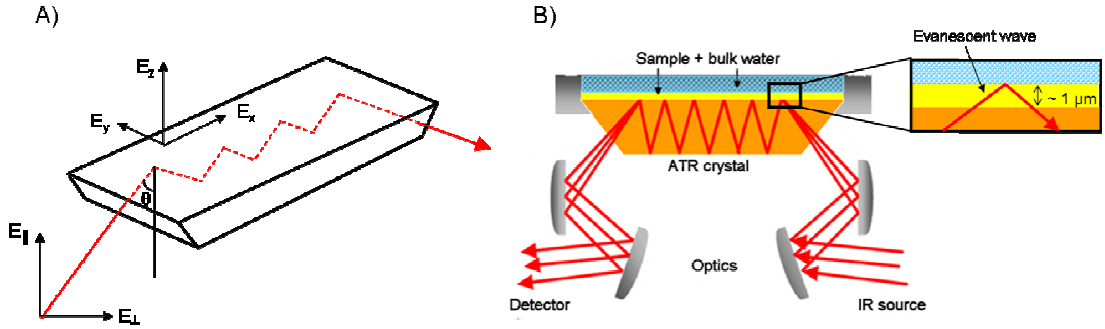


Figure 3.7. A) IR beam as it travels through a trapezoidal ATR crystal. The light enters the face normally and hits the interface between the crystal and the top at an angle θ. B) Total internal reflection at the interface of an IRE. The depth of penetration of the evanescent wave is approximately 1 µm.

Single Beam Sample reference (SBSR) is a pseudo double-beam method. Sample and reference compartments are prepared above each other on the same ATR crystal, mounted on a plate holder which is moved alternating up and down under computer control. At each position (R, S) a certain number of scans is measured before moving automatically to the other position, enabling quasi simultaneous collection of S and R single channel spectra. Both S and R are accessible via independent flow-through cuvettes (Figure 3.8).

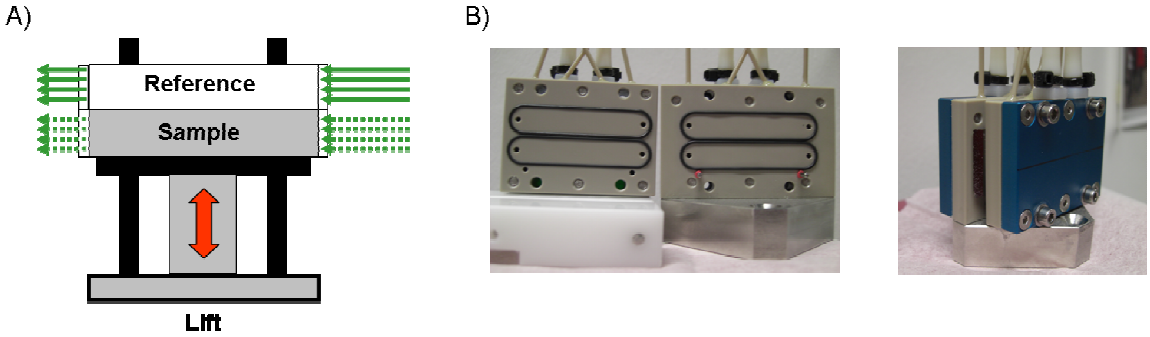


Figure 3.8. SBSR ATR attachment. A) S and R are brought into the IR beam by repetitive computer controlled lifting and lowering of the ATR cell body. B) S and R are mounted on the same IRE and accessible via independent tubing to flow-through cuvettes.

The peptide group, the structural repeat unit of proteins, gives up to 9 characteristic bands named amide A, B, and I – VII, in order of decreasing frequency (Table 3.4). There are three absorption bands of particular importance. The amide A band at 3200-3300 cm^{-1} that characterizes the N—H stretch vibration, the amide I band at 1600-1700 cm^{-1} that arises mainly from the C=O stretch vibration and other minor contributions (out of phase C—N stretching, C—C—N deformation and the N—H in plane bend) and the amide II band at 1510-1580 cm^{-1} that is the out of phase mode of the N—H in plane bending vibration and the C—N stretching vibrations with smaller contributions from the C=O in plane bend and the C—C and C—N stretching vibrations [197, 199, 200].

Table 3.4. The nine characteristic absorption bands for proteins in the mid-IR [196, 198, 199].

Band	**Frequency, ν (cm^{-1})**	**Vibration**
Amide A	≈3300	N—H stretching
Amide B	≈3100	N—H stretching
Amide I	1600-1700	Predominantly C=O stretching
Amide II	1500-1575	C—N stretching and N—H bending
Amide III	1230-1300	Complex in-plane modes, C—N stretching and N—H bending
Amide IV	625-767	Complex in-plane modes, O=C—N bending mixed with other modes
Amide V	550-700	Out-of-plane N—H bending
Amide VI	537-606	Out-of-plane C=O bending
Amide VII	≈200	Skeletal torsion

These 3 oscillations belong to the backbone of the polypeptide chain and are therefore relatively intense. These vibrations are not independent of each other. Because of the presence of particular hydrogen bonding patterns within the protein backbone that form secondary structures, they are coupled oscillators. In α-helices or β-strands the coupling of these oscillators is different and therefore the IR spectra of a protein are dependent on its secondary structure (Table 3.5). The amide I vibration is the most commonly used for secondary structure analysis. For the amide II

vibration of proteins the correlation between protein secondary structure and frequency is less straightforward since this band is usually quite complex.

The QCM measurements and ATR-IR experiments may provide complementary information concerning affinity and structure if the same surface is used.

Table 3.5. Position of the amide bands depending on the secondary structure of a protein/peptide [195, 198].

Conformation	**Vibration frequency, ν (cm^{-1})**		
	Amide A (N-H stretch)	**Amide I (C=O stretch)**	**Amide II (N-H bending)**
α-helix	3305	1648-1660	1540-1550
β-sheet	3230-3275	1625-1640 (strong)	1520-1530
β-turns and loops		various bands 1660-1685	
"random coil"	3250	1650-1660 (deuterated 1640-1648)	1520-1545
Anti-parallel β-sheet		1680-1695	
Aggregated strands (intermolecular β-sheets)		1615-1625	

The IRE used was a 51×20×1.5 mm^3 or 51×20×2 mm^3 Ge trapezoid with an angle of incidence of θ = 45° yielding 33 and 25 internal reflections, respectively. All spectra were recorded at 25 °C with a Bruker Vertex 70 spectrometer (Bruker, Germany) equipped with a lift-model SBSR ATR mirror attachment (Optispec, Neerach, Switzerland), with a hydrodynamically optimized and water-thermostatted SBSR cell (flow-through cuvette) made of Delrin® and with parallel (∥) and perpendicular (⊥) polarized IR light. A mercury-cadmium telluride (MCT) detector was used. All spectra were scanned at 4 cm^{-1} resolution. S and R compartments (area: 310 mm^2, thickness: 0.26 mm) were sealed by a viton O-ring (diameter: 1 mm) and had a volume of about 80 µL (Figure 3.7 B). Before each experiment, Ge ATR crystals were subjected to various cleaning procedures, including UV/ozone cleaning and rinsing with acetone, ultrapure water and ethanol, until there were no visible impurities left. Finally, the plate was mounted in the SBSR cell. All solutions used were degassed and transported to the flow-through cuvette with the help of a peristaltic pump (Ismatec SA, Switzerland) using viton tubings (inside diameter 1mm).

3.2.3. Surfaces

3.2.3.1. Hydrophilic vs Hydrophobic Surfaces

QCM-D gold crystals covered with SiO_2 and polystyrene were chosen as models of hydrophilic and hydrophobic surfaces, respectively. The SiO_2 surfaces were either used as purchased from Q-Sense or prepared by cleaning Au crystals followed by electron-beam evaporation to form a layer of SiO_2 (50 nm) on top. The gold and SiO_2 QCM-D sensor crystals were cleaned before experiments (besides the procedure described above for gold crystals) by exposure to ultraviolet (UV)/ozone for 5-10 min. The treatment is performed in an UV/ozone chamber in which a special lamp is fitted that generates light at the specific wavelengths 185 nm and 254 nm. The surface is treated both with the UV wavelength from the lamp and the generation of ozone by breakage of the O—O bond by the 185 nm wavelength. The treatment works in two ways, organic contaminants on the crystal surface are volatized and readily removed and the underlying surface is slightly oxidized. This treatment does not work for removal of thick organic films. The polystyrene surfaces were used as purchased from Q-Sense. Before starting each measurement, crystals were thoroughly rinsed with ultrapure water and ethanol alternatively, dried with N_2 and immediately assembled into the QCM-D chamber ready to use. In special cases, the crystals were rinsed with 2% Hellmanex® (Hellma, Mühlheim, Germany) and ultrapure water between runs.

3.2.3.2. Positively vs Negatively Charged Surfaces

In order to test the adsorption behaviour of Aβ peptides to oppositely charged surfaces, polyelectrolyte multilayers were prepared using the technique of layer-by-layer assembly (LbL) [201]. The multilayering process, which is achieved by sequential adsorption of oppositely charged polyelectrolytes, can be used to functionalize surfaces with properties widely different from those of the underlying substrate, and thin films can be constructed with a high degree of reproducibility. The polyelectrolytes used were (structures on Figure 3.9): (i) Poly(ethylenimine) (PEI, MW ~60,000), a cationic polyelectrolyte with monomers with a MW of 43.07 $g \cdot mol^{-1}$, obtained as a 50% m/v solution, (ii) Poly(sodium 4-styrenesulfonate) (PSS, MW ~70,000), an anionic polyelectrolyte constituted by monomers with a MW of 206.2 $g \cdot mol^{-1}$, and (iii) Poly(allylamine hydrochloride) (PAH, MW ~56,000), a cationic polyelectrolyte where the monomers have a MW of 93.5 $g \cdot mol^{-1}$.

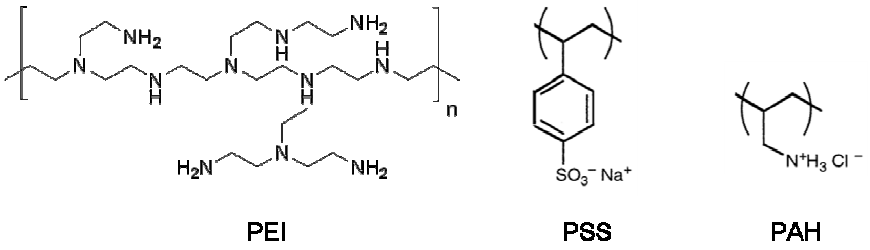


Figure 3.9. Structures of the polyelectrolytes used to prepare charged surfaces by LbL assembly.

Alternatively, positively charged and negatively charged polyelectrolyte solutions are in contact with the surface with water rinsing in between (Figure 3.10). The first (anchoring) layer was always 1 mM PEI, followed by 10 mM solution (with 1 M NaCl) of PSS, and 10 mM PAH solution (also with 1 M NaCl). This procedure was repeated until the desired surfaces were obtained, $PEI(PSS/PAH)_6$ and $PEI(PSS/PAH)_6PSS$. For QCM-D experiments, the preparation of the desired structures was done *in situ*, i.e., in the measurement chamber and the surface was not dried before peptide exposure. For ATR-IR measurements, the surfaces were prepared in advance and dried. Before peptide exposure, the polyelectrolyte multilayers were let to swell for at least 1 hour since it has been shown that the thickness of dry layers increases substantially when brought in contact with water, swelling 20-40% [202].

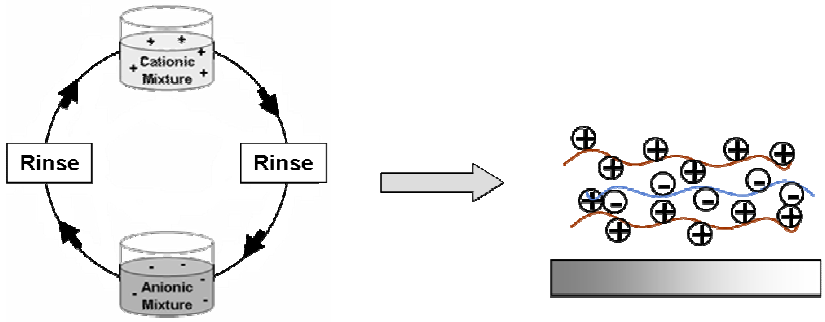


Figure 3.10. Schematic representation of the technique of LbL assembly to produce self-assembled multilayers on planar substrates.

3.2.2.3. Supported Lipid Bilayers

Two important examples of biomembrane model systems are unilamellar phospholipid vesicles and supported lipid bilayers (SLBs) [203]. In the former, a bilayer of amphiphilic phospholipid molecules forms a spherical shell, separating an "intracellular" liquid volume from the "extracellular" space, while SLBs are planar, two-dimensional, extended bilayers of the same

composition as vesicles, adsorbed on a suitable solid surface (Figure 3.11 A). SLBs are commonly prepared by a method pioneered by McConnell *et* al. [204] in which vesicles in a bulk liquid are allowed to interact with a suitable surface, the later inducing spontaneous vesicle rupture and fusion to a coherent planar bilayer [205] (Figure 3.11 B). For mixtures of zwitterionic lipid species in the fluid phase, in buffer at biologically relevant pH and salt concentration (with low Ca^{2+} concentration), the process mostly occurs in three successive phases on SiO_2 surfaces: (i) Initially, only vesicles populate the surface. (ii) At a critical coverage, vesicles start to rupture, fuse, and form bilayer islands, coexisting with vesicles and bare surface. (iii) Finally, a coherent SLB is formed, which covers the whole surface. Other behaviours have been observed with charged lipids and/or other pH values and electrolyte compositions, as well as on other substrates; however, SiO_2-based substrates are unique in their ability to facilitate spontaneous SLB formation. Moreover, lipid bilayers supported on silica substrates generally maintain a ≈10 Å layer of water between the membrane and the solid surface thus preserving many of the properties of free membranes. They are continuous with mobile components of both leaflets freely diffusing over the entire surface of the substrate.

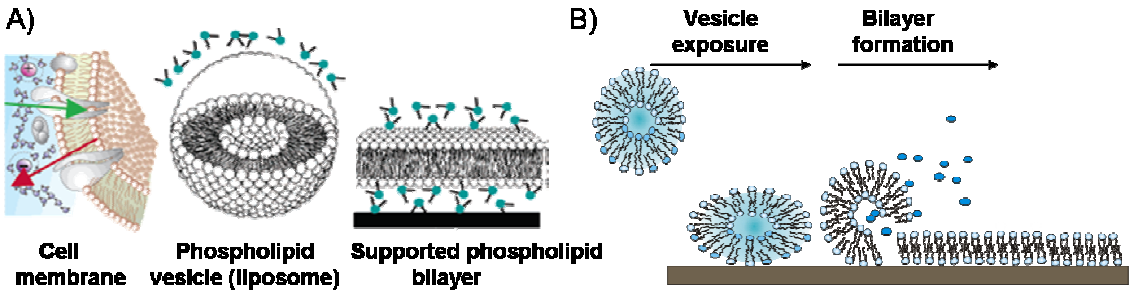


Figure 3.11. A) Cell membrane and biomembrane model systems. B) Lipid bilayer formation on SiO_2 substracts (*adapted from* [204]).

One advantage of this method is the possibility to incorporate functionalized molecules into the membrane for precise applications [206]. It is of considerable interest, for instance, to construct a biomimetic system for studies of ligand–receptor interactions on membranes. The objective herein was to use planar SLBs as the model system and incorporate components such as other lipids/molecules that confer, e.g., a different charge or rigidity to the lipid bilayers formed and to examine the adsorption of Aβ peptides onto these structures.

The QCM-D experiments were performed by injecting a solution of monodisperse vesicles which were prepared and characterized as described below into the measurement cells. All the

experiments were done with vesicles in their fluid state. Δ*f* and Δ*D* were recorded as functions of time until saturation/equilibrium was reached. The experiments were preformed at 25 °C.

Liposomes are vesicular structures consisting of hydrated bilayers which form spontaneously when phospholipids are dispersed in water [207], due to their amphiphilicity, i.e., they have defined polar and non polar regions. The non polar regions orient towards the interior, away from the aqueous phase, the polar regions are in contact with it. The main types of liposomes are listed in Table 3.6.

Table 3.6. Categories of liposomes.

Vesicle type	Abbreviation	Diameter	Number of lipid bilayers
Small unilamellar vesicles	SUV	20-100 nm	1 lipid bilayer
Large unilamellar vesicles	LUV	> 100 nm	1 lipid bilayer
Multilamellar vesicles	MLV	> 0.5 μm	5 - 20 lipid bilayers
Oligolamellar vesicles	OLV	0.1 - 1 μm	~ 5 lipid bilayers
Multivesicular vesicles	MMV	> 1 μm	Multicompartmental structure

There are many different strategies for the preparation of liposomes depending on the type of vesicles. In this work, liposomes were prepared by mechanical methods, (i) ultrasonication of a dispersion of phospholipids with a probe sonicator, or (ii) extrusion.

Lipid mixtures were obtained by addition of the appropriate volumes of stock lipid solutions in chloroform. Then the organic solvent was removed in a nitrogen flow. The resulting lipid film was dried overnight under vacuum. Lipids were re-hydrated with vortex at room temperature with the respective buffer at concentrations from 1 to 5 mM. Sonicated SUVs were produced by sonication to clarity (15-30 min) at room temperature with cooling in a tip sonicator. Titanium particles and large MLVs were removed by centrifugation (10 min at 5000 rpm). Extruded SUVs were prepared by mechanically extruding the lipid suspensions through a 50 or 100 nm polycarbonate membrane (Whatman Inc., Kent, UK) 21 times. PBS was used to prepare all the vesicles (10 mM phosphate buffer with 150 mM ionic strength adjusted by NaCl at pH 7.4). The studies were performed after diluting the SUV suspension to the indicated concentration.

The size of the lipid vesicles was measured by dynamic light scattering (DLS) on a Zeta Sizer Nano ZS (Malvern Instruments, Ltd., UK) at a scattering angle of 90° where the reflection effect is

minimized. SUVs of various compositions were diluted and the temperature equilibrated to 25 °C for all the samples. The autocorrelation function was obtained by the autocorrelator and fit by the method of cumulants. Only SUVs with a narrow size distribution were used. DLS measurements did not differentiate the hydrodynamic volumes of extruded/sonicated SUVs.

3.3. Results

3.3.1. Adsorption of Aβ Peptides on Hydrophilic vs Hydrophobic Surfaces

In a previous study, adsorption of Aβ40 at hydrophilic and hydrophobically modified silicon–liquid interfaces was characterized by neutron reflectometry [208]. The peptide was found to adsorb at positively charged hydrophilic and hydrophobic surfaces, whereas no adsorbed layer was detected on hydrophilic noncharged and negatively charged films. These studies provide information about the affinity of the Aβ to different substrates in aqueous solution, but not about the amount of adsorbed peptide or its structure. QCM-D was used to examine the behaviour of Aβ peptides when in contact with surfaces that exhibit different hydrophilicity and charge.

In Figure 3.12 is shown the adsorption of Aβ40 and Aβ42 to QCM-D gold crystals covered with polystyrene (third overtone) at room temperature. Both peptides adsorb onto the hydrophobic surface, as can be seen by the change in the resonance frequency of the crystals, Δf, which exhibits negative values indicating that the mass of the QCM-D crystal sensor has increased. Moreover, it is clear that after rinsing with buffer, not much of the adsorbed layer is removed, so most of the material stays attached to the crystal.

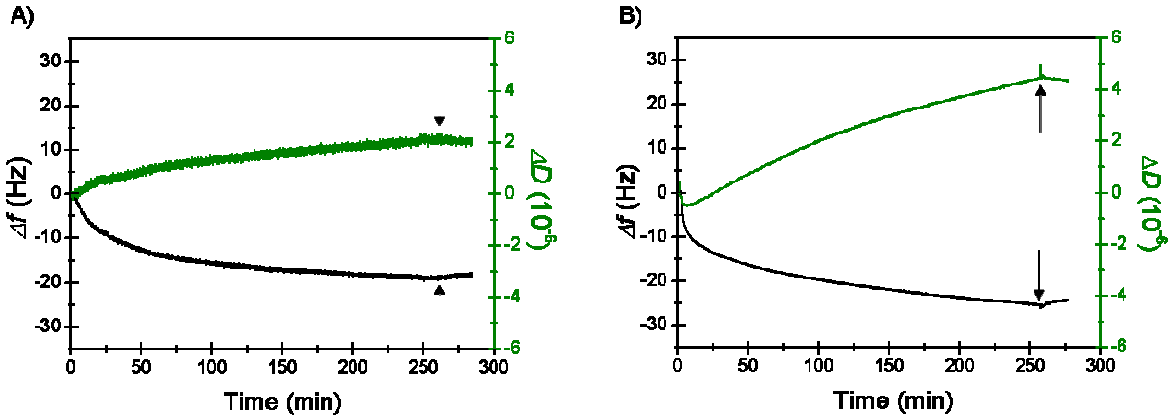


Figure 3.12. Adsorption of A) Aβ40 and B) Aβ42 50 μM in PBS to polystyrene coated surface at 22°C measured as changes in frequency, Δf (left axis, black line), and dissipation, ΔD (right axis, green line), of the QCM-D as a function of time. The arrows indicate rinsing with buffer after adsorption.

The AFM imaging of the QCM-D crystal sensor (Figure 3.13) shows that after rinsing there is a significant amount of peptide on the surface but its morphology is different for Aβ40 and Aβ42.

While in the case of Aβ40 all we can see are amorphous aggregates, for Aβ42, the same adsorption time (~4 hours) was enough to induce fibril formation on the hydrophobic polystyrene surface. This is not surprising considering that the longer alloform has two additional amino acid residues with hydrophobic character, Ile41 and Ala42, that significantly increase the contacts within the C-terminus and between the C-terminus and the CHC, shifting the conformational equilibrium of Aβ42 towards β structure that has an increased propensity to oligomerize and consequently to form fibrils [103].

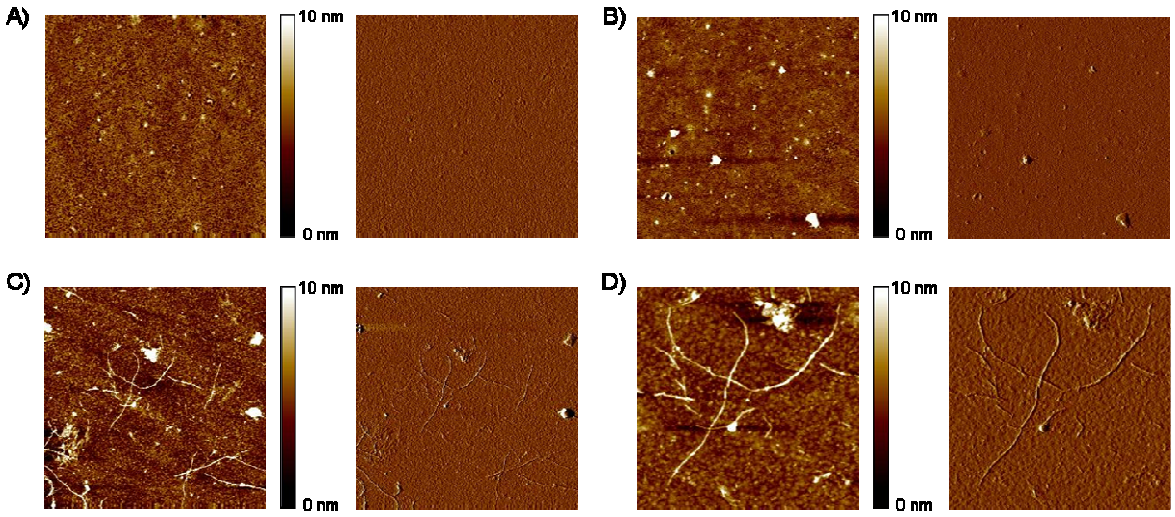


Figure 3.13. AFM imaging of polystyrene covered gold crystals. A) polystyrene surface; B) Aβ40 50 µM in PBS; C) and D) Aβ42 50 µM in PBS. The image size is 5×5 μm^2 x-y in A), B) and C) and 3×3 μm^2 x-y in D). The z-range is 10 nm.

Figure 3.14 shows the adsorption of Aβ40 and Aβ42 to QCM-D gold crystals covered with SiO_2 at room temperature. It is clear that Aβ40 adsorbed in much less extent (Δf of only about -10 Hz) than in the case of the polystyrene surface. If we look at the adsorption behaviour of Aβ42, the "amount" of adsorbed peptide (Δf ~ -25 Hz after 4 hours) does not look much different than in the case of the hydrophobic polystyrene substrate, but when the sensor crystal was rinsed with buffer material desorbed, as shown by the very fast *f* and *D* decrease, indicating that the affinity to the hydrophilic surface was lower.

The AFM images (Figure 3.15) support this assumption. In the case of Aβ40 there is almost no material left on the surface after PBS rinsing while for Aβ42 oligomers are observed at the surface. Probably these structures are not strongly attached to the surface.

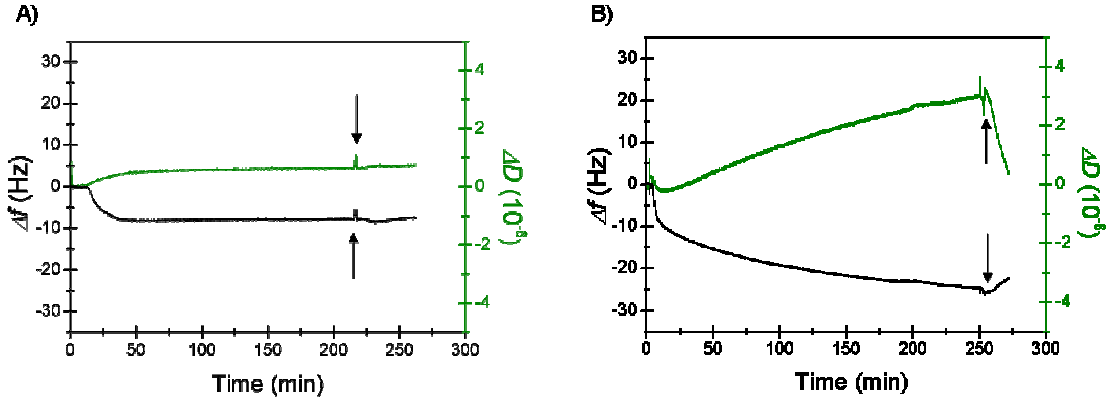


Figure 3.14. Adsorption of A) Aβ40 and B) Aβ42 50 μM in PBS to SiO_2 coated surface at 22°C measured as changes in frequency, Δf (left axis, black line), and dissipation, ΔD (right axis, green line), of the QCM-D as a function of time. The arrows indicate rinsing with buffer after adsorption.

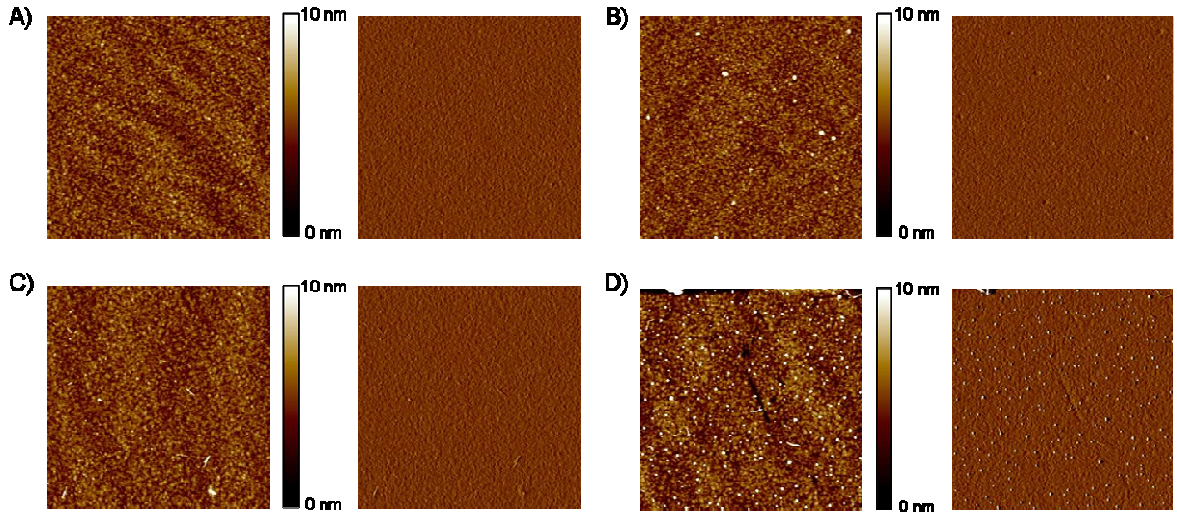


Figure 3.15. AFM imaging of SiO_2 covered gold crystals. A) SiO_2 surface; B) and C) Aβ40 50 μM in PBS; D) Aβ42 50 μM in PBS. The image size is 5×5 μm^2 x-y and the z-range is 10 nm.

3.3.2. Adsorption of Aβ Peptides on Positively vs Negatively Charged Surfaces

In order to check the adsorption behaviour of Aβ to oppositely charged surfaces, surfaces having either the positively charged PAH ($PEI(PSS/PAH)_6$) or the negatively charged PSS ($PEI(PSS/PAH)_6PSS$) as the last layer, were prepared by LbL deposition [201]. In the case of the QCM-D measurements the preparation of the surfaces was done *in situ* just before the measurement and the curves corresponding to the build up of the structures are illustrated in

Figure 3.16. There are some aspects that are worth to analyze such as the swelling mechanism and structural properties of the polyelectrolyte substrates. The complexation of anionic and cationic polyelectrolytes at the surface is accompanied by a regular increase in the adsorbed amount and in the layer thickness as more layers are deposited on the surface. The energy dissipation *D* and the differences between the overtones are fairly small during PSS and PAH adsorption. On the other hand, after PAH adsorption, during rinsing with pure water, the *D* values increase drastically, showing a very high discrepancy between overtones, and *f* decreases. The contrary happens in the rinsing step after PSS adsorption, *D* decreases and the overtones are nearly the same, while *f* increases. So at first glance it looks like the rinsing procedures lead to (i) a loss of mass after PSS adsorption and (ii) an increase of mass after PAH adsorption. But what happens are transitions from a rigid to a soft layer, alternately. PAH is a less strong polyelectrolyte and has a more extended conformation and after water rinse the chains are more flexible, exhibiting a viscoelastic behaviour. Besides, more water molecules will be immobilized within the adsorbed layer and thus the *f* decrease. PSS adsorption and rinse lead to a compaction, or to a decrease in the mobility of the polymers in the layer, that probably exhibit in this case a much greater interpenetration which causes water release from the structure and thus an increase in *f*.

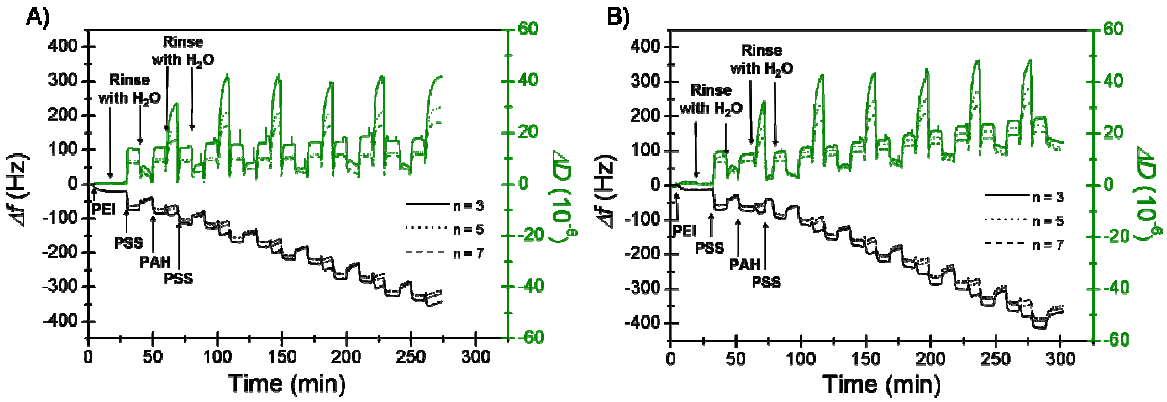


Figure 3.16. Construction of A) PEI(PSS/PAH)$_6$ and B) PEI(PSS/PAH)$_6$PSS multilayers monitored by QCM-D. The third, fifth and seventh overtones are shown.

This is a good example to demonstrate the advantages of modeling the QCM-D data in order to obtain information about the layer properties. In Figure 3.17 A is represented the thickness of the adsorbed layer calculated using the linear Sauerbrey equation for the third, fifth and seventh overtones. The film thickness increases linearly, following the shape of the QCM-D curves for Δ*f*, since it was calculated only from the frequency values without taking into account the Δ*D* values which, as described above, can reveal some interesting aspects about the behaviour of the system

concerning its viscoelastic properties. By applying the Voight model to the data (Figure 3.17 B), it is clear that film thickness increases linearly with the number of bilayers and that the growth is also linear if we consider each different step individually, PSS and PAH adsorption and rinsing. Looking, for instance, at the values obtained after water rinse when PAH is the outer layer, one can see that the thickness calculated using the Sauerbrey equation is underestimated. Moreover, it is also clear that the thickness determined using the Sauerbrey equation (Figure 3.17 A), when compared to the plots in Figure 3.17 B, has more similarities with the values obtained after pure water rinse when PSS in the outer layer, after PSS and PAH adsorption and at last with the step of rinsing after PAH adsorption. So the discrepancies increase with the decreasing rigidity of the layer.

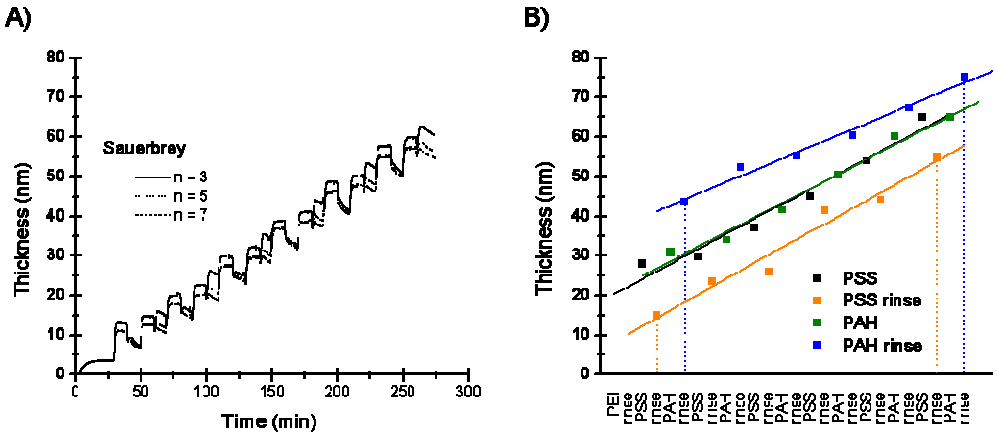


Figure 3.17. Layer thickness during polyelectrolyte multilayer construction followed by QCM-D. A) Sauerbrey equation applied to the third, fifth and seventh overtones. B) Voight modeling.

The advantage of using polyelectrolytes as charged hydrophilic surfaces is their high charge density. The zeta potential values for the polyelectrolytes were determined to be -20 mV for PSS as the outer layer and +20 mV for PAH as the outer layer after the deposition of three to four layers. The contact angles of water on the polyelectrolyte films depend on the number of adsorbed layers but a trend clearly shows a lower contact angle for multilayers with PSS as the outermost layer, that is, the PAH surface is more hydrophobic than the PSS surface [209, 210]. One explanation is the higher charge density of PSS as a strong polyelectrolyte compared with PAH as a weak polyelectrolyte. The pK values for PAH were estimated to be in the range between 9 and 10 and between 3.5 and 4.5 for PSS [211], so in the pH range of the experiments both are fully ionized. In our systems, the contact angles are 45º for PSS and 65º for PAH.

After the construction of the precursor multilayers $PEI(PSS/PAH)_6$ and $PEI(PSS/PAH)_6PSS$ the surfaces were brought to contact with Aβ40 solutions in water or PBS. The adsorption of the

peptide onto PSS and PAH-terminated films was followed by QCM-D and ATR-IR. Figure 3.18 shows representative QCM-D measurements. A) and B) correspond to Aβ40 (in water) adsorption on PEI(PSS/PAH)$_6$PSS and PEI(PSS/PAH)$_6$, respectively. There is a slight difference between the two measurements but it does not seem to be very significant. On the PSS-terminated surface the adsorption of the peptide leads to a Δf of ~ -7 Hz after 15 hours, and ΔD is lower than 10^{-6}. The values reached after the same time for the PAH-terminated surface are similar. In the same figure, C) and D) show the same experiment but the peptide is in a buffered salted solution. In this case, for the positively charged surface Δf is ~ -40 Hz after 15 hours and ΔD 4×10^{-6} while for the negatively charged surface there is a difference of ~25% (-30 Hz) on the observed frequency decrease.

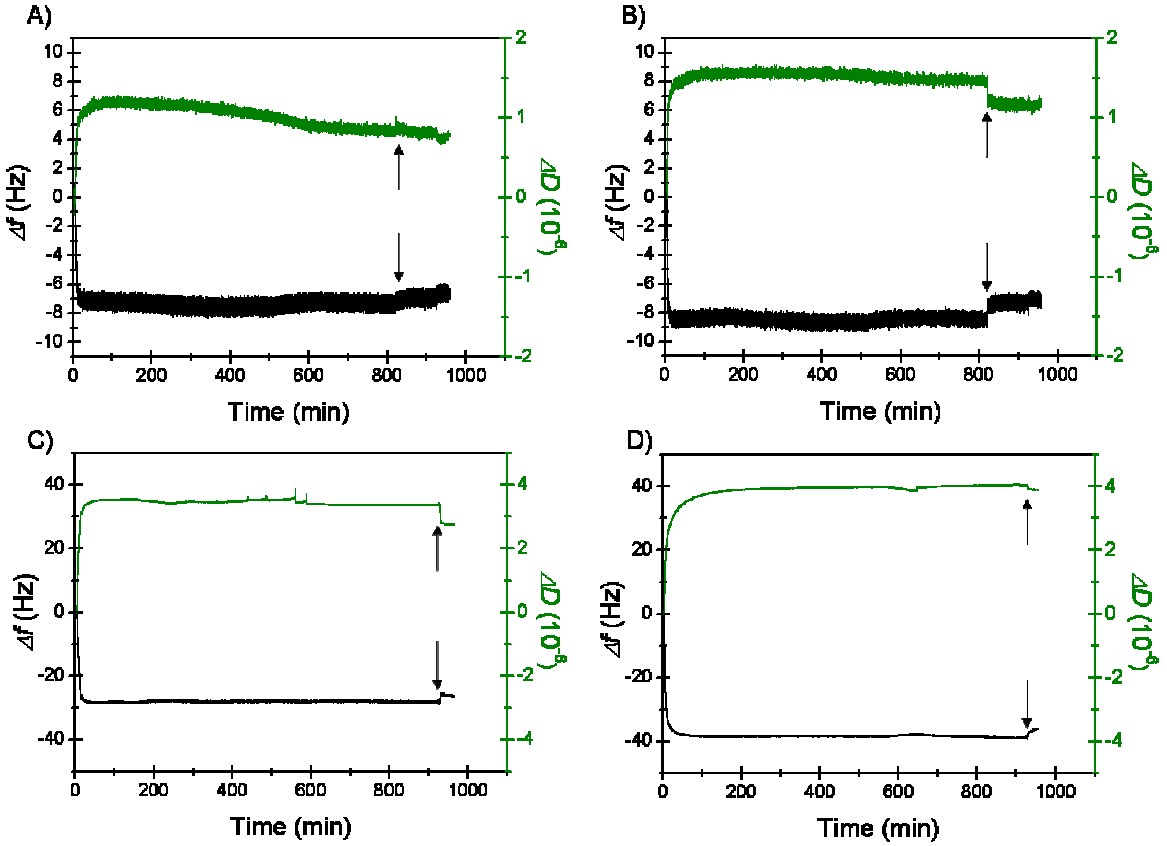


Figure 3.18. Adsorption of Aβ40 on polyectrolyte multilayer coated QCM-D gold crystals followed by QCM-D at 22°C, as changes in frequency, Δf (left axis, black line), and dissipation, ΔD (right axis, green line), as a function of time. The arrows indicate rinsing with buffer after adsorption. Aβ40 50 μM A) in water on PEI(PSS/PAH)$_6$PSS; B) in water on PEI(PSS/PAH)$_6$; C) in PBS on PEI(PSS/PAH)$_6$PSS and D) in PBS on PEI(PSS/PAH)$_6$.

From these results, it seems that even though the difference is small, specially if the peptide is in PBS the affinity is higher to the PEI(PSS/PAH)$_6$ substrate that, besides being positively charged, is also more hydrophobic as described above.

The QCM-D crystals were imaged with AFM after Aβ40 adsorption (Figure 3.19). One aspect, which can be directly observed, is that the PAH-terminated surface is rougher. The interaction between proteins or peptides and surfaces is strongly influenced by parameters such as surface energy, roughness and chemical composition. So in addition to the chemical nature of the surfaces this aspect should be also taken in consideration. Since QCM-D monitoring of the polyelectrolyte multilayer construction showed that the PAH exhibits a higher chain flexibility this might lead to a more disorganized surface upon N_2 drying.

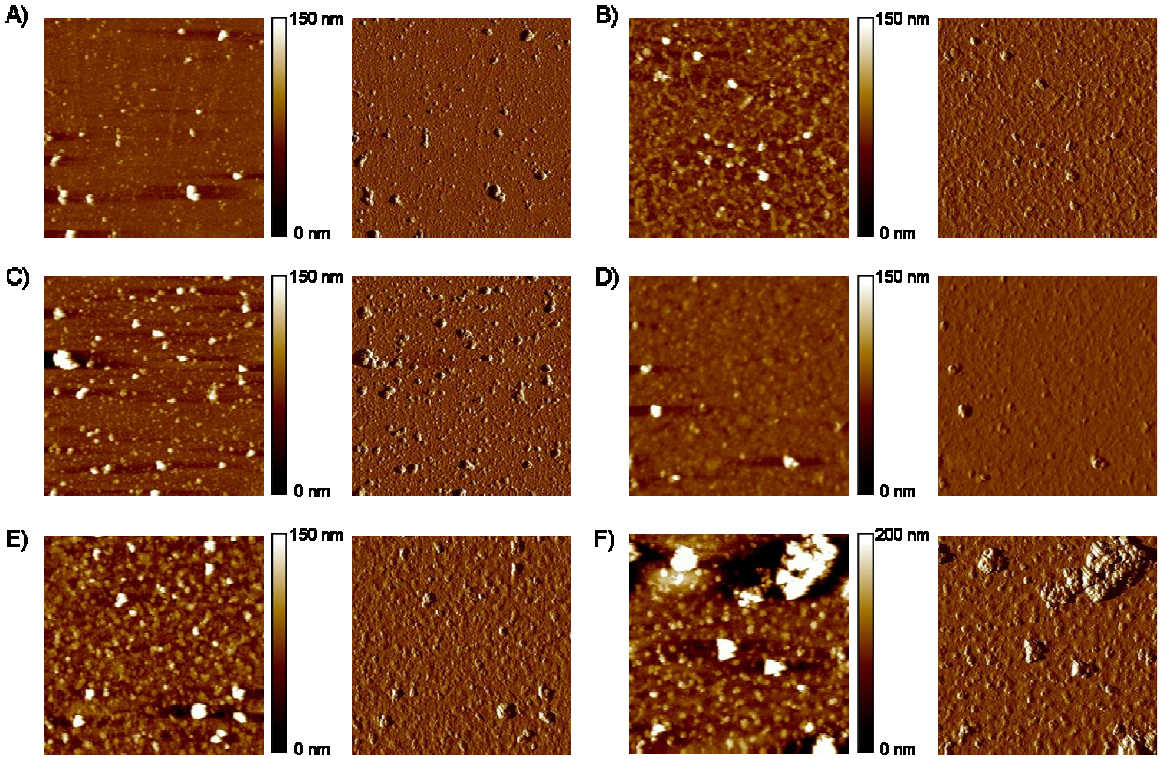


Figure 3.19. AFM imaging of Aβ40 adsorbed onto polyelectrolyte multilayer coated QCM-D gold crystals. The image size is 5×5 μm^2 x-y. A) Aβ40 50 µM in water on $PEI(PSS/PAH)_6PSS$; B) Aβ40 50 µM in water on $PEI(PSS/PAH)_6$; C) and D) Aβ40 50 µM in PBS on $PEI(PSS/PAH)_6PSS$; E) and F) Aβ40 50 µM in PBS on $PEI(PSS/PAH)_6$.

The IR spectrum of a peptide provides important information on structure and environment of the backbone and of the amino acid side chains. As a valuable tool ATR-IR spectroscopy represents a surface sensitive, integral method enabling *in situ* studies of processes at relevant surfaces on the molecular level. It is used for the analysis of material surfaces, so it is possible to get information about the structure of surface-bound peptides. This technique has the sensitivity required to observe the amide I and amide II vibration to obtain structural information. Moreover, information is obtained in the spectral region where the side chains of amino acid residues are known to

contribute [196]. The amide III region is rarely considered for secondary structure determination since it is very complex.

The adsorption of Aβ40 (5 μM solution in ultrapure H_2O) above the polyelectrolyte-coated Ge IRE was monitored and the evolution of the IR spectrum in the region 1800-1200 cm^{-1} due to adsorption onto $PEI(PSS/PAH)_6$ is shown if Figure 3.20 A. Three main absorbance bands are present, the first is centered at ~1628 cm^{-1} (correspondent to the amide I that characterizes the C=O stretch vibration), the second is a broad band centered at ~1560 cm^{-1} (amide II, N—H bending vibration) and the third band appears at 1400 cm^{-1}. There is also a fourth band at 1315 cm^{-1} (amide III). All of these bands have an increasing intensity with adsorption time until a certain point when the absorbances reach a constant value. Figure 3.20 B illustrates the time course of the absorbance at 1628 cm^{-1} during absorption of the peptide on $PEI(PSS/PAH)_6$ and $PEI(PSS/PAH)_6PSS$. This frequency was chosen since it is an indicator of the presence of β-sheet structure. In both cases, the absorbance reaches a constant value already after 8 minutes. However, in the case of the negatively charged surface the maximum value observed is only approximately half of that for the positively charged surface. This means that more peptide is adsorbed on the $PEI(PSS/PAH)_6$ surface in a β-sheet structure.

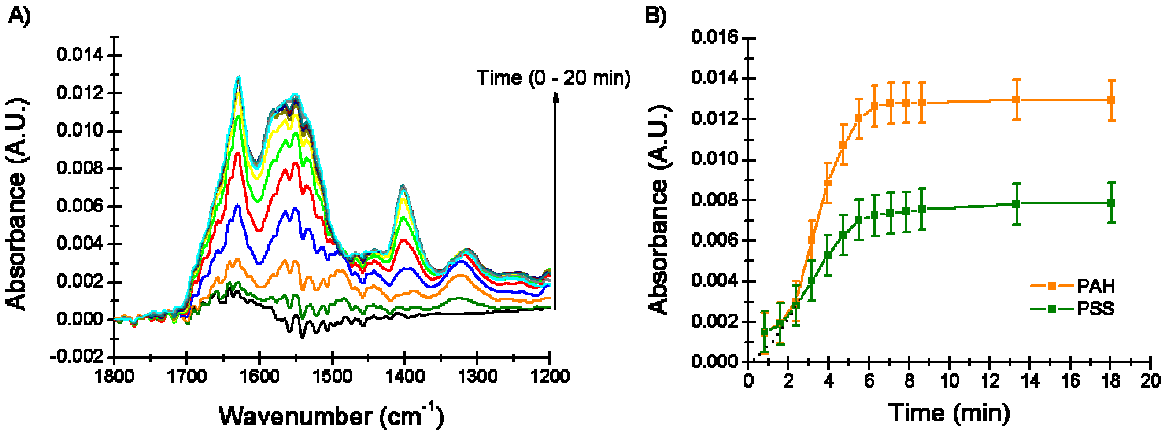


Figure 3.20. Adsorption of Aβ40 from a 5 μM solution in H_2O on polyelectrolyte coated Ge IREs. A) Evolution of the IR spectrum of Aβ40 in the region 1800-1200 cm^{-1} due to adsorption onto $PEI(PSS/PAH)_6$. B) Time course of the absorbance at 1628 cm^{-1} during absorption of the peptide on $PEI(PSS/PAH)_6$ and $PEI(PSS/PAH)_6PSS$.

Figure 3.21 shows the IR spectra obtained after Aβ40 adsorption and additional rinsing with water and NaCl to remove non-adsorbed peptide and, in the case of NaCl, to disrupt electrostatic interactions. If PAH is the outer layer, the absorbance decreases with water rinsing showing that the peptide is partially washed off. Even after NaCl and further water rinses, the band centered at 1628

cm^{-1}, that is indicative of the presence of β-sheet secondary structure, is still present. But the bands characteristic for antiparallel β-sheet and aggregated strands are not present. This is consistent with the amorphous aggregates observed by AFM (Figure 3.19 E and F). After Aβ40 adsorption on PSS, defined bands are not observed, with exception of the one at 1400 cm^{-1} (Figure 3.21 B). The band at 1630 cm^{-1}, that is very pronounced in the former case, appears as well but has a small shoulder at higher frequency (~1650 cm^{-1}) which can be attributed to an unordered conformation and/or α-helical structure. So it is reasonable to say that there is a mixture of several structures and, after NaCl rinsing almost no material was left.

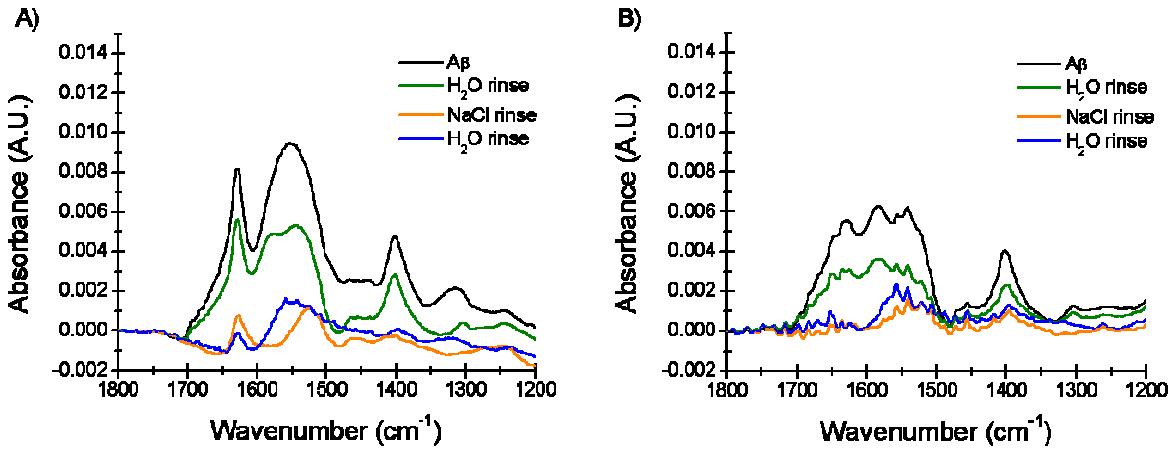


Figure 3.21. Evolution of the IR spectrum of Aβ40 from a 5 μM solution in H_2O in the region 1800-1200 cm^{-1} due to adsorption on A) $PEI(PSS/PAH)_6$ and B) $PEI(PSS/PAH)_6PSS$.

3.3.2. Interaction of Aβ Peptides with Supported Lipid Bilayers

A molecular understanding of the interaction of peptides and proteins with lipid bilayers requires experimental knowledge of the structure of the membrane bilayer, the transbilayer location of bound peptides, the structures adopted by the peptides, and the changes that occur in the bilayer structure as a result of partitioning. Because cellular membranes must be in a fluid state for normal cell function, it is the structure of fluid bilayers that is relevant for the understanding of the interactions with peptides.

Several investigations have been done concerning the transformation of lipid vesicles to SLBs in aqueous media in contact with SiO_2 surfaces. Seantier *et* al. [212] have distinguished two mechanistic pathways for SLB formation from dimyristoylphosphatidylcholine (DMPC) vesicles depending on the experimental parameters. The first pathway occurs when there is not a minimum in Δf and ΔD has a small value indicating that vesicles seem to break after a short interaction time

with the surface. This pathway is preferential, for instance, in the absence of salts when strong vesicle-surface interactions (van der Waals and electrostatic) take place, favoring a greater contact area and destabilizing the vesicles, which leads to a fast rupture process. However, the rate of SLB formation is slow which can be due to electrostatic repulsions.

The addition of salts modifies the pathway of SLB formation. With increasing ionic strength, the properties of the vesicle membrane and of the surface change due to charge shielding by electrostatic interactions. Thus, lower adhesion strength between the surface and the lipids stabilizes the vesicles on the surface. In these conditions, the adsorption of vesicles takes place until a critical density of vesicles on SiO_2, Θ_c, is reached, followed by their rupture and the SLB formation (Figure 3.22). These classical QCM-D curves suggest that the transition of intact vesicles to SLB seems to be caused by a combination of vesicle-surface and vesicle-vesicle interactions.

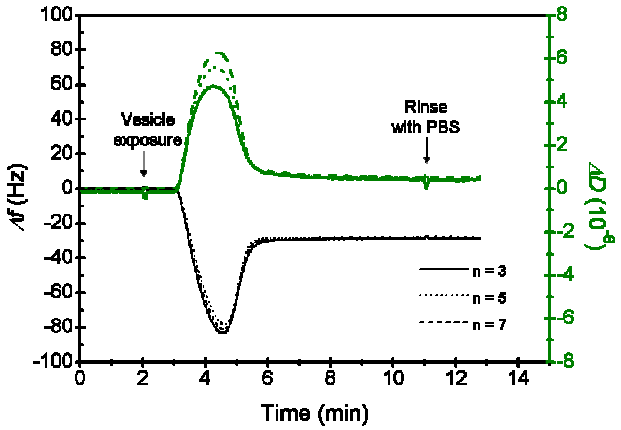


Figure 3.22. Typical QCM-D curves (for the third, fifth and seventh overtones) of SLB formation on SiO_2 displayed as Δf (left axis, black lines) and ΔD (right axis, green lines) from 0.2 mM egg PC vesicles (60 nm mean diameter) in PBS.

From the analysis of the curves shown in Figure 3.22 one can distinguish different stages:

1. Injection of SUVs initiates the irreversible adsorption of intact vesicles on the SiO_2 surface (t ~3 min) indicated by the decrease of f and the increase of D, as a result of the addition of relatively soft vesicles (high energy loss) on the sensor crystal surface.
2. At critical surface coverage Θ_c (t ~4.5 min), coalescence and rupture of vesicles gradually overcome the adsorption by releasing the water trapped inside and between the vesicles, reflected by the transitional cusps in Δf and ΔD. As vesicles continue to rupture and spread into planar bilayers (t = 5–6 min), f increases and D decreases, as a result of the formation of relatively rigid bilayers (lower energy loss) on the crystal surface.

3. Finally, a stable bilayer is formed (t > 6 min), showing steady Δf and ΔD without change after rinsing with buffer.

To interpret the QCM-D results, the Sauerbrey equation can be employed to calculate the mass adsorbed on the crystal surface, since after bilayer formation the adsorbed layer is supposed to be homogeneous and rigid (ΔD is close to zero). The mass obtained is ~500 ng·cm^{-2}. Moreover, using the software Q-Tool from the QCM-D supplier, the thickness of the lipid bilayer can be determined as well and it is ~5 nm. This value is close to the thickness determined using other methods [213]. The plots of the thickness and areal mass obtained employing the Sauerbrey equation for the process of SLB formation are shown in Figure 3.23.

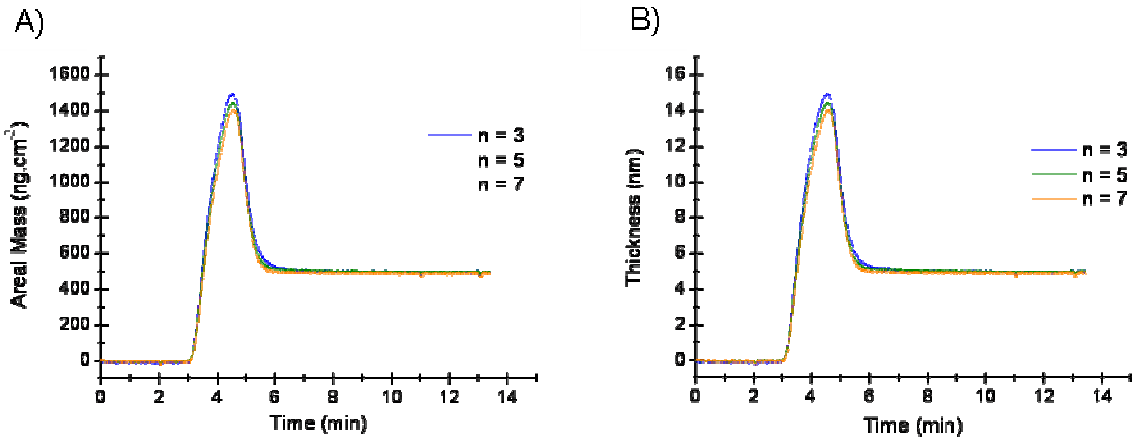


Figure 3.23. Thickness A) and areal mass B) calculated employing the Sauerbrey equation for the process of SLB formation monitored by QCM-D (for the third, fifth and seventh overtones).

AFM was also employed to monitor the bilayer formation, but it has some limitations as the inability to follow the adsorption kinetics in real time or the complex interactions between vesicles, SLB patches, the surface, and the imaging tip [214]. Also it is difficult to obtain accurate AFM estimates of vesicles and SLB coverage after rupture has begun because of both the rate at which the transformation proceeds and the increased risk of modifying the presumably metastable state of the system with the AFM probe (the "snapshots" shown in Figure 3.24 were always taken in the same spot). Moreover, after the desired exposure times, there was no exchange with pure buffer so non adsorbed vesicles were not removed contrarily to the QCM-D measurement that was done always with flow. Reihmult *et* al. [214] have deconvoluted AFM images and calculated a deformation ratio of 2:1 (width-to-height ratio), so we can assume that in Figure 3.24 the formation of patches of bilayer from vesicles with a mean diameter of 30 nm is observed on the SiO_2 surface.

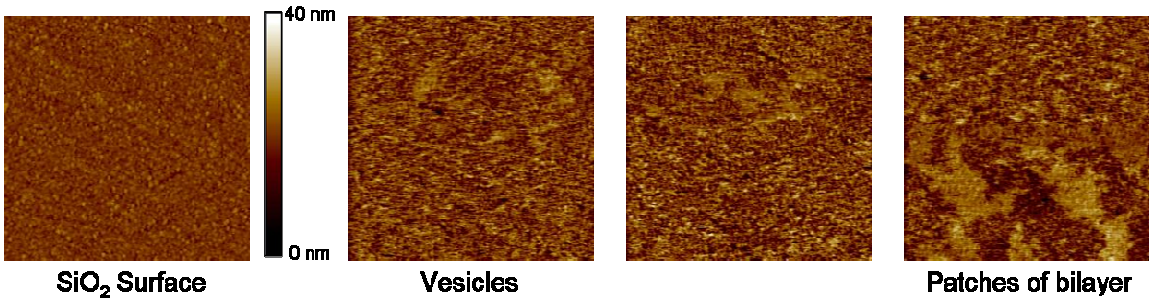


Figure 3.24. "Snapshots" of the SLB formation process for egg PC vesicles (60 nm mean diameter) on SiO_2 by AFM. The image size is 5×5 μm^2 x-y and the z-range is 40 nm.

On Figure 3.25 we can see that the kinetics of SLB formation is dependent on the concentration of the vesicles but the pathway of SLB formation is concentration independent. By increasing the concentration, the kinetics of SLB formation is accelerated since Θ_c is reached faster but the pathway stays the same [212]. The process of bilayer formation has been shown to be autocatalytic, meaning that SLB islands promote the rupture of intact vesicles on the surface, increasing the rate of SLB formation [203]. An informative way of analyzing the data is to plot ΔD versus Δf (Figure 3.25 B) which removes the time as an implicit parameter. A "cusp like" curve is obtained that is characteristic for the SLB formation process. Its shape defines clearly each step (adsorption and rupture of vesicles and bilayer formation) of the SLB construction mechanism.

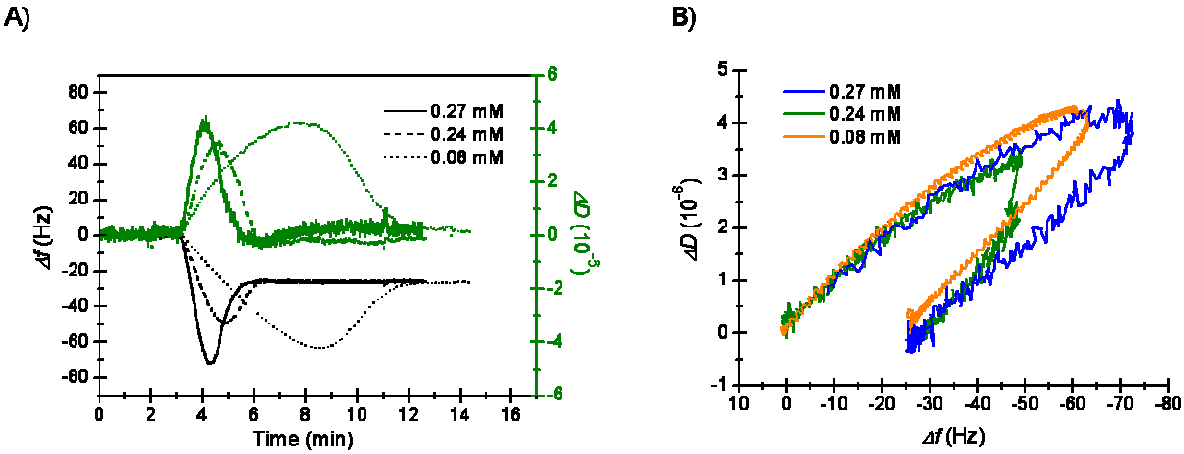


Figure 3.25. Dependence of SLB formation on vesicle concentration. A) QCM-D curves of SLB formation on SiO_2 displayed as Δf (left axis, black lines) and ΔD (right axis, green lines) from egg PC vesicles (60 nm mean diameter) in PBS. B) Plot of ΔD versus Δf.

The QCM-D results for vesicle fusion and bilayer formation of 100 mol% of egg PC and for vesicles composed of lipid mixtures with different compositions are shown in Figure 3.26.

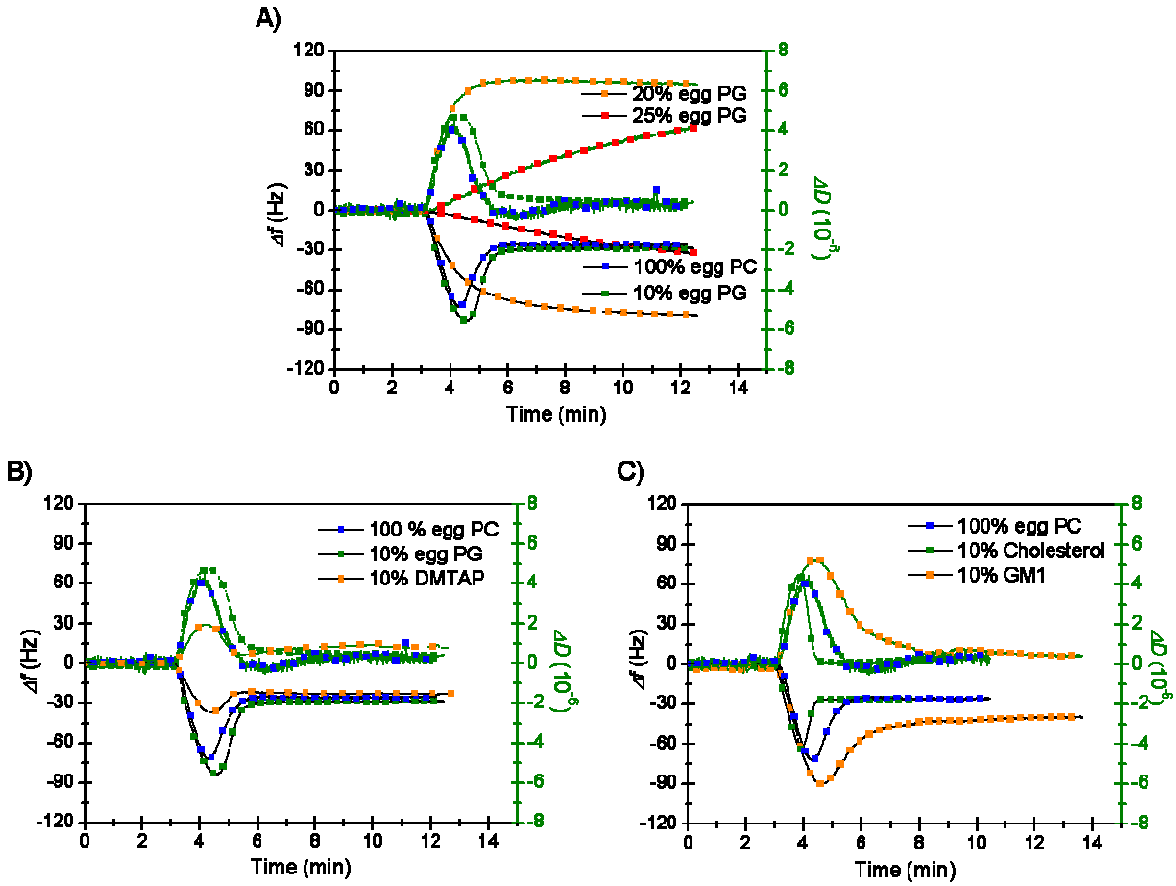


Figure 3.26. Changes in frequency, Δf (left axis, black lines) and dissipation, ΔD (right axis, green lines) as a function of time due to adsorption of vesicles with different mol% of lipids on SiO_2. A) Incorporation of different mol% of egg PG. B) Incorporation of 10 mol% of egg PG or DMTAP. C) Incorporation of 10 mol% of cholesterol or GM1.

Qualitatively, all ΔD and Δf curves followed the typical vesicle fusion behaviour on the SiO_2 surface as in Figure 3.21. However (Figure 3.26 A), when a percentage higher than 10% of egg PG was incorporated in the egg PC vesicles, it was not possible to form bilayers on SiO_2. This is not surprising since this is a negatively charged surface and thus, when the number of negative charges increases, the affinity to the surface decreases due to electrostatic repulsion. For 20 and 25% of egg PG, bilayers are not formed and for the last the adsorption of vesicles is dramatically lower. So for comparison purposes this was the percentage of other components incorporated in the egg PC vesicles in order to form SLBs. Vesicle charge is determinant and for the positively charged DMTAP component the SLB formation almost follows the previously described first pathway, vesicles start to rupture very soon after adsorption to the SiO_2 surface (Figure 3.26 B). Lipid fluidity is a distinctive feature of cell membranes. Increasing the cholesterol content leads to increased membrane rigidity and this seems to influence the kinetics of SLB formation as depicted on Figure 3.26 C. On the other hand, with incorporation of GM1 in the egg PC vesicles, the process becomes slower. GM1, besides

being negatively charged reduces the affinity to the SiO_2 surface. It is also a bigger molecule (MW 1,563.9) and, after SLB formation, the "standard" value for Δf of -25 to -30 Hz decreases to ~-40 Hz, due to the increased mass on top of the crystal.

Many studies exist concerning the interactions of Aβ peptides with model lipid bilayers and monolayers [215, 216, 217]. However, most of them concern the Aβ40 and phospholipids with defined fatty acid chain. Phospholipids are the main component of biomembranes, and PC is the major membrane phospholipid in eukaryotic cells. So egg PC, a natural product where the fatty acid chains vary is an appropriate model for membrane studies. The interaction of Aβ peptides, both Aβ40 and Aβ42, with SLBs only constituted by this zwiterionic lipid mixture was verified by QCM-D, and the results are displayed in Figure 3.27 A. Obviously, the peptides have different affinities for the purely zwiterionic bilayer. While Aβ40 does not cause any change in the frequency of the resonant crystal (Δf ~2 Hz), Aβ42 decreases the frequency in a gradual way that stabilizes after 2 hours. A change in the dissipation factor D is also observed, and after washing with PBS some material is washed out, indicating there is at least some reversible adsorption. It has been proposed from molecular dynamics simulations that Aβ40 and Aβ42 exist in solution in different conformational states due to the two additional Ile41 and Ala42 [103]. Denaturation profiles for both peptides were determined and for Aβ42 one apparent transition was found, with data fitting either a two-state trimer to unfolded monomer model (Tri ↔ 3U) or tetramer to unfolded monomer model (Tetra ↔ 4U). For Aβ40, the profile was accurately fitted by a two-state model (N ↔ U), where a folded, or native, monomer and an unfolded or denatured monomer are present in equilibrium [102]. So Aβ42 exists in solution in an equilibrium that involves oligomeric species while Aβ40 exists as a monomer. The difference between the behaviours of the peptides when in contact with the egg PC SLBs is attributable to the different conformational and oligomeric states and will be discussed in more detail.

The state at which Aβ42 is most likely to interact with the cell membrane is an important issue. In order to test this, a solution of freshly prepared Aβ42 and a solution aged for 6 days were compared in respect to the interaction with egg PC bilayers. After this period the peptide is already in a fibrillar state [184]. It can be seen that the interaction is again quite different (see Figure 3.27 B). For the aged solution, Δf exhibited a lower absolute value, indicating there is less material adsorbed on the surface. Moreover, the dissipation values D are more or less constant, so the fibrils seem to contribute slightly to a decrease in the frequency of the resonant crystal but the effect on the membrane structure is negligible. From the previous results, it is concluded that freshly prepared Aβ42, already containing oligomers, is the only sample able to interact in a significant way with the

zwiterionic egg PC SLB. So further experiments concerning Aβ42 interaction with SLBs with different compositions were performed.

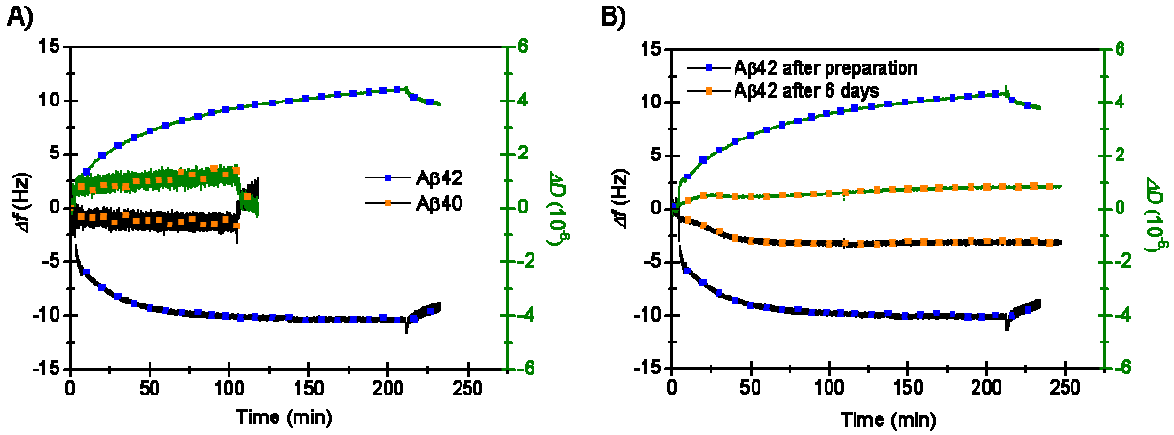


Figure 3.27. Interaction of Aβ peptides (50 μM in PBS) with egg PC SLBs monitored by QCM-D at 22°C, as changes in frequency, Δ*f* (leftt axis, black line), and dissipation, Δ*D* (right axis, green line), as a function of time. A is obtained from fresh Aβ peptides solution, B compares fresh Aβ42 with a solution aged for 6 days.

The interaction of Aβ42 with egg PC bilayers that have 10 mol% of other substances was checked (Figure 3.28). The limitation to include more than 10 mol% of other substances is due to the impossibility of forming SLBs in SiO_2 surfaces if this percentage is increased, and this was particularly notorious for the negatively charged lipids egg PG and GM1. Egg PG is negatively charged and prepared from egg PC by transphosphatidylation by the action of phospholipase D, so its fatty acid composition is the same, and consequently the fluidity of the SLB will also be similar. DMTAP is positively charged and a relatively small molecule. In Figure 3.28 A is shown the QCM-D response when Aβ42 was brought in contact with egg PC SLBs containing 10 mol% of egg PG or DMTAP. Two effects are directly perceptible: (i) there is more peptide adsorbed on the DMTAP containing bilayers than in the case of egg PG incorporation and (ii) the presence of charged molecules induces an irreversible adsorption of Aβ42 on the surface of the bilayer which can not be removed by washing with PBS. But there are other aspects worth to consider. For DMTAP the initial adsorption is fast, and this suggests a strong attraction between the SLB and the Aβ42 oligomeric species. Considering the pI of the peptide (5.2) this is not so surprising, even though all the measurements were done in high ionic strength (150 mM) so the counter ions should at least partially shield the charges thus reducing electrostatic interactions.

Links between cholesterol, Aβ and AD have been reported [218, 219]. There are evidences that in the presence of Aβ cell viability decreases either in the presence of both sialic acid and cholesterol or sialic acid alone, indicating that GM1 is an essential factor in inducing cytotoxicity

[217]. Figure 3.28 B shows the QCM-D response when 10 mol% of GM1 or cholesterol were incorporated in the egg PC SLB. In the case of the SLB with 10 mol% GM1, the peptide adsorption was very similar to that on the pure PC bilayer but with the clear difference that the material is not removed after PBS rinsing. Cholesterol, on the other hand, seems to decrease the amount of material adsorbed. All these aspects will be discussed in detail in the next section.

It should be always kept in mind that in any case the peptide may go through a structural conversion and aggregation that leads to some degree of irreversible adsorption and to variations of the dissipation values due to rearrangement that might affect both peptide and SLB.

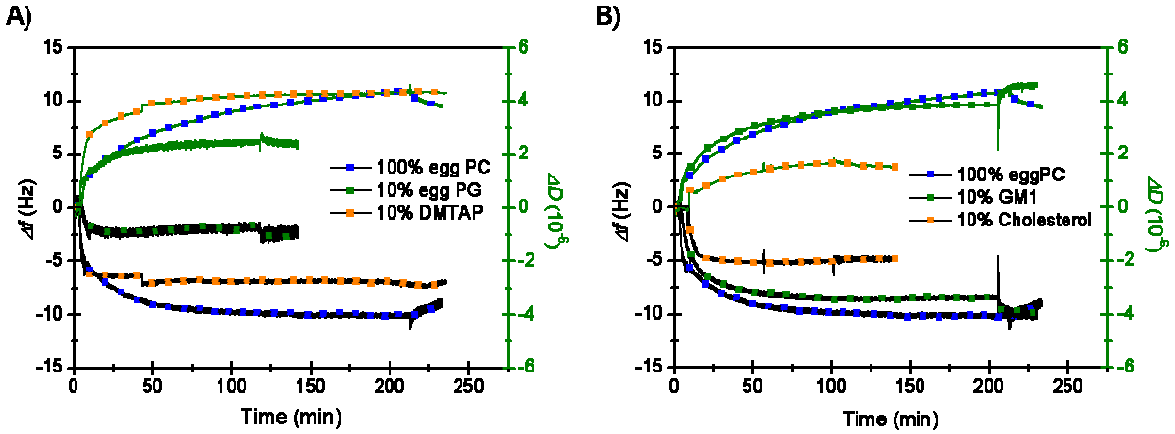


Figure 3.28. Interaction of Aβ42 (50 μM in PBS) with egg PC SLBs with 10 mol% of other constituents monitored by QCM-D at 22°C, as changes in frequency, Δ*f* (leftt axis, black line), and dissipation, Δ*D* (right axis, green line), as a function of time.

3.4. Discussion and Conclusions

Aβ, a 4 kDa amphiphilic peptide of 39 to 43 amino acid residues is a major fibrillar component of neuritic plaques in AD brains and is related to the pathogenesis of the disease. Aβ is a proteolytic product of the transmembrane protein APP and, due to its amphipathicity, it may be retained in the membrane, and this has been shown to be crucial for the cytotoxic activity exhibited by Aβ peptides. Hydrophobic and electrostatic interactions strongly influence its conformation and aggregation both in solution and at interfaces. By choosing appropriate solid sorbent surfaces it is expected to contribute to the understanding of the different interactions independently. In this effort, QCM-D, AFM and ATR-IR were employed for the investigation of the behaviour of Aβ peptides on solid planar surfaces, which include model lipid bilayers.

Since Aβ peptides are amphiphilic, the first model surfaces studied exhibited different hydrophilicity. QCM-D gold crystals covered with SiO_2 and polystyrene were chosen as models of hydrophilic and hydrophobic surfaces, respectively (Figure 3.29). The surfaces of silicon substrates bear an oxide layer with siloxane bonds (Si—O—Si) that, when in contact with water or air, switch to silanol groups (Si—OH), producing a hydrophilic surface. After the cleaning procedures described, which includes UV/ozone treatment, the SiO_2 surface is saturated with silanol groups. Above pH 2, the oxide surface is negatively charged and the charge density is almost constant over pH 3–8 [220]. Polystyrene is a vinyl polymer. Structurally, it is a long hydrocarbon chain, with a phenyl group attached to every other carbon atom. Polystyrene is produced by free radical vinyl polymerization, from the monomer styrene [221]. Unmodified polystyrene surfaces are hydrophobic and only bind biomolecules through passive hydrophobic interactions.

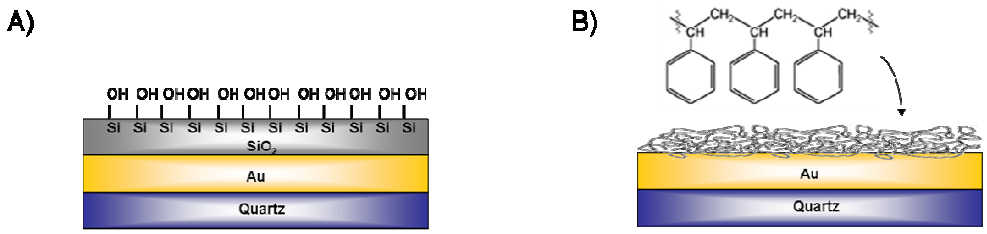


Figure 3.29. QCM-D AT-cut quartz crystal coated with gold and with a layer of A) SiO_2 and B) polystyrene.

QCM-D measurements have shown that Aβ peptides (50 μM in PBS) strongly adsorb to hydrophobic polystyrene surfaces. Aβ40 adsorbs in less extent and forms amorphous aggregates

while Aβ42 fibrillates as proved with AFM imaging. Aβ42 oligomers adsorb weakly to hydrophilic SiO_2 surfaces while for Aβ40 no material remained on the SiO_2 surface after PBS rinsing. The presentation of the QCM-D data as a plot of the energy dissipation versus the change in the frequency, makes it possible to directly compare the ratio between Δ*D* and Δ*f*, or the induced energy dissipation per coupled unit mass [222]. One is able to see directly the influence of the protein adsorption on the damping of the crystals and thus infer viscoelastic properties of the adsorbed layer. For example, a low Δ*D*/Δ*f* value indicates mass addition without significant dissipation increase, which is characteristic of a fairly rigid layer. In contrast, a large Δ*D*/Δ*f* value signals a soft, dissipative film (Figure 3.30).

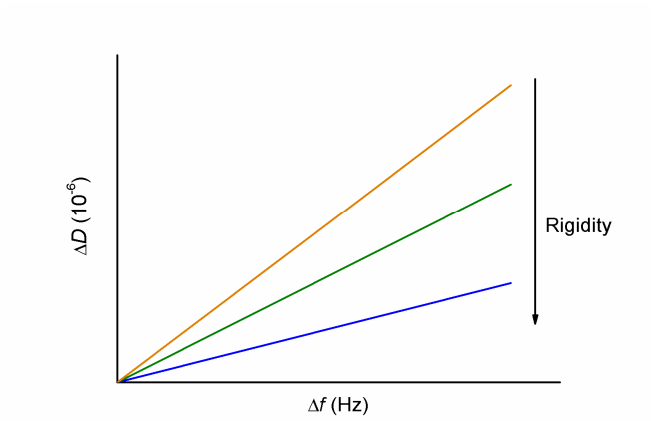


Figure 3.30. Change of dissipation (Δ*D*) versus frequency (Δ*f*). A steeper slope reflects a more viscolelastic layer.

Figure 3.31 A and B compare the Δ*D*/Δ*f* plots for the adsorption of Aβ40 and Aβ42, respectively, onto SiO_2 and polystyrene substrates (data from Figures 3.12 and 3.14). The projections of Δ*D* and Δ*f* versus time are also shown to assist in interpretation. During Aβ40 adsorption, in both cases (SiO_2 and polystyrene substrates) there is a clear linear relationship between the change in dissipation and the change in frequency during peptide uptake. The slopes of Δ*D*/Δ*f* are similar as well, suggesting there are no changes in the viscoelastic properties of the adsorbed layer. On the SiO_2 substrate a minor increase in the dissipation energy without any mass uptake (Δ*f* is constant) can be seen after ~30 min. In polystyrene, Δ*f* reaches much lower values (so as Δ*D* reaches higher ones), suggesting more material is adsorbed than in the hydrophilic layer and, moreover, a slight change in the slope after the same 30 min suggests that probably there is some conformational rearrangement and/or adsorption of peptide onto the first adsorbed Aβ40 layer since the initial process looks very similar for both surfaces. So it is proposed (Figure 3.31 C, on the left) that after the initial contact of Aβ40 with the surfaces by diffusion controlled adsorption from

the bulk solution in the case of the hydrophobic polystyrene substrate, the peptide interacts with it in a way that facilitates some aggregation and formation of interpeptide interactions which, together with a conformational change to a more β-enriched structure leads to the formation of amorphous aggregates that are not totally removed by rinsing. Contrarily to the monomers which are rinsed out with buffer. These assumptions are supported by the AFM imaging of the QCM-D crystal after the experiments (Figure 3.13 B 3.15 B for the polystyrene and SiO_2 substrates, respectively).

The behaviour of Aβ42 is not as simple as assumed from the first look at Figure 3.31 B. A curious observation is the initial decrease in the energy dissipation to negative values when the peptide first contacts with both surfaces (since Δf decreases there is mass uptake). As previously described, Aβ40 and Aβ42 exhibit different conformational states in solution due to increased intra- and interpeptide hydrophobic contacts [103]. Aβ42 exists in solution in an equilibrium that involves oligomeric species while Aβ40 exists as a monomer. Certain Aβ regions are predisposed towards β-strand and bend-like structures and it has been proposed that monomeric Aβ exists in solution as a metastable loop-like structure in which each monomer contains an antiparallel β-sheet [103]. It has been suggested that hydrophobic interactions and hydrogen bonds are chiefly responsible for stabilizing Aβ oligomers relative to monomers [136]. In a structural model proposed using solid-state NMR of Aβ40, in the protofilaments, contacts between β-sheet layers are side chain-side chain interactions along the hydrophobic faces created by side chains of the C-terminal segment and the CHC [131, 137]. The N-terminal residues are expected to be in random conformations.

As schematized in Figure 3.31 C on the right, it might be that the oligomeric nature of Aβ42, together with its already structured β-sheet domains makes this specie softer, and once it contacts with the solid surfaces there is a flattening/stiffening translated in the QCM-D response with a decrease in the energy dissipation while the adsorbed mass increases. After ~50 min, a linear change in dissipation with frequency occurs, but the slope is steeper for the uptake onto the hydrophobic polystyrene. The mass increase seems to be similar for up to 200 min for the two surfaces. These observations lead to the following assumptions, which are hampered by the AFM imaging of the QCM crystals shown in Figure 3.13 C and D and Figure 3.15 D. First, on the hydrophilic SiO_2 surface Aβ42 oligomers adsorb interacting mainly via the charged N-terminal residues and remain like that, not aggregating further into protofibrils or fibrils. Second, on the hydrophobic polystyrene surface, after the first soft diffuse conformation adsorption phase, the slope of $\Delta D/\Delta f$ becomes steeper, which suggests conformational rearrangements which lead to aggregation. This process is accompanied by an increase in the induced energy dissipation per coupled unit mass, as small oligomers are displaced by higher order aggregates. On the

hydrophobic surface, Aβ42 oligomers are immobilized towards in-plane interactions with the antiparallel β-sheet constituted by the C-terminal and the CHC. This is favorable for the establishment of contacts between β-sheet layers by side chains interactions along the hydrophobic faces leading to fibrillation.

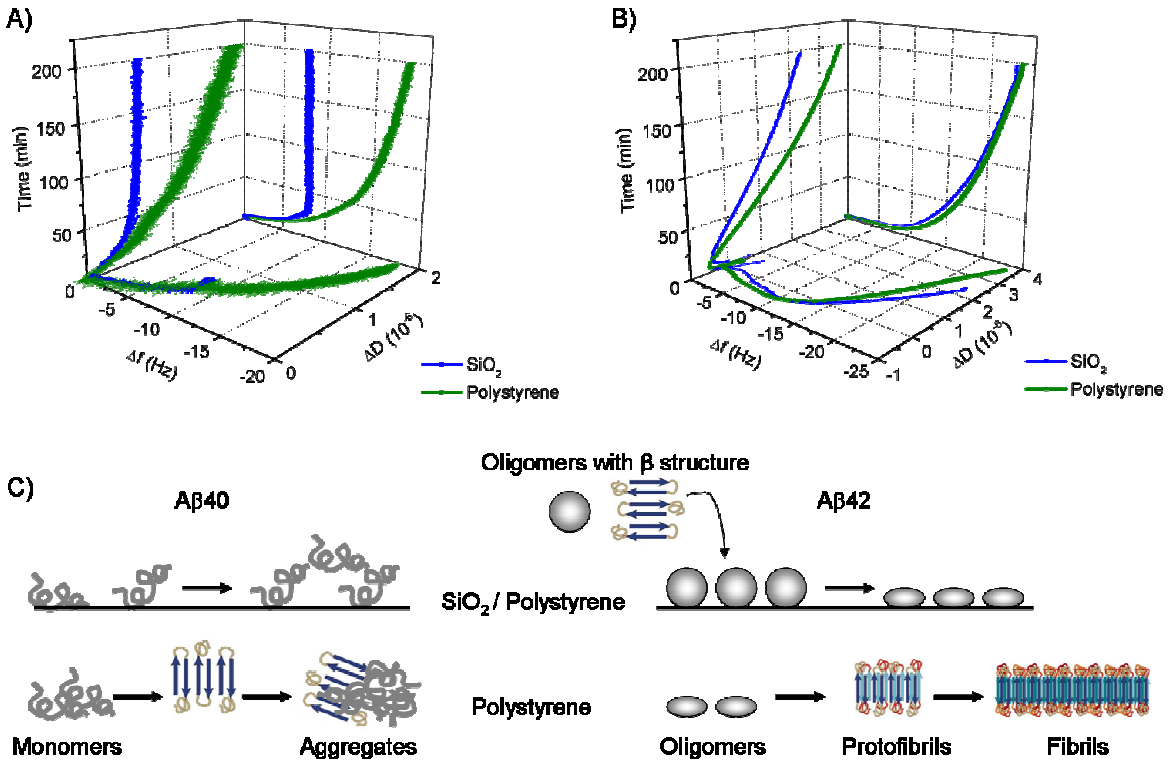


Figure 3.31. Change of dissipation (Δ*D*) versus frequency (Δ*f*) during the adsorption of A) Aβ40 50 μM in PBS and B) Aβ42 50 μM in PBS onto QCM-D gold crystals coated with SiO_2 or polystyrene. The projections of Δ*D* and Δ*f* evolution with time are also shown. C) Proposed model of the adsorption process.

Sequential LbL assembly of polyelectrolytes has proven to be a very efficient procedure for the fabrication of thin and well-defined films [201]. The build-up of multilayers of cationic PAH and anionic PSS was monitored using QCM-D. The interaction of the polyelectrolytes is dominated by electrostatic interactions and the layer thickness increases with increasing number of layers deposited. The ionic strength affects the structure of preformed polyelectrolyte multilayers. By employing QCM-D the changes in frequency and energy dissipation were monitored *in situ* during build up of the multilayer films. The adsorption of the polyelectrolyte (dissolved in 1 M NaCl) was followed by a rinsing step with ultrapure water in order to remove any excess before the next polyelectrolyte was adsorbed. An interesting observation was that during the rinse with water, when PAH was the outermost layer, a large increase in the dissipation occurred. In contrast, when

PSS was the outermost layer this effect was not observed. This leads to the conclusion that the conformation of an outer PAH layer is very sensitive to the presence of counterions in the solution whereas an outer PSS layer is not. When removing the salt in the solution by rinsing with water, the outer PAH layer expands and more and larger loops and tails are formed due to increased repulsion between the charged segments in the polyelectrolyte (Figure 3.32). This gives rise to a higher dissipation. By modelling the QCM signal according to Voinova [191] it was found that the outer layer of PAH extended about 20 nm out into solution after rinsing (Figure 3.17 B).

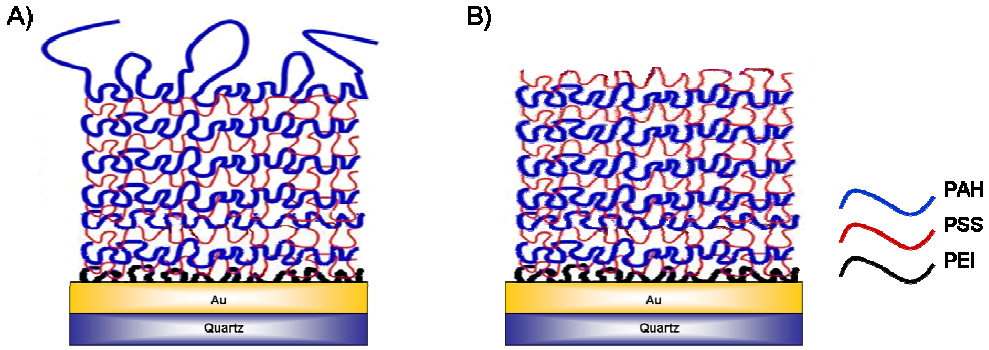


Figure 3.32. QCM-D AT-cut quartz crystal coated with gold and with A) $PEI(PSS/PAH)_6$ and B) $PEI(PSS/PAH)_6PSS$.

The adsorption of Aβ40 onto $PEI(PSS/PAH)_6$ and $PEI(PSS/PAH)_6PSS$ multilayers was monitored *in situ* by QCM-D and ATR-IR. For these complex systems only the behaviour of the monomeric less prone to aggregation peptide was tested. The same type of plots described for the QCM-D response to the adsorption of Aβ peptides onto SiO_2 and polystyrene substrates is depicted in Figure 3.33 A and B (data from Figure 3.18). In water, the adsorption process seems to be quite similar since the slopes of $\Delta D/\Delta f$ plots look alike. Also by AFM amorphous aggregates were detected in both cases after rinsing (Figure 3.19 A and B). In the case of PAH as outer layer, there seems to be a slight increase in D with time although Δf is constant. As said above, this suggests some conformational rearrangement of the deposited layer. When the peptide was dissolved in PBS more differences appeared: (i) there is less material deposited on the PSS terminated multilayer ($|\Delta f|$ lower), (ii) the slope of $\Delta D/\Delta f$ is steeper initially for the PSS terminated surface but the PAH terminated one exhibits a drastic change after ~20 min, as ΔD does not stabilize with time as Δf does. AFM images (Figure 3.19) show more and bigger aggregates for the $PEI(PSS/PAH)_6$ surface than for the PSS terminated one, although in both cases they have an amorphous appearance. In Figure 3.19 is also revealed that the PAH terminated surface is rougher, and the reason for this is the expansion of the polyelectrolyte chains after water rinsing. So one possible explanation for the

lower slope initially observed for $\Delta D/\Delta f$ is the increase in the rigidity of the underlying layer induced by the buffer (with high ionic strength) and the peptide itself. The abrupt change may be due to conformational rearrangement of the peptide and aggregation as suggested by the ATR-IR measurements (Figure 3.20).

The adsorption of Aβ40 on the polyelectrolyte-coated Ge IREs was monitored by ATR-IR, and the time course of the absorbance at 1628 cm^{-1} (indicator of the presence of β-sheets) shows that the adsorption is fast for both surfaces but more peptide is adsorbed on the $PEI(PSS/PAH)_6$ surface in a β-sheet structure. After the rinsing cycles (water, NaCl, water) to remove non-adsorbed peptide and disrupt electrostatic interactions, when PAH is the outer layer, the bands indicative of the presence of β-sheet secondary structure are still present. But the bands characteristic for antiparallel β-sheet and aggregated strands are not present. This is consistent with the amorphous aggregates observed by AFM (Figure 3.19 E and F). After Aβ40 adsorption on PSS, defined bands are not observed, with exception of one at 1400 cm^{-1} (Figure 3.21 B) indicating the presence of mixed undefined secondary structural elements. The pI of Aβ is 5.2 so in ultrapure water the peptide is slightly negatively charged. The larger amount of peptide found at the positively charged PAH ending film is thus compatible with the electrostatic nature of the peptide/multilayer interaction. Within the Aβ40 sequence there are 6 negatively charged residues (Asp1, Glu3, Asp7, Glu11, Glu22 and Asp23) that have a pKa of 4.5, so they are deprotonated and confer a negative charge to the peptide. Moreover, the Lys and Arg (pKa 10) and His (pKa 6.5) residues are positively charged (residues 5, 6, 13, 14, 16, 28), but the His residues are not fully protonated so the net charge of the peptide is negative. This would predict a less favorable interaction with the PSS terminated surface due to electrostatic repulsion. The region 1430–1390 cm^{-1} corresponds to the symmetric stretching vibration of the COO^- mode of unprotonated carboxyl group and shows the typical contributions of the Asp and Glu residues [196] for both $PEI(PSS/PAH)_6$ and $PEI(PSS/PAH)_6PSS$ multilayers. This leads to the possibility that not only electrostatic interactions are responsible for the increased β-sheet structure on the positively charged surface. As said, PAH is more hydrophobic than PSS and hydrophobic interactions drive β-sheet formation and aggregation as shown in the case of the hydrophobic polystyrene surface. Also the roughness of the structure seems to influence the process.

Aβ42 has been shown to aggregate and form fibrils more rapidly than Aβ40 [120, 217], and to have enhanced neurotoxicity [104, 106], althought Aβ40 is about 10 times more abundant in circulation [101]. In the time scale of the experiments reported herein, oligomeric and fibrillar species were only observed for Aβ42, while for Aβ40 amorphous aggregates were identified,

despite the presence of β-sheet enriched structures. It is suggested that the pathway of fibrillation differs, as previously indicated by others [102, 103].

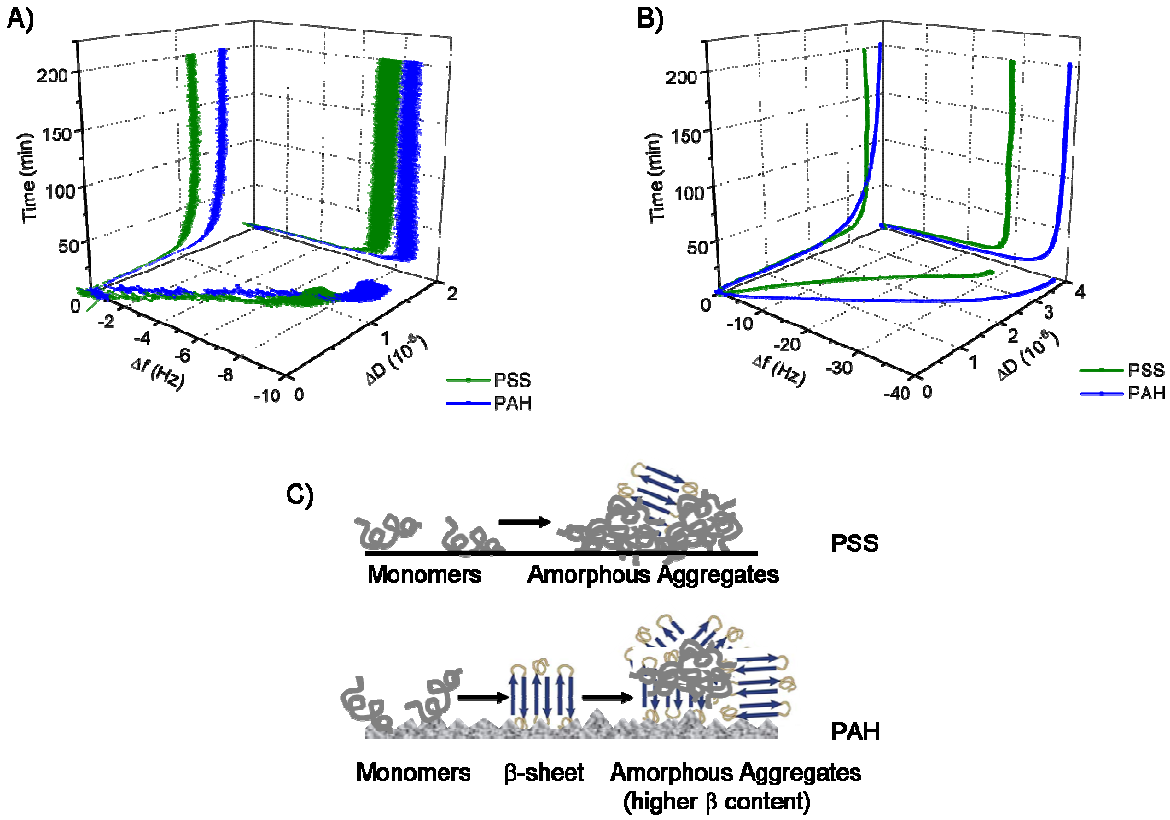


Figure 3.33. Change of dissipation (Δ*D*) versus frequency (Δ*f*) during the adsorption of A) Aβ40 50 μM in H_2O and B) Aβ40 50 μM in PBS into QCM-D gold crystals coated with $PEI(PSS/PAH)_6$ (PAH) or $PEI(PSS/PAH)_6PSS$ (PSS). The projections of Δ*D* and Δ*f* evolution with time are also shown. C) Proposed model of the adsorption process.

It is established that membrane binding and permeabilization are pivotal steps in amyloid-forming proteins and peptides cytotoxicity. These membrane associated mechanisms include membrane depolarization and destabilization, pore or ion channel-formation and membrane associated free-radical formation [143, 144, 145, 75]. Studies have shown that there is a substantial modulation of Aβ interfacial behaviour at lipid bilayers and monolayers by specific and non specific protein-lipid interactions which are controlled by a number of physical and chemical factors such as lipid composition, charge and phase [215, 216, 217]. SLBs are the biomembrane model system chosen to study the interaction with Aβ peptides, focusing on the more amyloidogenic Aβ42. They were prepared by spontaneous vesicle rupture and fusion to a bilayer on SiO_2 substrate. PC and sphingomyelin (SM) are major zwitterionic phospholipids in mammalian cells. Phospholipids are

amphipatic molecules. They have a hydrophilic polar headgroup and hydrophobic non polar tails constituted by long chain fatty acids (Figure 3.34 A). In a bilayer, the hydrophilic heads orient towards the aqueous media and the hydrophobic tails away from it (Figure 3.34 B). The presence of unsaturated lipids (fatty acid chains with unsaturated bonds) confers a fluid character to the bilayer.

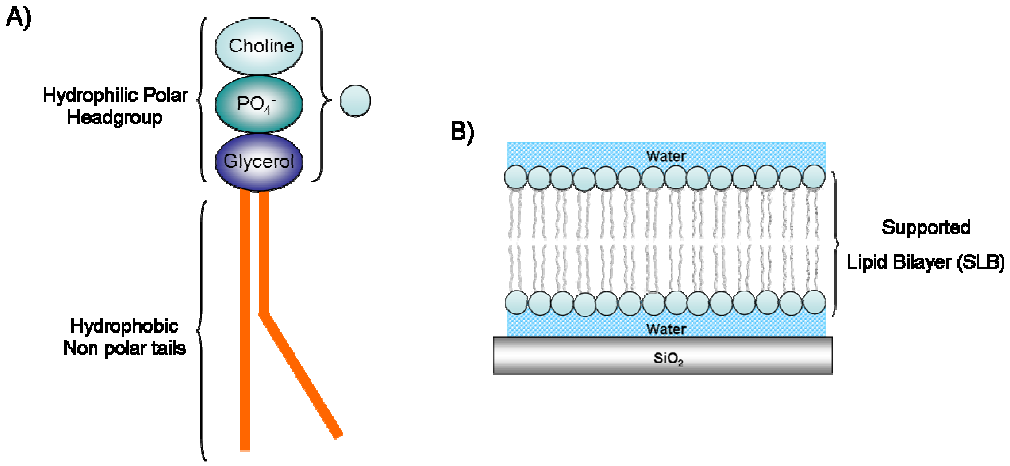


Figure 3.34. A) Structure of PC. B) SLB on SiO_2 substrate.

SLBs of 100 mol% egg PC (composition concerning fatty acids in Table 3.1) and of egg PC with 10 mol% of other substances were prepared on SiO_2 substrates and their interaction with Aβ peptides was followed by QCM-D. Freshly prepared Aβ40 (monomeric) and Aβ42 (oligomeric), and an aged solution of Aβ42 (fibrillar) were brought into contact with the 100 mol% egg PC SLBs. This is important in order to infer about the state at which Aβ is most likely to interact with the main constituent of cell membranes. The QCM-D data from Figure 3.27 is shown in Figure 3.35 A. When analyzing the data it is important to remember that in the case of SLBs the variations in energy dissipation may arise also from perturbations of the lipid bilayer and not only from the adsorbed peptide layer. Aβ40 does not seem to interact in an appreciable extent with the pure zwitterionic SLB. However, Aβ42 does, since both ΔD and Δf change after peptide exposure. In the $\Delta D/\Delta f$ plot one can distinguish two different processes, one with a small slope and a second one (~10 min) with a much steeper slope, with very little mass uptake but high energy dissipation. In the first one, Aβ42 oligomers, when finding the lipidic interface, flatten when they start to interact with it, as one can see that Δf changes fast but the dissipation does not (as for Aβ42 adsorption onto SiO_2 and polystyrene). Afterwards, the peptide can at least partially insert in the hydrophobic transmembranar part of the bilayer due to its hydrophobic domains. This leads to a disturbance of the membrane structure, and thus the increase in ΔD with a small increase in the adsorbed material can be explained. The process might also induce some further peptide aggregation onto

protofibrills and even fibrils but this can not be proved by the methods used (this should be dependent of the proportion of bilayer-buried and exposed regions of the molecule). The membrane fluidity may allow peptide assemblies to float at the water-membrane interface and easily orient to an energetically favorable state. But certainly there should be insertion in the SLB and perturbation of its structure that contributes to the increase of *D*. It is also possible that the burying of the peptide in the hydrophobic core of the bilayer will prevent extensive interactions with other peptides nearby. Fibrillar Aβ also does not interact strongly with the egg PC bilayer. There is a small increase in the mass but a very small dissipation variation (flat $\Delta D/\Delta f$ plot). It is likely that the high molecular weight species which is too big to insert in the bilayer sits on the surface, even though to a small extent, having the contrary effect of oligomers, which means the SLB is "compressed", becoming even more rigid. All the proposed interactions are schematized in Figure 3.35 B.

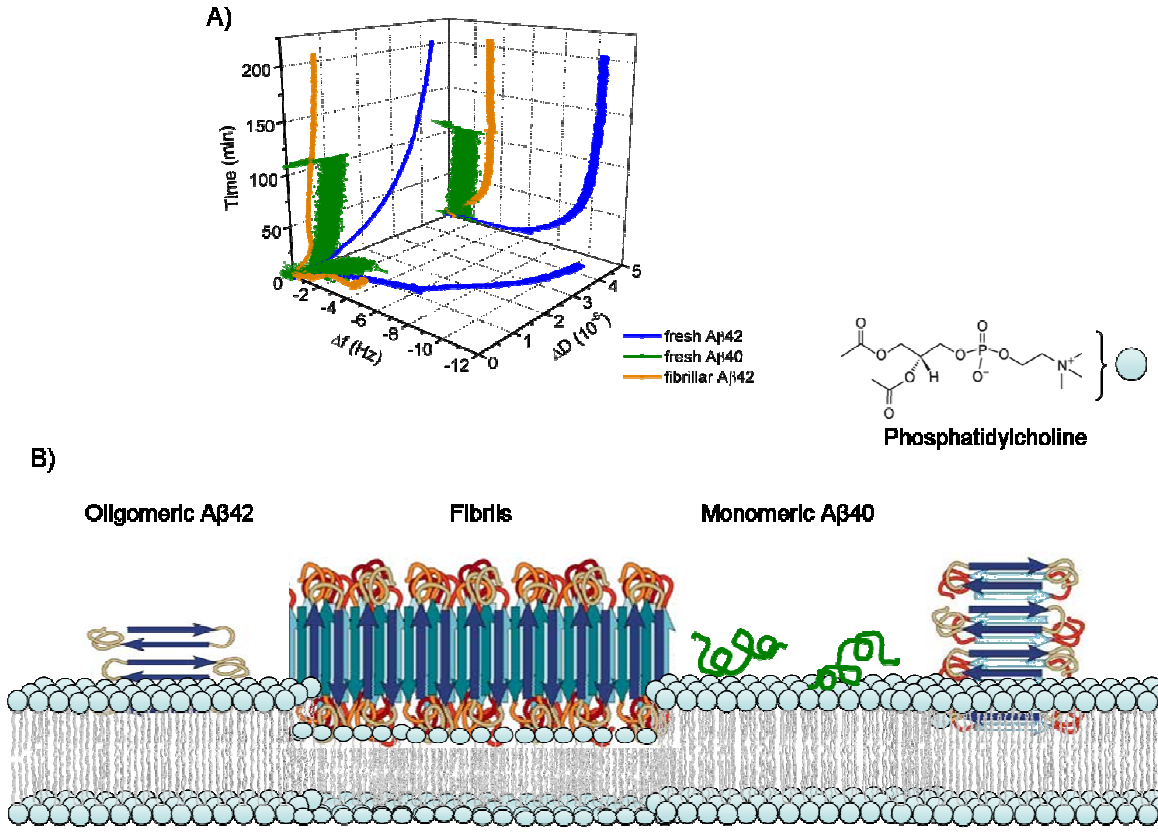


Figure 3.35. A) Change of dissipation (ΔD) versus frequency (Δf) during the interaction of Aβ peptides with egg PC SLBs. The projections of ΔD and Δf evolution with time are also shown. B) Proposed effects on the bilayer structure.

Although there are many studies concerning the interactions of Aβ peptides with lipid model systems there is also some controversy. But several previous reports support the effects proposed above. Most studies using CD, dye release assay and other methods, have reported that freshly solubilized Aβ40 as well as Aβ42 (assumed to be a monomer) do not interact with PC at neutral pH [223], although weak interaction has been also reported [224]. A recent molecular dynamics study suggested that on dipalmitoylphosphatidylcholine (DPPC) bilayers, independently of peptide charge, Aβ42 sits parallel to the bilayer surface near the interface between the headgroup and the hydrophobic core regions of the bilayer [225]. Finally, it has been reported that aggregated Aβ tends to interact with PC decreasing the membrane fluidity [226].

The incorporation of 10 mol% of egg PG or DMTAP conferred a partial negative or positive charge to the SLBs, respectively. The choline of the polar headgroup of egg PC is replaced by glycerol in egg PG. DMTAP is a small molecule and does not have a phosphate group, and thus, it should allow the appearance of "gaps" at the bilayer surface. The results from Figure 3.28 A are shown in Figure 3.36 A. Aβ42 does not seem to interact strongly with the SLB when egg PG is present, the mass uptake is very low (Δf ~2 Hz), although a small increase in ΔD was observed, as shown by the steep $\Delta D/\Delta f$ curve after 15 min. The isoelectric point of Aβ is 5.2 and at physiological pH, which was used in the experiments, the peptide will thus be negatively charged. Despite the presence of salt, we can admit an electrostatic repulsion to a certain extent, although these are positively charged residues, Arg5, His6 (N-terminus) and Lys28. So oligomeric species of Aβ42 do not insert in the bilayer and stay at the surface (Figure 3.36 B). When DMTAP was added to the SLB, the mass increase of the sensor crystal was higher than in the previous situation (Δf ~6 Hz) but lower when compared to the pure egg PC bilayer. After peptide exposure to the bilayer there is a fast mass uptake with almost no change in the energy dissipation, that only starts to increase later, when Δf is not decreasing anymore (~10 min). Aβ42 has 6 negatively charged residues at pH 7.4; 4 are in the unordered N-terminus (Asp1, Glu3, Asp7 and Glu11) and Glu22 and Asp23 are in the central region right next to the CHC. These residues could be responsible for a fast, electrostatically driven, interaction with the DMTAP molecules buried in the bilayer (Figure 3.36 C). Some peptide rearrangement might be possible, including further aggregation into protofibrils or higher molecular weight oligomers. Besides this, as described for the pure egg PC SLB, the peptide can still insert in some areas to the hydrophobic core thus allowing a certain change in the membrane structure that can be responsible as well for the ΔD increase.

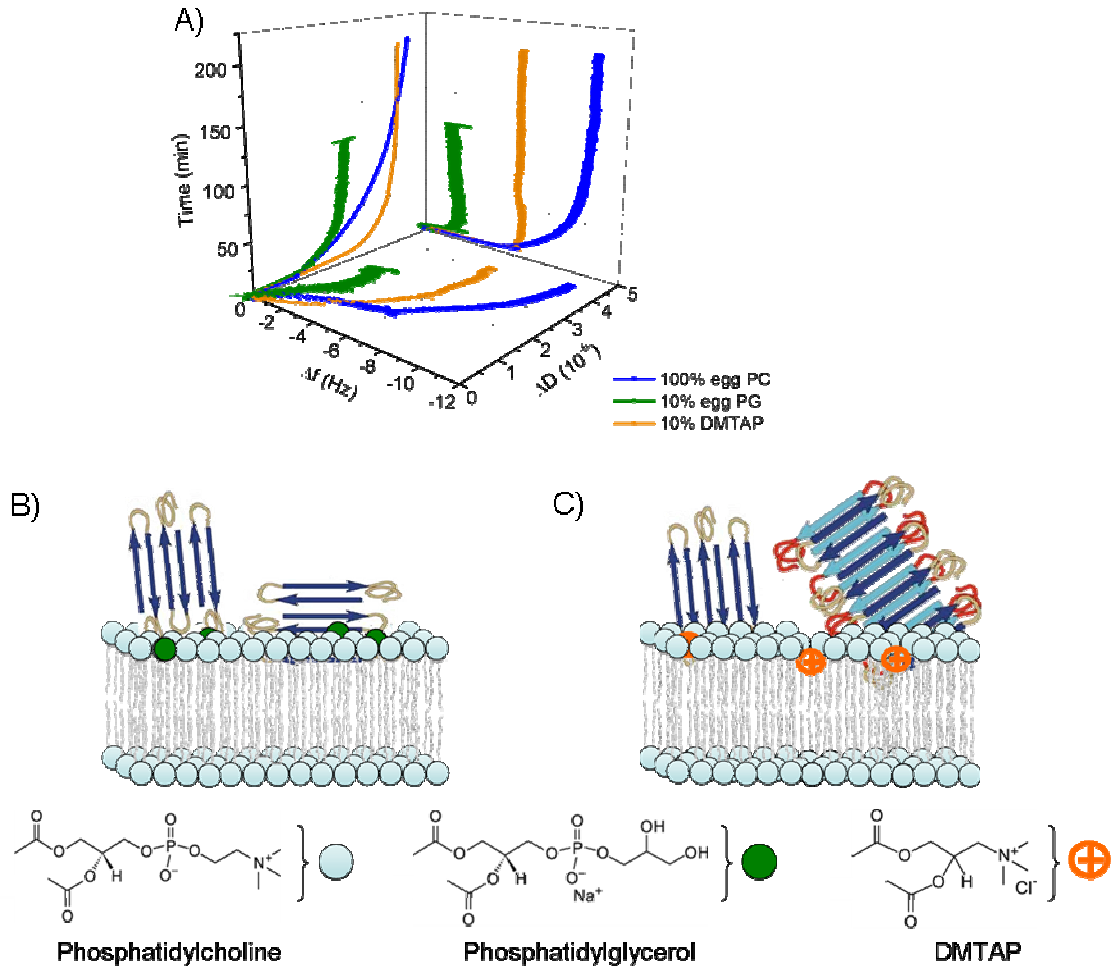


Figure 2.36. A) Change of dissipation (Δ*D*) versus frequency (Δ*f*) during the interaction of Aβ peptides with egg PC SLBs incorporating 10 mol% of egg PG or 10 mol% of DMTAP. The projections of Δ*D* and Δ*f* evolution with time are also shown. B) and C) Proposed interactions.

Even though in natural occurring mammalian membranes lipids with a net positive charge are not present, DMTAP was used to look for the effect of charge itself. Therefore there are not many studies concerning the interaction of Aβ peptides with positively charged membranes. But the interaction of Aβ with acidic phospholipids is again controversial. Regarding PG, no [227] or only weak [226] interaction was observed at neutral pH in the presence of a physiological concentration of salt (100–150 mM), which were the conditions of the measurements described herein. However, CD studies showed that at a very low ionic strength, Aβ40 binds to PG containing membranes, forming an α-helix or a β-sheet (depending on the peptide-to-lipid ratio) [216]. There are many studies indicating that the physical properties of the lipid-water interface are influenced by the presence of charged headgroups and dipoles which interact with water molecules [181]. This turns the local ion concentration, the ionic strength and the pH quite different from those in bulk. Under

low ionic strength conditions, the local pH near the membrane surface is significantly lowered compared to the bulk value, because protons are concentrated at the negatively charged surface by electrostatic attraction. Thus, the peptide takes the electrically neutral form that may bind to lipid bilayers. Indeed, stronger interaction of Aβ40 and Aβ42 with PG was reported at pH 6 than pH 7 in the presence of a physiological concentration of salt [223]. Lin *et* al. have determined affinity constants between liposomes and Aβ40 calculated by a Langmuir binding model which suggest that fresh Aβ40-liposome interaction is electrostatically driven while for 1 day incubated Aβ40 and various liposomes the interactions were mainly attributed to hydrophobic interactions [217]. The main difference concerned PC indicating a different binding mechanism, and at the same time the affinity for PG was dramatically decreased. Well, one can say that the 1 day incubated Aβ40 should have more similarities with the fresh Aβ42 used in these measurements (oligomers are formed and β-sheet content is increased).

Gangliosides are sialic acid-containing glycosphingolipids abundant in the neuronal system [186] and among them GM1 has been shown to bind Aβ that serves as seed on the plasma membrane to promote aggregation of further peptide [228]. Also a neurotoxic form of Aβ is generated during the aggregation process on liposomes containing GM1 clusters [229]. The data presented in Figure 3.28 B is shown in the $\Delta D/\Delta f$ plot in Figure 3.37 A. The slope of the plot, compared with the pure egg PC SLB is a bit steeper although they look like. GM1 is negatively charged and the sialic acid residues have been shown to be important for the cytotoxicity of Aβ [217]. It might be that Aβ binds the exposed domains acting as seeds to induce further aggregation, leaving less peptide available for insertion into the membrane (thus the reduced mass uptake compared with 100 mol% egg PC) - Figure 3.37 B). But with the data shown here this is speculative and based on previous reports. For GM1 containing liposomes a higher affinity constant was determined than for dipalmitoylphosphatidylglycerol (DPPG) liposomes [217].

The structure of cholesterol is very different from that of other membrane lipids [219]. Cholesterol is a steroid with a flat shape and rigid rings that allows interdigitation between phospholipids. At one end of this planar ring system is a hydroxyl group and at the other end is a hydrocarbon tail, so cholesterol has both hydrophilic and hydrophobic poles that determine its positioning within the lipid bilayer (Figure 3.37 C). Cholesterol is known for decreasing the area per phosphopilid molecule, thereby increasing the cohesiveness of lipids and the bilayer stiffness [230]. So it is not surprising that cholesterol affected the amount of Aβ42 adsorbed onto the egg PC bilayer (Figure 3.37 A). After adsorption, there is a drastic change in the slope of $\Delta D/\Delta f$ indicating that the rigid domains act as templates able to increase the peptide concentration and to drive its oligomerization. Evidence suggests that an elevated cholesterol level is a risk factor of AD [231].

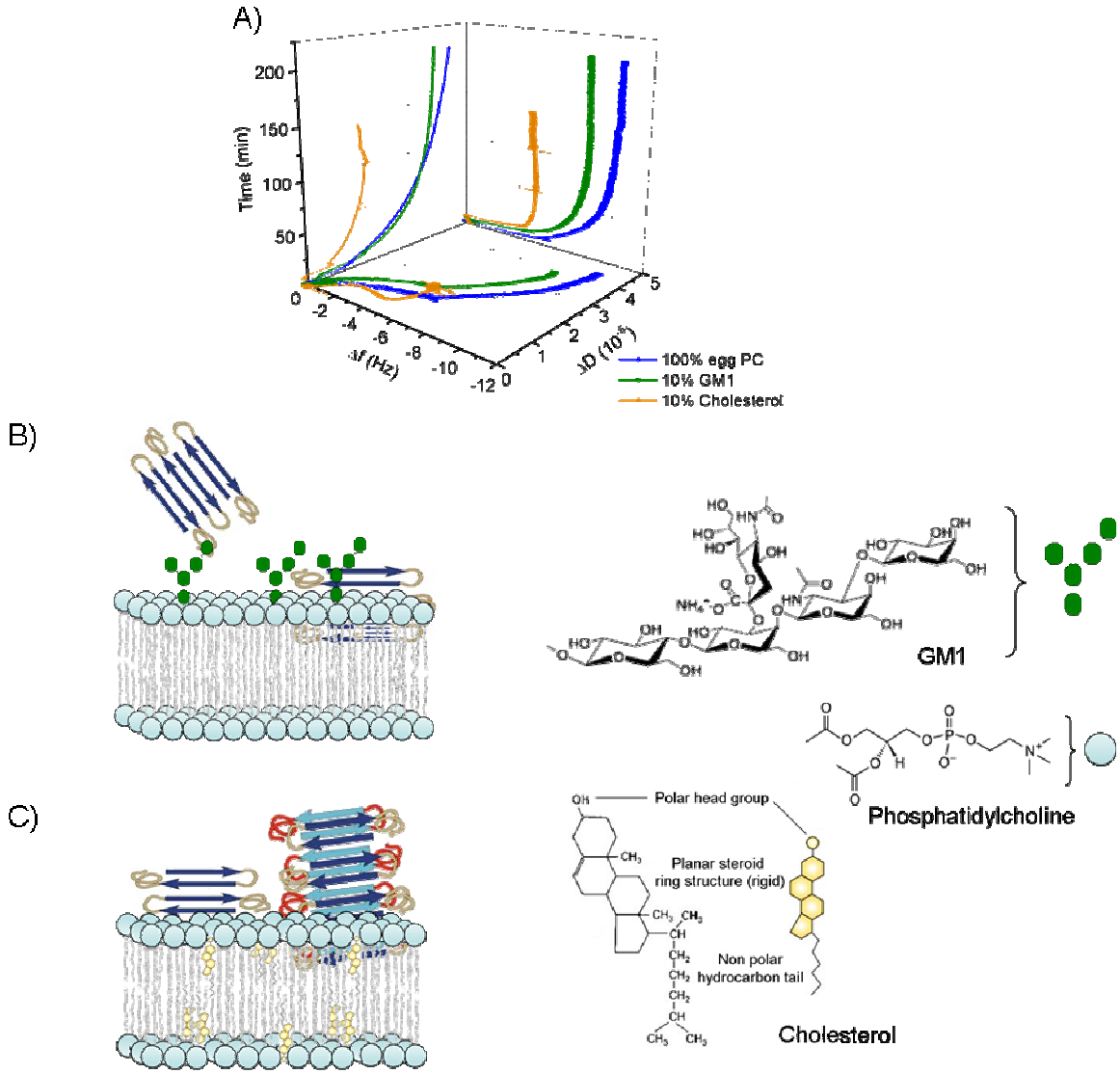


Figure 3.37. A) Change of dissipation (Δ*D*) versus frequency (Δ*f*) during the interaction of Aβ peptides with egg PC SLBs incorporating 10 mol% of GM1 or 10 mol% of cholesterol. The projections of Δ*D* and Δ*f* evolution with time are also shown. Proposed interactions for SLBs containing 10 mol% of GM1 B) and cholesterol C).

The QCM-D study presented for the interaction of Aβ42 with SLBs is in agreement with the mechanism proposed by Davis and Berkowitz based on molecular simulations, concerning the influence of hydrophobic and electrostatic interactions with the bilayer surface on the aggregation [225]. Initially, the Aβ peptide is brought close to the surface of a bilayer due either to diffusion (through interaction with sugar groups on lipids, such as gangliosides) or to cleavage from the APP. Once the peptide is close enough to the surface, it will favorably bind with the lipids. If this binding occurs on a mostly zwitterionic bilayer, the peptide will strongly interact with the interface at the hydrophobic core of the bilayer, precluding extensive interactions with other nearby peptides.

However, if this binding occurs on an anionic bilayer, the peptide will not be as strongly associated with the bilayer core and will be more exposed to the solvent and other bound peptides. If the anionic headgroups of lipids are able to lower the local pH by one to two units, the hydrophobic portion of the peptide will become exposed, and more likely to interact with other nearby peptides, thus driving oligomerization. In addition, previous research has shown that fibrilization occurs more rapidly in solution at a lower pH 5, close to the pI of Aβ [43]. Therefore, lowering the pH near the anionic lipid surface may also promote aggregation by increasing protein-protein interactions through a reduction in the electrostatic repulsion between peptides. Under normal conditions, most of the negatively charged lipids are found on the inner leaflet of the membrane but it has been shown that during aging or due to disease the membrane composition may be altered, resulting in increased charged density on the outer leaflet [230]. This can explain, at least partially, the increased prevalence of AD with aging.

In the outer leaflet, glycosphingolipids, SM and cholesterol (and PC with saturated acyl chains) form a lipid microdomain in the liquid ordered phase, in which the acyl chains are highly ordered like in the gel state, whereas the lipids are laterally mobile like in the fluid state. Proteins important for signal transduction are proposed to be located in this microdomain, which is dubbed as a "lipid raft", although their existence in biomembranes remains controversial [232]. Biochemically, lipid rafts are defined as detergent-insoluble fractions of biomembranes [233]. It is conceivable that lipid rafts serve as a platform for the aggregation of Aβ since the production of Aβ occurs, at least partly, in lipid rafts [93].

All these processes can be implied in the cytotoxicity of Aβ oligomers associated to increased plasma membrane permeability. Different mechanisms have been proposed to be involved in membrane permeabilization such as pore formation [144] and disorder of the membrane structure [145, 146].

4. Controlling Aβ Oligomerization with Nanoparticles

4.1. Introduction

As shown in the previous chapter, studies of the interactions of Aβ peptides with planar surfaces draw attention to the fact that conformational changes and aggregation may occur upon adsorption. As one changes from a flat surface to particles, and the particles become smaller (eventually approaching the size of the proteins themselves), the composition and organization will change, departing from the simple limiting case of flat surfaces. For instance, there is the potential that highly curved surfaces (very small NPs) can suppress protein adsorption, an effect likely to be selective to larger proteins, offering a route to differential control of protein adsorption [234].

Since Aβ is a physiological peptide which is constantly anabolized and catabolized [87, 111, 112], steady state levels of Aβ monomers are controlled by 3 factors (i) production; (ii) degradation and (iii) aggregation, which is a concentration dependent process. So the most effective treatments for AD should be directed towards (i) decreasing Aβ production, (ii) increasing Aβ removal, or (iii) preventing Aβ fibril formation. One therapeutic strategy is, in principle, to inhibit and preferably reverse the aggregation itself, because this appears to be the first step in the pathogenic process not associated with some natural biological function. Several findings suggest that a conformational transition from random coil/α-helix structure to β-sheets is responsible for aggregation [31, 107, 164]. So an attractive solution would be the re-conversion of Aβ conformation by adsorption or complexation to a third component such as NPs (Figure 4.1).

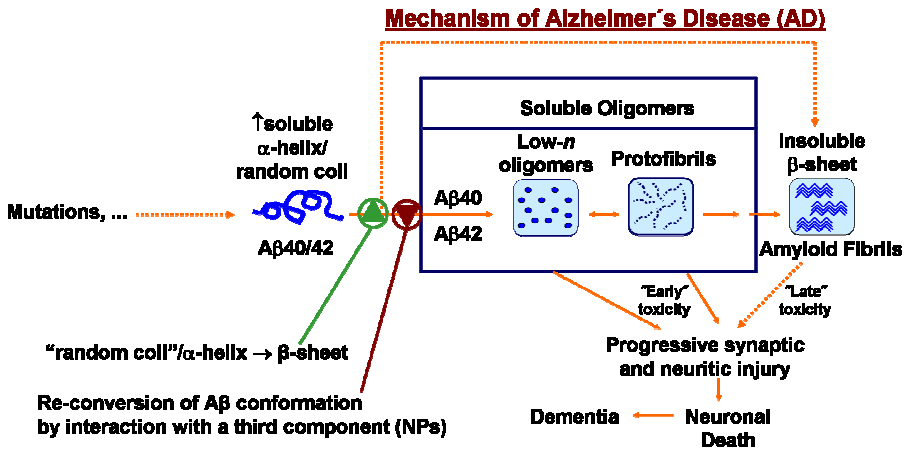


Figure 4.1. Mechanism of AD highlighting the strategy proposed for the use of nanoparticles to re-convert Aβ conformation in order to inhibit aggregation.

The principal difficulty in CNS drug development is the BBB, which is formed by the brain capillary endothelium [235, 236]. BBB is a unique membranous barrier that tightly segregates the brain from the circulating blood [237]. The CNS is constituted by blood capillaries which are structurally different from the blood capillaries in other tissues; these structural differences result in a permeability barrier between the blood within brain capillaries and the extracellular fluid in brain tissue. Capillaries of the vertebrate brain and spinal cord lack the small pores that allow rapid movement of solutes from circulation into other organs; these capillaries are lined with a layer of special endothelial cells that are sealed with tight junctions. Tight epithelium, similar in nature to this barrier, is also found in other organs (skin, bladder, colon, and lung) [237]. Ependymal cells lining the cerebral ventricles and glial cells are of three types, (i) astrocytes, which form the structural frame work for the neurons and control their biochemical environment; (ii) oligodendrocytes that shield axons and (iii) microglias, the blood derived mononuclear macrophages (Figure 4.2) [235].

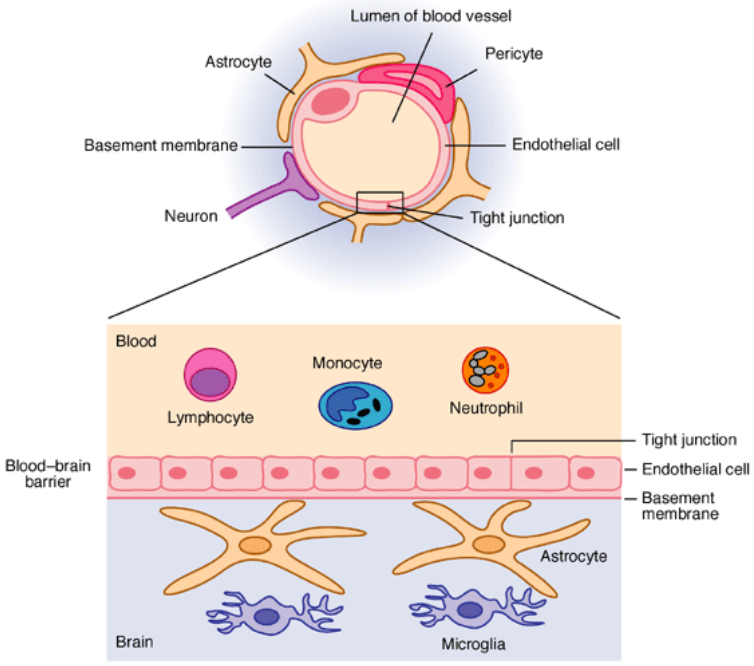


Figure 4.2. The BBB. The BBB is created by the tight apposition of endothelial cells lining blood vessels in the brain, forming a barrier between the circulation and the brain parenchyma (astrocytes, microglia). Blood-borne immune cells such as lymphocytes, monocytes and neutrophils can not penetrate this barrier. A thin basement membrane, comprising lamin, fibronectin and other proteins, surrounds the endothelial cells and associated pericytes, and provides mechanical support and a barrier function (*from* [240]).

The BBB also has an additional enzymatic aspect. Solutes crossing the cell membrane are subsequently exposed to degrading enzymes present in large numbers inside the endothelial cells that contain large densities of mitochondria, metabolically highly active organelles. Finally, the BBB is further reinforced by a high concentration of P-glycoprotein, an active efflux transporter that actively removes a broad range of drug molecules from the endothelial cell cytoplasm before they cross into the brain parenchyma [235].

The BBB prevents >98% of all drugs from entering the CNS and consequently effective pharmaceuticals are not available to treat the vast majority of CNS diseases (e.g. AD, PD, Huntington's, brain cancer, stroke) [237]. So the poor BBB permeability has to be overcome for the targeting of CNS disorders.

Polymers offer advantages since it is possible to modulate their properties and surfaces in order to control the adsorption and interaction processes. Properly engineered polymeric NPs can pass through the BBB and have a good bioavailability and constitute a promising strategy to be exploited to promote drug delivery to the CNS [235, 238, 239]. NPs consisting of complexes of polyampholytes and dodecanoic or perfluorododecanoic acid (polyampholyte dressed micelles exhibiting a large surface) were synthesized [241]. According to previous work, fluorinated NPs induce α-helix rich structures in Aβ40 whereas the hydrogenated analogues are less efficient [242]. These results have encouraged the use polymeric nanostructures for induction of conformational conversions with the aim to contribute substantially for the understanding of the mechanisms underlying protein misfolding diseases.

In order to test the influence of the zeta potential of the particles on the peptide structure, NPs without fluorine atoms but with high charge densities were required. Polymerization in microemulsion leading to sulfonated polystyrene microgels and heterophase polymerization with reactive surfactants leading to sulfated polystyrene latexes were used to create the desired NPs. Studies about the principal factors responsible for the conformational behaviour and aggregation/oligomerization of Aβ peptides in the presence of polymeric nanostructures were performed. Here is reported the formation, structure and cytotoxic activity of Aβ42 oligomeric species prepared in the absence and presence of NPs.

4.2. Materials and Methods

4.2.1. Synthesis of Fluorinated Nanoparticles

Fluorinated NPs and their hydrogenated analogues were synthesized as previously reported [241]. Poly(N,N-diallyl-N,N-dimethylammonium-*alt*-maleamic carboxylate), a polyampholyte with alternating cationic and anionic monomers was synthesized. A solution of 0.1 g of polyampholyte in 100 mL of water was adjusted to pH 8 using an aqueous solution of 0.1 M sodium hydroxide and heated to 90°C. An aqueous solution (100 mL, 90 °C) of 1.0 equiv of the dodecanoic acid and perfluorododecanoic acid, respectively, was added in droplets to the polyampholyte solution, which was then adjusted to pH 8. The stoichiometries were calculated with respect to the charges such that the ratio of anionic surfactant headgroups (carboxylate) to cationic monomers (ammonium) was 1 to 1. The mixture was stirred for further 60 min at 90 °C after the addition of surfactant to the polyampholyte and then cooled to room temperature. The mechanism of dressed micelle formation is shown in Figure 4.3.

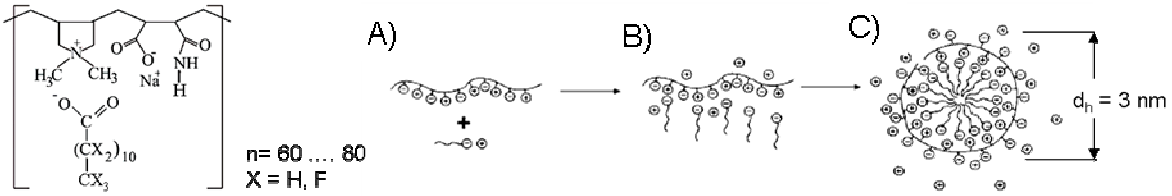


Figure 4.3. Complexes of polyampholytes with dodecanoic acid (X = H) and perfluorododecanoic acid (X = F). On the right is shown the formation of dressed micelles: A) the polyampholyte and the sodium dodecanoate were mixed; B) loose aggregates were formed by the complexation of polyampholyte and dodecanoate moieties (charge ratio, 1 positive to 1 negative); C) reorganization of the complex to a compact polyampholyte dressed micelle (*adapted from* [241]).

4.2.2. Synthesis of Sulfonated and Sulfated Nanoparticles

Heterogeneous polymerization is a generic term for a variety of heterophase polymerization techniques (suspension, microsuspension, dispersions, emulsion, microemulsion and miniemulsion polymerization; the common feature is the formation of a new phase, the polymeric phase) (Table 4.1) [243]. This was the approach used to synthesize sulfonated and sulfated NPs.

4.2.2. 1. Polymerization in Microemulsion leading to Microgels

Microemulsion is defined as at least a ternary mixture of two immiscible liquids stabilized with a surfactant or a mixture of surface active agents. Microgels are small polymer networks of well-defined mesoscopic size, low polydispersity, and highly perfect spherical shape [244, 245]. These polymer microgels may be functionalized in a second step by polymer analogous reaction resulting in polyelectrolyte microgels of the same geometry. Such polyelectrolyte microgels can be regarded as highly charged, spherical polyelectrolyte networks swollen in aqueous solution.

Table 4.1. Heterophase polymerization techniques [243].

Polymerization technique	Monomer	Nucleation phenomenon
Ab initio emulsion or dispersion	Feed or droplets[a)]	Phase formation at the very beginning of the polymerization
Suspension and microsuspension	Stable monomer droplets under the influence of shear forces	Point of particle identity and polymer solubility in the monomer determines phase formation[c)]
Microemulsion and miniemulsion	Stable droplets also in the absence of shear forces[b)]	Polymer solubility in the monomer determines phase formation[c)]
Seed techniques	Feed or droplets	Suppress phase formation

a) The presence of a free monomer phase in the reactor is not necessary.
b) Microemulsions are thermodynamically stable; miniemulsions are kinetically stable.
c) It is assumed that reactions in the continuous phase are suppressed.

The molecular properties of the microgels (more or less loosely cross-linked) are controlled by the ratio mono- to bifunctional monomer used in the synthesis [246]. A cross linking density of 1/20 that covers the size range of 6 nm < R < 70 nm (for the swollen microgels) was used. It should also be mentioned that for smaller particles with R < 12 nm counterion modified surfactants such as cetyltrimethylammonium terephthalate and tartate are used, whereas in other systems the cationic surfactants cetyltrimethylammonium chloride (CTMA) and benzethonium are used for microemulsification. Microgels were synthesized as previously reported [244, 245], only with minor modifications (Figure 4.4 A). Briefly, freshly distilled styrene, the estimated amount of cross-linker (m-diisopropenylbenzene, m-DIB), and the initiator (azobis(isobutyronitril), AIBN) are mixed to form the oil phase. A solution of CTMA in deionized water was prepared separately. Oil and water phases were mixed by vigorous stirring with a high-speed stirrer. After equilibrium is approached, the reaction mixtures were heated for 48 hours at 60 °C. The polymerized microgel was dried in vacuum at 50 °C, dissolved in tetrahydrofuran (THF) and reprecipitated in methanol two times. The

surfactants were removed by Soxhlet extraction with boiling methanol for 72 hours, and the resulting microgels were dried in vacuum at 50 °C.

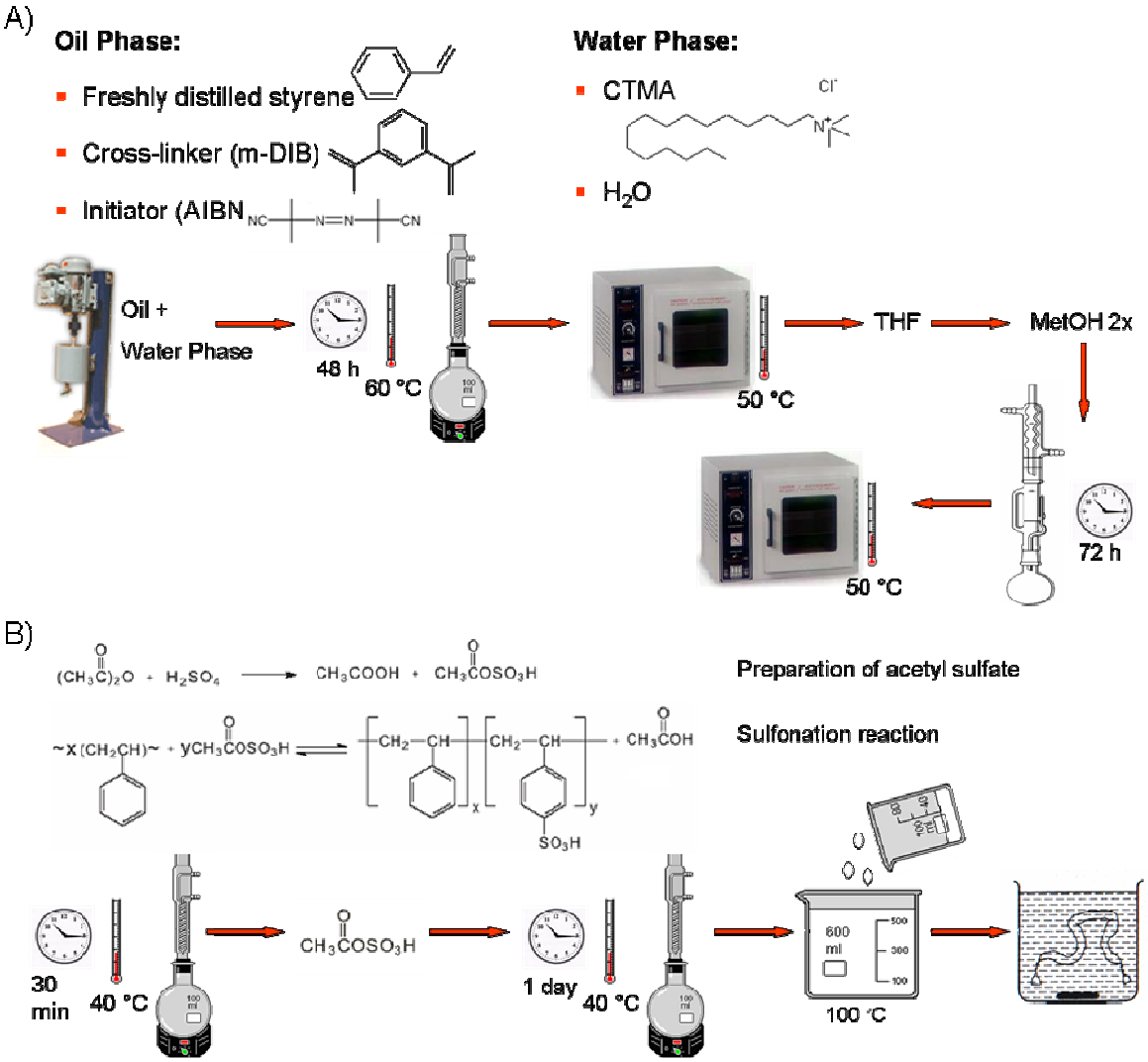


Figure 4.4. Scheme of the experimental procedure for the synthesis of microgels A) and subsequent sulfonation B).

Sulfonation was performed with H_2SO_4/acetic oxide in 1,2-dichloroethane at 55 °C (Figure 4.4 B) [247]. The acetyl sulfate was freshly prepared prior to the sulfonation reaction by mixing a fixed amount of dichloromethane and acetic anhydride under inert atmosphere (N_2). The solution was cooled to 0 °C, and 95-97% sulfuric acid was carefully added followed by stirring until a homogeneous and clear solution was obtained at room temperature. During the preparation, an excess of acetic anhydride was used to scavenge any trace of water, if present. The microgel was dissolved in dichloromethane, and the solution was heated to 40 °C in order to obtain total

solubilization and purged with N_2 for 30 min. The freshly prepared acetyl sulfate solution was added and the reaction mixture was maintained at 40 °C under stirring for a day. The solution became clear yellow after adding the sulfonating agent. The reaction was interrupted by adding an excess of 2-propanol for 30 min and cooling to room temperature. Finally, the sulfonated polymer was precipitated by dripping into a large volume of boiling water. The resulting product was washed with water, filtered, dialyzed and dried under vacuum up to constant weight.

The microgels were characterized by TEM, DLS (to determine D_h) and zeta potential measurements. Since the zeta potential is a crucial property of the NPs for the present study, a brief description of this parameter will be done.

The development of a net charge at the particle surface affects the distribution of ions in the surrounding interfacial region, resulting in an increased concentration of counter ions close to the surface [248]. Thus an electrical double layer exists around each particle. The liquid layer surrounding the particle has two parts, (i) an inner region, the Stern layer, where the ions are strongly bound and (ii) an outer, diffuse, region where they are less firmly attached. Within the diffuse layer there is a notional boundary inside which the ions and particles form a stable entity. When a particle moves, ions within the boundary move with it, but any ions beyond the boundary do not. This boundary is called the surface of hydrodynamic shear or slipping plane. The potential that exists at this boundary is known as the zeta potential (Figure 4.5). Zeta potential is measured by applying an electric field across the dispersion. Particles with a zeta potential will migrate toward the electrode of opposite charge with a velocity proportional to the magnitude of the zeta potential.

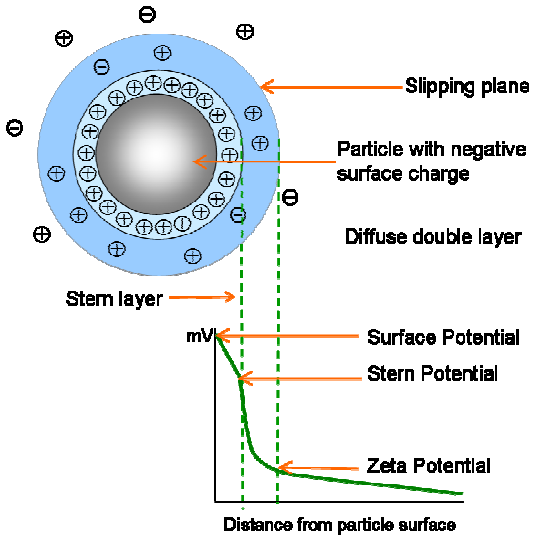


Figure 4.5. Schematic showing the distribution of ions around a charged particle.

Zeta potential is one of the main forces that mediate interparticle interactions, and its magnitude gives an indication of the potential stability of the colloidal system. If all the particles in suspension have a large negative or positive zeta potential then they will tend to repel each other and there is no tendency to flocculate. However, if the particles have low zeta potential values, there is no electrostatic force to prevent the particles coming together and flocculating. The most important factor that affects zeta potential is pH.

DLS and zeta potential measurements were performed on a Malvern HPPS 500 instrument (Southborough, MA, U.S.A.). TEM of the NPs was performed using a Zeiss EM 912 Omega microscope at an acceleration voltage of 120 kV (Carl Zeiss, Oberkochen, Germany). The samples were applied as drops on copper grids and air-dried.

4.2.2.2. Heterophase Polymerization with Reactive Surfactants

Over the past few years, copolymerizable emulsifiers have become of increasing interest for the application in emulsion polymerization [249, 250]. The promise of this new group of surfactants is connected to the capability to react with the monomers during the free-radical polymerization and to be chemically bound to the resulting polymer. The emulsifier is thus incorporated in the polymer particle and should offer higher latex stability and less coagulation during polymerization [249].

The basic ingredients in emulsion polymerization are monomers, water, emulsifiers and an initiator system. The water-insoluble monomers are emulsified by the employed emulsifier, in most cases emulsifiers from the groups of sulphonates, sulphate esters, sulphosuccinic acid esters or phosphate esters or nonionic surfactants. During polymerization polymer particles are formed which are stabilised by the emulsifier. Classical emulsifiers adsorb onto the particles by physical interaction of the hydrophobic part and prevent the coagulation of the polymer particles by electrostatic or steric stabilization.

Copolymerizable emulsifiers offer the promise of being incorporated in the polymer backbone to contribute to enhanced stability of the polymer dispersion [250]. The chemical bond between polymer and emulsifier makes it impossible to sheer off the emulsifier by shear forces or other external impacts. Furthermore during film formation – when the solvent evaporates and the polymer film is formed from the polymer dispersion – copolymerizable surfactants are unable to migrate to the surface or to form nests of surfactants. In the ideal case the emulsifier is buried

inside the film. This should lead to improved film properties, e.g. less water take up or whitening of the film when it comes into contact with water.

In this approach, different ratios of reactive surfactant (1-(allyloxy polyalkoxy)-3-phenyloxy propyl polyethylene glycolethersulphate, ammonium salt, named APG 2019 (Clariant, Frankfurt/Main, Germany) and non reactive surfactant (SDS) were used to produce sulfated latexes with different charge density. APG 2019 is incorporated in the final particle. APG 2019 is an allyl-phenyl-glycerol derivative with a phenol group as a hydrophobic moiety and an allyl group as a copolymerizable moiety (structure in Figure 4.6). The hydrophilic moiety is a polyethylene glycol ethersulphate group with ammonium as counterion. APG 2019 is a clear, yellowish liquid about 90% active; the pH of a 1% aqueous solution ranges from 6 to 8.

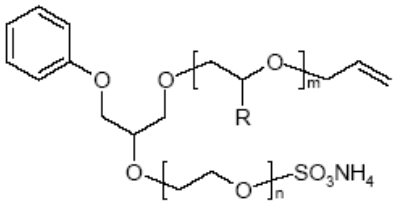


Figure 4.6. Structure of 1-(Allyloxy polyalkoxy)-3-phenyloxy propyl polyethylene glycolethersulphate, ammonium salt (n = 5, 10 or 20)

Aqueous solutions of initiator (ammonium persulphate (APS) or PEGA-200) and surfactant (APG 2019 and/or SDS) were prepared (Figure 4.7). Freshly distilled styrene (final concentration 12 $mg \cdot mL^{-1}$) was mixed with initiator and surfactant solutions (final concentration 1.6 $mg \cdot mL^{-1}$ and 4 $mg \cdot mL^{-1}$, respectively) in a final volume of 15 mL. The mixtures were kept at 70 °C for 24 hours with slow rotation. The resulting suspension was dialyzed. At the end the solid content was estimated and the NPs were characterized by TEM, DLS and zeta potential measurements as described above.

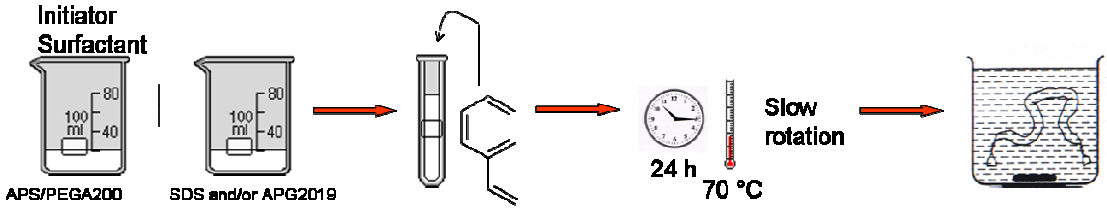


Figure 4.7. Scheme of the experimental procedure for the synthesis of sulfonated latexes.

4.2.3. Instrumentation and Methodologies

4.2.3.1. Circular Dichroism

As mentioned in the previous chapter, a number of spectroscopic methods are used to estimate protein secondary structure content (Table 3.3). Because of its simplicity, CD spectroscopy is widely used to determine the secondary structure of proteins and peptides.

A beam of light has time dependent electric and magnetic fields associated with it. If the light is polarized by passing through suitable prisms or filters, its electric field, *E*, will oscillate sinusoidally in a single plane, meaning this *E* has varying magnitude and constant direction orthogonal to the line of propagation (Figure 4.8) [251, 252].

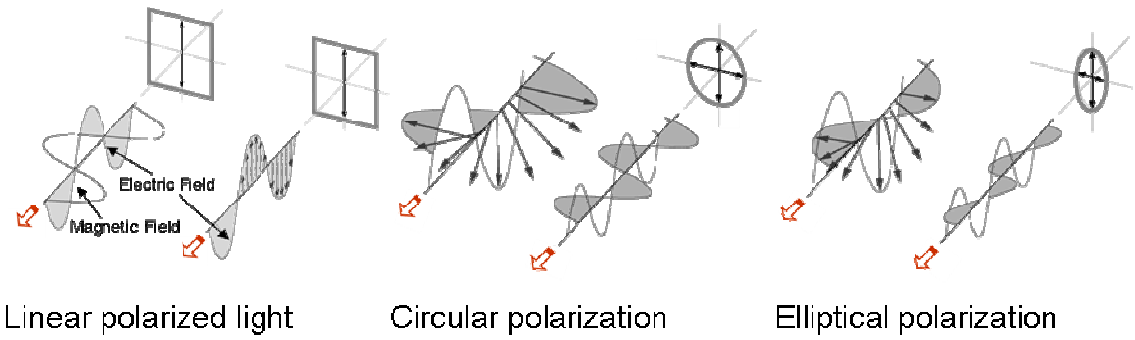


Figure 4.8. Linear polarized light can be visualized as a sine wave oscilating in a plane and its electric field vector has varying magnitude and constant direction orthogonal to the line of propagation. Circularly polarized light has an electric field vector of constant magnitude that changes its direction as a function of time on the plane orthogonal to the propagation.

When viewed from the front, the sinusoidal wave can be visualized as the resultant of two vectors of equal length, which trace out circles, one that rotates clockwise is called right handed (E_R) and the other that rotates counterclockwise denominated left handed (E_L) (Figure 4.9). The two circularly polarized waves have physical existence. The waves are 90º out of phase with each other and can be separated using a variety of prisms or electronic devices that utilize the Pockel's effect. When asymmetric molecules interact with light, they may absorb right- and left-handed circularly polarized light in different extents. The result is that the plane of the light wave is rotated and that the addition of the E_R and E_L vectors results in a vector that traces out an ellipse and the light is said to be elliptically polarized (Figure 4.9).

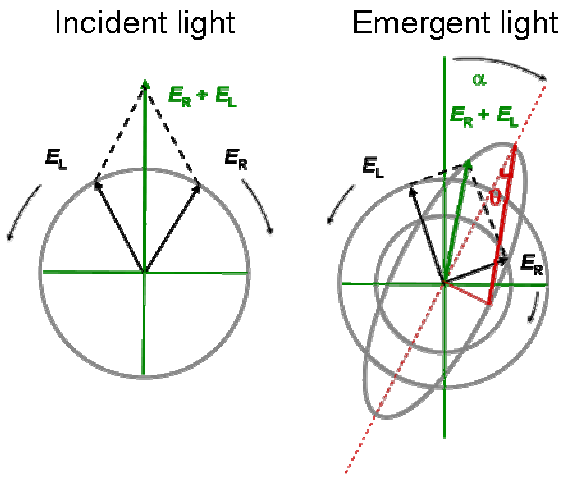


Figure 4.9. Linear polarized light is a sum of left- and right-handed circularly polarized components with equal length. When it passes a solution with an optically active substance the left and right components of the linear polarized light are absorbed in different amounts. The components are recombined and the emergent light is elliptically polarized.

The word chiroptical is descriptive of the techniques that use optical detection devices that are selective towards optically active (chiral) materials and/or molecules [253]. They are used for structural investigation and analytical determination. There are three chiroptical techniques: (i) optical rotation (OR), which deals with the angular rotation of plane polarized light at a single wavelength (λ) (or ellipticity resulting from absorption of linearly polarized light by chiral molecules); (ii) optical rotatory dispersion (ORD), in which the angular rotation of the plane polarized light is measured as a function of λ; and (iii) CD, in which the angular rotation is measured as a function of λ but the light is circularly polarized. CD and ORD are mathematically related by an integral transform (the Kronig-Kramerr transform).

CD is a form of light absorption spectroscopy that measures the difference in absorbance of right- and left-circularly polarized light (rather than the commonly used absorbance of isotropic light) by a substance (Figure 4.10). Inherently asymmetric chromophores (nearly all the molecules synthesized by living organisms are optically active) or symmetric chromophores in asymmetric environments will interact differently with right- and left-circularly polarized light resulting in circular dichroism. As a result, right- and left-circularly polarized light will be absorbed in different extents at some wavelengths due to differences in extinction coefficients for the two polarized rays (the refractive index is also different for the two forms of light). A curiosity, the word dichroism is derived from ancient Greek and means "two colours", because the sample under analysis has one colour if illuminated with the right-handed polarized light and a different color if illuminated with the left-handed one, as color is related with light absorption.

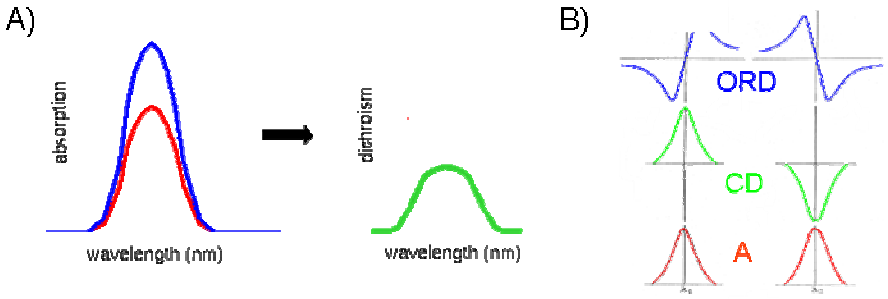


Figure 4.10. A) CD is a form of light absorption spectroscopy that measures the difference in absorbance of right- and left-handed circularly polarized light. B) The absorption band of a typical UV transition of an optically active molecule is illustrated on the left (red), and also the associated CD band (green), and ORD of the band (blue). CD spectra are coincident with the absorption spectra of molecules. However, ORD spectra are dispersive and have long "tails" of rotation to longer and shorted wavelengths than the absorption spectra. Thus ORD measurements can be made of the rotation of light by molecules in regions where they do not absorb light (*adapted from* [253]).

At a given λ,

$$\Delta A = A_L - A_R \qquad (4.1)$$

where ΔA is the difference between absorbance of left circularly polarized light (A_L) and right circularly polarized light (A_R). It can also be expressed, applying the Beer-Lambert´s law, as:

$$\Delta A = \varepsilon_L.C.l - \varepsilon_R.C.l \qquad (4.2)$$

where ε_L and ε_R are the molar extinction coefficients for left circularly polarized light and right circularly polarized light, respectively, C is the molar concentration and l is the path length in cm. Then,

$$\Delta\varepsilon = \varepsilon_L - \varepsilon_R \qquad (4.3)$$

is the molar CD. Although ΔA is usually measured, for historical reasons most measurements are reported in degrees of ellipticity. Molar CD and molar ellipticity $[\theta]$ are readily interconverted by the equation:

$$[\theta] = 3298.\Delta\varepsilon \qquad (4.4)$$

The main applications of CD Spectroscopy, taking into account its benefits and drawbacks (Table 4.2) are: (i) estimation of protein and nucleic acid conformation; (ii) monitoring of

conformational changes due to interactions of asymmetric molecules; (iii) evaluation of thermodynamics and kinetics of folding and unfolding; and (iv) determination of binding constants (direct titrations, serial dilutions of complexes, changes in stability due to thermal or chemical denaturation).

Table 4.2. Benefits and drawbacks of CD spectroscopy.

Benefits	Drawbacks
▪ Low concentrations/amounts of sample ▪ Non-destructive; measurements in solution phase ▪ Microsecond time resolution; kinetics of conformational changes ▪ Relative changes due to influence of environment	▪ Interference with solvent absorption in the UV region ▪ Absolute measurements subject to a number of experimental errors ▪ Average accuracy of fits about +/- 10% ▪ CD spectropolarimeter is relatively expensive

Within the far-UV region (180-240 nm, or even lower in the case of synchrotron CD), the same chromophores responsible for the absorption bands in proteins (peptidic bond, aromatic amino acid residues and disulfide bridges) give rise to the CD signals. The absorbing group is principally the peptide bond. There is a weak but broad $n \rightarrow \pi^*$ transition centered around 220 nm and an intense $\pi \rightarrow \pi^*$ transition, at about 190 nm [252]. Studies of far UV CD can be used to assess quantitatively the overall secondary structure content of the protein, since it has been known for many years that the different forms of regular secondary structure found in peptides and proteins exhibit distinct spectra (Figure 4.11 A). The intensity and energy of these transitions depends on the angles the peptide bond assumes (ψ and Φ angles) and therefore on the secondary structure of the protein (Figure 4.11 B and Table 4.3).

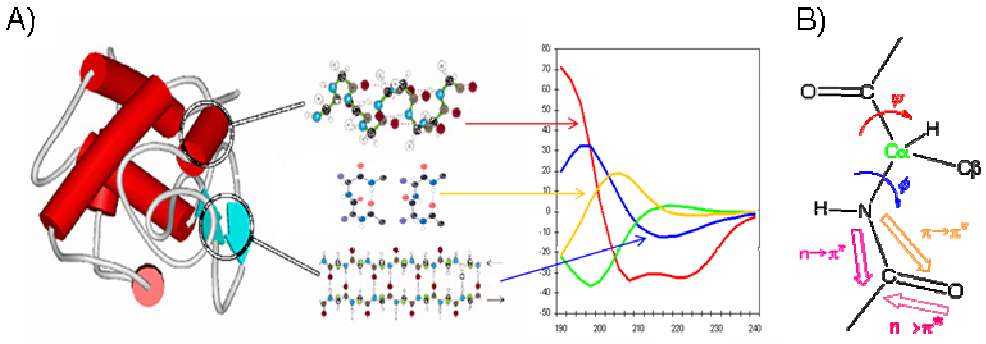


Figure 4.11. A) Representative CD curves corresponding to common secondary structural elements. (—) α-helix; (—) β-sheet; (—) β-turn; (—) "random coil". B) The transitions of the peptide bond responsible for CD adsorption bands. These transitions are dependent of the ψ and Φ angles.

Table 4.3. CD adsorption bands and responsible transitions in the far-UV observed for pure secondary structures of proteins.

Sec. Structure	Bands	Transition
α	negative; 222 nm	nπ*
	negative; 208 nm	ππ*
	positive; 190 nm	ππ*
β	negative; 218 nm	nπ*
	positive; 197 (± 5) nm	ππ*
"random coil"	217 nm (very weak)	ππ*
	negative;195 nm	nπ*
β-turns	variable	

Knowing the base spectra of the α-helix, β-sheet, β-turns and the disordered conformation, the secondary structure content of a protein/peptide can be estimated by a mathematical component analysis of the CD spectrum [251, 254]. Basically, all the analytical methods to analyze CD data assume that the spectrum of a protein can be represented by a linear combination of the spectra of the secondary structural elements plus a noise term which includes the contribution of aromatic chromophores and prosthetic groups (Table 4.4):

$$\theta_\lambda = \sum \varepsilon_i S_{\lambda i} + noise \qquad (4.5)$$

where θ_λ is the CD of the protein as a function of wavelength, ε_i is the fraction of each secondary structure i and $S_{\lambda i}$ is the ellipticity at each wavelength of each i^{th} secondary structural element. In

constrained fits the sum of all the fractional weights, ε_i, must equal one, and all of the fractional contributions must be greater than or equal to zero.

Table 4.4. Analytical methods to determine protein secondary structure from CD spectra [251, 254].

Method	Application
Multilinear Regression-Unconstrained Fit (MLR)	Samples with unknown concentration
Linear Regression-Constrained Fit (G&F, LINCOMB)	Polypeptide conformation
Convex Constrint Algorithm (CCA)	Folding states in a set of spectra
Ridge Regression (CONTIN)	Polypeptide conformation
Variable Selection (VARSLC)	Globular Proteins in solution
Variable Selection-Self Consistent Method (SELCON)	Globular Proteins in solution
Neural Network Analysis (K2D, CDNN)	Globular Proteins in solution

One of the strengths of CD is that various aspects of protein structure can be measured (Figure 4.12).

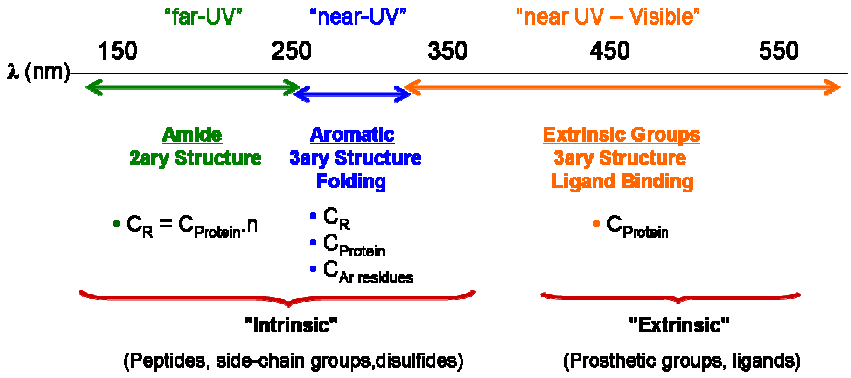


Figure 4.12. Characteristics of protein structure measured in the UV range by CD.

In the far UV, the peptide bond is the principal absorbing group; studies in this region can give information on the secondary structure [254]. In the near UV, the aromatic amino acids side chains (Phe, Tyr and Trp) absorb in the range 250 to 290 nm. The tertiary folding of the polypeptide chain can place these side chains in chiral environments, thus giving rise to CD spectra which can serve as

characteristic fingerprints of the native structure. In addition, non-protein components or cofactors, or added ligands, may absorb in regions of the spectrum well separated from those of amino acids and peptide bonds. The CD signals in these regions can be used to provide detailed information on the environment, and possible interactions between these cofactors or ligands and the protein.

CD measurements were carried out at room temperature on a JASCO J-720 spectrometer (Jasco Co., Tokyo, Japan). Each spectrum was an average of 6–10 scans using quartz cells having path length of 0.1 cm. Spectra were recorded in the range 260–180 nm at a speed of 50 nm/min with a resolution of 0.2 nm and are presented on a per residue basis ($deg \cdot cm^2 \cdot decimol^{-1}$). The mean residue molar ellipticity θ_{MRW} was calculated using the formula, $\theta_{MRW} = \theta/10 \times Cr \times l$, where MRW is the mean residue weight (molecular weight/number of residues) of the peptide, Cr is the mean residue molar concentration ($Cr = n \times Cp$, where n is the number of peptide bonds and Cp is the molar concentration in $mol \cdot L^{-1}$), l is the path length in cm, and θ is the ellipticity in mdeg. The baselines (pure buffer and NPs) were subtracted from the measured spectra.

4.2.3.2. Isothermal Titration Calorimetry

Characterization of the thermodynamics of binding interactions is important in improving the understanding of biomolecular processes, and forms an essential part of the rational drug design practice. Isothermal titration calorimetry (ITC) is becoming the method of choice for the determination of the thermodynamic parameters associated with the non-covalent interaction of two (or more) molecules [255]. It is a delicate method for the study of the heat effect of ligand binding to proteins or the study of protein association. ITC has matured into a highly sensitive technique requiring only small volumes (~1 mL) and low concentrations (μM), and reasonably short measuring times. The power of ITC lies in its unique ability to measure binding reactions by titrating one binding partner with another while measuring the heat released in a calorimeter cell, so there is no need of immobilization. Since heat change occurs during many physicochemical processes, ITC has a broad application, ranging from chemical and biochemical binding studies to more complex processes as enzyme kinetics.

Most of the commonly used isothermal titration calorimeters are based on a cell feedback network to differentially measure and compensate for heat produced or absorbed between the sample and a reference cell. This is known as differential power compensation. Twin coin-shaped cells are mounted in a cylindrical adiabatic environment, and connected to the outside through narrow access tubes (Figure 4.13). A thermoelectric device measures the temperature difference

between the two cells and a second device measures the temperature difference between the cells and the jacket. As chemical reactions occur in the sample cell, heat is generated or absorbed. The temperature difference between the sample and reference cells (ΔT_1) is kept at a constant value (i.e., the baseline) by the addition or removal of heat to the sample cell, as appropriate. The integral of the power required to maintain ΔT_1 constant over time is a measure of total heat resulting from the process being studied. Figure 4.13 is a schematic drawing of the ITC equipment design. A computer controlled syringe is used to titrate a solution of the binding molecule into the sample cell. Thus, the surroundings are constantly trying to cool the sample cell but heat is applied to keep it warmer and at a constant temperature.

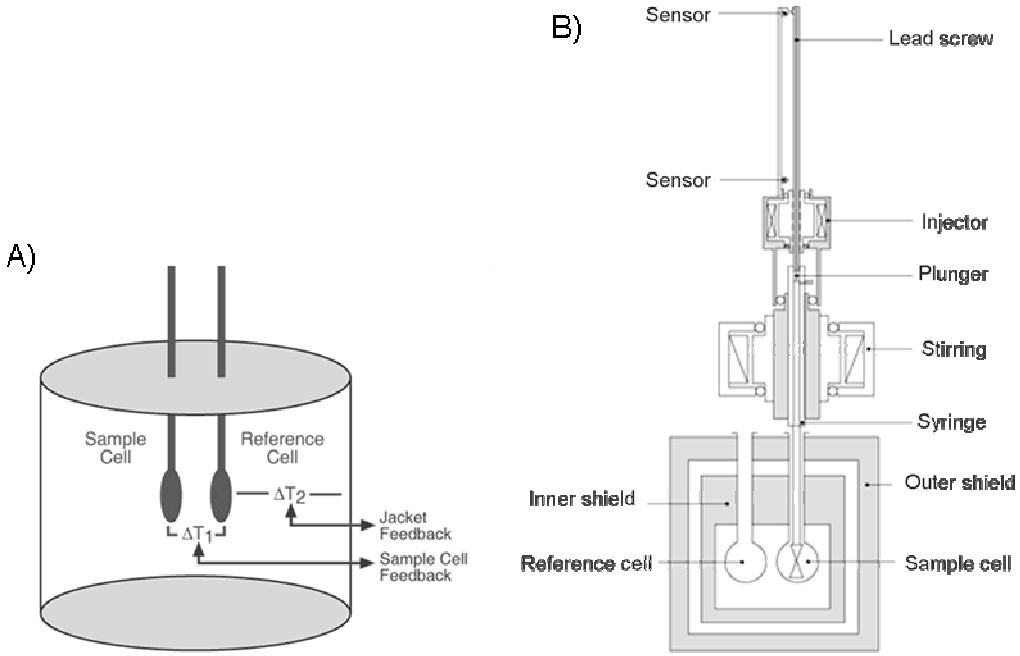


Figure 4.13. Diagram of ITC cells and syringe. The syringe rotates in place during the ITC experiment. The end of the syringe has been adapted to provide continuous mixing in the ITC cell. The plunger is computer-controlled and injects precise volumes of ligand (*adapted from* [256]).

As a molecule is titrated into the sample cell heat may be absorbed or generated depending on whether binding is endothermic or exothermic, respectively. If it is endothermic, more heat will need to be added to the sample cell to keep its temperature constant, while if it is exothermic less heat will need to be added. In both cases the change in heat flow into the sample cell required to maintain a constant temperature represents the heat of binding. As more titrant is added, the binding sites will become filled and once saturation is achieved, no further change will be observed except for a heat associated with dilution. In the raw data for a typical ITC experiment each peak

represents the heat change associated with an injection of binding molecule into the sample cell. The area under each peak is the total heat associated with the binding of all the material in that injection.

Analysis of the ITC provides the stoichiometry (*n*, number of binding sites), the enthalpy (ΔH^o) and entropy (ΔS^o) of binding, as well as the binding constant (*K*). In a single experiment, a complete thermodynamic profile of the molecular interaction can be determined. For a ligand X binding to a single set of n identical sites on a macromolecule M, i.e.,

$$M + X = MX$$
$$MX + X = MX_2$$
$$\cdot\ \cdot$$
$$MX_{n-1} + X = MX_n$$

the single-site binding constant is (filled sites)

$$K = \frac{[\text{filled sites}]}{[\text{empty sites}][X]} \qquad (4.6)$$

and

$$\Delta G^0 = -RT\ln K = \Delta H^0 - T\Delta S^0 \qquad (4.7)$$

here ΔG^0, ΔH^0 and ΔS^0 are the free energy, enthalpy, and entropy change for single site binding.

By non-linear least squares fit of calorimetric titration data, the parameters *K*, ΔH^0, and *n* are determined directly in a single experiment and ΔG^0 and ΔS^0 may then be calculated.

Measuring the binding isotherm at a second temperature allows additional determination of the change in heat capacity of binding through the relation:

$$\Delta Cp = \frac{\Delta H^0{}_{T_2} - \Delta H^0{}_{T_1}}{T_2 - T_1} \qquad (4.8)$$

It is expected to understand thermodynamically the effect of the synthesized nanoparticles on Aβ conformational changes.

ITC was carried out on a VP-ITC calorimeter (MicroCal LLC, Northampton, MA). Typically, 1.8 mL of 5 µM Aβ40/42 was loaded into the calorimetric cell into the injection syringe. Before experiments, all solutions were degassed by stirring under vacuum in a Thermovac unit supplied with the instrument. Following thermal equilibration at 25 °C and the initial 2 min delay, 25 serial injections of 10 µL were made into the cell from the syringe using a 300 rpm stirring speed and 10 min intervals. Separate experiments were conducted to measure heats of dilution. Baseline

correction and integration of the calorimeter response were carried out with the Origin software (MicroCal) provided with the calorimeter.

4.2.3.3. Thioflavine T Fluorescence Assay

ThT is a benzothiazole dye that exhibits enhanced fluorescence upon binding to amyloid fibrils and is commonly used to diagnose amyloid fibrils, both *ex vivo* and *in vitro* [43]. The dye associates rapidly with aggregated fibrils of Aβ peptides, undergoing a characteristic red shift of its excitation giving rise to a new excitation maximum at 450 nm and enhanced emission at 482 nm, as opposed to the 385 nm (ex) and 445 nm (em) of the free dye. This change is dependent on the aggregation state as monomeric or dimeric peptides do not react. The structure of ThT (Figure 4.14) has a hydrophobic end with a dimethylamino group attached to a phenyl group, linked to a more polar benzothiazole group containing the polar N and S.

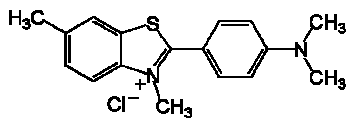


Figure 4.14. Structure of Thioflavine T.

This combination of polar and hydrophobic regions creates the possibility for ThT to form micelles in aqueous solutions, with hydrophobic interiors and the positively charged N pointing toward the solvent. Micelles are formed above the critical micellar concentration (cmc, 4 μM) that bind to amyloid fibrils causing changes in the excitation spectra and enhanced fluorescence [257].

The aggregation state of the samples analyzed by CD was checked 24 h after preparation using the ThT fluorescence assay. ThT was purchased from Fluka and stock solutions were prepared by dissolving ThT powder in 1 mL 50 mM glycine/NaOH buffer pH 9. The solution was filtered through 0.22 μm syringe filters and the concentration was determined spectrofotometrically using an extinction coefficient of 2.2×10^{-4} $M^{-1}\cdot cm^{-1}$ at 411 nm. The concentration of the stock was determined and the amount of ThT from stock needed in the assay (1 mL total volume) to obtain a final concentration of 30 μM was calculated. The stock solution was stored at 4 °C covered with foil. Excitation spectra were recorded on a Jasco FP-770 spectrofluorometer (Jasco Co., Tokyo, Japan) at 25 ºC with 30 μM ThT in 50 mM glycine/NaOH buffer, pH 9.0 in a 1 mL assay volume, with emission at 482 nm (10 nm slits) and the spectrum was recorded between 400 and 500 nm with 5 nm slits.

4.2.3.4. Immuno-Dot Blot Assay

Protein detection using the dot blot protocol allows the identification and analysis of proteins of interest. In dot blot methodology sample proteins are spotted through circular templates onto membranes or paper substrate as a discrete spot (dot) and hybridized with an antibody probe. Semi-quantitative measurements can be made of the spots.

A11 is a polyclonal antibody that recognizes a conformationally unique epitope common to soluble oligomers regardless of sequence (Figure 4.15 B) [120]. Also, A11 blocks the toxicity of Aβ oligomers, indicating they are the primary toxic species. A11 was produced by mimicking the structural organization of Aβ in oligomers by attaching the C-terminus of Aβ40 to colloidal gold particles via a thioester bond (Figure 4.15 A). New Zealand white rabbits were immunized with this micellar mimics of Aβ oligomers to raise antibodies. This antibody was used to monitor Aβ oligomer formation.

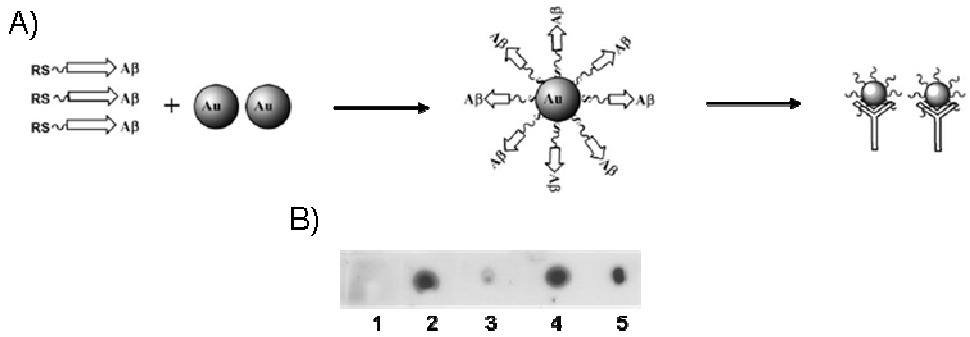


Figure 4.15. A) Strategy used to produce A11 anti-oligomer antibody. B) Characterization of oligomer-specific immunoreactivity of the antibody A11*. 1 – Aβ monomer; 2 - Aβ oligomer; 3 – fibrillar Aβ; 4 – synuclein oligomer; 5 – IAPP oligomer.
* test strips were kindly provided by Dr. Charles Glabe, Department of Molecular Biology and Biochemistry, University of California, Irvine, U.S.A.

Bam-10 is an antibody that recognizes an epitope within amino acid residues 1-12 of the Aβ sequence and was used to verify the exposure of this epitope. Monoclonal anti-Aβ (mouse IgG1 isotype) is derived from the Bam-10 hybridoma produced by the fusion of mouse myeloma cells and splenocytes from an immunized BALB/c mouse. Synthetic Aβ40 conjugated to KLH was used as the immunogen. Bam-10 antibody specifically stains amyloid plaques within the cortex and amyloid deposits in blood vessels of AD brain tissue.

HFIP-treated Aβ peptides were resuspended in PBS (20 mM, 150 mM NaCl, pH 7.4) to a final concentration of 50 μM in the absence or presence of NPs. The dot blot assay was performed as

previously described by Kayed *et* al. with minor modifications [120]. A 2.5 µL aliquot of each sample was hand-spotted onto nitrocellulose membranes (Amersham Bioscience) and blocked with 10% non-fat milk in TBS-T buffer for 1 hour at room temperature. The membranes were washed 3 times for 5 min with TBS-T and incubated for 1 hour at room temperature with antibody A11 (Biosource) diluted 1:1000 or with a mouse monoclonal anti-Aβ (clone Bam-10, Sigma, 1:1500), in 3% BSA/TBS-T. The membranes were washed again and incubated with secondary antibody horseradish peroxidase-conjugated anti-rabbit or anti-mouse Ig diluted 1:5000 in 3% BSA/TBS-T for 1 hour at room temperature. Detection was performed with ECL (enhanced chemiluminescence; GE Healthcare).

4.2.3.5. SDS Polyacrylamide Gel Electrophoresis

The term electrophoresis describes the migration of charged particle under the influence of an electric field. *Electro* refers to the energy of electricity. *Phoresis*, from the Greek verb *phoros*, means "to carry across". Thus, gel electrophoresis refers to the technique in which molecules are forced across a span of gel (colloid in a solid form), driven by an electrical current. Activated electrodes at either end of the gel provide the driving force. Many biological molecules such as amino acids, peptides, proteins, nucleotides, and nucleic acids, possess ionisable groups and, therefore, at any given pH, exist in solution as electrically charged species. Depending on the nature of the net charge, the charged particles will migrate either to the cathode or to the anode. Their rate of migration depends on the strength of the field, on the net charge, size, shape and relative hydrophobicity of the molecules, and also on the ionic strength, viscosity and temperature of the medium in which the molecules are moving. After staining, the separated macromolecules in each lane can be seen in a series of bands spread from one end of the gel to the other. As an analytical tool, electrophoresis is simple, rapid and highly sensitive and it is used analytically to study the properties of a single charged species, and as a separation technique.

In electrophoresis, the force moving the macromolecule results from the electrical field, *E*. the electrophoretic mobility of the molecule, μ, is the ratio of the particle velocity, *V*, to the electrical field [258]. Electrophoretic mobility is also equal to the net charge of the molecule, *Z*, divided by the frictional coefficient, *f*. Thus:

$$\mu = \frac{V}{E} = \frac{Z}{f} \qquad (4.9)$$

The frictional force of the gel material acts as a "molecular sieve," separating the molecules by size. There are two basic types of materials used to make gels: agarose and polyacrylamide. Agarose is a natural polymer extracted from sea weed. Agarose gels have large "pore" size and are used primarily to separate macromolecules such as nucleic acids, large proteins and protein complexes. Agarose gels can be processed faster than polyacrylamide gels, but their resolution is inferior.

The polyacrylamide gel electrophoresis (PAGE) technique was introduced by Raymond and Weintraub [259]. Polyacrylamide is the same material that is used for skin electrodes and in soft contact lenses. The pore size of the gel may be varied to produce different molecular sieving effects for separating proteins of different sizes. By controlling the percentage (from 3% to 30%), precise pore sizes can be obtained, usually from 5 to 2000 kDa. This is the ideal range for gene sequencing, protein, polypeptide, and enzyme analysis.

SDS is an anionic detergent which denatures proteins by "wrapping around" the polypeptide backbone, binding to proteins fairly specifically in a mass ratio of 1.4:1 [260]. In doing so, SDS confers a negative charge to the polypeptide in proportion to its length and the denatured polypeptides acquire equal charge densities per unit length. It is usually necessary to reduce disulphide bridges and this is done with 2-mercaptoethanol or dithiothreitol. In denaturing SDS-PAGE separations therefore, migration is determined not by intrinsic electrical charge of the polypeptide, but by molecular weight.

Proteins can be visualized after electrophoresis by staining them with dyes or metals that bind to the proteins but not to the gel itself [261]. All stains interact differently with different proteins. No stain will universally stain all proteins in a gel in proportion to the mass present. Coomassie blue staining is the most common stain for polyacrylamide gels. Silver staining is another popular method for detection that involves the fixation of the proteins in the gel matrix. Silver ions are then attached to the proteins in differing manners and can be viewed after a reduction step with formaldehyde. This allows direct visualization in the gel. In any case, each band on the gel represents a different protein (or a protein subunit); smaller proteins are found near the bottom of the gel. Sometimes proteins are transferred to membranes via western blotting for immunoblotting detection.

Aliquots (1.5 ng of peptide) of each reaction mixture prepared for immuno-dot blot assay were analyzed for SDS-stable LMW species. Aβ samples were separated by electrophoresis at 40 mV for 1 hour at room temperature, using 15% SDS-polyacrylamide gels. SDS and β-mercaptoethanol were present in both running and sample buffers but the samples were not preheated. LMW

markers purchased from Sigma were used as molecular weight standards. The gels were stained by a silver staining.

4.2.3.6. Cell Culture and Evaluation of Toxicity

The cell line used in all the cytotoxicity assays is the SH-SY5Y (human neuroblastoma cell line). This cell line is a thrice-cloned sub-line of bone marrow biopsy-derived SK-N-SH that had been established in 1970 from the bone marrow biopsy of a 4-year-old girl with metastatic neuroblastoma [262]. SH-SY5Y has a dopamine-β-hydroxylase activity and will form tumors in nude mice in approximately 3-4 weeks. The loss of neuronal characteristics has been described with increasing passage numbers. Therefore it is recommended not to be used after passage 20 or verify specific characteristics such as noradrenalin uptake or neuronal tumor markers. Morphologically these are epithelial-/neuronal-like elongated cells growing as monolayer and in cell clusters and they do not grow to complete confluence.

SH-SY5Y cells were propagated in 25 cm^2 flasks and maintained at 37 °C in a 95% humidified atmosphere and 5% CO_2. Cells were grown in Ham's F12:MEM (minimum essential media) (EBSS) (1:1) (Gibco BRL) supplemented with 2 mM L-Glutamine (Gibco BRL), 1% non essential amino acids (NEAA) (Gibco BRL) and 15% fetal bovine serum (FBS) (Gibco BRL). To split sub-confluent cultures (70-80% confluency) cells were seeded at 1×10^3 to 1×10^4 viable cells/cm^2 and trypsinized using 0.25% solution.

Evidences suggest links between deposition of Aβ, oxidative stress, and apoptosis associated with AD [154] and Aβ has been shown to induce apoptosis in neurons, which may contribute to the neuronal degeneration in AD [155]. Caspases (Cysteine-requiring Aspartate protease) are a family of proteases that mediate cell death and are important to the process of apoptosis. Caspases are regulated at a post-translational level, ensuring that they can be rapidly activated. Caspases exist as inactive precursor molecules called procaspases, which are activated through a proteolytic step. This proteolytic processing occurs at critical aspartic acid residues that conform to the caspase recognition sequence. As a result caspases often function in cascades. There are two types of apoptotic caspases: initiator caspases and effector (executioner) caspases. Initiator caspases (e.g. caspase-2, -8, -9, -10) cleave inactive pro-forms of effector caspases, thereby activating them. Effector caspases (e.g. caspase-3, -6, -7) in turn cleave other protein substrates within the cell, to trigger the apoptotic process. Within the caspase cascade, a model has been proposed in which an "initiator or upstream" protease, such as caspase-8, gets activated by an apoptic stimulus. This

activated caspase-8 then activates an amplifier protease, such as caspase-1 by cleavage at the recognition sequence. This, in turn, activates a "machinery" protease such as caspase-3 or caspase-7 (Figure 4.16).

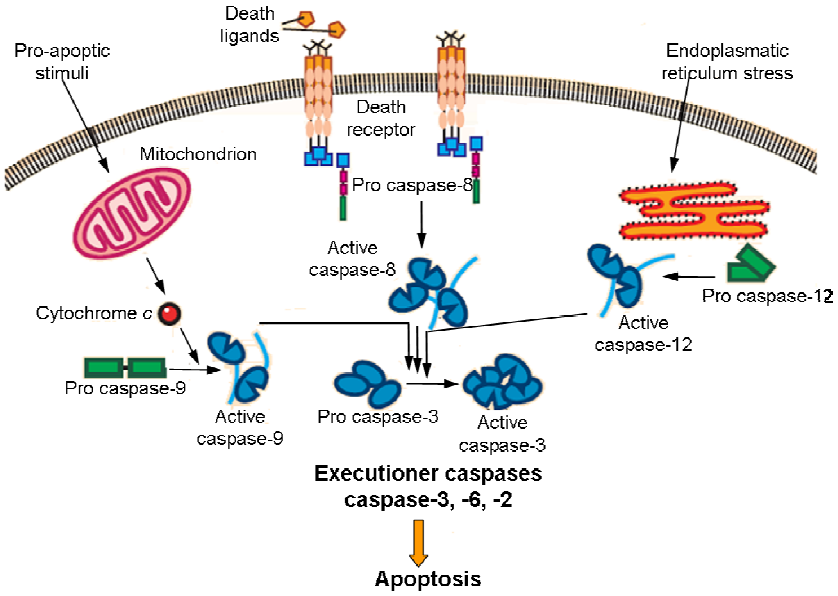


Figure 4.16. Caspase-mediated apoptosis. Caspases are typically activated in the early stages of apoptosis through two main pathways. The extrinsic pathway involves the binding of "death inducing ligands" to cell surface receptors. This pathway results in the activation of caspase-8. The intrinsic pathway is initiated by cellular stress and generally involves changes to the mitochondria that release cytochrome *c*, which activates caspase-9. Regardless of the activation pathway, both lead to a caspase cascade, where effector caspases are activated through proteolysis.

Caspase-3 (also referred to as CPP32, Yama, and apopain) is one of the critical enzymes of apoptosis mediating mitochondrion initiated apoptosis and is the most studied of mammalian caspases [151]. It can process caspase-2, 6, 7, and 9 proenzymes and specifically cleave most caspase related substrates known to date, and also plays a central role in mediating nuclear apoptosis. Caspase-3 activity is tissue, cell type, or death stimulus specific. Brain tissue from AD patients contains deposits of oxidized Aβ [151] and activated caspase-3 [156]. So the caspase-3 activity is an indicator of apoptosis and subsequent cell death induced by Aβ.

The caspase-3 fluorometric assay is based on the hydrolysis of the peptide substrate acetyl-Asp-Glu-Val-Asp-7-amido-4-methylcoumarin (Ac-DEVDAMC) by caspase-3, resulting in the release of the fluorescent 7-amino-4-methylcoumarin (AMC) moiety (Figure 4.17). The excitation and emission wavelengths of AMC are 360 nm and 460 nm, respectively.

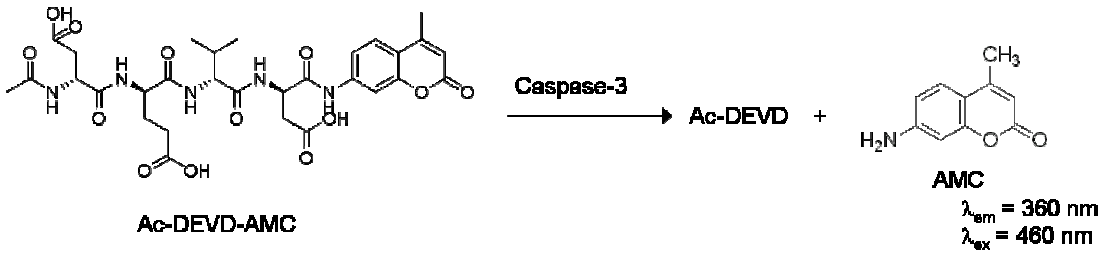


Figure 4.17. The caspase-3 fluorimetric assay.

MTT assay is a laboratory test and a standard colorimetric assay for measuring cellular proliferation widely used to determine cytotoxicity of potential medicinal agents and other toxic materials [263]. The MTT assay has been shown to be a measure of oxidative metabolism and vesicle trafficking induced by Aβ [102]. MTT enters the cells by endocytosis and is reduced to formazan by NADH reductase and other enzymes, which can be measured spectrophotometrically. Yellow MTT (a tetrazole) is reduced to purple formazan in the mitochondria of living cells (Figure 4.18). A solubilization solution (usually either DMSO or a solution of the SDS in dilute HCl) is added to dissolve the insoluble purple formazan product into a colored solution. The absorbance of this colored solution can be quantified by measuring at a certain wavelength (usually between 500 and 600 nm) by a spectrophotometer.

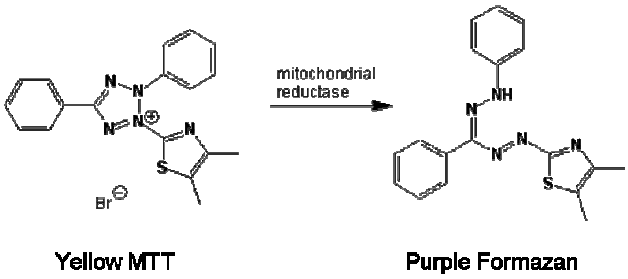


Figure 4.18. Reduction of MTT to formazan by mitochondrial enzymes.

This reduction takes place only when mitochondrial reductase enzymes are active, and therefore conversion is directly related to the number of viable cells. When the amount of purple formazan produced by cells treated with an agent is compared with the amount of formazan produced by untreated control cells, the effectiveness of the agent in causing death of cells can be deduced.

The procedure for producing Aβ oligomers was the same for both assays. Briefly, Aβ42 was pre-treated with HFIP and re-dissolved in DMSO at 2 mM. 10 μM peptide pre-incubated for 48 hours in F12 media (Gibco BRL) with or without nanoparticles at 4ºC with shaking, were added to

80% confluent cells in Dulbecco's MEM with 1% FBS, and further incubated for 24 hours, at 37 ºC. The cell tolerance to the NPs was verified and the maximum dose that allowed cells to grow normally was used in all the cytotoxicity assays performed.

Activation of caspase-3 was measured using the CaspACE fluorimetric 96-well plate assay system (Sigma), following the manufacturer's instructions. After incubation of cells with Aβ in the presence or absence of NPs, each well was trypsinized and the cell pellet was lysed in 100 µL of hypotonic lysis buffer (Sigma). 40 µL of each cell lysate were used in duplicates for determination of caspase-3 activation. The remaining cell lysate was used to measure total cellular protein concentration with the Bio-Rad protein assay kit (Bio-Rad), using BSA as standard. Values shown are the mean of duplicates and the experiment was performed three times. Comparison between groups was made using the Student's t test. A p value of less than 0.05 was considered statistically significant.

Alternatively, adherent cells were released from their substrate by trypsinization and resuspended at 4×10^4 per mL. In a 24-well plate, 400 µL of cellular suspension were plated in each well and incubated for 4 hours at 37 °C, in a 95% humidified atmosphere and 5% CO_2. The culture media was removed and wells were rinsed twice with PBS. 100 µL of complete culture media without phenol red and 10 µL of 5 $mg{\cdot}mL^{-1}$ MTT in PBS were added to each well followed by gentle homogenization. The plate was placed in the incubator for additional 4 hours, after which the supernatant was discarded. Remaining MTT-formazan crystals were dissolved with 100 µL of DMSO and the plate agitated for 5 min at 200 rpm. The content of each well was centrifuged at 13000 rpm for 2 min and 90 µL aliquots of the supernatant were transferred to a 96-well plate. Absorbance was read on a microplate spectrophotometer at 540 nm with background subtraction at 690 nm.

4.3. Results

4.3.3.1. Fluorinated vs Hydrogenated Nanoparticles

4.3.1.1. Effect on Aβ Secondary Structure and Aggregation

The NPs used in this study have a hydrophobic core (surfactant chains) and a hydrophilic shell (polyampholyte). The mean D_h are of about 3 to 5 nm and the zeta potentials of −50 mV when fluorinated and of +25 mV when hydrogenated. Thus, the NPs are electrostatically stabilized and they will not tend to coagulate or flocculate. They have high specific surface areas of approximately 1000 $m^2 \cdot g^{-1}$ which is expected to be useful in providing extensive interactions with the peptide (Figure 4.3) [241]. The secondary structure of Aβ peptides in the absence and presence of NPs was analyzed by CD spectroscopy. The peptides were pretreated with HFIP, a solvent that disrupts peptide-peptide interactions and facilitates the formation of α-helical structure as depicted in Figure 4.19 [183].

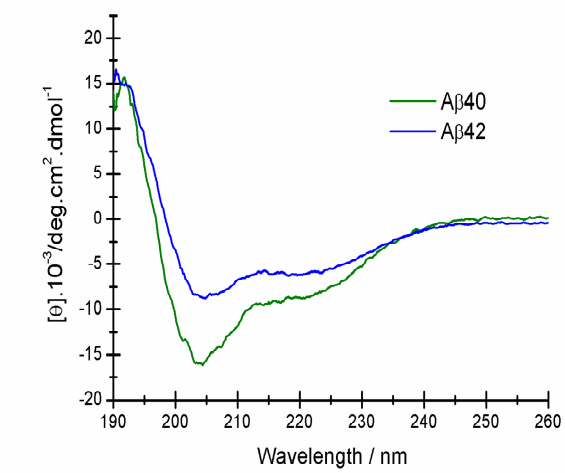


Figure 4.19. CD spectra of Aβ peptides 50 μM in HFIP.

The far-UV CD spectra obtained are shown in Figure 4.20. Immediately after resuspension in buffer (pH 7) at 50 μM, Aβ40 and Aβ42 show evidence of different secondary structural properties. While Aβ40 is mostly unordered (one single minimum at ~200 nm), Aβ42 is folded in a β-sheet structure, as the spectrum has the characteristic features of this structure - minimum at 217 nm and maximum at ~200 nm. It has been proposed that even monomeric Aβ exists in solution as a metastable loop-like structure containing an antiparallel β-sheet [135] and recently was

demonstrated by molecular dynamics simulations that the two additional hydrophobic residues at the Aβ42 C-terminus, Ile41 and Ala42, significantly increase contacts within the C-terminus and between the C-terminus and the CHC [103]. As a result, the β-structure of Aβ42 is more stable than that of Aβ40, and the conformational equilibrium in Aβ42 shifts towards β-structure. Fluorinated complexes, at a concentration of 8 mg·mL^{-1}, induce a very significant random coil → α-helix conformational conversion in Aβ40, as shown by the appearance of the two characteristic minima at 208 nm and 222 nm and a maximum at ~190 nm in the spectrum A of Figure 4.20. In the case of Aβ42, at lower NP concentration (2 mg·mL^{-1}), the predominant β-sheet content was not significantly altered as shown by the CD spectra (Figure 4.20 B). In contrast, the spectrum was reminiscent of α-helix structure at a NP concentration of 8 mg·mL^{-1}. The maximum was shifted to lower wavelengths and its intensity increased. Also the minimum at ~220 nm typical for the β-sheet secondary structure is broadened and shows a small shoulder around the characteristic 208 nm minimum for α-helix secondary structure.

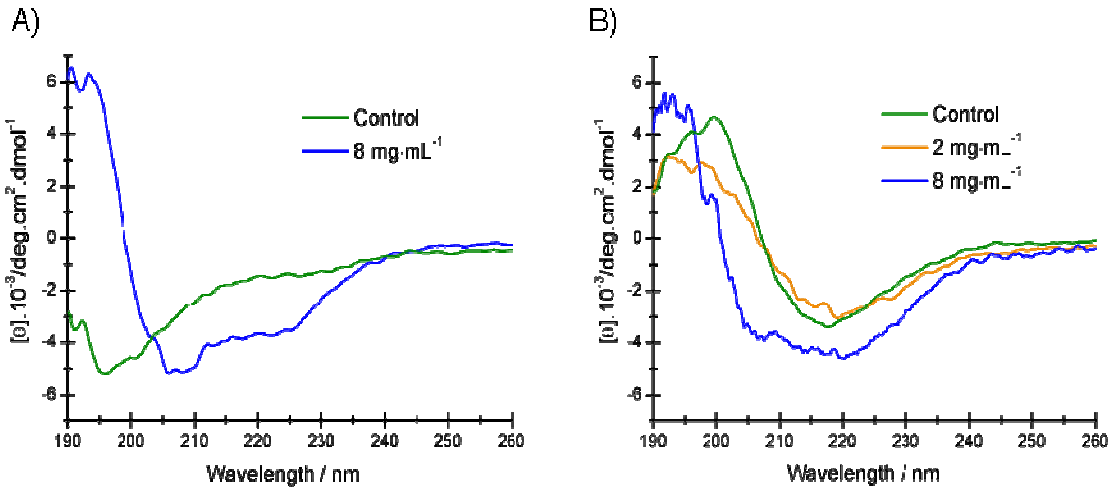


Figure 4.20. CD spectra of Aβ peptides before and after titration with 8 mg·mL^{-1} fluorinated NPs. A), Aβ40 50 µM in phosphate buffer 10 mM, pH 7; B), Aβ42 50 µM in phosphate buffer 10 mM, pH 7.

The CD spectra of Aβ42 titrated with increasing fluorinated NP concentration intersect at ~200 nm, with positive ellipticity values, thus the spectrum of the titration with complexes at 2 mg·mL^{-1} can be considered a superposition of CD spectra for β and α structures as the amount of NPs is not enough to recruit and change the conformation of all Aβ molecules. Together, these spectral changes are a good indicator that less peptide is in a β-sheet conformation and more in α-helical one. In any case the CD spectra are distorted due to light scattering and this effect could not be totally eliminated by reference measurements. Therefore the discussion here is restricted to relative changes since determination of secondary structure content would be a complicated task and

probably not very accurate. The CD spectrum of Aβ42 in the presence of hydrogenated complexes was measured but is not shown since the S/N ratio is very low due to scattering effects which is an indicator of aggregation.

The aggregation state of the samples analyzed by CD was checked 24 hours after preparation using the ThT fluorescence assay. ThT fluorescence excitation was measured with emission at 482 nm and the spectrum was recorded between 400 and 500 nm (Figure 4.21). As shown in Figure 4.21, the fluorinated NPs decrease the intensity of the ThT excitation peak at 440 nm, which means the peptides are less aggregated when these NPs are present. It is not totally clear why in the presence of hydrogenated analogues the intensity of the 440 nm excitation peak is also diminished, since CD results have shown that both peptides are more aggregated and have increased β-sheet content in the presence of hydrogenated NPs.

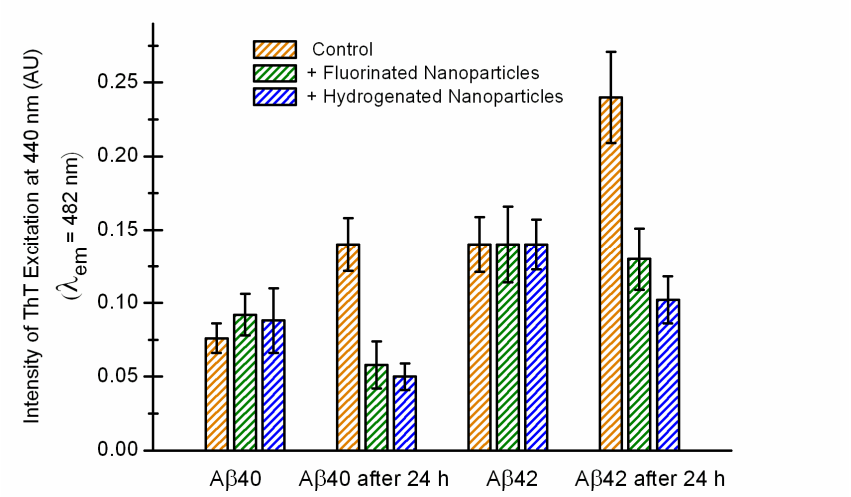


Figure 4.21. ThT fluorescence excitation intensity at 440 nm (λ_{em} = 482 nm) of Aβ solutions in the absence or presence of NPs. Experiments were performed in duplicates and the error bars indicate the standard deviations.

To have an idea about the process in terms of aggregation in real time, AFM was employed. After HFIP pretreatment and re-dispersion in PBS, Aβ42 looks like a dense and homogeneous film of non-aggregated peptide (Figure 4.22 A). After 1 day, oligomers with a diameter of ~ 3 nm, determined by section analysis, were observed in agreement with previously reported data [184]. After 3 days, fibrillar structures with small height are detected together with oligomers. In the presence of 8 mg·mL^{-1} fluorinated NPs, AFM imaging suggests that the peptide interacts strongly with these structures as the homogeneous field observed in the case of Aβ42 alone seems to be around the NPs, leaving more areas "empty". The cross section analysis shows that it does not seem to be much material in the vicinity of the fluorinated NPs, so the peptide should be at their surface.

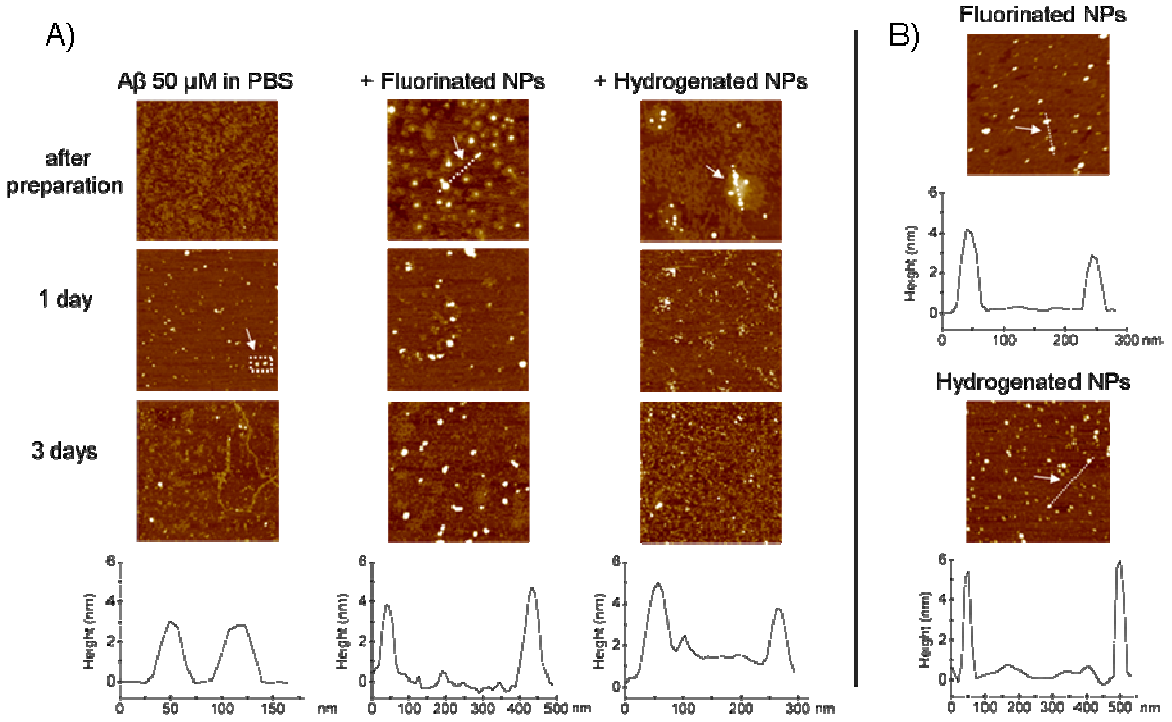


Figure 4.22. AFM analysis of Aβ42 aggregation. In A, Aβ42 was incubated in PBS (20 mM, 150 mM NaCl, pH 7.4) at room temperature without stirring (50 μM final concentration) alone or in the presence of 8 mg·mL^{-1} of fluorinated and hydrogenated NPs. In B, NPs were incubated in PBS (8 mg·mL^{-1}) for 3 days. 5 μL aliquots were spotted on freshly cleaved mica. The image size is 1×1 μm^2 x-y and the z-range is 5 nm. Section analysis correspondent to the dotted lines indicated by white arrows are shown.

In these images, the NPs look bigger than measured by dynamic light scattering (3-5 nm diameter), but this is frequently observed in AFM experiments. Figure. 4.22 B shows the AFM images of the NPs alone incubated for 3 days, which look like the images obtained at the beginning of the experiment (observed for both NPs, data not shown). The cross section analysis shows a similar profile but the area occupied seems to be slightly bigger in the case of co-incubation with the peptide, so we can attribute the differences to the adsorption of Aβ42 at the NP surface. Up to 3 days of incubation, there are no major changes and even oligomeric structures are not abundant; the peptide seems to be mostly in a monomeric state. The picture changed considerably when Aβ42 was incubated in the presence of the hydrogenated analogues. Immediately after preparation, the image exhibits the NPs surrounded by peptide but in a more dispersed way, so the interaction is not as strong as before. The cross section analysis in Figure 4.22 A, if compared to the one in Figure 4.22 B for the hydrogenated NPs alone, displays a different profile since the peaks are much broader and the height between them is ~1.5 nm. These observations might be explained by the conversion of Aβ42 to a more aggregated state. After 1 day, oligomers and even small protofibrils

are clustered around the complexes. After 3 days, a big network of shorter fibrillar structures is observed all over the surface. The AFM shows a clear difference between the state of association of Aβ42 incubated with fluorinated and hydrogenated NPs.

4.3.1.2. Energetics of the Interactions

To better understand the mechanism and important factors in the formation and stability of interactions between Aβ and NPs and the driving force of conformational changes thermodynamic approaches were employed. ITC is a method of choice for the determination of thermodynamic parameters associated with non-covalent interactions [255]. The observed heat includes heats of binding, of dilution of both protein and NPs, and of mixing. It includes not only contributions directly attributable to the binding event, but also solvent effects and conformational changes that might occur.

Oligomer formation is favored at physiological pH (7.4) and ionic strength (150 mM) [184] where hydrophobic interactions in the C-terminal region may predominate. But high salt concentrations diminish the effective surface charge of the NPs and this charge shielding would consequently be expected to reduce the electrostatic interactions between charged residues on the surface of Aβ and charged groups of NPs. It has been shown that addition of salt, at 37 °C, reduces the α-helical inducing effect in the case of Aβ40 [242]. In the present work PBS (with exception of CD measurements) was always the buffering system used since it mimics better the physiological medium. It is expected that electrostatic interaction is reduced but still present, as AFM analysis (done with PBS) shows that the NPs were efficient.

By analyzing the thermodynamic data in PBS, the contribution of hydrophobic interactions can be estimated since the presence of salt will reduce the electrostatic interactions. As shown in Figure 4.23, there is a strong interaction between the fluorinated NPs and both Aβ40 and Aβ42 in PBS that does not exist in the case of titration of the peptide with the hydrogenated NPs. The hydrogenated NPs with positive zeta potentials may interact electrostatically with the charged N-terminus of the peptide (pI of Aβ is 5.2). This could lead to conformational changes which allow also interactions with the negatively charged residues in the central region (Glu22 and Asp23). So important here is the observation that in the presence of high ionic strength the interaction is more favorable in the case of the fluorinated NPs, which indicates that hydrophobic interactions play a very important role since perfluorododecanoic acid is more hydrophobic than dodecanoic acid. Therefore, fluorinated NPs should be able to interact to a larger extent with hydrophobic parts of the peptide.

It is worth to stress that the complete thermodynamic characterization of a non-covalent interaction is only of real value if the parameters are understood in the context of changes which occur in the system on going from the free state to the bound state. In the experiment described here, ligand binding is coupled to a conformational transition and it is hard to evaluate these contributions, so the data was not fitted with any binding model.

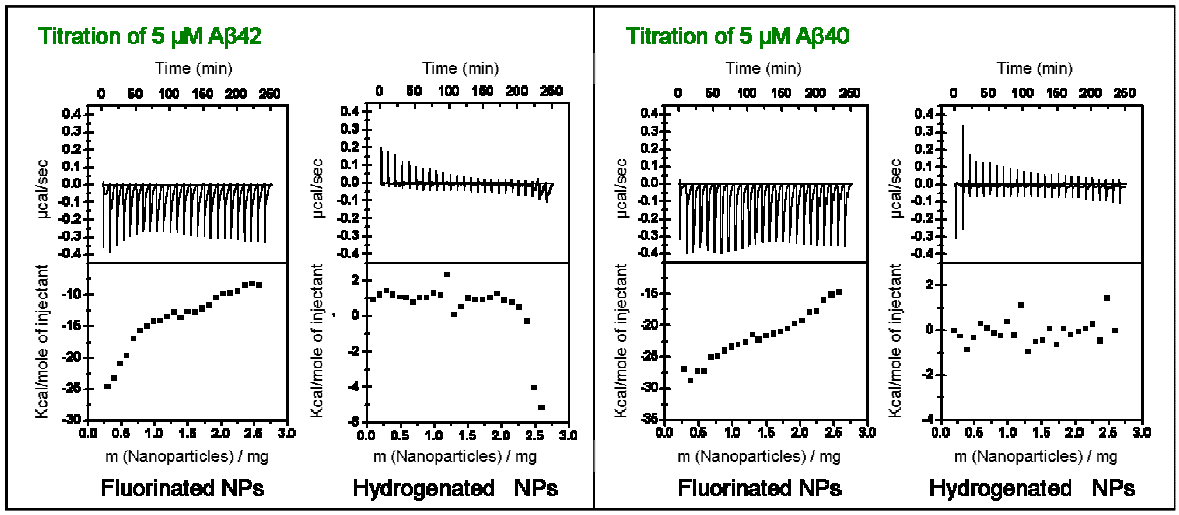


Figure 4.23. Isothermal titration calorimetry. Each panel shows in the upper part the heat evolving from titration of 10 mg·mL^{-1} NP solution into 5µM Aβ peptides in PBS. Peaks correspond to 10 µL injections with 10 min intervals and they are corrected for the heats of dilution. In the bottom of each panel are the binding isotherms integrating the raw data.

4.3.1.3. Effect on Aβ Oligomer Formation

It is at present recognized that not monomers or insoluble fibrils may be responsible for neurotoxicity but soluble oligomers of Aβ. A11 is a polyclonal antibody that recognizes a conformationaly unique epitope common to soluble oligomers regardless of the sequence [120]. A11 does not recognize the Aβ monomer, or Aβ fibrils and blocks the toxicity of Aβ oligomers. We have used this antibody to monitor oligomer formation and confirm the AFM analysis suggesting that the conformational change into α-helix enriched structures affects oligomer formation. Bam-10 is a monoclonal Anti-β-Amyloid Protein (mouse IgG1 isotype) antibody that recognizes an epitope within amino acid residues 1-12 of the Aβ sequence and was used to verify the exposure of this epitope. SDS-PAGE has been used in literature to characterize Aβ oligomers preparations. Walsh *et* al. reviewed evidences that Aβ toxicity is likely to be mediated by different multiple Aβ assembly forms, and that the earliest symptoms of the disease are attributable to soluble, SDS-stable *low-n* oligomers [264].

Aliquots of 50 μM Aβ40 and Aβ42 in the absence or presence of 8 $mg \cdot mL^{-1}$ of fluorinated or hydrogenated NPs were removed at various times and tested in parallel by immunoblotting and SDS-PAGE. We have used this concentration of complexes since according to CD and AFM results this is the amount of fluorinated NPs needed to have a significant increase in α-helical content of the peptide secondary structure with concomitant anti-aggregation activity. Samples were spotted onto nitrocellulose membranes and probed with A11 and Bam-10 antibodies. For Aβ42, oligomer-specific immunoreactivity formed within 2 days and was stable for 5 days (Figure 4.24 A). Bam-10 reactivity diminished as aggregation proceeded. The same was observed for Aβ40 (Figure 4.24 B) but, as the oligomerization process is slower, for the same concentration of peptide, oligomer-directed detection was achieved only after 5 days. Accordingly, Bam-10 immunoreaction only started to faint after 7 days of incubation. This behaviour was previously described for monoclonal antibodies 6E10 and 4G8 [265], which recognize epitopes in the N-terminal and internal regions of the peptide sequence, respectively. For 4G8, this is attributable to the fact that the CHC has a central role in oligomerization, so its immunoreactivity should disappear early as oligomerization proceeds. Since the rates of fibril nucleation and elongation are favored by incubation at 37 °C [266, 267] and proceed through a mechanism that is closely related with concentration [184], Bam-10 immunodetection changes with incubation time, peptide concentration and temperature were checked (Figure 4.24 C). As expected, Bam-10 immunoreaction is weaker as oligomerization proceeds, with increasing time, temperature and peptide concentration.

The effect of NPs is shown in Figure 4.24 A and B. Strong A11 immunoreactivity was never detected in the case of Aβ40 and Aβ42 incubated with fluorinated NPs, suggesting these complexes inhibited oligomer formation whereas Bam-10 reacted strongly during the first 7 days, similarly to the control. Fuorinated NPs might interact with crucial regions for Aβ oligomerization in the very beginning of the nucleation process, shielding them from interaction with other peptide molecules as suggested by AFM. As a result, the oligomerization reaction stops. In the case of incubation with the hydrogenated analogues, none of the antibodies reacted strongly since the beginning of the reaction for Aβ42. Accordingly to the AFM images, these NPs might provide a high concentration of peptide on the surface in a conformation that favors fast aggregation. Hence, both epitopes are shielded and immunodetection is not achieved. In this case, the lack of immunoreactivity with A11 is attributed not to the ability of the complexes to abrogate oligomer formation but instead to their capability to accelerate Aβ aggregation. The apparent different accessibility of epitopes confirms the conformational differences between the samples. However, the epitope is recognized in the Aβ40 species, presumably also due to a different conformation. The reason for this is not totally clear.

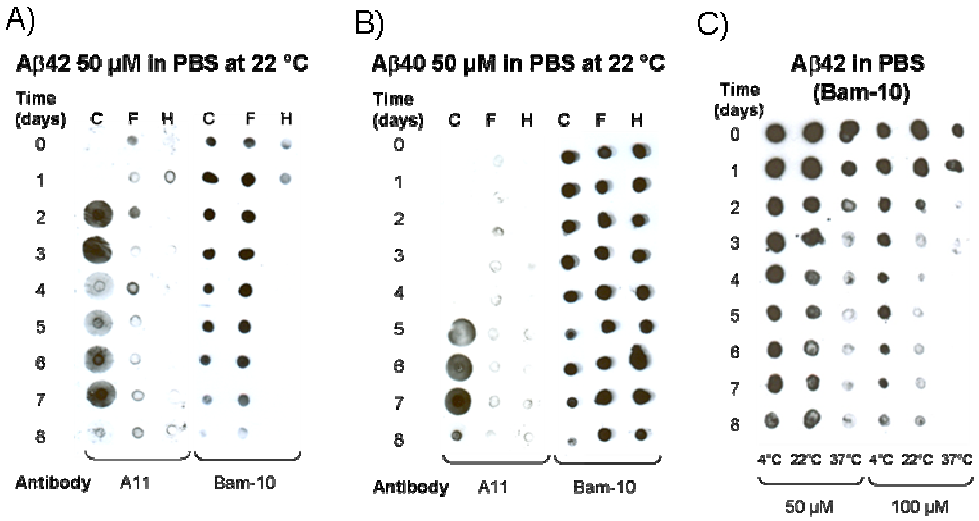


Figure 4.24. Time course of Aβ oligomerization detected by immunoblotting. A) Aβ42 was incubated for up to 8 days in PBS, pH 7.4 at room temperature without stirring (50 μM final concentration) in the absence (C) or presence of 8 mg·mL^{-1} of fluorinated (F) and hydrogenated (H) NPs. Aliquots were spotted onto nitrocellulose membranes and probed with A11 and Bam-10 antibodies. B) Aβ40 was incubated under the same conditions described for A). Aliquots were spotted onto nitrocellulose membranes and probed with A11 and Bam-10 antibodies. C) 50 μM and 100 μM Aβ42 was incubated for up to 8 days in PBS, pH 7.4 at 4 °C, 22 °C and 37 °C. Aliquots were spotted onto nitrocellulose membranes and probed with Bam-10 antibody.

To corroborate the effect of NPs in the oligomerization process of Aβ, assessment of size using standard denaturating gel conditions was performed with the reaction mixtures tested by immunoblotting. The silver staining shows that SDS-stable Aβ42 oligomeric species are present 1 day after preparation of a 50 μM solution (Figure 4.25). These have relative molecular masses of ~14,000 and ~19,000, which may be attributable to trimers and tetramers. Chen and Glabe determined a denaturation profile for Aβ42 and one apparent transition was found, with data fitting either a two-state trimer to unfolded monomer model (Tri ↔ 3U) or tetramer to unfolded monomer model (Tetra ↔ 4U) [102]. By photochemical cross-linking, paranuclei of Aβ42 ranging from tetramer to octamer that are in rapid equilibrium have been observed [268]. Possibly the trimeric and tetrameric species observed represent the paranuclei observed by cross-linking. This apparent discrepancy can be simply explained by the possibility that the photochemical cross-linking products are mixtures that result from the cross-linking of a trimer/tetramer and the random collisional cross-linking of additional monomeric subunits that are in rapid equilibrium. In the case of co-incubation with fluorinated NPs, the appearance of oligomers was delayed and SDS-stable trimers and tetramers are observed only after 3 days. Both are less abundant than in the case of the peptide alone and the relative amount of trimers is lower. This suggests that these small oligomers may be important for nucleation.

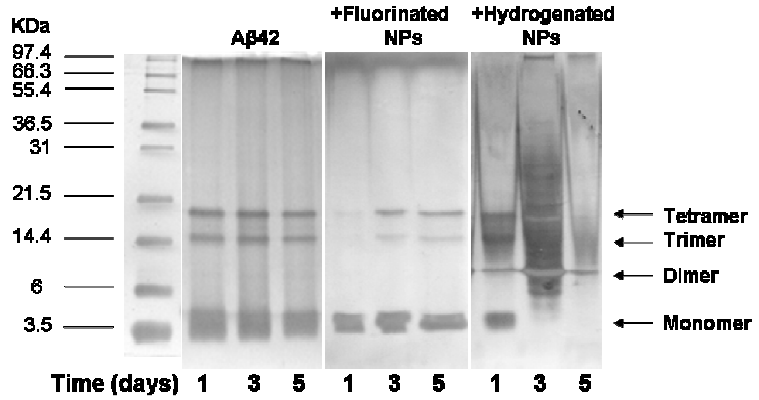


Figure 4.25. SDS-PAGE electrophoretic migration of Aβ42. Aβ42 was incubated in PBS, pH 7.4 at room temperature without stirring (50 μM final concentration) in the absence or presence of 8 $mg \cdot mL^{-1}$ of fluorinated and hydrogenated NPs. Aβ42 (0.2 pmol/lane) SDS-stable oligomers were separated using denaturating and reducing conditions and visualized using a silver staining protocol.

In the case of Aβ40 (Figure 4.26), dimers are visualized after 1 day of preparation. For this peptide the denaturation profile was accurately fit by a two-state model (N ↔ U), where a folded, or native, monomer and an unfolded or denatured monomer are present at equilibrium (similar for small proteins) [102]. It likely adopts a collapsed structure as previously reported [269]. When Aβ40 was co-incubated with fluorinated NPs, SDS-stable dimers were not observed for up to 5 days.

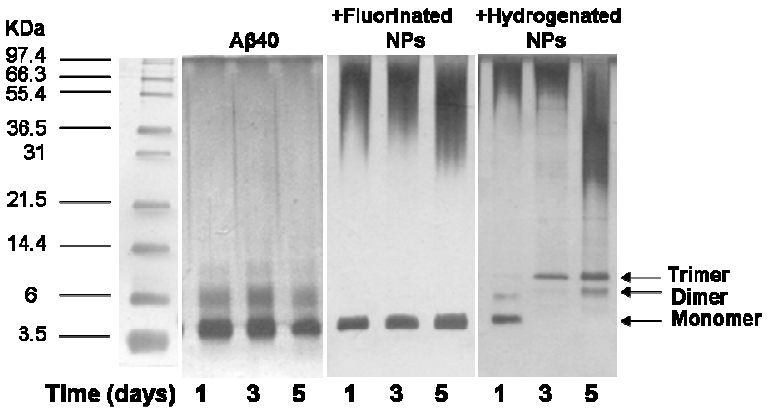


Figure 4.26. SDS-PAGE electrophoretic migration of Aβ40. Aβ40 was incubated in PBS, pH 7.4 at room temperature without stirring (50 μM final concentration) in the absence or presence of 8 $mg \cdot mL^{-1}$ of fluorinated and hydrogenated NPs. Aβ40 (0.2 pmol/lane) SDS-stable oligomers were separated using denaturating and reducing conditions and visualized using a silver staining protocol.

The hydrogenated NPs, which induce aggregation as determined by CD, AFM and immunobloting, promote the formation of SDS-stable Aβ42 homodimers that were not observed in the previous cases, and after 3 days both Aβ40 and Aβ42 monomers are not detected anymore.

Schmechel *et* al. [138] demonstrated for the first time that a biochemically defined assembly of Aβ into dimers probably represents the initial step in amyloidogenesis. For Aβ40 trimers were also visualized, and this can be explained by a higher rate of aggregation, as the one observed for Aβ40 but detection is not due to a equilibrium since monomers are not detected anymore after 3 days.

3.3.1.4. Effect on Aβ-induced Cytotoxicity

Several substances, such as small compounds and short peptides, have been shown to prevent cell death induced by Aβ in cell culture systems, usually by interfering with signalling pathways triggered by cell contact with amyloidogenic toxic species [176, 270]. It was hypothesized that differences in Aβ conformation and oligomerization state induced by NPs may influence bioactivity. Soluble aggregates of Aβ40 and Aβ42 produced *in vitro* are both toxic, but the latter are much more so by a factor of about 100 [271]. Therefore the effect of the NPs on the peptide induced cytotoxicity was only evaluated for the more bioactive Aβ42 oligomers since they are good therapeutic targets. The cell line used in all the cytotoxicity assays was SH-SY5Y. To produce Aβ42 oligomers, HFIP-pretreated peptide was dissolved in DMSO and diluted in phenol red-free F12. After a pre-incubation of 48 hours, the mixtures were incubated for 24 hours with the cells.

The cytotoxicity of Aβ42 oligomers was firstly assessed by interference with MTT reduction, shown to be a measure of oxidative metabolism and vesicle trafficking [218]. According to the MTT reduction assay, the application of 10 μM Aβ42 affected cellular redox activity in SH-SY5Y cells, causing decreased MTT reduction into formazan (84±17% of control, n=5) and thus reduced cell viability (Figure 4.27). When fluorinated NPs were incubated with Aβ42 during oligomerization, cell viability increased slightly (91±33%, n=5), so these structures interfered with Aβ42 induced decrease of MTT reduction. In contrast, the hydrogenated analogues had very little influence on the cytotoxicity of Aβ42 when compared with the control (80±10%, n=5), yet showing a tendency to potentiate it as cytotoxicity is possibly related to its effect on aggregation. It should be noticed that the error bars on both control and treated samples are very high, and this could indicate a poor reproducibility and low sensitivity of the assay for this particular experiment, since the oligomers did not significantly reduce the amount of MTT metabolically reduced by the cells when compared with non treated wells. In parallel with the MTT assay an alternative method to estimate the impact of the polymeric nanostructures on the Aβ induced cytotoxicity was used.

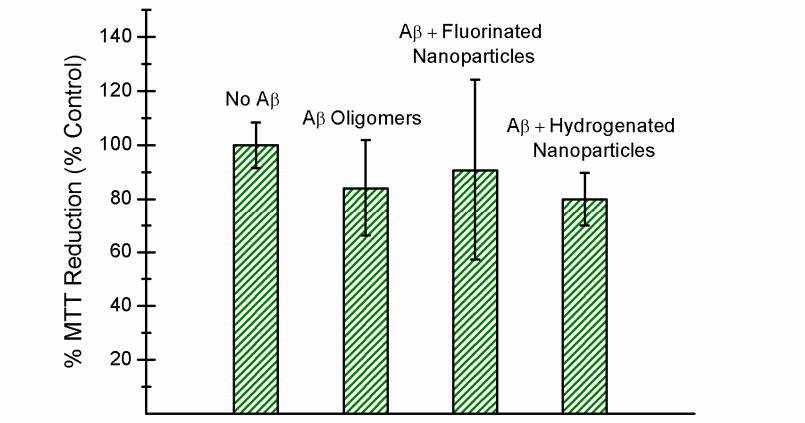


Figure 4.27. Aβ42-mediated inhibition of neuronal MTT reduction. 10 μM Aβ42 pre-incubated for 48 hours in F12 media with or without NPs (100 μg/mL of culture for fluorinated NPs and 50 μg/mL of culture for the hydrogenated analogues) at 4 ºC with shaking, was added to 80% confluent SH-SY5Y cells and further incubated for 24 hours, at 37 ºC. For each experiment, the data shown are the averages of 5 wells.

Evidences suggest links between deposition of Aβ, oxidative stress, and apoptosis associated with AD [154] and Aβ has been shown to induce apoptosis in neurons, which may contribute to neuronal degeneration [155]. Brain tissue from AD patients contains deposits of oxidized Aβ [151] and activated caspase-3 [156], a cysteine protease that mediates mitochondrion initiated apoptosis. So the caspase-3 activity is an indicator of apoptosis and subsequent cell death induced by Aβ. The caspase-3 fluorometric assay is based on the hydrolysis of a peptide substrate by caspase-3, resulting in the release of a fluorescent moiety. The results obtained are shown in Figure 4.28.

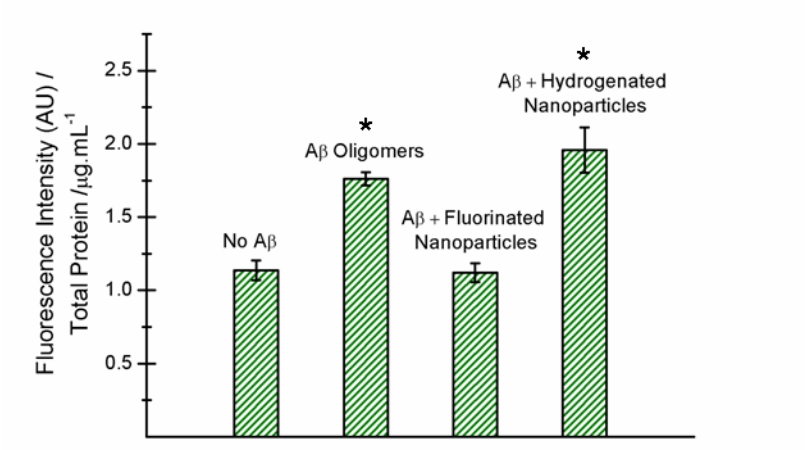


Figure 4.28. Aβ42-induced caspase-3 activation in cultured neurons. 10 μM Aβ42 pre-incubated for 48 hours in F12 media with or without NPs (100 μg/mL of culture for fluorinated NPs and 50 μg/mL of culture for the hydrogenated analogues) at 4 ºC with shaking, was added to 80% confluent SH-SY5Y cells and further incubated for 24 hours, at 37 ºC. For each experiment, the data shown are the averages of 3 wells. * indicates values significantly different from those for control cells as calculated by Student's t-test ($P < 0.05$).

Even though the ratio NPs:Aβ42 used in the cell assays was considerably lower than in the other experiments, the NPs were efficient, what means that they inhibit or enhance bioactivity, in accordance to the conclusions drawn from CD, AFM, immunoblotting and SDS-PAGE experiments. To clarify this, a dose dependent assay of the inhibitor activity of fluorinated NPs was performed (Figure 4.29). When Aβ42 was pre-incubated in the presence of lower concentrations of NPs than the one used in the previous assay (Figure 4.29), no protection is observed. If the concentration of NPs is higher then the cell tolerance pre-determined (100 μg/mL of culture), toxicity is increased due to the cytotoxicity of the NPs themselves.

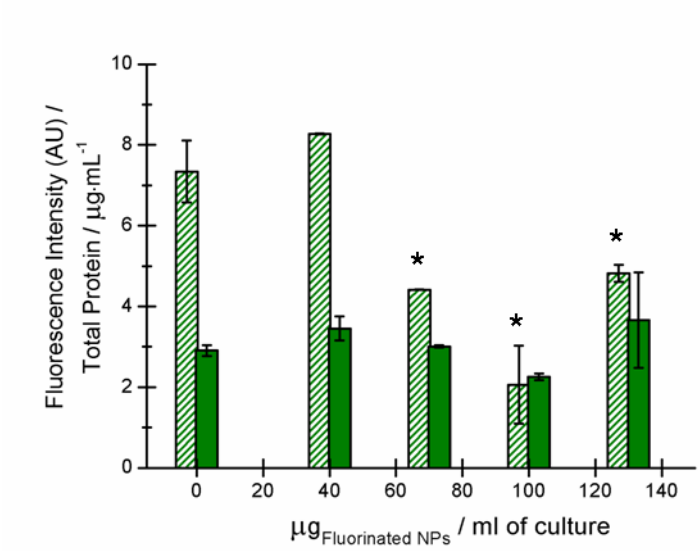


Figure 4.29. Dose dependent assay of the inhibitor activity of fluorinated NPs. 10 μM Aβ42 pre-incubated for 48 hours in F12 media in the absence (pattern) or presence (filled) of increasing NPs concentrations (40, 70, 100 and 130 μg/mL of culture) at 4 ºC with shaking, was added to 80% confluent SH-SY5Y cells and further incubated for 24 hours, at 37 ºC. For each experiment, the data shown are the averages of 3 wells. * indicates values significantly different from those for control cells (incubated with Aβ42 without NPs) as calculated by Student's t-test ($P < 0.05$).

4.3.2. Sulfonated and Sulfated Nanoparticles

43.3.2.1. Nanoparticles Synthesis and Characterization

Spherical polystyrenesulfonate NPs were synthethized via (i) crosslinking copolymerization in microemulsion and subsequent sulfonation via polymer reactions yelding microgels, and (ii) heterophase polymerization with copolymerizable surfactants leading to polystyrene latexes. Microgels are small polymer networks of well-defined mesoscopic size, low polydispersity, and

perfect spherical shape [244, 245]. These polymer microgels were functionalized in a second step by polymer analogous reaction resulting in polyelectrolyte microgels. Such polyelectrolyte microgels can be regarded as highly charged, spherical polyelectrolyte networks swollen in aqueous solution. The NPs obtained have a D_h of 40±12 nm measured by DLS and a zeta potential of -46±7 mV. The TEM micrographs are shown in Figure 4.30 A to D. It can be straightforwardly seen that the microgels do not look like a homogeneous population. The particle cross-linking density, i.e., the compactness of the particle structure can offer a possible explanation for this observation. The synthesis did not consist of a single step approach, with sulfonation taking place only after synthesis of the polystyrene microgel. It might have happened that the initial population of particles was not uniform and the networks were differently swollen, and so sulfonation did not occur always to the same extent and even took place in the interior of the microgels, as can be seen from the electronic density in TEM images. This raises the concentration of hydrophilic groups also inside the particles, which will make them almost randomly compacted. It should be noticed that the higher the degree of sulfonation the more ionic groups the microgel will carry and consequently the more extended the chains will be. On the other hand, the more sulfonated groups are trapped in the particle, the more the particle can swell by incorporating water molecules. Moreover, the drying process might have influenced the heterogeneity of the population for the same reasons stated above (different amounts of water trapped in the microgel).

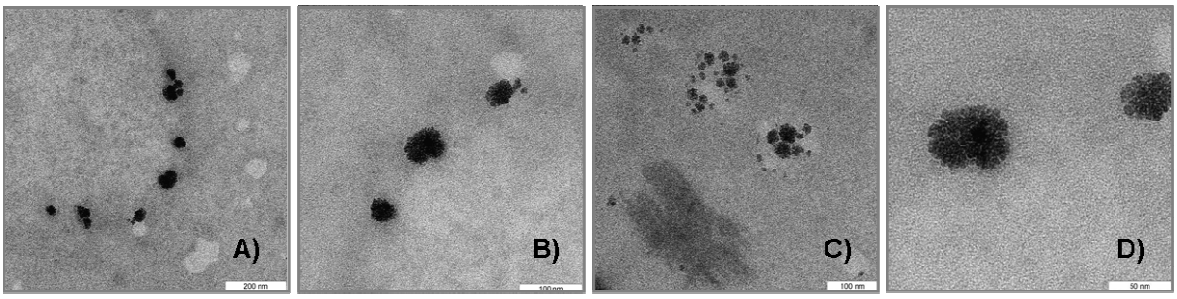


Figure 4.30. TEM images of polystyrene sulfonated microgel. The scale bars indicate 200 nm in A), 100 nm in B) and C) and 50 nm in D).

Over the past few years, copolymerizable emulsifiers have become of increasing interest for application in emulsion polymerization [249, 250]. During polymerization polymer particles are formed and the promise of copolymerizable surfactants is connected to the capability to react with monomers during the free-radical polymerization. The emulsifier is thus incorporated in the polymer particle and should offer higher latex stability and less coagulation during polymerization, contributing to enhanced stability of the polymer dispersion. Additionally, one of the main

drawbacks of polymerization of oil-soluble monomers in microemulsions to produce small polymer particles at a nanoscale range is the need of considerable amounts of surfactants and cosurfactants, most often larger than the amount of monomer itself. In order to recover the polymer produced, a long and wasteful process is needed. An obvious solution to such a problem is to use a polymerizable surfactant, which might be incorporated in the final polymer.

The D_h and zeta potential of the sulfated latexes are shown in Figure 4.31. It was expected that as the relative amount of APG 2019 increases, so the size and negative charge of the NPs do. But this was not exactly the case.

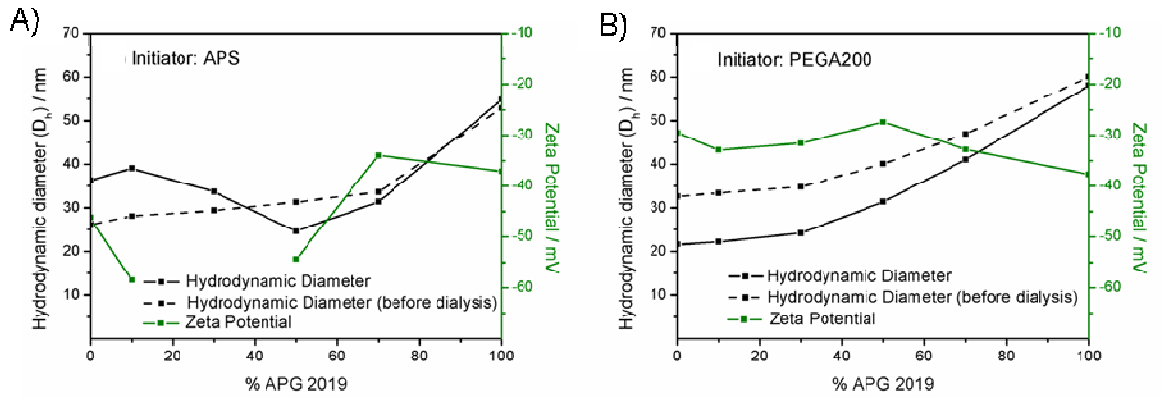


Figure 4.31. Hydrodynamic diameter (left axis, black lines) and zeta potential (right axis, green lines) of the polystyrene latexes synthesized with APG 2019 and SDS as surfactants, using APS as initiator A) or PEGA200 B). The zeta potential of the latex synthesized using 30% of APG2019 in the surfactant mixture was not considered because of value instability.

On Figure 4.32 A to D, are representative TEM images of the sulfated polystyrene latexes synthesized using the reactive surfactant APG2019. Even though the D_h values determined by DLS vary depending on the relative amount of each surfactant, all batches were fairly homogeneous. Contrarily to the microgel synthesis this is a one step process and the sulfation of the NPs occurs during styrene polymerization. So it is not surprising to observe identical particles with homogeneous size and electron density. Aggregates were formed, and this was noticeable especially after dialysis as the unreacted surfactants that still contribute to latex stability were removed.

In both cases, the introduction of strong acid groups ($-CSO_3^-$ and $-COSO_3^-$) to polystyrene had a noticeable effect on the solubility behaviour because of the big difference in polarity between the ionic group, the hydrocarbon main chain and the phenyl group. Moreover, there is an electrostatic stabilization shown by the highly negative zeta potentials (see table in Figure 4.33), so the NPs will not tend to coagulate or flocculate, as shown by the TEM images.

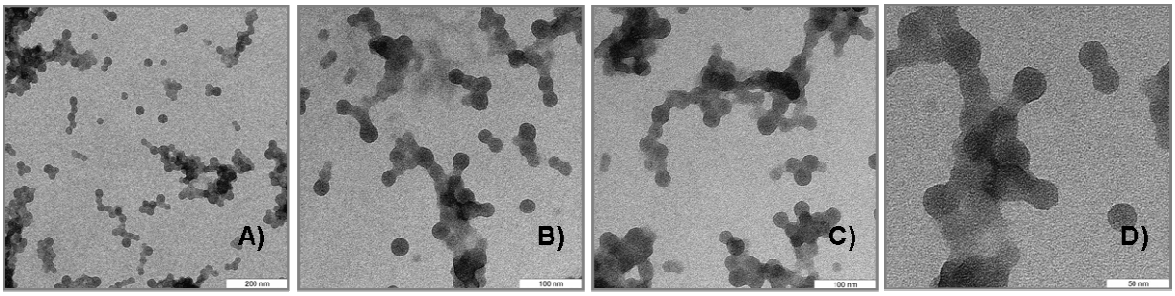
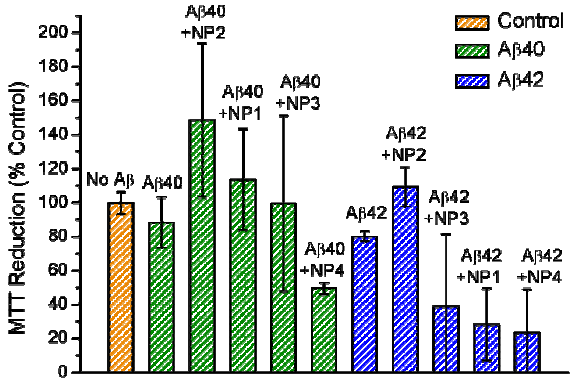


Figure 4.32. TEM images of polystyrene sulfated latex. The scale bars indicate 200 nm in A), 100 nm in B) and C) and 50 nm in D).

From all the latexes synthesized one batch had to be chosen to use in further studies. The first choice was the one with the more negative zeta potential, since in principle it would be the NP more similar to the fluorinated NPs previously studied, even though the size is considerably bigger (fluorinated NPs have a diameter of ~4 nm). However, first a screening was made, based on the cell tolerance to all the NPs (by microscopy, data not shown). The impact of selected NP on Aβ-induced cytotoxicity to cultured neurons was tested in a second step. The cell line used in all the cytotoxicity assays was SH-SY5Y. It is at present recognized that not monomers or insoluble fibrils may be responsible for neurotoxicity but soluble oligomers of Aβ. To produce Aβ oligomers, HFIP-pretreated peptide was dissolved in DMSO and diluted in phenol red-free F12. After a pre-incubation of 48 hours, the mixtures were incubated for 24 hours with the cells. The cytotoxicity of Aβ oligomers and sulfonated latexes was assessed by interference with MTT reduction. According to the MTT assay, the application of 10 μM Aβ affected cellular redox activity in SH-SY5Y cells, causing decreased MTT reduction into formazan (88±15% of control, n=5) for Aβ40 and Aβ42 (80±3% of control, n=5). It should be remembered that despite the small structural difference between the two peptides Aβ40 and Aβ42, they display distinct clinical, biological and biophysical behaviour. So it is not surprising that the bioactivity of Aβ40 is lower than the one of Aβ42. Taking into consideration the results, the latex named NP2 in Figure 4.33, synthesized with APG2019 as surfactant was chosen to perform further studies. The D_h amounts to ~55 nm (close to the one of the microgel, ~50 nm) and the zeta potential is -37±2 mV.



Nanoparticle	% APG 2019	Initiator	D_h (nm)	Zeta Potential (mV)
1	50	APS	24.6±0.8	-54.4±1.9
2	100	APS	54.8±3.4	-37.1±2.4
3	0	PEGA200	21.6±1.2	-29.5±1.3
4	50	PEGA200	31.4±0.9	-27.4±2.1

Figure 4.33. Aβ-mediated inhibition of MTT reduction by neuronal cells in the presence and absence of sulfated latexes. The data shown is the average of 5 wells and the error bars indicate the standard deviations. The table shows the properties of the latexes used.

4.3.2.2. Effect on Aβ Secondary Structure and Aggregation

The far-UV CD spectra of peptides and proteins provide information about their secondary structural properties and it was measured for both Aβ40 and Aβ42 in the absence and presence of sulfonated and sulfated NPs (Figure 4.34). Immediately after resuspension in buffer at 50 μM, Aβ40 and Aβ42 show evidence of different secondary structures. While Aβ40 is mostly unordered (one single minimum at ~200 nm), Aβ42 is folded in a β-sheet rich structure, as the spectrum exhibits β characteristic ellipticity - minimum at 217 nm and maximum at ~200 nm. The arguments for explaining the shift of the conformational equilibrium in Aβ42 towards β-structure are stated before. Both sulfonated microgel and sulfated latex tend to stabilize an unordered conformation of both peptides. The CD spectrum of Aβ40 (Figure 4.34 A) is almost the same after titration with the NPs. In the case of the more amyloidogenic Aβ42 (Figure 4.34 B), the shape of the spectrum changes drastically. The maximum at ~200 nm turns into a broad minimum and the minimum at ~217 nm is flattened. Such spectrum can be considered as a sum of CD spectra typical for both unordered and β-sheet structures. Therefore, one can assume that the NPs are able to transform a β-sheet structure, at least partially, into an unfolded structure. The signal is low and noisy due to scattering effects, so there are aggregates that can be constituted of peptide alone and/or peptide and NPs.

A ThT fluorescence assay was performed with the samples analyzed by CD 24 hours after preparation (Figure 4.35). The sulfonated microgel decreased the intensity of the ThT excitation peak at 440 nm for both Aβ40 and Aβ42, indicating that the peptides are less aggregated when this

structure is present. ThT fluorescence assay was not suitable for application in the case of the sulfated latex since the NP interferes with the behaviour of the ThT (data not shown).

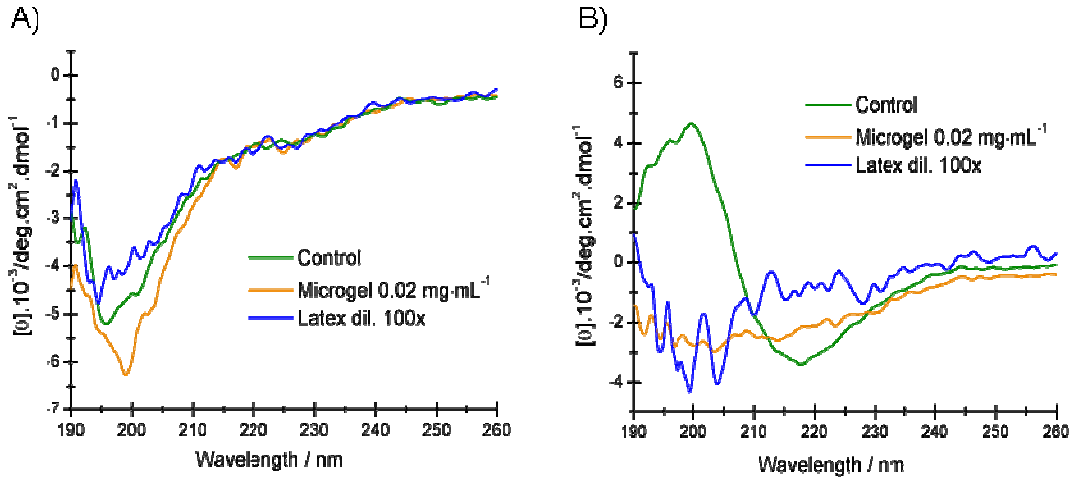


Figure 4.34. CD spectra of Aβ peptides in the absence and presence of NPs. In A), Aβ40 50 μM in phosphate buffer 10 mM pH 7; B), Aβ42 50 μM in phosphate buffer 10 mM pH 7.

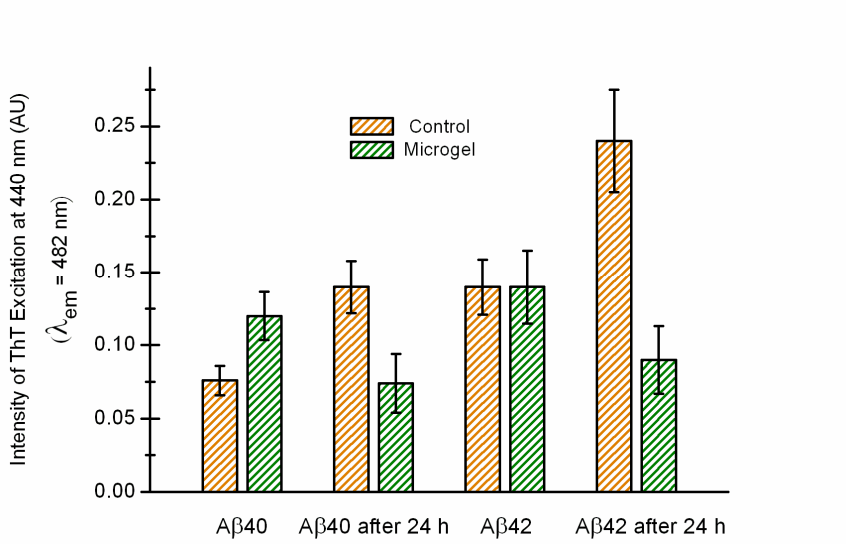


Figure 4.35. ThT fluorescence excitation intensity at 440 nm (λ_{em} = 482 nm) of Aβ solutions in the absence or presence of sulfonated microgel. Experiments were performed in duplicates and the error bars indicate the standard deviations.

A curious situation occurred when an "aged solution" of Aβ40 was titrated with NPs. "Aged solution" is a solution left aging at room temperature for several days, and this should lead to aggregation and fibrillation. This is confirmed by the β-sheet spectrum with low signal intensity (Figure 4.36). The NPs induced a significant increase of the spectra intensity that exhibit much more pronounced maxima at 195 nm and minima at 217 nm. The turbidity of the solution also decreased (data not shown). It can be concluded that the aggregates were solubilized in a certain extent by

these highly charged particles, since usually the signal arises from soluble species and not from insoluble aggregates. After 1 week the spectra look like at the beginning probably due to NP precipitation.

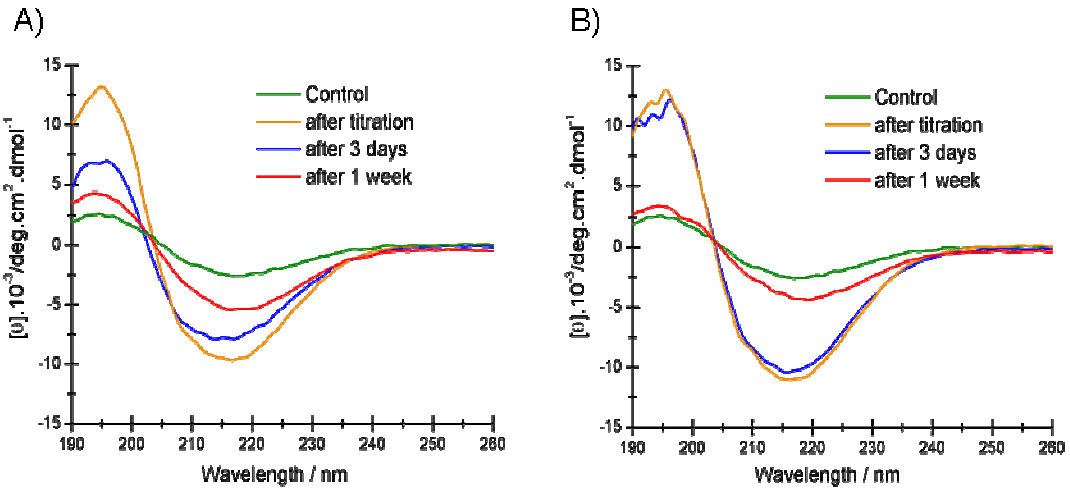


Figure 4.36. CD spectra of "aged solution" of Aβ40 50 µM in phosphate buffer 10 mM pH7 before and after titration with NPs. A) titration with 0.02 mg·mL^{-1} of sulfonated microgel. B) titration with a dispersion of sulfated latex diluted 100 times.

4.3.2.3. Effect on Aβ Oligomer Formation

As already referred, oligomer formation is favored at physiological pH and ionic strength [184] but high salt concentrations diminish the effective surface charge of the NPs and especially in the case of the microgels the added salt will reduce the structuring of these macroions in solution. This charge shielding is consequently expected to reduce the electrostatic interactions between charged residues on the surface of Aβ and charged groups of NPs. As in the case of the fluorinated NPs, it is expected that electrostatic interactions are reduced but still present.

Since oligomers of Aβ are considered bioactive in the pathogenesis, it is important to know if the NPs affect oligomer formation. A11 antibody was used to monitor oligomer formation and Bam-10 to verify the exposure of the epitope within amino acid residues 1-12 of the Aβ sequence. SDS-PAGE was employed to look for SDS-stable low-*n* oligomers. Aliquots of 50 µM Aβ40 and Aβ42 incubated in the absence and presence of NPs (0.02 mg·mL^{-1} for the microgel and ~0.01 mg·mL^{-1} for the latex) were removed at various times and tested in parallel by immunoblotting and SDS-PAGE. Samples were spotted onto nitrocellulose membranes and probed with A11 and Bam-10 antibodies (Figure 4.37). Oligomer-specific immunoreactivity formed within 2 days for Aβ42 and

5 days for Aβ40 and was stable till up to 7 days. Accordingly, Bam-10 immunoreaction only started to faint after 7 days of incubation.

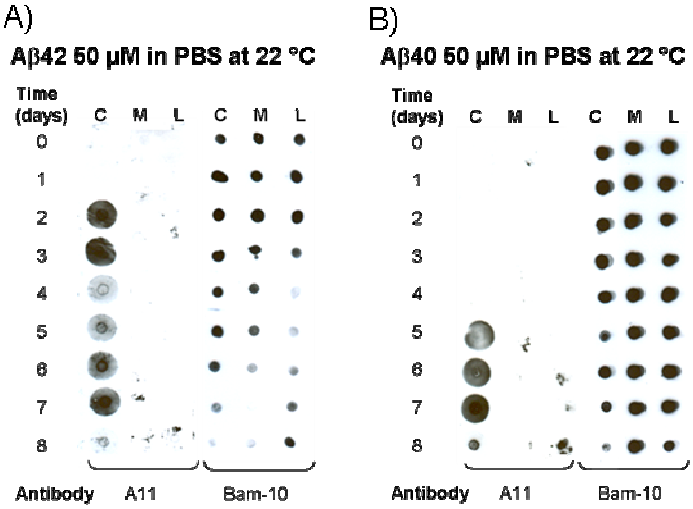


Figure 4.37. Time course of Aβ oligomerization detected by immunobloting. A) Aβ42 was incubated for up to 8 days in PBS, pH 7.4 at room temperature without stirring (50 μM final concentration) in the absence (C) or presence of 0.02 $mg \cdot mL^{-1}$ of sulfonated microgel (M) and ~0.01 $mg \cdot mL^{-1}$ of sulfated latex (L). Aliquots were spotted onto nitrocellulose membranes and probed with A11 and Bam-10 antibodies. B) Aβ40 was incubated in the same conditions described for A). Aliquots were spotted onto nitrocellulose membranes and probed with A11 and Bam-10 antibodies.

Strong A11 immunoreactivity was never detected when Aβ42 (Figure 4.37 A) and Aβ40 (Figure 4.37 B) were incubated with both NPs, suggesting inhibition of oligomer formation. However, Bam-10 immunodetection started to fade after 6 days when Aβ42 was incubated with sulfonated microgel and in the case of the sulfated latex only after 4 days, yet reappearing after 7 days. For Aβ40 the epitope was always detected. As for the case of the fluorinated NPs and their hydrogenated analogues, the apparent different accessibility of epitopes confirms the conformational differences between the samples. Probably the charged N-terminal residues are involved in extensive interactions that allow adsorption of the peptide to the NPs and so the epitope is shielded and immunodetection is not achieved. For the microgels it is possible that the peptide is trapped inside the polyelectrolyte network swollen in solution. This will be more extensively discussed in the discussion section.

SDS-PAGE analysis by silver staining shows that SDS-stable Aβ42 oligomers are present 1 day after preparation of a 50 μM solution (Figure 4.38). These have relative molecular masses of M_R ~14,000 and ~19,000, which correspond to trimers and tetramers. In the case of co-incubation with NPs, the appearance of oligomeric species was delayed and the bands correspondent to SDS-stable

trimers and tetramers are much less intense. Both are less abundant than in the case of the peptide alone and the relative amount of trimers is also lower. This suggests that these small oligomers may be important for nucleation. Dimers, even though very discretely, started to appear when the peptide was co-incubated with the nanostructures. It might be that the conversion of dimers into trimers/tetramers is faster than the dimerization, and moreover there are multiple possibilities for oligomer formation. Interaction with the NPs reduces the rate of transformation of dimers to trimers and tetramers and this can be the reason for the very small amounts of detected dimers when the peptide was co-incubated with NPs. Co-incubation of Aβ40 with NPs has no significant effect on the oligomerization behaviour of the peptide even though dimers seem to be a bit more abundant in the case of the presence of NPs (Figure 4.39).

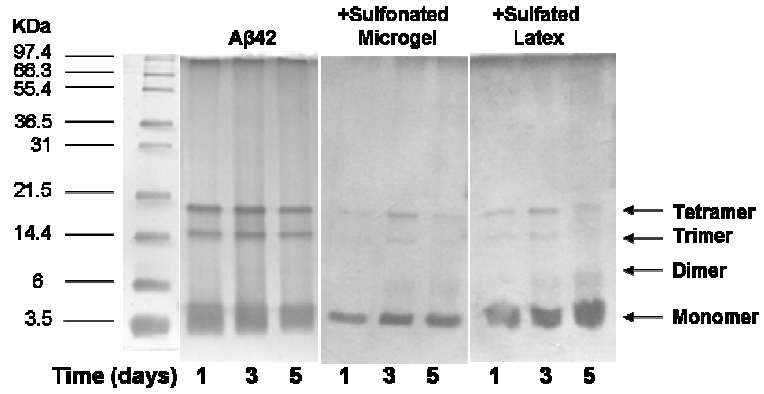


Figure 4.38. SDS-PAGE electrophoretic migration of Aβ42. Aβ42 was incubated in PBS, pH 7.4 at room temperature without stirring (50 μM final concentration) in the absence or presence of 0.02 mg·mL^{-1} of sulfonated microgel and ~0.01 mg·mL^{-1} of sulfated latex. Aβ42 (0.2 pmol/lane) SDS-stable oligomers were separated using denaturating and reducing conditions and visualized using a silver staining protocol.

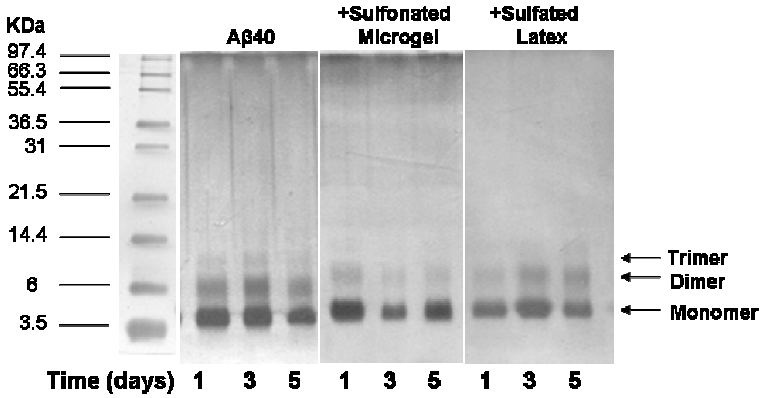


Figure 4.39. SDS-PAGE electrophoretic migration of Aβ40. Aβ40 was incubated in PBS, pH 7.4 at room temperature without stirring (50 μM final concentration) in the absence or presence of 0.02 mg·mL^{-1} of sulfonated microgel and ~0.01 mg·mL^{-1} of sulfated latex. Aβ42 (0.2 pmol/lane) SDS-stable oligomers were separated using denaturating and reducing conditions and visualized using a silver staining protocol.

4.3.2.4. Effect on Aβ-induced Cytotoxicity

As previously shown for the selection of the sulfated latex suitable for this study, Aβ42 affected cellular redox activity in SH-SY5Y cells, causing decreased MTT reduction into formazan (84±17% of control, n=5) and thus reduced the viability of the cells. When Aβ42 was incubated with NPs during oligomerization, the differences in the MTT assay are hardly recognized because of the very large error bars, as shown in Figure 4.40. Even with this reservation a trend is observed. In the presence of the NPs, cell viability increased, as shown by the higher MTT reduction compared to the wells treated with Aβ oligomers - (92±27%, n=5) for the microgel and (96±11%, n=5) for the latex.

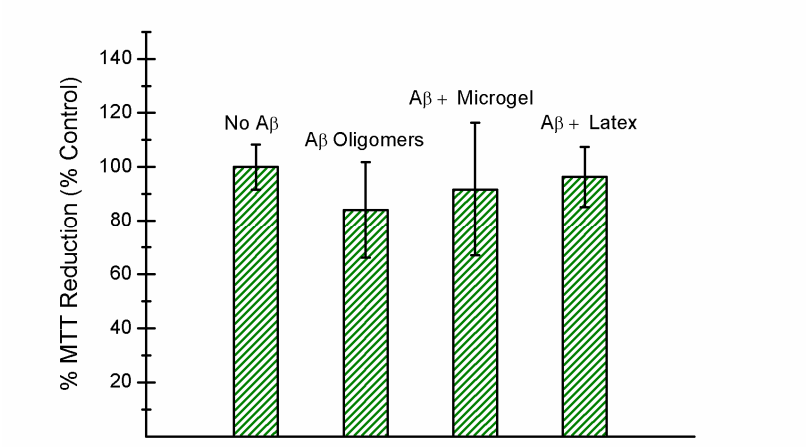


Figure 4.40. Aβ42-mediated inhibition of neuronal MTT reduction. 10 μM Aβ42 pre-incubated for 48 hours in F12 media with or without NPs (1.6 μg per mL of culture in the case of sulfonated microgel and 80 μL of a 100 times diluted suspension per mL of culture for the sulfated latex) at 4 ºC with shaking, was added to 80% confluent SH-SY5Y cells and further incubated for 24 hours, at 37 ºC. For each experiment, the data shown are the averages of 5 wells.

In parallel with the MTT assay the caspase-3 fluorimetric assay was used to estimate the impact of the polymeric nanostructures on the Aβ induced cytotoxicity. The results obtained are shown in Figure 4.41. The tendency obtained by the MTT is supported by the caspase-3 activity. The Aβ42 oligomers increased enzyme activation and both NPs could significantly attenuate this effect, and especially the sulfated latex particles seem to be very efficient. In the presence of sulfonated microgel, the enzymatic activity was also decreased relative to the control (1.3±0.3 of fluorescence intensity per mg of protein).

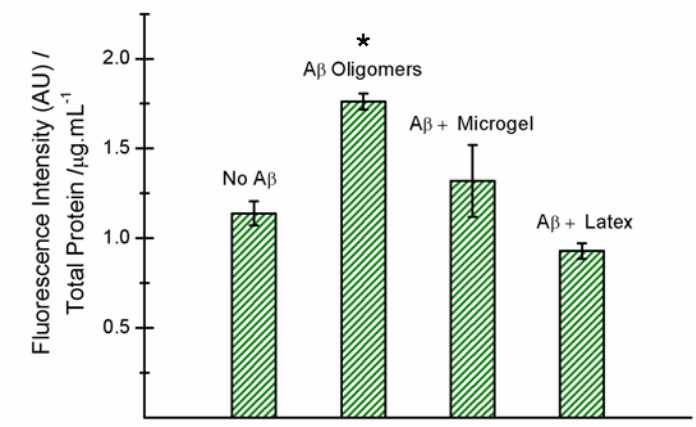


Figure 4.41. Aβ42-induced caspase-3 activation in cultured neurons. 10 μM Aβ42 pre-incubated for 48 hours in F12 media with or without NPs (1.6 μg per mL of culture in the case of sulfonated microgel and 80 μL of a 100 times diluted suspension per mL of culture for the sulfated latex) at 4 ºC with shaking, was added to 80% confluent SH-SY5Y cells and further incubated for 24 hours, at 37 ºC. For each experiment, the data shown are the averages of 3 wells. * indicates values significantly different from those for control cells as calculated by Student's t-test (P < 0.05).

4.4. Discussion and Conclusions

This work was driven by the motivation to induce different conformational behaviours in Aβ peptides and to interfere with aggregation aiming to contribute to the understanding of the mechanisms underlying protein misfolding diseases. To achieve this purpose, a strategy chosen was the re-conversion of Aβ conformation by adsorption or complexation to a third component, the NPs.

The results reported indicate that fluorinated NPs, with a highly negative zeta potential, which promote an increase in α-helical secondary structure of Aβ peptides exert a combination of antioligomeric and antiapoptotic effects, increasing cell viability in the presence of Aβ42 oligomers. Their hydrogenated analogues have the opposite effect, promoting aggregation and enhancing cytotoxicity. In order to test the influence of the zeta potential of the NPs on the peptide structure, sulfonated and sulfated NPs were produced.

Polystryrene NPs were synthethized via (i) crosslinking copolymerization in microemulsion and subsequent sulfonation via polymer reactions yelding microgels and, (ii) heterophase polymerization with copolymerizable surfactants leading to sulfated polystyrene latexes. Polyelectrolyte microgels can be regarded as highly charged, spherical polyelectrolyte networks swollen in aqueous solution. In the second approach, the emulsifier APG2019 is incorporated in the polymer particle offering high latex stability and less coagulation during polymerization, improving the stability of the polymer dispersion. CD measurements show that sulfonated and sulfated NPs with highly negative zeta potentials promote a randomization of the secondary structure of Aβ peptides and are able to revert fibrillation. Moreover, they retard oligomerization, thus reducing Aβ42-induced cytotoxicity. Gong *et* al. have studied the α-helical inducing effect of sulfonated polystyrene NPs and PSS on the conformation of apo cytochrome c and showed that for a concentration of 0.035 $mg \cdot mL^{-1}$ PSS has a stronger effect in inducing α-helix than the NPs [272]. Only at higher concentrations a sharp increase in the α-helical content was observed for the NPs that were 36% charged. Also in this study was shown that at very low concentration, the NPs can still interact with the protein but without inducing a significant conformational transformation. We have used a lower concentration due to scattering effects in measuring CD spectra (0.02 $mg \cdot mL^{-1}$ for the microgel ~0.01 $mg \cdot mL^{-1}$ for the latex assuming a solid content of ~1%) and it is therefore plausible that if the concentration was higher α-helix induction would be observed and not only a randomization of the structure.

Two major driving forces control protein aggregation and fibrillogenesis: (i) hydrophobic interactions; and (ii) polar hydrogen bonding among side-chain groups. It has been demonstrated that the CHC in the Leu17-Ala21 region is essential for the aggregation of Aβ peptides [129-132]. A large number of studies suggest that the Asp23-Lys28 loop region connected to the CHC and the second hydrophobic domain in the C-terminus is involved in Aβ fibril growth. In structure-activity investigations on Aβ(25-35) and Aβ42, the turn in the Val24-Trp27 region and the second hydrophobic domain were reported to be necessary for aggregation [133]. Furthermore, CD and NMR (1H, 15N, and 13C) measurements showed that the oxidation of the Met35 side chain to methionine sulfoxide (Met35(O)) diminishes the tendency of both WT-Aβ40 and WT-Aβ42 to aggregate [134, 135]. These results explicitly indicate that these three distinct regions may be involved in aggregation. Fundamental characteristics of the Aβ sequence, which displays β-extended chain structure propensity in the regions 17-21 and 31-36 even as a soluble monomer, might also influence aggregation [135]. Certain localized peptide regions are predisposed towards β-strand and bend-like structures and it has been proposed that monomeric Aβ exists in solution as a metastable loop-like structure in which each monomer contains an antiparallel β-sheet [103]. NMR studies propose that in protofilaments contacts between β-sheet layers are side chain-side chain interactions along the hydrophobic faces created by side chains of the C-terminal segment and the CHC. The N-terminal residues are expected to be in random conformations. The core of the protofilament is hydrophobic with the exception of the oppositely charged side chains of Asp23 and Lys28, which form salt bridges [44]. Other NMR experiments show that Aβ oligomers are stabilized by the in-register parallel arrangement of the molecules, presumably with all hydrophobic C-terminus tails clustered together [132].

Vieira *et* al. [273] demonstrated the effectiveness of different fluorinated alcohols for the β-to-α refolding process on fibrillar aggregated Aβ40. The effect of the $-CF_3$ group on the observed conformational changes was interpreted as a result of alterations in the hydration shell of the peptides and hydrophobic effects of fluorogroups. Montserret et al. [274] have shown that while for highly hydrophilic, amphipatic α-helical peptides the folding in micellar solutions of SDS is mostly driven by electrostatic interactions, when we consider hydrophobic peptides, SDS-peptide hydrophobic interactions may be sufficiently strong to bring about the whole folding process into a α-helical rich structure. Dodecanoic acid is less hydrophobic than perfluorododecanoic and this could explain why the fluorinated particles are able to interact in a larger extent with hydrophobic peptide regions. Perfluorododecanoic acid is a stronger acid than dodecanoic, suggesting that the acidic character plays as well a key role in α-helix induction. In agreement with the results obtained,

previous studies have shown that hydrophobic Teflon particles with a size of 200 nm and a zeta potential of -47 mV are able to induce α-helix structure in Aβ40 [182].

The strong acid groups (sulfonate and sulfate) of NPs will be totally dissociated at physiological pH. Consequently, NPs can interact with charged residues of the N-terminal region destabilizing the secondary structure of monomers. Moreover, unsulfonated phenyl groups may also contribute with hydrophobic interactions and disturb contacts between C-terminal segment and the CHC of monomers in the fibrils. Hence solubilization of fibrils can occur by monomer depletion or destruction of the structure. More than 10 years ago, Pollack *et* al. have reported that several sulfonated dyes as Congo Red attenuate Aβ toxicity and that the protective effect appears specific for compounds whose sulfonate groups can interact with the β-pleated structure of aggregated amyloid [275].

Aβ is an amphipathic peptide that readily self-associates into oligomers that are toxic to cultured cells. The so-called ADDLs [64] or protofibrils [65] cause subtle injury to cultured neurons and injection in rats of Aβ oligomers can inhibit long-term potentiation in the hippocampus, which is required for memory formation [67]. Composition and surface of NPs seem to be of extreme importance in defining the ability to influence Aβ biochemical and biophysical behaviour. As shown by immuno-dot blot and SDS-PAGE the fluorinated NPs that induce a β→α conformational transition delay appreciably the oligomerization of Aβ42, and therefore lower the peptide-induced cytotoxicity. The hydrogenated NPs may promote high local concentration of Aβ monomers and oligomers on the surface, increasing the nucleation and aggregation rate. Moreover, equilibrium may exist between Aβ on the hydrogenated NP surface and Aβ in solution, which could lead to the production of soluble toxic oligomers. Immuno-dot blot and SDS-PAGE show that sulfonated NPs that promote an unordered conformation also postpone the appearance of Aβ oligomers, and peptide-induced cytotoxicity is reduced.

The structures of the NPs used in these studies have a good balance between hydrophilic moieties making them water soluble and hydrophobic chains that allow interactions with crucial Aβ regions involved in oligomerization. The fluorinated NPs are not "hard" particles but dynamic structures where the stiff fluorinated chains are in contact with the hydrophilic phase. In the case of hydrogenated NPs the flexible -CH_3 groups are caught by the hydrophilic heads. Each group has a significant role in the inhibitory effect of the fluorinated NPs, but -CF_3 and -COOH groups have crucial functions (Figure 4.42). -CF_3 groups can interact with hydrophobic peptide residues, preventing interpeptide hydrophobic interactions. The introduction of the strong electron withdrawing -CF_3 group significantly increases the acidic nature of -COOH. This group with acidic character plays a key role in binding to the peptide possibly to one or both Lys residues (Lys16 and

Lys28). There is also a specific geometric preference for the interaction between C—F and side-chain amides of Glu (Gln15) and Asn (Asn27) residues [276]. So the fluorinated NPs might be able to interact with the two stretches of hydrophobic residues (Leu17-Ala21) and (Ala30-Ala42) believed to be the key for oligomerization or with residues in their vicinity, exploiting the same intermolecular interaction formed in Aβ assembly and consequently disrupt the potential further aggregation. A conformationally tightened state is produced by the interplay of ionic and hydrophobic characters of both peptide and fluorinated NP, and this prevents fibrillation. Electrostatic interactions with charged amino acid residues might play a role as anchors but this can not be the only effect since the hydrogenated NPs are also charged. After a first electrostatic interaction, the hydrophobic interactions dominate creating a hydrophobic cluster by exclusion of water molecules. This might lead to the stabilization of peptide intramolecular hydrogen bonds in expense of intermolecular hydrogen bonding with water and to formation of a stable α-helical structure and stabilization of the particle-peptide interaction. Ferrão-Gonzales *et* al. showed that 1-anilino-8-naphthalene sulfonate (ANS)-derived molecules inhibit aggregation due to their dual nature, with hydrophobic regions and charged groups [277].

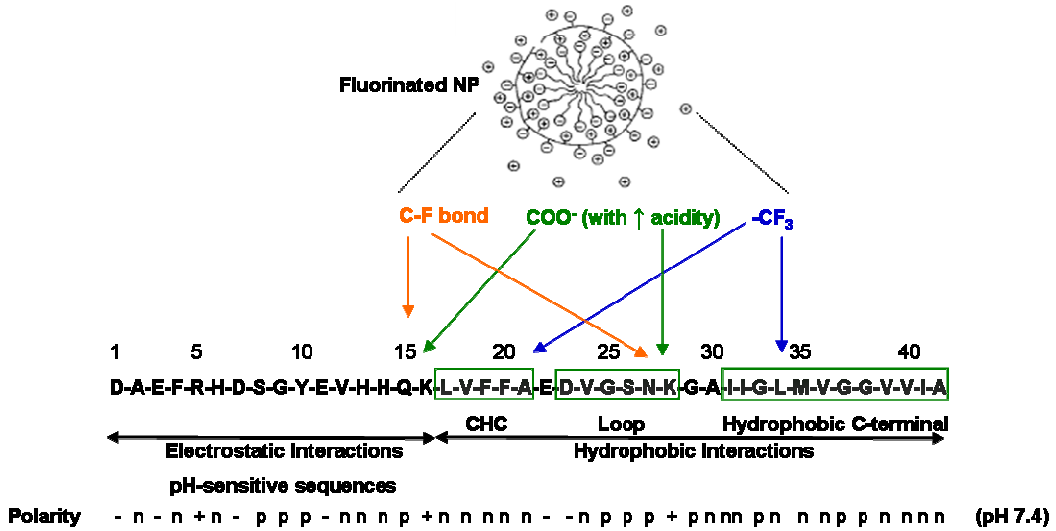


Figure 4.42. Schematic representation of the possible interactions of fluorinated NPs and Aβ peptides leading to inhibition of the oligomerization process. Primary sequence of Aβ42 and polarity of its amino acid residues at pH 7.4 are shown. Fluorinated NPs might interact with the two stretches of hydrophobic residues (17-21) and (30-42). The introduction of the -CF_3 group increases the acidic nature of -COOH and this group with acidic character plays a key role in binding to the peptide possibly to one or both Lys residues (Lys16 and Lys28). There is also a geometric preference for the interaction between C-F and side-chain amides of Gln15 and Asn27. After a first anchoring by electrostatic interaction, -CF_3 groups can interact with hydrophobic peptide residues, preventing interpeptide hydrophobic interactions and consequently disrupting potential further aggregation.

In addition, fluorinated compounds are synthesized in pharmaceutical research on a routine basis and many marketed compounds contain fluorine. There are many examples illustrating that the replacement of an oxidizable C—H group by a C—F group increases metabolic stability of the molecule [278]. Therefore, fluorinated NPs might have a good bioavailability and could interact with Aβ in the brain and influence its aggregation.

Essafi *et* al. [279] found that highly sulfonated polystyrene could form hydrophobic domains in water and this can be important in particular for the sulfonated microgels. Besides this, as previously referred, unsulfonated phenyl groups can interact with hydrophobic peptide residues, preventing interpeptide hydrophobic interactions. The acidic sulfonate and sulfate groups may also play a key role in binding to the peptide, possibly to positively charged residues (Lys16 and Lys28). So the sulfonated/sulfated NPs have properties that allow them to interact with the hydrophobic stretches and neighboring residues such as the fluorinated NPs do (Figure 4.43). Since the hydrophobic interface is the driving force of nucleation, the process is disturbed by complexation with the NPs and less peptide is available to aggregate. Moreover, due to their size (D_h ~50 nm), the NPs are appropriate multivalent compound amplifying the interactions and the adsorption of monomers/small oligomers lowers the concentration of peptide available to oligomerize and moves the equilibrium away from aggregation. Even though the concentration of NPs used in the cell assays was considerably lower than in the other experiments they were efficient, inhibiting Aβ bioactivity according to the conclusions drawn from CD, immunoblotting and SDS-PAGE experiments. The importance of the sulfonated moieties is supported by previous studies. Glycopolymers carrying sulfated saccharides with modest sugar content were found to suppress the aggregation of Aβ peptides [280], and the sulfated group was shown to be indispensable for the inhibitory effect. In another study, sulfated glycosaminoglycans and sulfated glycans inhibit formation of the abnormal isoform of prion protein in prion-infected cells [281].

The relatively lower amount of trimers and tetramers detected by SDS-PAGE when the peptide was co-incubated with fluorinated and sulfonated/sulfated NPs before cell incubation can be a decisive factor for the lower Aβ42-induced cytotoxicity determined in the presence of these polymeric nanostructures. Cleary *et* al. provided experimental evidence that defined molecular species of the Aβ interfere with cognitive function [141]. This demonstration that cognitive deficits are directly attributable to low amounts of naturally assembled Aβ oligomers indicates that trimers may be particularly active. The hydrogenated NPs, which induce aggregation and enhance cytotoxicity, promote the formation of SDS-stable Aβ dimers. There are several reports on Aβ dimers occurring *in vivo*. Schmechel *et* al. [138] demonstrated for the first time that a biochemically defined assembly of Aβ into dimers probably represents the initial step in amyloidogenesis. The

presence of Aβ dimers in the cortex has been suggested to initiate the accumulation of Aβ in the human brain [139] and dimeric Aβ is proposed to initiate aggregation by accumulation in lipid rafts [140]. Nonfibrillar SDS-stable dimers have been characterized as neurotoxic derivatives [64] and selectively blocked hippocampal long term potentiation in the absence of monomers, protofibrils, or fibrils [67].

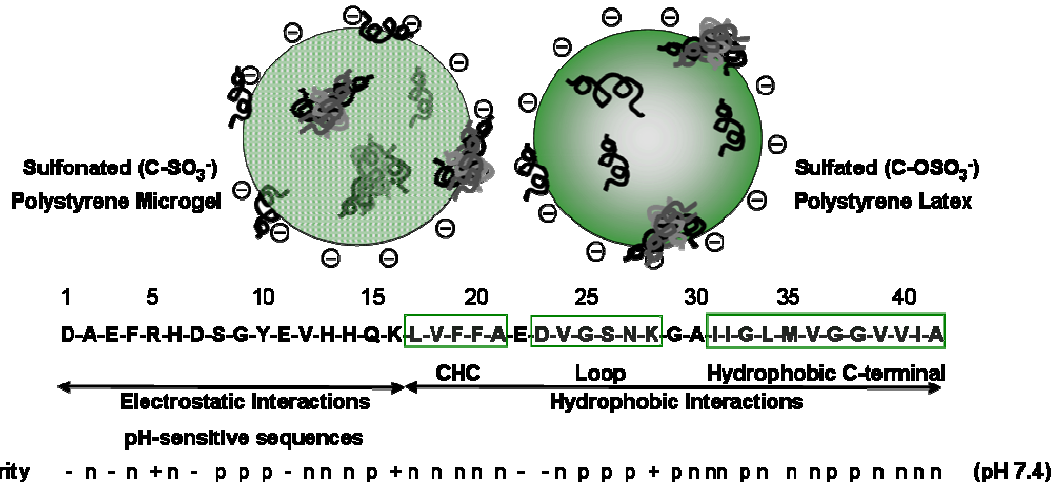


Figure 4.43. Schematic representation of the possible interactions of sulfonated and sulfated NPs and Aβ peptides that inhibit oligomerization. Primary sequence of Aβ42 and polarity of its amino acid residues at pH 7.4 are shown. Strong acid groups $–CSO_3^-$ and $–COSO_3^-$ may bind to positively charged residues. Highly sulfonated polystyrene can form hydrophobic domains in water and unsulfonated phenyl groups can interact with hydrophobic peptide residues, preventing interpeptide hydrophobic interactions. For the sulfonated microgels it is possible that the peptide is trapped inside the polyelectrolyte network swollen in solution.

In the case of the sulfonated and sulfated NPs, dimeric species appeared but they were not abundant. It is possible that some LMW species are toxic leading to cell death and the ones trapped in the presence of the NPs are not. They might have different sizes and/or conformations. Since there was no immunoreaction with the anti-oligomer antibody A11, an apparent different accessibility of epitopes confirms the conformational differences between the samples. Also the detection with Bam-10 diminished with time. This polymorphism in terms of differential epitope accessibility has been previously described for prion oligomers [282] and also for Aβ oligomers [266]. Probably there is a polymorphism on the epitopes accessibility and the unordered conformation of the peptide in the presence of these polymeric NPs leads to the formation of amorphous aggregates instead of structured oligomers and protofibrils whose soluble, SDS-stable low-*n* species are detected by the antibody A11. For the microgels it is possible that the peptide is

trapped inside the polyelectrolyte network swollen in solution, and thus immunodetection is not achieved.

Helical forms of Aβ have been suggested to be intermediates in the aggregation process of the peptide in aqueous phase [283], micelles [284] and membranes [285]. The results presented here support the concept that formation of β-sheets is related with the nucleation process, since hydrogenated NPs promote β-sheet formation and also aggregation.

Nanostructures are being used as drug carriers in the CNS for several applications but NP based systems and the interaction mechanism with Aβ peptides was not explored in AD research [240]. In literature few works have reported in detail the effect of nanogels [286], PEGylated phospholipid nanomicelles [287] and polymeric nanostructures [288] on Aβ fibrillation [286-288] and cytotoxicity [286, 287] but none of these studies has focused on Aβ oligomer formation.

5. Concluding Remarks

Folding of proteins is an important but not fully understood process. A number of cellular mechanisms that prevent misfolding and misassembly exist and, in addition, molecular chaperones aid in the folding process. Yet, protein misfolding and aggregation occur and are linked to several diseases, causing problems due to loss of function or, in the case of amyloid disorders, gain of toxic function. Amyloid diseases comprise many prevalent pathological conditions such as AD, PD and type II diabetes mellitus. The biochemistry of amyloid proteins has been a fascinating and important area of research because of its contribution to the understanding of protein folding dynamics and assembly and of the pathogenic mechanisms of human disease.

Aβ peptides play a central role in the mechanism of AD, the most common cause of dementia in elderly. Aβ amyloid formation and deposition are due to a conformational switching from an unordered or α-helical form to β-enriched structure during amyloidogenesis. However, the relevance of the amyloid plaques to the pathogenesis is unclear and even questioned by many investigators since there is a weak correlation between the number of amyloid deposits detected by neuropathological analysis of postmortem brains and the degree of cognitive impairment experienced by the patients in life. Several evidences indicate that Aβ toxicity is likely to be mediated by multiple different Aβ assembly forms, and that the earliest symptoms of the disease are attributable to soluble, low-*n* oligomers. The overall aim of this thesis was to contribute for the understanding of Aβ properties and assembly in order to trigger undesirable effects.

Due to the high concentration of macromolecules inside cells, the cellular environment is very crowded, and many surfaces and interfaces exist. These macromolecular crowding effects have a strong influence on the protein folding dynamics. The protein lipid environment seems to be a physiological factor playing a crucial role both in aggregation kinetics and cytotoxicity. Protein-lipid interactions can affect the oligomerization process and, on the other hand, aggregates may change the membrane structure and affect the membrane permeability. The research presented in Chapter 3 was motivated by the call to better understand the role of surfaces with different properties in the assembly of Aβ peptides that have an amphipatic character.

Several techniques were employed to examine the Aβ behaviour when in contact with planar surfaces, including model lipid bilayers. From these experiments it was confirmed that hydrophobic interactions are a driving force of Aβ misfolding and aggregation. The change in the monomer : oligomer : fibril ratios caused by surfaces stresses the importance of hydrophobic interactions in the

assembly process of the Aβ peptide. Such studies may represent an important step towards a detailed understanding of the initial stages of aggregation and hence assist in the design of inhibitors and development of therapeutic strategies against AD.

Based on the results presented, different adsorption models of Aβ peptides on surfaces were proposed, depending on the peptide oligomerization state (monomer or oligomer). After the initial contact of monomeric Aβ with the surfaces by diffusion controlled adsorption from the bulk solution, the peptide will aggregate or not depending on its affinity to the substrate. Concerning oligomeric Aβ, it was shown that these species are soft and when in contact with a solid surface flattening and stiffening occurs. It is well established that membrane binding and permeabilization are pivotal steps in amyloid-forming peptides and proteins cytotoxicity. Different mechanisms have been proposed to be involved in membrane permeabilization such as pore formation and disorder of the membrane structure. Since recent debate has focused on soluble oligomers as the main neurotoxic species that contribute to neurodegeneration and dementia in neuropathic protein deposition diseases, the viscoelastic nature of Aβ42 oligomers described herein might be an important common property of protein oligomers related with their neurotoxicity. Moreover, contrarily to monomers and fibrils, oligomers are able to interact with neutral lipid bilayers most likely by insertion into the hydrophobic transmembranar part. This observation might also be related with the different physical properties of monomers and oligomers.

Aβ42 has been shown to fibrillate faster than Aβ40 and to have enhanced neurotoxicity, althought Aβ40 is about 10 times more abundant in circulation. In the time scale of the experiments reported herein, fibrillar species were only observed for Aβ42, while for Aβ40 only β-sheet enriched amorphous aggregates were identified. It is suggested that the pathway of fibrillation differs as previously indicated by others. It might be that the amorphous aggregates are removed by cellular mechanisms and disposed into the proteasomal machinery for degradation. Thus, in the folding energy landscape of Aβ, several intermediates seem to occur on different folding trajectories parallel to each other that depend on the peptide alloform. The slower fibrillation rate of Aβ40 might be coupled to the formation of transient intermediates that are less stable than the ones formed by Aβ42 that lead to a fast aggregation into the most energetically stable structure, the amyloid fibrils. This could be one of the reasons for the predominance of Aβ42 in the neuritic plaques of AD patients' brains and to the lower cytotoxicity of Aβ40.

This work was also driven by the motivation to induce different conformational behaviours in Aβ peptides and to interfere with aggregation aiming to reduce the peptide cytotoxicity. The strategy chosen was the re-conversion of Aβ conformation by interaction with NPs. The studies presented in the Chapter 4 were based on the application of properly engineered NPs as very

valuable tools to achieve this purpose. The use of polymeric NPs for preventing β-sheet formation and oligomerization was presented and evaluated as was the impact of such structures on Aβ-induced cytotoxicity.

The experimental results show that dynamic fluorinated NPs interact with Alzheimer´s disease Aβ peptides increasing its α-helical content. The fluorinated NPs exert a combination of antioligomeric and antiapoptotic effects, increasing the viability of cells trated with Aβ oligomers. The hydrogenated analogues, however have the contrary effect, inducing the formation β-sheet enriched structure more prone to aggregate and more cytotoxic. Sulfonated and sulfated polystyrene NPs interact with Aβ peptide inducing randomization of its structure. As consequence, the oligomerization process is disturbed and the peptide induced toxicity to neuroblastoma cells is reduced. In both cases, the proper balance between hydrophilic moieties that allow solubility and hydrophobic chains to exploit the intermolecular interactions of Aβ assembly seem to be an essential feature of the effective NPs. The results presented comprise attractive achievements for the development of new approaches for protein misfolding diseases study and therapy.

Data relative to the cytotoxic Aβ species is confusing, and several oligomers have been reported as toxic. Stabilizing monomers rather than target later stages of the fibrillation pathway seems to be a good approach in order to eliminate the accumulation of toxic species as early as possible. The interaction with native states of proteins and peptides prone to unfold and aggregate might prevent pathogenic effects, especially if the toxicity mechanism is not well known. Many of the therapeutics studies have reported inhibitors of Aβ fibril formation. This raises the question about the merits of fibril-disrupting compounds, as they may shift the equilibrium of Aβ aggregation to more hazardous oligomeric species. Hence, a more important goal is to find compounds capable of blocking Aβ oligomerization.

In the case of the diseases as AD that occur in the brain, we have to consider the existence of the BBB. Unlike peripheral capillaries that allow relatively free exchange of substance across/between cells, the BBB strictly limits transport into the brain through both physical (tight junctions) and metabolic (enzymes) barriers. Thus, the BBB is often the rate-limiting factor in determining permeation of drugs into the brain. Properly engineered NPs can pass through the BBB and have a good bioavailability. In addition, NPs can enter the cells reaching subcellular locations and thereby access a vast range of biological processes. NPs possess very high surface free energy which introduces large adsorption capacities; they have a very large surface to volume ratio, so even small amounts of NPs present extremely large surface areas available for peptide/protein binding.

More than 20 diseases have been identified which are caused by the deposition of amyloid. The oligomeric forms of amyloidogenic proteins appear to have similar structures and to act as common toxic intermediates in amyloid fibril formation from a variety of precursor proteins. If the oligomeric pathway is required for toxicity, the assembly dynamics and folded structures of the peptides/proteins are therefore essential for the etiology of protein misfolding diseases. In the particular case of AD, part of the controversy surrounding the Aβ structure-function relation results from the lack of methods to effectively study Aβ assembly and characterize conditions that influence this process. Molecules able to induce different conformational behaviours and interfere with aggregation could lead to the understanding of the driving forces behind inter- and intraprotein interactions as well as the structural motifs responsible for them. NPs as the ones presented here could also be used as lead structures for the development of drugs against protein misfolding diseases.

Properties and conventions associated with the standard amino acids [258].

Amino acid	3-letter code	1-letter code	Linear structure formula	MW (g.mol^{-1})	pK$_a$ (side chain)	pI (25 ℃)	Hydropathy index	Occurence in Proteins (%)
Nonpolar, aliphatic R groups								
Glycine	Gly	G	NH_2-CH_2-COOH	75.0669	-	5.97	-0.4	7.5
Alanine	Ala	A	CH_3-CH(NH_2)-COOH	89.0935	-	6.01	1.8	9.0
Valine	Val	V	$(CH_3)_2$-CH-CH(NH_2)-COOH	117.1469	-	5.97	4.2	6.9
Leucine	Leu	L	$(CH_3)_2$-CH-CH_2-CH(NH_2)-COOH	131.1736	-	5.98	3.8	7.5
Isoleucine	Ile	I	H_3C-CH_2-CH(CH_3)-CH(NH_2)-COOH	131.1736	-	6.02	4.5	4.6
Proline	Pro	P	NH-$(CH_2)_3$-CH-COOH |_____|	115.1310	-	6.48	-1.6	4.6
Aromatic R groups								
Phenylalanine	Phe	F	Phenyl-CH_2-CH(NH_2)-COOH	165.1900	-	5.48	2.8	3.5
Tyrosine	Tyr	Y	HO-p-Phenyl-CH_2-CH(NH_2)-COOH	181.1894	10.07	5.66	-1.3	3.5
Tryptophan	Trp	W	Phenyl-NH-CH=C-CH_2-CH(NH_2)-COOH |_____|	204.2262		5.89	-0.9	1.1
Polar, uncharged R groups								
Serine	Ser	S	HO-CH_2-CH(NH_2)-COOH	105.0930	13.60	5.68	-0.8	7.1
Threonine	Thr	T	H_3C-CH(OH)-CH(NH_2)-COOH	119.1197	13.60	5.87	-0.7	6.0
Cysteine	Cys	C	HS-CH_2-CH(NH_2)-COOH	121.1590	10.28	5.07	2.5	2.8
Methionine	Met	M	H_3C-S-$(CH_2)_2$-CH(NH_2)-COOH	149.2124	-	5.74	1.9	1.7
Asparagine	Asn	N	H_2N-CO-CH_2-CH(NH_2)-COOH	132.1184	-	5.41	-3.5	4.4
Glutamine	Gln	Q	HOOC-$(CH_2)_2$-CH(NH_2)-COOH	146.1451	-	5.65	-3.5	3.9
Negatively charged R groups								
Aspartic acid	Asp	D	HOOC-CH^2-CH(NH^2)-COOH	133.1032	3.65	2.77	-3.5	5.5
Glutamic acid	Glu	E	H_2N-CO-$(CH_2)_2$-CH(NH_2)-COOH	147.1299	4.25	3.22	-3.5	6.2
Positively charged R groups								
Lysine	Lys	K	H_2N-$(CH_2)_4$-CH(NH_2)-COOH	146.1882	10.53	9.74	-3.9	7.0
Arginine	Arg	R	HN=C(NH_2)-NH-$(CH_2)_3$-CH(NH_2)-COOH	174.2017	12.48	10.76	-4.5	4.7
Histidine	His	H	NH-CH=N-CH=C-CH_2-CH(NH_2)-COOH |_____|	155.1552	6.00	7.59	-3.2	2.1

References

1. Ellis, R. J. and Minton, A. P. (2003) *Join the crowd*. Nature **425**, 27–8.
2. Gething, M-J. and Sambrook, J. (1992) *Protein folding in the cell*. Nature **355**, 33–45.
3. Anfinsen, C.B., Haber, E., Sela, M. and White, F.H. Jr. (1961) *The kinetics of formation of native ribonuclease during oxidation of the reduced polypeptide chain*. Proc. Natl. Acad. Sci. U.S.A. **47**, 1309-1314.
4. Anfinsen, C. B. (1973) *Principles that govern the folding of protein chains*. Science **181**, 223-230.
5. Levinthal, C. (1968) *Are there pathways for protein folding?* J. Chim. Phys. **65**, 44–45.
6. Dill, K. A. and Chan, H. S. (1997) *From Levinthal to pathway funnels*. Nat. Struct. Biol. **4**, 10-19.
7. Baldwin, R. L. (1994) *Matching speed and stability*. Nature **369**, 183-184.
8. Ramos, C. H. I. and Ferreira, S. T. (2005) *Protein folding, misfolding and aggregation: evolving concepts and conformational diseases*. Protein Pept. Lett. **121**, 213-222.
9. Pace, C. N., Shirley, B. A., McNutt, M. and Gajiwala, K. (1996) *Forces contributing to the conformational stability of proteins*. FASEB J. **10**, 75-83.
10. Kauzmann, W. (1987) *Thermodynamics of unfolding*. Nature **325**, 763-764.
11. Dill, K. A. (1990) *Dominant forces in protein folding.* Biochemistry **29**, 7133-7155.
12. Rahim, Z. and Barman, B. N. (1978) *The van der Waals criterion for hydrogen bonding*. Acta Cryst. **A34**, 761-764.
13. Doig, A. J., Sternberg, M. J. E. (1995) *Side-chain conformational entropy in protein folding*. Prot. Sci. **4**, 2247-51.
14. Watanabe, K., Masuda, T., Ohashi, H., Mihara, H. and Suzuki, Y. (1994) *Multiple proline substitutions cumulatively thermostabilize Bacillus cereus ATCC7064 oligo-1,6-glucosidase. Irrefragable proof supporting the proline rule*. Eur. J. Biochem. **226**, 277-283.
15. Creamer, T. P. (2001) *Methods in Molecular Biology, vol. 168: Protein Structure, Stability and Folding*. Humana Press Inc., Totowa, New Jersey.
16. Pauling, L. and Corey, R. B. (1951) *Atomic coordinates and structure factors for two helical configurations of polypeptide chains*. Proc. Natl. Acad. Sci. U.S.A. **37**, 235-240; Pauling, L. and Corey, R. B. (1951) *The structure of synthetic polypeptides*. Proc. Natl. Acad. Sci. U.S.A. **37**, 241-250; Pauling, L. and Corey, R. B. (1951) *The pleated sheet, a new layer configuration of polypeptide chains*. Proc. Natl. Acad. Sci. U.S.A. **37**, 251-256; Pauling, L. and Corey, R. B. (1951) *The structure of feather rachis keratin*. Proc. Natl. Acad. Sci. U.S.A. **37**, 256-261; Pauling, L. and Corey, R. B. (1951) *The structure of hair, muscle, and related proteins*. Proc. Natl. Acad. Sci. U.S.A. **37**, 261-271; Pauling, L. and Corey, R. B. (1951) *The structure of fibrous proteins of the collagen-gelatin group*. Proc. Natl. Acad. Sci. U.S.A. **37**, 272-281; Pauling, L. and Corey, R. B. (1951) *The polypeptide-chain configuration in hemoglobin and other globular proteins*. Proc. Natl. Acad. Sci. U.S.A. **37**, 282-285.
17. Ramachandran, G. N. (1963) *Stereochemistry of polypeptide chain configurations*. J. Mol. Biol. **7**, 95-99.
18. Kendrew, J. C., Bodo, G., Dintzis, H. M. and Parrish, R. G. (1958) *A three-dimensional model of the myoglobin molecule obtained by x-ray analysis*. Nature **181**, 662-666.
19. Hardesty, B. and Kramer, G. (2001) *Folding of a nascent peptide on the ribosome*. Prog. Nucleic Acid Res. Mol. Biol. **66**, 41–66.
20. Hartl, F. U. and Hayer-Hartl, M. (2002) *Molecular chaperones in the cytosol: from nascent chain to folded protein*. Science **295**, 1852–1858.
21. Schlesinger, M. J. (1990) *Heat shock proteins*. J. Biol. Chem. **265**, 12111–12114.
22. Bukau, B. and Horwich, A.L. (1998) *The Hsp70 and Hsp60 chaperone machines*. Cell **92,** 351-366.
23. Schiene, C. and Fischer, G. (2000) *Enzymes that catalyse the restructuring of proteins*. Curr. Opin.

Struct. Biol. **10**, 40–45.
24. Wang, J. D. and Weissman, J. S. (1999) *Thinking outside the box: new insights into the mechanism of GroEL-mediated folding*. Nat. Struct. Biol. **6**, 597–600.
25. Hammon, C. and Helenius, A. (1995) *Quality control in the secretory pathway*. Curr. Opin. Cell. Biol. **7,** 523–529.
26. Wilson, M. R. and Easterbrook Smith, S. B. (2000) *Clusterin is a secreted mammalian chaperone*. Trends Biochem. Sci. **25**, 95–98.
27. Bence, N. F., Sampat, R. M. and Kopito, R. R. (2001) *Impairment of the ubiquitin–proteasome system by protein aggregation*. Science **292**, 1552–1555.
28. Dobson, C. M. (2003) *Protein folding and misfolding*. Nature **426**, 884-890.
29. Dobson, C. M. (2004) *Principles of protein folding, misfolding and aggregation*. Semin. Cell Dev. Biol. **15**, 3-16.
30. Chiti, F. and Dobson, C. M. (2006) Protein *misfolding, functional amyloid and human disease*. Annu. Rev. Biochem. **75**, 333-366.
31. Cohen, F. E. and Kelly, J. W. (2003) *Therapeutic approaches to protein-misfolding diseases*. Nature **426**, 905-909.
32. Virchow, R. (1854) *Zur Cellulose – Frage*. Virchows Arch. **6**, 416-426.
33. Divry, P. (1927) *Etude histochimique des plaques seniles (histochemical study of senile plaques)*. J. Belg. Neurol. Psychiatry **9**, 643–657.
34. Cohen, E. S. and Calkins, S. (1959) *Electron microscopic observations on a fibrous component in amyloid of diverse origins*. Nature **183**, 1202–1203.
35. Glenner, G. G. and Wong, C. W. (1984) *Alzheimer´s disease: initial report of the purification and characterization of a novel cerebrovascular amyloid protein*. Biochem. Biophys. Res. Commun. **120**, 885-890.
36. Tan, S. Y. and Pepys, M. B. (1994) *Amyloidosis*. Histopathology **25**, 403–414.
37. Pepys, M. B. (2005) *Amyloidosis*. Annu. Rev. Med. **57**, 8.1-8.19.
38. Sunde, M., Serpell, L. C., Bartlam, M., Fraser, P. E., Pepys, M. B. and Blake, C. F. (1997) *Common core structure of amyloid fibrils by synchrotron X-ray diffraction*. J. Mol. Biol. **273**, 729–39.
39. Bonar, L., Cohen, A. S. and Skinner, M. (1967) *Characterization of the amyloid fibril as a cross-β Protein*. Proc. Soc. Expt. Biol. Med. **131**, 1373-1375.
40. Jaroniec, C. P., MacPhee, C. E., Bajaj, V. S., McMahon, M. T., Dobson, C. M. and Griffin, R. G. (2004) *High-resolution molecular structure of a peptide in an amyloid fibril determined by magic angle spinning NMR spectroscopy*. Proc. Natl. Acad. Sci. U.S.A. **101**, 711–716.
41. Serpell, L. C., Sunde, M., Benson, M. D., Tennent, G. A., Pepys, M. B. and Fraser, P. E. (2000) *The protofilament substructure of amyloid fibrils*. J. Mol. Biol. **300**, 1033–1039.
42. Nilsson, M. R. (2004) *Techniques to study amyloid fibril formation in vitro*. Methods **34**, 151-160.
43. LeVine III, H. (1993) *Thioflavine T interaction with synthetic Alzheimer's disease β-amyloid peptides: detection of amyloid aggregation in solution*. Protein Sci. **2**, 404–410.
44. Tycko, R. (2003) *Insights into the amyloid folding problem from solid-state NMR*. Biochemistry **42**, 3151-3159.
45. Sachse, C., Xu, C., Wieligmann, K., Diekmann, S., Grigorieff, N. and Fändrich, M. (2006) *Quaternary structure of a mature amyloid fibril from Alzheimer's Aβ(1-40) peptide*. J. Mol. Biol. **362**, 347-354.
46. Jimenez, J. L., Nettleton, E. J., Bouchard, M., Robinson, C. V., Dobson, C. M. and Saibil, H. R. (2002) *The protofilament structure of insulin amyloid fibrils*. Proc. Natl Acad. Sci. U.S.A. **99**, 9196–9201.
47. Wilson, M. R., Yerbury, J. J.and Poon, S. (2007) *Potential roles of abundant extracellular chaperones in the control of amyloid formation and toxicity*. Mol. BioSyst. **4**, 42-52.
48. Ecroyd, H., Koudelka, T., Thorn, D. C., Williams, D. M., Devlin, G., Hoffmann, P. and Carver, J. A. (2008) *Dissociation from the oligomeric state is the rate-limiting step in amyloid fibril formation by kappa-casein*. J. Biol. Chem. **283**, 9012–9022.
49. Jahn, T. R. and Radford, S. (2005) *The Yin and Yang of protein folding*. FEBS J. **272**, 5962-5970.

50. Merlini, G. and Bellotti, V. (2003) *Molecular mechanisms of amyloidosis*. N. Engl. J. Med. **349**, 583-596.
51. Jarrett, J. T. and Lansbury, P. T. Jr. (1993) *Seeding "one-dimensional crystallization" of amyloid: a pathogenic mechanism in Alzheimer's disease and scrapie?* Cell **73**, 1055-1058.
52. Fandrich, M., Forge, V., Buder, K., Kittler, M., Dobson, C. M. and Diekmann, S. (2003) *Myoglobin forms amyloid fibrils by association of unfolded polypeptide segments*. Proc. Natl. Acad. Sci. U.S.A. **100**, 15463–15468.
53. Chiti, F., Taddei, N., Bucciantini, M., White, P., Ramponi, G. and Dobson, C. M. (2000) *Mutational analysis of the propensity for amyloid formation by a globular protein*. EMBO J. **19**, 1441–1449.
54. Otzen, D. E., Kristensen, O. and Oliveberg, M. (2000) *Designed protein tetramer zipped together with a hydrophobic Alzheimer homology: A structural clue to amyloid assembly*. Proc. Natl. Acad. Sci. U.S.A. **97**, 9907-9912.
55. Wurth, C., Guimard, N. K. and Hecht, M. H. (2002) *Mutations that reduce aggregation of the Alzheimer's Aβ42 peptide: an unbiased search for the sequence determinants of Aβ amyloidogenesis*. J. Mol. Biol. **319**, 1279-1290.
56. Chiti, F., Calamai, M., Taddei, N., Stefani, M., Ramponi, G. and Dobson, C. M. (2002) *Designing conditions for in vitro formation of amyloid protofilaments and fibrils*. Proc. Natl. Acad. Sci. U.S.A. **99**, 16419–16426.
57. Williams, A. D., Portelius, E., Kheterpal, I., Guo, J-T., Cook, K. D., Xu, Y. and Wetzel, R. (2004) *Mapping Aβ amyloid fibril secondary structure using scanning proline mutagenesis*. J. Mol. Biol. **335**, 833-842.
58. Fändrich, M. and Dobson, C. M. (2002) *The behaviour of polyamino acids reveals an inverse side chain effect in amyloid structure formation*. EMBO J. **21**, 5682-5690.
59. Kazmirski, S. L., Howard, M. J., Isaacson, R. L. and Fersht, A. R. (2000) *Elucidating the mechanism of familiar amyloidosis-Finnish type: NMR studies of human gelsolin domain 2*. Proc. Natl. Acad. Sci. U.S.A. **97** 10706-10711.
60. Nilsson, M., Driscoll, M. and Raleigh, D. P. (2002) *Low levels of asparagine deamidation can have a dramatic effect on aggregation of amyloidogenic peptides: implications for the study of amyloid formation*. Prot. Sci. **11**, 342-349.
61. Zhang, Q., Powers, E. T., Nieva, J., Huff, M. E., Dendle, M. A., Bieschke, J., Glabe, C. G., Eschenmoser, A., Wentworth, P. Jr., Lerner, R. A., and Kelly, J. W. (2004) *Metabolite-initiated protein misfolding may trigger Alzheimer's disease*. Proc. Natl. Acad. Sci. U.S.A. **101**, 4752-4757.
62. Bush, A. I. (2003) *The metallobiology of Alzheimer's disease*. Trends Neurosci. **26**, 207-214.
63. Yan S. D., Zhu H., Zhu A., Golabek, A., Du, H., Roher, A., Yu, J., Soto, C., Schmidt, A. M., Stern, D. and Kindy, M. (2000) *Receptor-dependent cell stress and amyloid accumulation in systemic amyloidosis*. Nat. Med. **6**, 643-651.
64. Lambert, M. P., Barlow, A. K., Chromy, B. A., Edwards, C., Freed, R., Liosatos, M., Morgan, T. E., Rozovsky, I., Trommer, B., Viola, K., Wals, L., Zhang, P. C., Finch, C. E., Krafft, G. A., and Klein, W. L. (1998) *Diffusible, nonfibrillar ligands derived from Aβ1–42 are potent central nervous system neurotoxins*. Proc. Natl. Acad. Sci. U.S.A. **95**, 6448-6453.
65. Hartley, D. M., Walsh, D. M., Ye, C. P., Diehl, T., Vasquez, S., Vassilev, P. M., Teplow, D. B., and Selkoe, D. J. (1999) *Protofibrillar intermediates of amyloid β-protein induce acute electrophysiological changes and progressive neurotoxicity in cortical neurons*. J. Neurosci. **19**, 8876-8884.
66. Sousa, M. M., Cardoso, I., Fernandes, R., Guimarães, A. and Saraiva, M. J. (2001) *Deposition of transthyretin in early stages of familial amyloidotic polyneuropathy: evidence for toxicity of nonfibrillar aggregates*. Am. J. Pathol. **159**, 1993–2000.
67. Walsh, D. M., Klyubin, I., Fadeeva, J. V., Cullen, W. K., Anwy, R., Wolfe, M. S., Rowan, M. J., and Selkoe, D. J. (2002) *Naturally secreted oligomers of amyloid-β protein potently inhibit hippocampal long-term potentiation in vivo*. Nature **416**, 535-539.

68. Hardy, J. and Selkoe, D. J. (2002) *The amyloid hypothesis of Alzheimer's disease: progress and problems on the road to therapeutics*. Science **297**, 353-356.
69. Alzheimer, A. (1907) *Uber eine eigenartige Erkrankung der Hirnrinde*. Allgemeine Zeitschrift fur Psychiatrie und Psychish-Gerichtliche Medizin **64**,146-148.
70. Selkoe, D. J. (2001) *Alzheimer's disease: genes, proteins, and therapy*. Physiol. Rev. **81**, 741-766.
71. Blennow, K., de Leon, M. J. and Zetterberg, H. (2006) *Alzheimer's disease*. Lancet **368**, 387-403.
72. Gotz, J., Chen, F., Van Dorpe, J. and Nitsch, R. M. (2001) *Formation of neurofibrillary tangles in P301l tau transgenic mice induced by Abeta 42 fibrils*. Science **293**, 1491-1495.
73. Braak, H. and Braak, E. (1998) *Evolution of neuronal changes in the course of Alzheimer's disease*. J. Neural Transm. Suppl. **53**, 127–140.
74. Dickson, D. W. (1997) *Neuropathological diagnosis of Alzheimer's disease: a perspective from longitudinal clinicopathological studies*. Neurobiol. Aging **18**, S21–S26.
75. Mattson, M. P. (2004) *Pathways towards and away from Alzheimer's disease*. Nature **430**, 631-639.
76. Terry, R. D., Masliah, E., Salmon, D. P., Butters, N., DeTeresa, R., Hill, R., Hansen, L. A. and Katzman, R. (1991) *Physical basis of cognitive alterations in Alzheimer's disease: synapse loss is the major correlate of cognitive impairment*. Ann. Neurol. **30**, 572-580.
77. Hardy, J. (1992) *Alzheimer´s disease: the amyloid cascade hypothesis*. Science **256**, 184-185.
78. Masters, C. L., Simms, G., Weinman, N. A., Multhaup, G., McDonald, B. L. and Beyreuther, K. (1985) *Amyloid plaque core protein in Alzheimer disease and Down syndrome*. Proc. Natl. Acad. Sci. U.S.A. **82**, 4245-4249.
79. Selkoe, D. J. (1994) *Alzheimer´s disease: a central role for amyloid*. J. Neuropathol. Exp. Neurol. **53**, 438-447.
80. Hardy, J. (1997) *The Alzheimer family of diseases: many ethiologies, one pathogenesis?* Proc. Natl. Acad. Sci. U.S.A. **94**, 2095-2097.
81. Kirschner, D. A., Abraham, C. and Selkoe, D. J. (1986) *X-ray diffraction from intraneuronal paired helical filaments and extraneuronal amyloid fibers in Alzheimer disease indicates cross-beta conformation*. Proc. Natl. Acad. Sci. U.S.A. **83**, 503-507.
82. Gouras, G. K., Almeida, C. G. and Takahashi, R. H. (2005) *Intraneuronal Abeta accumulation and origin of plaques in Alzheimer's disease*. Neurobiol. Aging **26**, 1235-1244.
83. Bartus, R. T., Emerich, D. F. (1999) *Cholinergic markers in Alzheimer's disease*. J. Am. Med. Assoc. **282**, 2208–2209.
84. Auld, D. S., Kornecook, T. J., Bastianetto, S. and Quirion, R. (2002) *Alzheimer's disease and the basal fore brain cholinergic system: relations to β-amyloid peptides, cognition and treatment strategies*. Prog. Neurobiol. **68**, 209–245.
85. Bowen, D. M., Palmer, A. M., Frances, P. T., Procter, A. W. and Lowe, S. L. (1988) *Classical neurotransmitters in Alzheimer's disease*. In: Terry RD (ed) *Aging and the Brain*. Raven Press, New York, 115–128.
86. Turner, P. R., O'Conner, K., Tate, W. P. and Abraham, W. L. (2003) *Roles of amyloid precursor protein and its fragments in regulating neural activity, plasticity and memory*. Prog. Neurobiol. **70**, 1–32.
87. Seubert, P., Oltersdorf, T., Lee, M. G., Barbour, R., Blomquist, C., Davis, D. L., Bryant, K., Fritz, L. C., Galasko, D., Thal, L. J., Lieberburg, I., and Schenk, D. B. (1993) *Secretion of β-amyloid precursor protein cleaved at the amino terminus of the β-amyloid peptide*. Nature **361**, 260–263.
88. Mattson, M. P. (1997) *Cellular actions of beta-amyloid precursor protein and its soluble and fibrillogenic derivatives*. Physiol. Rev. **77**, 1081–1132.
89. Allinson, T. M. J., Parkin, E. T., Turner, A. J. and Hooper, N. M. (2003) *ADAMs family members as amyloid precursor protein secretases*. J. Neurosci. Res. **74**, 342-352.
90. Vassar, R. (2004) *BACE1: the β-Secretase enzyme in Alzheimer's disease*. J. Mol. Neurosci. **23**, 105-114.
91. Iwatsubo, T. (2004) *The gamma-secretase complex: machinery for intramembrane proteolysis*.

Curr. Opin. Neurobiol. **14**, 379-83.
92. Selkoe, D. J. and Wolfe, M. S. (2007) *Presenilin: running with scissors in the membrane*. Cell **131**, 215-221.
93. Thinakaran, G. and Koo, E. H. (2008) *Amyloid precursor protein trafficking, processing, and function*. J. Biol. Chem. **283**, 29615-29619.
94. Gandy, S. (2005) *The role of cerebral amyloid β accumulation in common forms of Alzheimer disease*. J. Clin. Invest. **115**, 1121-1129.
95. Sian, A. K., Frears, E. R., El-Agnaf, O. M. A., Patel, B. P., Manca, M. F., Siligardi, G., Hussain, R. and Austen, B. M. (2000) *Oligomerization of β-amyloid of the Alzheimer´s and the Dutch-cerebral-haemorrhage types*. Biochem J. **349**, 299-308.
96. Bitan, G., Vollers, S. S. and Teplow, D. B. (2003) *Elucidation of primary structure elements controlling early amyloid β-protein oligomerization*. J. Biol. Chem. **278**, 34882–34889.
97. Liu, R., McAllister, C., Lyubchenko, Y. and Sierks, M. R. (2004) *Residues 17-20 and 30-35 of beta-amyloid play critical roles in aggregation*. J. Neurosci. Res. **75**, 162-171.
98. El-Agnaf, O. M. A., Guthrie, D. J. S., Walsh, D. M. and Irvine, G. B. (1998) *The influence of the central region containing residues 19–25 on the aggregation properties and secondary structure of Alzheimer's b-amyloid peptide*. Eur. J. Biochem. **256**, 560–569.
99. Johansson, A. S., Berglind-Dehlin, F., Karlsson, G., Edwards, K., Gellerfors, P. and Lannfelt, L. (2006) *Physiochemical characterization of the Alzheimer's disease-related peptides Aβ1-42Arctic and Aβ1-42wt*. FEBS J. **273**, 2618−2630.
100. Suzuki, N., Cheung, T. T., Cai, X-D., Odaka, A., Otvos, L. Jr., Eckman, C. B., Golde, T. E. and Younkin, S. G. (1994) *An increased percentage of long amyloid β protein secreted by familial amyloid β protein precursor (βAPP717) mutants*. Science **264**, 1336-1340.
101. Gravina, S. A., Ho, L., Eckman, C. B., Long, K. E., Otvos, L. Jr., Younkin, L. H., Suzuki, N. and Younkin, S. G. (1995) *Amyloid β protein (Aβ) in Alzheimer´s disease Brain*. J. Biol. Chem. **270**, 7013-7016.
102. Chen, Y-R and Glabe, C. G. (2006) *Distinct early folding and aggregation properties of Alzheimer amyloid-β peptides Aβ40 and Aβ42*. J. Biol. Chem. **281**, 24414-24422.
103. Yang, M. and Teplow, D. B. (2008) *Amyloid β-protein monomer folding: free-energy surfaces reveal alloform-specific differences*. J. Mol. Biol. **384**, 450-464.
104. Younkin, S. G. (1995) *Evidence that Aβ42 is the real culprit in Alzheimer´s disease*. Ann. Neurol. **37**, 287-288.
105. Selkoe, D. J. (1999) *Translating cell biology into therapeutic advances in Alzheimer´s disease*. Nature **399**, A23-A31.
106. Dahlgren, K. N., Manelli, A. M., Stine, W. B. Jr., Baker, L. K., Krafft, G. A. and LaDu, M. J. (2002) *Oligomeric and fibrillar species of amyloid-β peptides differentially affect neuronal viability*. J. Biol. Chem. **277**, 32046-32053.
107. Murphy, R. M. (2002) *Peptide aggregation in neurodegenerative disease*. Annu. Rev. Biomed. Eng. **4**, 155-174.
108. Kyte, J. and Doolittle, R. F. (1982) *A simple method for displaying the hydropathic character of a protein*. J. Mol. Biol. **157**, 105-132.
109. Scheuner, D. E. C., Jensen, M., Song, X., Citron, M., Suzuki, N., Bird, T. D., Hardy, J., Hutton, M., Kukull, W., Larson, E., Levy-Lahad, L., Viitanen, M., Peskind, E., Poorkaj, P., Schellenberg, G., Tanzi, R., Wasco, W., Lannfelt, L., Selkoe, D. and Younkin, S. (1996) *Secreted amyloid β-protein similar to that in the senile plaques of Alzheimer's disease is increased in vivo by the presenilin 1 and 2 and APP mutations linked to familial Alzheimer's disease*. Nat. Med. **2**, 864-870.
110. Tilley, L., Morgan, K., and Kalsheker, N. (1998) *Genetic risk factors in Alzheimer's disease*. J. Clin. Pathol. Mol. Pathol. **51**, 293−304.
111. Iwata, N., Higuchi, M. and Saido, T. C. (2005) *Metabolism of amyloid-β peptide and Alzheimer´s disease*. Pharmacol. Ther. **108**, 129-148.

112. Selkoe, D. J. (2001) *Clearing the brain's amyloid cobwebs*. Neuron **32**,177–180.
113. Forman, M. S., Trojanowski, J. Q. and Lee, V. M. (2004) *Neurodegenerative diseases: a decade of discoveries paves the way for therapeutic breakthroughs*. Nat. Med. **10**, 1055– 1063.
114. Lee, E. K., Park, Y. W., Shin, D. Y., Mook-Jung, I. and Yoo, Y. J. (2006) *Cytosolic amyloid-β peptide 42 escaping from degradation induces cell death*. Biochem. Biophys. Res. Commun. **344**, 471–477.
115. Billings, L. M., Oddo, S., Green, K. N., McGaugh, J. L. and Laferla, F. M. (2005) *Intraneuronal Aβ causes the onset of early Alzheimer's disease related cognitive deficits in transgenic mice*. Neuron **45**, 675–688.
116. Klein, W. L., Krafft, G. A. and Finch, C. E. (2001) *Targeting small Aβ oligomers: the solution to an Alzheimer´s disease conundrum?* Trends Neurosci. **24**, 219-224.
117. Hyman, B. T. (1997) *The neuropathological diagnosis of Alzheimer´s disease: clinical-pathological studies*. Neurobiol. Aging **18**, S27-S32.
118. McLean, C. A., Cherny, R. A., Fraser, F. W., Fuller, S. J., Smith, M. J., Beyreuther, K., Bush, A. I. and Masters, C. L. (1999) *Soluble pool of Abeta amyloid as a determinant of severity of neurodegeneration in Alzheimer's disease*. Ann. Neurol. **46**, 860–866.
119. Kuo, Y. M., Emmerling, M. R., Vigo-Pelfrey, C., Kasunic, T. C., Kirkpatrick, J. B., Murdoch, G. H., Ball, M. J. and Roher, A. E. (1996) *Water-soluble Abeta (N-40, N-42) oligomers in normal and Alzheimer disease brains*. J. Biol. Chem. **271**, 4077–4081.
120. Kayed, R., Head, E., Thompson, J. L., McIntire, T. M., Milton, S. C., Cotman, C. W. and Glabe, C. G. (2003) *Common structure of soluble amyloid oligomers implies common mechanism of pathogenesis*. Science **300**, 486-489.
121. Gong, Y., Chang, L., Viola, K. L., Lacor, P. N., Lambert, M. P., Finch, C. E., Krafft, G. A. and Klein, W. L. (2003) *Alzheimer's disease-affected brain: Presence of oligomeric Aβ ligands (ADDLs) suggests a molecular basis for reversible memory loss*. Proc. Natl. Acad. Sci. U.S.A. **100**, 10417–10422.
122. Conway, K. A., Lee, S. J., Rochet, J. C., Ding, T. T., Williamson, R. E. and Lansbury, P. T. Jr. (2000) *Acceleration of oligomerization, not fibrillization, is a shared property of both α-synuclein mutations linked to early-onset Parkinson's disease: Implications for pathogenesis and therapy*. Proc. Natl. Acad. Sci. U.S.A. **97**, 571-576.
123. Scherzinger, E., Lurz, R., Turmaine, M., Mangiarini, L., Hollenbach, B., Hasenbank, R., Bates, G. P., Davies, S. W., Lehrach, H. and Wanker, E. E. (1997) *Huntingtin-encoded polyglutamine expansions form amyloid-like protein aggregates in vitro and in vivo*. Cell **90**, 549-558.
124. Bucciantini, M., Calloni, G., Chiti, F., Formigli, L., Nosi, D., Dobson, C. M. and Stefani, M. (2004) *Prefibrillar amyloid protein aggregates share common features of cytotoxicity*. J. Biol. Chem. **279**, 31374-31382.
125. Walsh, D. M., A. Lomakin, G. B. Benedek, Condron, M. M. and Teplow, D. B. (1997) *Amyloid β-protein fibrillogenesis. Detection of a protofibrillar intermediate*. J. Biol. Chem. **272**, 22364-22372.
126. Harper, J. D., Wong, S. S., Lieber, C. M. and Lansbury, P. T. Jr. (1997) *Observation of metastable Aβ amyloid protofibrils by atomic force microscopy*. Chem. Biol. **4**, 119-125.
127. Walsh, D.M., Hartley, D.M., Kusumoto, Y., Fezoui, Y., Condron, M. M., Lomakin, A., Benedek, G. B., Selkoe, D. J. and Teplow, D. B. (1999) *Amyloid β-protein fibrillogenesis. Structure and biological activity of protofibrillar intermediates*. J. Biol. Chem. **274**, 25945-52.
128. Klein, W. L. (2002) *ADDLs & protofibrils - the missing links?* Neurobiol. Aging **23**, 231-5.
129. Török, M., Milton, S., Kayed, R., Wu, P., McIntire, T., Glabe, C. G. and Langen, R. (2002) *Structural and dynamic features of Alzheimer's Aβ peptide in amyloid fibrils studied by site-directed spin labeling*. J. Biol. Chem. **277**, 40810-40815.
130. Tjernberg, L. O., Näslund, J., Lindqvist, F., Johansson, J., Karlströmi, A. R., Thyberg, J., Terenius, L. and Nordstedt, C. (1996) *Arrest of β-Amyloid fibril formation by a pentapeptide ligand*. J. Biol. Chem. **271**, 8545-8548.
131. Petkova, A. T., Yau, W-M. and Tycko, R. (2006) *Experimental constraints on quaternary structure in Alzheimer´s β-amyloid fibrils* . Biochemistry **45**, 498-512.

132. Antzutkin, O. N., Balbach, J. J. and Tycko, R. (2003) *Site-specific identification of non-β-strand conformations in Alzheimer´s β-amyloid fibrils by solid-state NMR*. Biophys. J. **84**, 3326-3335.
133. Pike, C. J., Walencewicz-Wasserman, A. J., Kosmoski, J., Cribbs, D. H., Glabe, C. G. and Cotman, C. W. (1995) *Structure-activity analyses of β-amyloid peptides: contributions of the 25-35 region to aggregation and neurotoxicity*. J. Neurochem. **64**, 253-265.
134. Bitan, G., Tarus, B., Vollers, S. S., Lashuel, H. A., Condron, M. M., Straub, J. E. and Teplow, D. B. (2003) *A molecular switch in amyloid assembly: Met 35 and amyloid β-protein oligomerization*. J. Am. Chem. Soc. **125**, 15359-15365.
135. Hou, L., Shao, H., Zhang, Y., Li, H., Menon, N. K., Neuhaus, E. B., Brewer, J. M., Byeon, I-J. L., Ray, D. G., Vitek, M. P., Iwashita, T., Makula, R. A., Przybyla, A. B., and Zagorski, M. G. (2004) *Solution NMR studies of the Aβ(1-40) and Aβ(1-42) peptides establish that the Met35 oxidation state affects the mechanism of amyloid formation*. J. Am. Chem. Soc. **126**, 1992-2005.
136. Guo, M., Gorman, P. M., Rico, M., Chakrabartty, A., Laurents, D. V. (2005) *Charge substitution show that repulsive electrostatic interactions impede the oligomerization of Alzheimer amyloid peptides*. FEBS Lett. **579**, 3574-3578.
137. Paravastu, A. K., Leapman, R. D., Yau, W-M. and Tycko, R. (2008) *Molecular structural basis for polymorphism in Alzheimer´s β-amyloid fibrils*. Proc. Natl. Acad. Sci. U.S.A. **105**, 18349-18354.
138. Schmechel, A., Zentgraf, H., Scheuermann, S., Fritz, G., Pipkorn, R., Reed, J., Beyreuther, K., Bayer, T. A. and Multhaup, G. (2003) *Alzheimer β-amyloid homodimers facilitate Aβ fibrillization and the generation of conformational antibodies*. J. Biol. Chem. **278**, 35317–35324.
139. Enya, M., Morishima-Kawashima, M., Yoshimura, M., Shinkai, Y., Kusui, K., Khan, K., Games, D., Schenk, D., Sugihara, S., Yamaguchi, H. and Ihara, Y. (1999) *Appearance of sodium dodecyl sulfate-stable amyloid β-protein (Aβ) dimer in the cortex during aging*. Am. J. Pathol. **154**, 271–279.
140. Kawarabayashi, T., Shoji, M., Younkin, L. H., Wen-Lang, L., Dickson, D. W., Murakami, T. Matsubara, E., Abe, K., Ashe, K. H. and Younkin, S. G. (2004) *Dimeric amyloid β protein rapidly accumulates in lipid rafts followed by apolipoprotein E and phosphorylated tau accumulation in the Tg2576 mouse model of Alzheimer's disease*. J. Neurosci. **24**, 3801-3809.
141. Cleary, J. P., Walsh, D. M., Hofmeister, J. J., Shankar, G. M., Kuskowski, M. A., Selkoe, D. J. and Ashe, K. H. (2005) *Natural oligomers of the amyloid-β protein specifically disrupt cognitive function*. Nat. Neurosci. **8**, 79-84.
142. Davis, C. H. and Berkowitz, M. L. (2009) *Interaction between amyloid-β (1-42) peptide and phospholipid bilayers: a molecular dynamics study*. Biophys J. **96**, 785-97.
143. Glabe, C. G. (2006) *Common mechanisms of amyloid oligomer pathogenesis in degenerative disease*. Neurobiol. Aging **27**, 570-575.
144. Verdier, Y., Zarándi, M. and Penke, B. (2004) *Amyloid β-peptide interactions with neuronal and glial cell plasma membrane: binding sites and implications for Alzheimer´s disease*. J. Peptide Sci. **10**, 229-248.
145. Sokolov, Y., Kozak, J.A., Kayed, R., Chanturiya, A., Glabe, C. and Hall, J. E. (2006) *Soluble amyloid oligomers increase bilayer conductance by altering dielectric structure*. J. Gen. Physiol. **128**, 637-647.
146. Roychaudhuri, R., Yang, M., Hoshi, M. M. and Teplow, D. B. (2009) *Amyloid β-protein assembly and Alzheimer disease*. J. Biol. Chem. **284**, 4749-4753.
147. Curtain, C. C., Ali, F., Volitakis, I., Cherny, R. A,. Norton, R. S., Beyreuther, K., Barrow, C. J., Masters, C. L., Bush, A. I. and Barnham, K. J. (2001) *Alzheimer's disease amyloid-β binds copper and zinc to generate an allosterically ordered membrane-penetrating structure containing superoxide dismutase-like subunits*. J. Biol. Chem. **276**, 20466–20473.
148. Minicozzi, V., Stellato, F., Comai, M., Serra, M. D., Potrich, C., Meyer-Klaucke, W. and Morante, S. (2008) *Identifying the minimal Cu and Zn binding site sequence in amyloid beta peptides*. J. Biol. Chem. **283**, 10784–10792.
149. Butterfield, D. A., Drake, J., Pocernichan, C. and Castegna, A. (2001) *Evidence of oxidative*

damage in Alzheimer's disease brain: central role for amyloid β–peptide. Trends Mol. Med. **7**, 548-554.
150. Smith, D. G., Cappai, R. and Barnham, K. J. (2007) *The redox chemistry of the Alzheimer´s disease amyloid β peptide*. Biochim. Biophys. Acta **1768**, 1976-1990.
151. Head, E., Garzon-Rodriguez, W., Johnson, J. K., Lott, I. T., Cotman, C. and Glabe, C. (2001) *Oxidation of Aβ and plaque biogenesis in Alzheimer's disease and Down syndrome*. Neurobiol. Dis. **8**, 792–806.
152. LaFerla, F. M. (2002) *Calcium dyshomeostasis and intracellular signaling in Alzheimer's disease*. Nature Rev. Neurosci. **3**, 862–872.
153. Kerr, J. F. (2002) *History of the events leading to the formulation of the apoptosis concept*. Toxicology **182**, 471–474.
154. Marx, J. (2001) *New leads on the 'how' of Alzheimer's*. Science **293**, 2192–2194.
155. Yankner, B. A. (1996) *Mechanisms of neuronal degeneration review in Alzheimer's disease*. Neuron **16**, 921–932.
156. Stadelmann, C., Deckwerth, T. L., Srinivasan, A., Bancher, C., Bruck, W., Jellinger, K. and Lassmann, H. (1999) *Activation of caspase-3 in single neurons and autophagic granules of granulovacuolar degeneration in Alzheimer's disease*. Am. J. Pathol. **155**, 1459–1466.
157. Glabe, C. G. (2001) *Intracellular mechanisms of amyloid accumulation and pathogenesis in Alzheimer's disease*. J. Mol. Neurosci. **17**, 137–145.
158. Oddo, S., Caccamo, A., Shepherd, J. D., Murphy, M. P., Golde, T. E., Kayed, R., Metherate, R., Mattson, M. P., Akbari, Y. and LaFerla, F. M. (2003) *Amyloid deposition precedes tangle formation in a triple transgenic model of Alzheimer's disease*. Neurobiol. Aging **24**, 1063–1070.
159. Nakagawa, T., Zhu, H., Morishima, N., Li, E., Xu, J., Yankner, B. A. and Yuan, J. (2000) *Caspase-12 mediates endoplasmic-reticulum-specific apoptosis and cytotoxicity by amyloid-β*. Nature **403**, 98–103.
160. Shintani, T. and Klionsky, D. J. (2004) *Autophagy in health and disease: a double-edge sword*. Science **306**, 990-995.
161. Akiyama, H., Barger, S., Barnum, S., Bradt, B., Bauer, J., Cole, G. M., Cooper, N. R., Eikelenboom, P., Emmerling, M., Fiebich, B. L., Finch, C. E., Frautschy, S., Griffin, W. S., Hampel, H., Hull, M., Landreth, G., Lue, L., Mrak, R., Mackenzie, I. R., McGeer, P. L., O'Banion, M. K., Pachter, J., Pasinetti, G., Plata-Salaman, C., Rogers, J., Rydel, R., Shen, Y., Streit, W., Strohmeyer, R., Tooyoma, I., Van Muiswinkel, F. L., Veerhuis, R., Walker, D., Webster, S., Wegrzyniak, B., Wenk, G. and Wyss-Coray, T. (2000) *Inflammation and Alzheimer's disease*. Neurobiol. Aging **21**, 383–421.
162. McGeer, P. L. and McGerr, E. G. (2001) *Inflammation autotoxicity and Alzheimer's disease*. Neurobiol. Aging **22**, 799–809.
163. Atwood, C. S., Obrenovich, M. E., Liu, T., Chan, H., Perry, G., Smith, M. A. and Martins, R. N. (2003) *Amyloi-β: a chameleon walking in two worlds: a review of the trophic and toxic properties of amyloid-β*. Brain Res. **43**, 1–46.
164. Wolfe, M. S. (2004) *Therapeutic strategies for Alzheimer´s disease*. Nat. Rev. Drug Discov. **1** 859-866.
165. Walsh, D. M. and Selkoe, D. J. (2007) *Aβ oligomers - a decade of discovery*. J. Neurochem. **101**, 1172–1184.
166. Götz, J., Streffer, J. R., David, D., Schild, A., Hoerndli, F., Pennanen, L., Kurosinski, P. and Chen, F. (2004) *Transgenic animal models of Alzheimer´s disease and related disorders: histopathology, behavior and therapy*. Mol. Psychiatry **9**, 664-683.
167. Citron, M. (2004) *Strategies for disease modification in Alzheimer´s disease*. Nat. Rev. Neurosci. **5**, 677-685.
168. Weggen, S., Eriksen, J. L., Das, P., Sagi, S. A., Wang, R., Pietrzi, C. U., Findlay, K. A., Smith, T. E., Murphy, M. P., Bulter, T., Kang, D. E., Marquez-Sterling, N., Golde, T. E. and Koo, E. H. (2001) *A subset of NSAIDs lower amyloidogenic A42 independently of cyclooxygenase activity*. Nature **414**,

212-216.
169. Nitsch, R. M., Slack, B. E., Wurtman, R. J. and Growdon, J. H. (1992) *Release of Alzheimer amyloid precursor derivatives stimulated by activation of muscarinic acetylcholine receptors*. Science **258**, 304–307.
170. Haass, C. and Selkoe, D. J. (2007) *Soluble protein oligomers in neurodegeneration: lessons from the Alzheimer´s amyloid β-peptide*. Nat. Rev. Mol. Cell Biol. **8**, 101-112.
171. Qiu, W. Q., Walsh, D. M., Ye, Z., Vekrellis, K., Zhang, J., Podlisny, M. B., Rosner, M. R., Safavi, A., Hersh, L. B. and Selkoe, D. J. (1998) *Insulin-degrading enzyme regulates extracellular levels of amyloid beta-protein by degradation*. J. Biol. Chem. **273**, 32730–32738.
172. Tucker, H. M., Kihiko, M., Caldwell, J. N., Wright, S., Kawarabayashi, T., Price, D., Walker, D., Scheff, S., McGillis, J. P., Rydel, R. E. and Estus, S. (2000) *The plasmin system is induced by and degrades Amyloid-β aggregates*. J. Neurosci. **20**, 3937-3946.
173. Mueller-Steiner, S., Zhou, Y., Arai, H., Roberson, E. D., Sun, B., Chen, J., Wang, X., Yu, G., Esposito, L., Mucke, L. and Gan, L. (2006) *Antiamyloidogenic and neuroprotective functions of cathepsin B: implications for Alzheimer's disease.* Neuron **51**, 703-714.
174. Stains, C. I., Mondal, K. and Ghosh, I. (2007) *Molecules that target beta-Amyloid*. ChemMedChem **2**, 1674-1692.
175. Gervais, F., Paquette, J., Morissette, C., Krzywkowski, P., Yu, M., Azzi, M., Lacombe, D., Kong, X., Aman, A., Laurin, J., Szarek, W. A. and Tremblay, P. (2006) *Targeting soluble Aβ peptide with Tramiprosate for the treatment of brain amyloidosis*. Neurobiol. Aging **28**, 537-547.
176. LeVine III, H. (2007) *Small molecule inhibitors of Aβ assembly*. Amyloid **14**, 185-197.
177. Soto, C., Sigurdsson, E. M., Morelli, L., Kumar, R. A., Castano, E. M. and Frangione, B. (1998) *β-sheet breaker peptides inhibit fibrillogenesis in a rat brain model of amyloidosis: Implications for Alzheimer's therapy*. Nat. Med. **4**, 822–826.
178. Permanne, B., Adessi, C., Saborio, G. P., Fraga, S., Frossard, M. J., Van Dorpe, J., Dewachter, I., Banks, W. A., Van Leuven, F. and Soto, C. (2002) *Reduction of amyloid load and cerebral damage in a transgenic mouse model of Alzheimer's disease by treatment with a β-sheet breaker peptide*. FASEB J. **16**, 860–862.
179. Cherny, R. A., Atwood, C. S., Xilinas, M. E., Gray, D. N., Jones, W. D., McLean, C. A., Barnham, K. J., Volitakis, I., Fraser, F. W., Kim, Y., Huang, X., Goldstein, L. E., Moir, R. D., Lim, J. T., Beyreuther, K., Zheng, H., Tanzi, R. E., Masters, C. L. and Bush, A. I. (2001) *Treatment with a copper-zinc chelator markedly and rapidly inhibits β-amyloid accumulation in Alzheimer's disease transgenic mice*. Neuron **30**, 665-676.
180. Orgogozo, J. M., Gilman, S., Dartigues, J. F., Laurent, B., Puel, M., Kirby, L. C., Jouanny, P., Dubois, B., Eisner, L., Flitman, S., Michel, B. F., Boada, M., Frank, A. and Hock, C. (2003) *Subacute meningoencephalitis in a subset of patients with AD after Aβ42 immunization*. Neurology **61**, 46-54.
181. Relini, A., Cavalleri, O., Rolandi, R. and Gliozzi, A. (2009) *The two-fold aspect of the interplay of amyloidogenic proteins with lipid membranes*. Chem. Phys. Lipids **158**, 1-9.
182. Giacomelli, C. E. and Norde, W. (2005) *Conformational changes of the amyloid beta-peptide (1-40) adsorbed on solid surfaces*. Macromol. Biosci. **5**, 401-407.
183. Tanaka, K., Waki, H., Ido, Y., Akita, S., Yoshida, Y. and Yoshida, T. (1998) *Protein and polymer analyses up to m/z 100 000 by laser ionization time-of-flight mass spectrometry*. Rapid Commun. Mass Spectrom. **2**, 151-153.
184. Stine, W. B., Jr., Dahlgren, K. N., Krafft, G. A. and LaDu, M. J. (2005) *In vitro characterization of conditions for amyloid-β peptide oligomerization and fibrillogenesis*. J. Biol. Chem. **278**, 11612-11622.
185. Gurtovenko, A. A., Patra, M., Karttunen, M. and Vattulainen, I (2004) *Cationic DMPC/DMTAP lipid bilayers: molecular dynamics study*. Biophys. J. **86**, 3461–3472.
186. Derry, D. M. and Wolfe, L. S. (1967) *Gangliosides in isolated neurons and glial cells*. Science **158**,

1450-1452.
187. Mocchetti, I. (2005) *Exogenous gangliosides, neuronal plasticity and repair, and the neurotrophins*. Cell. Mol. Life Sci. **62**, 2283–94.
188. Rodahl, M., Höök, F., Fredriksson, C., Keller, C. A., Krozer, A., Brzezinski, P., Voinova, M. and Kasemo, B. (1997) *Simultaneous frequency and dissipation factor QCM measurements of biomolecular adsorption and cell adhesion*. Faraday Discuss. **107**, 229–246.
189. Marx, K. A. (2003) *Quartz crystal microbalance: a useful tool for studying thin polymer films and complex biomolecular systems at the solution-surface interface*. Biomacromolecules **4**, 1099-1120.
190. Sauerbrey, G. (1959) *Verwendung von Schwingquarzen zur Wägung dünner Schichten und zur Mikrowägung*. Zeitschrift für Physik **155**, 206-222.
191. Voinova, M. V., Rodahl, M., Jonson, M. and Kasemo, B. (1999) *Viscoelastic acoustic response of layered polymer films at fluid-solid interfaces: continuum mechanics approach*. Phys. Scr. **59**, 391-396.
192. Santos, N. C. and Castanho, M. A. R. B. (2004) *An overview of the biophysical applications of atomic force microscopy*. Biophys. Chem. **107**, 133-149.
193. Binnig, G., Quate, C. F. and Gerber, C. (1986) *Atomic force microscope*. Phys. Rev. Lett. **56**, 930–933.
194. Fotiadis, D., Scheuring, S., Müller, S. A., Engel, A. and Müller, D. J. (2002) *Imaging and manipulation of biological structures with the AFM*. Micron **33**, 385-97.
195. Tamm, L. K. and Tatulian, S. A. (1997) *Infrared spectroscopy of proteins and peptides in lipid bilayers*. Quarterly Reviews of Biophysics **30**, 365-429.
196. Barth, A. (2007) *Infrared spectroscopy of proteins*. Biochim. Biophys. Acta **1767**, 1073-1101.
197. Sigurdsson, E. M. (2005) *Methods in Molecular Biology, vol.299: Amyloid Proteins – Methods and Protocols*. Humana Press, Totowa, New Jersey.
198. Chittur, K. K. (1998) *FTIR/ATR for protein adsorption to biomaterial surfaces*. Biomaterials **19**, 357-369.
199. Pelton, J. T. and McLean, L. R. (2000) *Spectroscopic methods for analysis of protein secondary structure*. Anal. Biochem. **277**, 167-176.
200. Parker, F. S. (1971) *Applications of infrared spectroscopy in biochemistry, biology, and medicine*., Plenum Press, New York.
201. Decher, G. (1997) *Fuzzy nanoassemblies: toward layered polymeric multicomposites*. Science **277**, 1232-1237.
202. Sukhorukov, G. B., Susha, A. S., Davis, S., Leporatti, S., Donath, E., Hartmann, J. and Möhwald, H. (2002) *Precipitation of inorganic salts inside hollow micrometer-sized polyelectrolyte shells*. J. Colloid Interface Sci. **247**, 251-254.
203. Reimhult, E., Höök, F. and Kasemo, B. (2003) *Intact vesicle adsorption and supported biomembrane formation from vesicles in solution: influence of surface chemistry, vesicle size, temperature, and osmotic pressure*. Langmuir **19**, 1681-1691.
204. McConnell, H. M., Watts, T. H., Weis, R. M. and Brian, A. A. (1986) *Supported planar membranes in studies of cell-cell recognition in the immune system*. Biochim. Biophys. Acta **864**, 95-106.
205. Glasmästar, K., Larsson, C., Höök, F. and Kasemo, B. (2002) *Protein adsorption on supported phospholipid bilayers*. J. Colloid Interface Sci. **246**, 40–47.
206. Sackmann, E. (1996) *Supported membranes: scientific and practical applications*. Science **271**, 43-48.
207. Bangham, A. D., Standish, M. M. and Watkins, J. C. (1965) *Diffusion of univalent ions across the lamellae of swollen phospholipids*. J. Mol. Biol. **13**, 238-252.
208. Rocha, S., Krastev, R., Thünemann, A. F., Pereira, M. C., Möhwald, H. and Brezesinski, G. (2005) *Adsorption of amyloid β-peptide at polymer surfaces: a neutron reflectivity study*. ChemPhysChem **6**, 2527-2534.
209. Wong, J. E., Rehfeld, F., Hänni, P., Tanaka, M. and von Klitzing, R. (2004) *Swelling behavior of*

polyelectrolyte multilayers in saturated water vapor. Macromolecules **37**, 7285-7289.
210. Hsieh, M. Ch., Farris, R. J. and McCarthy, T. J. (1997) *Surface "priming" for layer-by-layer deposition: polyelectrolyte multilayer formation on alkylamine plasma-modified polytetrafluoroethylene*. Macromolecules **30**, 8453-8458.
211. Arys, X., Jonas, A. M., Laschewsky, A., Legras, R. (2000) *Supramolecular polymers*. Marcel Dekker New York, 505–563.
212. Seantier, B., Breffa, C., Félix, O. and Decher, G. (2005) *Dissipation-enhanced quartz crystal microbalance studies on the experimental parameters controlling the formation of supported lipid bilayers*. J. Phys. Chem. B **109**, 21755-21765.
213. Johnson, S. J., Bayerl, T. M., McDermott, D. C., Adam, G. W., Rennie, A. R., Thomas, R. K. and Sackmann, E. (1991) *Structure of an adsorbed dimyristoylphosphatidylcholine bilayer measured with specular reflection of neutrons*. Biophys. J. **59**, 289-194.
214. Reimhult, E., Zäch, M., Höök, F. and Kasemo, B. (2006) *A multitechnique study of liposome adsorption on Au and lipid bilayer formation on SiO_2*. Langmuir **22**, 3313-3319.
215. Maltseva, E. and Brezesinski, G. (2005) *Adsorption of amyloid beta (1–40) peptide at phospholipid monolayers*. ChemPhysChem **5**, 1185-1190.
216. Terzi, E., Hölzemann, G. and Seelig, J. (1997) *Interaction of Alzheimer β-amyloid peptide(1-40) with lipid membranes*. Biochemistry **36**, 14845-14852.
217. Lin, M.-S., Chen, L.-Y., Wang, S. S.-S., Chang, Y and Chen, W.-Y. (2007) *Examining the levels of ganglioside and cholesterol in cell membrane on attenuation the cytotoxicity of beta-amyloid peptide*. Colloids Surf., B **65**, 172-177.
218. Liu, Y., Peterson, D. A. and Schubert, D. (1998) *Amyloid β peptide alters intracellular vesicle trafficking and cholesterol homeostasis*. Proc. Natl. Acad. Sci. U.S.A. **95**, 13266-13271.
219. Maxfield, F. R. and Tabas, I (2005) *Role of cholesterol and lipid organization in disease*. Nature **438**, 612-621.
220. Iler R. K. (1979) *The chemistry of silica*, Wiley, New York.
221. Irie, S., Horii, H. and Irie, M. (1980) *Radical Ions of Vinyl Polymers Having Aromatic Side Groups. Polystyrene and Poly(2-vinylaphthalene)*. Macromolecules **13**, 1355–1360.
222. Feiler, A. A., Sahlholm, A., Sandberg, T. and Caldwell, K. D (2007) *Adsorption and viscoelastic properties of fractionated mucin (BSM) and bovine serum albumin (BSA) studied with quartz crystal microbalance (QCM-D)*. J. Colloid Interface Sci. **315**, 475-481.
223. McLaurin, J. and Charkrabartty, A. (1996) *Membrane disruption by Alzheimer β-amyloid peptides mediated through specific binding to either phospholipids or gangliosides*. J. Biol. Chem. **271**, 26482–26489.
224. Amborggio, E. E., Kim, D. H., Separovic, F., Barrow, C. J., Barnham, K. J., Bagatolli, L. A. and Fidelio, G. D. (2005) *Surface behavior and lipid interaction of Alzheimer β-amyloid peptide 1–42: a membrane-disrupting peptide*. Biophys. J. **88**, 2706–2713.
225. Davis, C. H. and Berkowitz, M. L. (2009) *Interaction between amyloid-β (1-42) peptide and phospholipid bilayers: a molecular dynamics study*. Biophys. J. **96**, 785-797.
226. Kremer, J. J., Pallitto, M. M., Sklansky, D. J. and Murphy, R. M. (2000) *Correlation of β-amyloid aggregate size and hydrophobicity with decreased bilayer fluidity of model membranes*. Biochemistry **39**, 10309–10318.
227. Matsuzaki, K. and Horikiri, C. (1999) *Interactions of amyloid β-peptide (1-40) with ganglioside-containing membranes*. Biochemistry **38**, 4137-4142.
228. Yanagisawa, K., Odaka, A., Suzuki, N. and Ihara, Y. (1995) *GM1 ganglioside-bound amyloid β-protein (Aβ): a possible form of preamyloid in Alzheimer's disease*. Nat. Med. **1**, 1062-1066.
229. Hayashi, H., Kimura, N., Yamaguchi, H., Hasegawa, K., Yokoseki, T., Shibata, M., Yamamoto, N., Michikawa, M., Yoshikawa, Y., Terao, K., Matsuzaki, K., Lemere, C. A., Selkoe, D. J., Naiki, H. and Yanagisawa, K. (2004) *A seed for Alzheimer amyloid in the brain*. J. Neurosci. **24**, 4894–4902.
230. Wong, P. T., Schauerte, J. A., Wisser, K., Ding, H., Lee, E., Steel, D. and Gafni, A. (2009) *Amyloid-β*

membrane binding and permeabilization are distinct processes separately influenced by membrane charge and fluidity. J. Mol. Biol. **386**, 81-96.
231. Wolozin, B. (2004) *Cholesterol and the biology of Alzheimer´s disease*. Neuron **41**, 7-10.
232. Simons, K. and Ikonen, E. (1997) *Functional rafts in cell membranes*. Nature **385**, 569-572.
233. Matsuzaki, K. (2007) *Physicochemical interactions of amyloid β-peptide with lipid bilayers*. Biochim. Biophys. Acta **1768**, 1935-1942.
234. Klein, J. (2007) *Probing the interactions of proteins and nanoparticles*. Proc. Natl. Acad. Sci. U.S.A. **104**, 2029-2030.
235. Misra, A., Ganesh, S. and Shahiwala, A. (2003) *Drug delivery to the central nervous system: a review*. J. Pharm. Pharmaceut. Sci. **6**, 252-273.
236. Silva, G. A. (2005) *Small neuroscience: the nanostructure of the central nervous system and emerging nanotechnology applications*. Curr. Nanosci. **1**, 225-236.
237. Begley, D. J. (1996) *The blood–brain barrier: principles for targeting peptides and drugs to the central nervous system*. J. Pharm. Pharmacol. **48**, 136–146.
238. Kabanov, A. V. and Gendelman, H. E. (2007) *Nanomedicine in the diagnosis and therapy of neurodegenerative disorders*. Prog. Polym. Sci. **32**, 1054–1082.
239. Roney, C., Kulkarni, P., Arora, V., Antich P., Bonte, F., Wu, A., Mallikarjuana, N. N., Manohar, S., Liang, H-F., Kulkarni, A. R., Sung, H-W., Sairam, M. and Aminabhavi, T. M. (2005) *Targeted nanoparticles for drug delivery through the blood–brain barrier for Alzheimer's disease*. J. Control. Release **108**, 193–214.
240. Francis, K., van Beek, J., Canova, C., Neal, J. W. and Gasque, P. (2003) *Innate immunity and brain inflammation: the key role of complement*. Exp. Rev. Mol. Med. **5**, 1-19.
241. Thunemann, A. F., Sander, K., Jaeger, W. and Dimova, R. (2002) *Polyampholyte-dressed micelles of fluorinated and hydrogenated dodecanoic acid*. Langmuir **18**, 5099-5105.
242. Rocha, S., Thünemann, A. F., Pereira, M. C., Coelho, M. A. N., Mohwald, H. and Brezesinki, G. (2008) *Influence of fluorinated and hydrogenated nanoparticles on the structure and fibrillogenesis of amyloid beta-peptide*. Biophys. Chem. **137**, 35-42.
243. Tauer, K., Schllenberg, C. and Zimmermann, A. (2000) *Nucleation in heterophase polymerizations*. Macromol. Symp. **150**, 1-12.
244. Antonietti, M., Bremser, W., Rosenauer, D. C., Schupp, B. and Schmidt, M. (1991) *Synthesis and size control of polystyrene polymerization in microemulsion*. Macromolecules **24**, 6636-6643.
245. Antonietti, M., Briel, A. and Förster, S. (1996) *Intrinsic viscosity of small spherical polyelectrolytes: Proof for the intermolecular origin of the polyelectrolyte effect*. J. Chem. Phys. **105**, 7795-7807.
246. Gröhn, F. and Antonietti, M. (2000) *Intermolecular structure of spherical polyelectrolyte microgels in salt-free solution. 1. Quantification of the attraction between equally charged polyelectrolytes*. Macromolecules **33**, 5938-5949.
247. Martins, C. R., Ruggeri, G. and De Paoli, M-A. (2003) *Synthesis in pilot plant scale and physical properties of sulfonated polystyrene*. J. Braz. Chem. Soc. **14**, 797-802.
248. Malver Instruments, Zetasizer Nano Series User Manual. ed. 2003.
249. Aslamazova, T. and Tauer, K. (2004) *On the colloidal stability of polystyrene particles prepared with different kinds of surface active initiators*. Colloids Surf., A **239**, 3-10.
250. Favero, C., Graillat, C. and Guyot, A. (2000) *Reactive surfactants in styrene microemulsion polymerization*. Macromol. Symp. **150**, 235-240.
251. Greenfield, N. J. (2007) *Using circular dichroism spectra to estimate protein secondary structure*. Nat. Protoc. **1**, 2876-2890.
252. Kelly, S. M. and Price, N. C. (2000) *The use of circular dichroism in the investigation of protein structure and function*. Curr. Protein Pept. Sci. **1**, 349-384.
253. Greenfield, N. J. and Fasman, G. D. (1971) *Polypeptides, characterization*. Encyclopedia of polymer science and technology. J. Wiley and Sons, N.Y. **15**, 410-429.
254. Sreerama, N. and Woody, R. W. (2004) *Computation and analysis of protein circular dichroism*

spectra. Meth. Enzymol. **383**, 318-351.
255. Ababou, A. and Ladbury, J. E. (2006) *Survey of the year 2004: literature on applications of isothermal titration calorimetry*. J. Mol. Recognit. **19**, 79-89.
256. MicroCal LLC, VP-ITC MicroCalorimeter User's Manual.
257. Khurana, R., Coleman, C., Ionescu-Zanetti, C., Carter, S. A., Krishna, V., Grover, R. K., Roy, R. and Singh, S. (2005) *Mechanism of thioflavin T binding to amyloid fibrils*. J. Struct. Biol. **151**, 229–238.
258. Lehninger, A. L., Nelson, D. L. and Cox, M. C. (1993) *Principles of Biochemistry*. Worth Publishers, N. Y., 2nd edition.
259. Raymond, S. and Weintraub, L. (1959) *Acrylamide gel as a supporting medium for zone electrophoresis*. Science **130**, 711.
260. Laemmli, U. K. (1970) *Cleavage of structural proteins during the assembly of the head of bacteriophage T4*. Nature **227**, 680 – 685.
261. Syrový, I. and Hodný, Z. (1990) *Staining and quantification of proteins separated by polyacrylamide gel electrophoresis*. J. Chromatogr. **569**, 175-196.
262. Biedler, J. L., Helson, L. and Spengler, B. A. (1973) *Morphology and growth, tumorigenicity, and cytogenetics of human neuroblastoma cells in continuous culture*. Cancer Res. **33**, 2643-2652.
263. Mosmann T. (1983) *Rapid colorimetric assay for cellular growth and survival: application to proliferation and cytotoxicity assays*. J. Immunol. Methods. **65**, 55–63.
264. Walsh, D. M., Klyubin, I., Fadeeva, J. V., Rowan, M. J. and Selkoe, D. J. (2002) *Amyloid-β oligomers: their production, toxicity and therapeutic inhibition*. Biochem. Soc. Trans **30**, 552-557.
265. Necula, M., Kayed, R., Milton, S. and Glabe, C. G. (2007) *Small molecule inhibitors of aggregation indicate that amyloid β oligomerization and fibrillization pathways are independent and distinct*. J. Biol. Chem. **282**, 10311-10324.
266. Kusumoto, Y., Lomakin, A., Teplow, D. B. and Benedek, G. B. (1998) *Temperature dependence of amyloid β-protein fibrillization*. Proc. Natl. Acad. Sci. U.S.A. **95**, 12277-12282.
267. Sabaté, R., Gallardo, M. and Estelrich, J. (2005) *Temperature dependence of the nucleation constant rate in β amyloid fibrillogenesis*. Int. J. Biol. Macromol. **35**, 9-13.
268. Bitan, G., Kirkitadze, M. D., Lomakin, A., Vollers, S. S., Benedek, G. B., and Teplow, D. B. (2003) *Amyloid β -protein (Aβ) assembly: Aβ40 and Aβ42 oligomerize through distinct pathways*. Proc. Natl. Acad. Sci. U.S.A. **100**, 330-335.
269. Zhang, S., Iwata, K., Lachenmann, M. J., Peng, J. W., Li, S., Stimson, E. R., Lu, Y., Felix, A. M., Maggio, J. E. and Lee, J. P. (2000) *The Alzheimer's peptide Aβ adopts a collapsed coil structure in water*. J. Struct. Biol. **130**, 130–141.
270. Ioudina, M., Uemura, E. (2003) *A three amino acid peptide, Gly-Pro-Arg, protects and rescues cell death induced by amyloid β-peptide*. Exp. Neurol. **184**, 923-929.
271. Hoshi, M., Sato, M., Matsumoto, S., Noguchi A., Yasutake, K., Yoshida, N. and Sato, K. (2003) *Spherical aggregates of β-amyloid (amylospheroid) show high neurotoxicity and activate tau protein kinase I/glycogen synthase kinase-3β*. Proc. Natl. Acad. Sci. U.S.A. **100**, 6370-6375.
272. Gong, J., Yao, P., Duan, H., Jiang, M., Gu, S. and Chunyu, L. (2003) *Structural transformation of cytochrome c and apo cytochrome c induced by sulfonated polystyrene*. Biomacromolecules **4**, 1293-1300.
273. Vieira, E. P., Hermel, H. and Möhwald, H. (2003) *Change and stabilization of the amyloid-β(1-40) secondary structure by fluorocompounds*. Biochim. Biophys. Acta **1645**, 6-14.
274. Montserret, R., McLeish, M. J., Böckmann, A., Geourjon, C. and Penin, F. (2000) *Involvement of electrostatic iInteractions in the mechanism of peptide folding induced by sodium dodecyl sulfate binding*. Biochemistry **45**, 8362-8373.
275. Pollack, S. J., Sadler, I. I. J., Hawtin, S. R., Tailor, V. J. and Shearman, M. S. (1995) *Sulfonated dyes attenuate the toxic effects of β-amyloid in a structure-specific fashion*. Neurosci. Lett. **197**, 211-214.
276. Mueller, K., Faeh, C. and Diederich, F. (2007) *Fluorine in pharmaceuticals: looking beyond*

intuition. Science **317**, 1881-1886.
277. Ferrão-Gonzalez, A., Robbs, B. K., Moreau, V. H., Ferreira, A., Juliano, L., Valente, A. P., Almeida, F. C. L., Silva, J. L. and Foguel, D. (2005) *Controlling β-amyloid oligomerization by the use of naphtalene sulfonates*. J. Biol. Chem. **280**, 43747-34754.
278. Bohm, H.-J., Banner, D., Bendels, S., Kansy, M., Kuhn, B., Müller, K., Obst-Sander, U. and Stahl, M. (2004) *Fluorine in medicinal chemistry*. ChemBioChem **5**, 637-643.
279. Essafi, W., Lafuma, F. and Williams, C. E. (1995) *Elffect of solvent quality on the behaviour of highly charged polyelectrolytes*. J. Phys. II **5**, 1269-1275.
280. Miura, Y., Yasuda, K., Yamamoto, K., Koike, M., Nishida, Y. and Kobayashi, K. (2007) *Inhibition of Alzheimer amyloid aggregation with sulfated glycopolymers*. Biomacromolecules **8**, 2129-2134.
281. Yamaguchi, S., Nishida, Y., Sasaki, K., Kambara, M., Kim, C-L., Ishiguro, N., Nagatsuka, T., Uzawa, H. and Horiuchi, M. (2006) *Inhibition of PrPSc formation by synthetic O-sulfated glycopyranosides and their polymers*. Biochem. Biophys. Res. Commun. **349**, 485-491.
282. Chien, P., Weissman, J. S. and DePace, A. H. (2004) *Emerging principles of conformation-based prion inheritance*. Annu Rev. Biochem. **73**, 617-656.
283. Kirkitadze, M. D., Condron, M. M. and Teplow, D. B. (2001) *Identification and characterization of key kinetics intermediates in amyloid β-protein fibrillogenesis*. J. Mol. Biol. **312**, 1103-1119.
284. Fezoui, Y. and Teplow, D. B. (2002) *Kinetic studies of amyloid β-protein fibril assembly. differential effects of α-helix stabilization*. J. Biol. Chem. **277**, 36948-36954.
285. Terzy, E., Holzemann, G., and Seelig, J. (1997) *Interaction of Alzheimer β-amyloid peptide (1-40) with lipid membranes*. Biochemistry **36**, 14845-14852.
286. Okada, T., Sawada, S., Akiyoshi, K. and Matsuzaki, K. (2006) *Inhibition of the formation of amyloid beta-protein fibrils using biocompatible nanogels as artificial chaperones*. FEBS Lett. **580**, 6587-6595.
287. Pai, A. S., Rubinstein, I. and Onyuksel, H. (2006) *PEGylated phospholipid nanomicelles interact with β-amyloid$_{(1-42)}$ and mitigate its beta-sheet formation, aggregation and neurotoxicity in vitro*. Peptides **27**, 2858-2866.
288. Cabaleiro-Lago, C., Quinlan-Pluck, F., Lynch, I., Lindman, S., Minogue, A. M., Thulin, E., Walsh, D. M., Dawson, K. A. and Linse, S. (2008) *Inhibition of amyloid Beta protein fibrillation by polymeric nanoparticles*. J. Am. Chem. Soc. **130**, 15437-15443.

List of Figures

Figure 2.1 Protein folding energy landscapes 6

Figure 2.2 Schematic illustrating the formation of a hydrogen bond and a hydrophobic bond during the folding of a protein 7

Figure 2.3 A) Peptide bonds and dihedral angles. B) Ramachandran plot 11

Figure 2.4 The α-helix 13

Figure 2.5 The structure of the β-sheet 15

Figure 2.6 A) β-turn; B) β-hairpin 16

Figure 2.7 Examples of some common structural motifs in proteins 17

Figure 2.8 Regulation of protein folding in the ER 21

Figure 2.9 Free-energy diagram showing to what extent a given sequence under native conditions prefers a normally folded conformation 23

Figure 2.10 X-ray diffraction signature of amyloid fibrils 27

Figure 2.11 Amyloid fibrils and protofilaments 28

Figure 2.12 Representation of the amyloid forming pathway 29

Figure 2.13 A schematic energy landscape for protein folding and aggregation 30

Figure 2.14 Histopathological lesions in AD 33

Figure 2.15 AD results in shrinkage of brain regions involved in learning and memory 34

Figure 2.16 Proteolytic processing of APP 36

Figure 2.17 Primary sequence of Aβ42, polarity of its amino acid residues and secondary structures prediction 38

Figure 2.18 Structure of APP around the Aβ domain, secretase cleavage sites, and location of some familial AD missense mutations 39

Figure 2.19 Metabolism of Aβ 40

Figure 2.20 Mechanism of AD according to the updated amyloid hypothesis where oligomeric species of Aβ are the main neurotoxic species 42

Figure 2.21 TEM and NMR based structural models of Aβ40 protofilaments 43

Figure 2.22 The neurotoxic action of Aβ involves generation of ROS and disruption of cellular calcium homeostasis 48

Figure 2.23 The amyloid cascade hypothesis suggests several possibilities of therapeutic intervention for disease modification in AD 51

Figure 3.1 MALDI-TOF mass spectrometry profile of Aβ peptides 56

Figure 3.2 Chemical structures of lipids and other substances used to prepare SLBs 58

Figure 3.3 A) AT-cut of a quartz crystal and a view of TSM of oscillation. B) Δf is related with the mass adsorbed; ΔD provides information about viscolelastic properties 60

Figure 3.4 Application of the Voight model to characterize viscoelastic films 61

Figure 3.5 Principle of the AFM 63

Figure 3.6 Comparison between the two AFM scanning types 63

Figure 3.7 A) IR beam as it travels through a trapezoidal ATR crystal. B) Total internal reflection at the interface of an IRE 67

Figure 3.8 SBSR ATR attachment 67

Figure 3.9 Structures of the polyelectrolytes used to prepare charged surfaces by LbL assembly 71

Figure 3.10 Technique of LbL assembly to produce self-assembled multilayers 71

Figure 3.11 A) Cell membrane and biomembrane model systems. B) Lipid bilayer formation on SiO_2 72

Figure 3.12 Adsorption of Aβ40/42 to polystyrene coated surface measured as changes in frequency, Δf, and dissipation, ΔD, of the QCM-D 75

Figure 3.13 AFM imaging of polystyrene covered gold crystals before and after Aβ40/42 adsorption 76

Figure 3.14 Adsorption of Aβ to SiO_2 coated surface measured as changes in frequency, Δf, and dissipation, ΔD, of the QCM-D 77

Figure 3.15 AFM imaging of SiO_2 covered gold crystals before and after Aβ40/42 adsorption 77

Figure 3.16 Construction of $PEI(PSS/PAH)_6$ and $PEI(PSS/PAH)_6PSS$ monitored by QCM-D 78

Figure 3.17 Layer thickness during polyelectrolyte multilayer construction. A) Sauerbrey equation. B) Voight modeling 79

Figure 3.18 Adsorption of Aβ40 on polyectrolyte multilayer coated QCM-D gold crystals followed by QCM-D 80

Figure 3.19 AFM imaging of Aβ40 adsorbed onto polyelectrolyte multilayer coated QCM-D gold crystals 81

Figure 3.20 Adsorption of Aβ40 on polyelectrolyte coated Ge IRE. A) Evolution of the IR spectrum in the region 1800-1200 cm^{-1} due to adsorption onto $PEI(PSS/PAH)_6$. B) Time course of the absorbance at 1628 cm^{-1} during absorption on $PEI(PSS/PAH)_6$ and $PEI(PSS/PAH)_6PSS$ 82

Figure 3.21 Evolution of the IR spectrum of Aβ40 in the region 1800-1200 cm^{-1} due to adsorption on A) $PEI(PSS/PAH)_6$ and B) $PEI(PSS/PAH)_6PSS$ 83

Figure 3.22 Typical QCM-D curves of SLB formation on SiO_2 displayed as Δf and ΔD 84

Figure 3.23 Thickness A) and areal mass B) calculated employing the Sauerbrey equation for the process of SLB formation 85

Figure 3.24 "Snapshots" of the SLB formation process on SiO_2 by AFM 86

Figure 3.25 Dependence of SLB formation on vesicle concentration 86

Figure 3.26 Changes in frequency, Δf and dissipation, ΔD, due to adsorption of vesicles with different mol% of lipids on SiO_2 87

Figure 3.27 Interaction of Aβ peptides with egg PC SLBs monitored by QCM-D 89

Figure 3.28 Interaction of Aβ42 with egg PC SLBs with 10 mol% of other constituents monitored by QCM-D 90

Figure 3.29 QCM-D quartz crystal coated with gold and with A) SiO_2 and B) polystyrene 91

Figure 3.30 Change of ΔD versus Δf. A steeper slope reflects a more viscolelastic layer 92

Figure 3.31 Change of ΔD versus Δf during the adsorption of Aβ onto QCM-D gold crystals coated with SiO_2 or polystyrene. C) Proposed model of the adsorption process . 94

Figure 3.32 QCM-D quartz crystal coated with gold and with A) $PEI(PSS/PAH)_6$ and B) $PEI(PSS/PAH)_6PSS$ 95

Figure 3.33 Change of ΔD versus Δf during the adsorption of Aβ40 into QCM-D gold crystals coated with $PEI(PSS/PAH)_6$ and $PEI(PSS/PAH)_6PSS$. C) Proposed model of the adsorption process 97

Figure 3.34 A) Structure of PC. B) SLB on SiO_2 substrate 98

Figure 3.35 A) Change of ΔD versus Δf during the interaction of Aβ peptides with egg PC SLBs. B) Proposed effects on the bilayer structure 99

Figure 3.36 A) Change of Δ*D* versus Δ*f* during the interaction of Aβ peptides with egg PC SLBs incorporating 10 mol% of egg PG or 10 mol% of DMTAP. B) and C) Proposed interactions 101

Figure 3.37 A) Change of Δ*D* versus Δ*f* during the interaction of Aβ peptides with egg PC SLBs incorporating 10 mol% of GM1 or 10 mol% of cholesterol. Proposed interactions for SLBs containing 10 mol% of GM1 B) and cholesterol C) 103

Figure 4.1 Mechanism of AD highlighting the strategy proposed for the use of NPs 105

Figure 4.2 The blood–brain barrier 106

Figure 4.3 Complexes of polyampholytes with dodecanoic acid and perfluorododecanoic acid 108

Figure 4.4 Scheme of the experimental procedure for the synthesis of sulfonated microgels 110

Figure 4.5 Schematic representation of zeta potential 111

Figure 4.6 Structure of APG2019 113

Figure 4.7 Scheme of the experimental procedure for the synthesis of sulfated latexes 113

Figure 4.8 Linear and circularly polarized light 114

Figure 4.9 Linear polarized light is a sum of left- and right-handed circularly polarized components with equal length 115

Figure 4.10 CD measures the difference in absorbance of right- and left-handed circularly polarized light 116

Figure 4.11 Representative CD curves corresponding to common secondary structural elements 118

Figure 4.12 Characteristics of protein structure measured in the UV range by CD 119

Figure 4.13 Diagram of ITC cells and syringe 121

Figure 4.14 Structure of Thioflavine T 123

Figure 4.15 A) Strategy used to produce A11 anti-oligomer antibody. B) Characterization of oligomer-specific immunoreactivity 124

Figure 4.16 Caspase-mediated apoptosis 128

Figure 4.17 The caspase-3 fluorimetric assay 129

Figure 4.18 Reduction of MTT to formazan by mitochondrial enzymes 129

Figure 4.19 CD spectra of Aβ peptides in HFIP 131

Figure 4.20 CD spectra of Aβ peptides before and after titration with fluorinated NPs 132

Figure 4.21 ThT fluorescence excitation intensity at 440 nm (λem = 482 nm) of Aβ solutions in the absence and presence of fluorinated and hydrogenated NPs 133

Figure 4.22 AFM analysis of Aβ42 aggregation in the absence and presence of fluorinated and hydrogenated NPs 134

Figure 4.23 Isothermal titration calorimetry. Titration of 10 $mg \cdot mL^{-1}$ NP solution into 5 µM Aβ peptides in PBS 136

Figure 4.24 Time course of Aβ oligomerization detected by immunoblotting in the absence and presence of fluorinated and hydrogenated NPs 138

Figure 4.25 SDS-PAGE electrophoretic migration of Aβ42 in the absence and presence of fluorinated and hydrogenated NPs 139

Figure 4.26 SDS-PAGE electrophoretic migration of Aβ40 in the absence and presence of fluorinated and hydrogenated NPs 139

Figure 4.27 Aβ42-mediated inhibition of neuronal MTT reduction in the absence and presence of fluorinated and hydrogenated NPs 141

Figure 4.28 Aβ42-induced caspase-3 activation in cultured neurons in the absence and presence of fluorinated and hydrogenated NPs 141

Figure 4.29 Dose dependent assay of the inhibitor activity of fluorinated NPs 142

Figure 4.30 TEM images of polystyrene sulfonated microgel 143

Figure 4.31 Hydrodynamic diameter and zeta potential of the polystyrene latexes..... 144

Figure 4.32 TEM images of polystyrene sulfated latex 145

Figure 4.33 Aβ42-mediated inhibition of MTT reduction by neuronal cells in the absence and presence of sulfated latexes 146

Figure 4.34 CD spectra of Aβ peptides in the absence and presence of sulfonated and sulfated NPs 147

Figure 4.35 ThT fluorescence excitation intensity at 440 nm (λ_{em} = 482 nm) of solutions of Aβ in the presence of sulfonated microgel 147

Figure 4.36 CD spectra of "aged solution" of Aβ40 before and after titration with in the absence and presence of sulfonated and sulfated NPs 148

Figure 4.37 Time course of Aβ oligomerization detected by immunobloting in the absence and presence of sulfonated and sulfated NPs 149

Figure 4.38 SDS-PAGE electrophoretic migration of Aβ42 in the absence and presence of sulfonated and sulfated NPs 150

Figure 4.39 SDS-PAGE electrophoretic migration of Aβ40 in the absence and presence of sulfonated and sulfated NPs 151

Figure 4.40 Aβ42-mediated inhibition of neuronal MTT reduction in the absence or presence of sulfonated and sulfated NPs 151

Figure 4.41 Aβ42-induced caspase-3 activation in cultured neurons in the absence or presence of sulfonated and sulfated NPs 152

Figure 4.42 Schematic representation of the possible interactions of fluorinated NPs and Aβ peptides 156

Figure 4.43 Schematic representation of the possible interactions of sulfonated NPs and Aβ peptides 158

List of Tables

Table 2.1 Human diseases associated with formation of amyloid 24

Table 3.1 Fatty acid content of egg PC 57

Table 3.2 Molecular weight of the molecules shown in Figure 2.2 58

Table 3.3 Spectroscopic methods for probing protein structure 64

Table 3.4 The nine characteristic absorption bands for proteins in the mid-IR 68

Table 3.5 Position of the amide bands depending on the secondary structure of a protein/peptide 69

Table 3.6 Categories of liposomes 73

Table 4.1 Heterophase polymerization techniques 109

Table 4.2 Benefits and drawbacks of CD spectroscopy 117

Table 4.3 CD adsorption bands and responsible transitions in the far-UV observed for pure secondary structures of proteins 118

Table 4.4 Analytical methods to determine protein secondary structure from CD spectra 119

Acknowledgements

I wish to acknowledge the following people for contributing to this thesis or just being there as good friends and co-workers.

Most of the research presented was done at the Max Planck Institute of Colloids and Interfaces (MPIKG, Golm, Germany). I deeply thank Prof. Helmuth Möhwald for this opportunity and, besides of expressing my gratitude, I would like to express my reverence for the fantastic working atmosphere existing in the Interfaces Department. My stay here has been a very rewarding experience, and I have learned a lot on many levels. Prof. Dr. Gerald Brezesinski received me in his group at the Max Planck Institute. He was always helpful, hopeful and friendly which made easier to overcome the difficulties and frustrations of being a PhD student. I really appreciate the brain storming and scientific discussions.

I thank Prof. Maria do Carmo Pereira and Prof. Manuel Coelho (FEUP, Porto, Portugal) for accepting me as a coworker in the Faculty of Engineering of the University of Porto, and for encouraging me to continue the work as Ph.D. student. Their support and suggestions were always essential.

Many thanks to all co-authors who made this thesis possible, especially Dr. Isabel Cardoso from Instituto de Biologia Molecular e Celular (IBMC, Porto, Portugal) for the precious help with the immuno and cytotoxicity assays concerning the interaction of Aβ with nanoparticles. I thank to Prof. Dr. Klaus Tauer (MPIKG, Golm, Germany) for suggesting the application of reactive surfactants and for helping me with the synthesis and characterization of sulfated latexes. Dr. Cristoph Wieland (Fraunhofer IAP, Golm, Germany) is acknowledged for helping with microgel synthesis.

I owe my gratitude to Prof. Massimo Stefani and Dr. Monica Bucciantini (University of Florence, Florence, Italy) that welcomed me during a short visit to Florence for some experiments. I really appreciated the nice atmosphere in the lab and the sympathy from all the coworkers.

Everyone in the Interfaces Department for the work support, the trips we made, party evenings, and lots more. I had a great time working with you! Very deep thanks to Heidi Zastrow and Anne Heilig for helping me to solve my light scattering and AFM problems, respectively. To all present and former members of my group (no one mentioned, no one forgotten) many thanks. Dr. Élodie Soussan and Prof. Dr. Gerald Brezesinski are acknowledged for helping me with the French and German versions of the abstract, respectively.

A special thank to Ana β (Teles), Ana Δ (Queirós), Audrée, Dani, Élodie, Erwan, Fix, Jelena, John, Magda, Marlene, Micha, Miles, Milan, Munish, Pedro, Petia, Silke, … to all my partners in crime many thanks for all the good times during these years. You all have made my life much easier! To Manel, I am glad that you stand by me with comprehension. To the friends from ever, that even being far were always present: many times I felt as I had never left... And I owe that to all of you!

Last but not least, the most felt acknowledgment is to my Family. It has been quite hard for me to be away for such a long time, and I know for You as well. Mãe, Pai, Pedro, Teca, João, Avós e Tios: Muito Obrigada for your constant support! A special thanks to my Aunt Maria João for being a very inspiring example and for all the suggestions concerning the work, you have helped me learning not to turn down a challenge.

I am thankful to Fundação para a Ciência e a Tecnologia (FCT) for a PhD Fellowship (SFRH/BD/18465/2004. The work was supported by the Max Planck Society and the FCT research project PTDC/BIO/69359/2006.

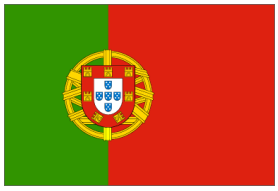
FCT
Fundação para a Ciência e a Tecnologia
MINISTÉRIO DA CIÊNCIA, TECNOLOGIA E ENSINO SUPERIOR

Ciência.Inovação 2010
Programa Operacional Ciência e Inovação 2010
MINISTÉRIO DA CIÊNCIA, TECNOLOGIA E ENSINO SUPERIOR

U.PORTO

Max Planck Institute
of Colloids and Interfaces





Legal Regulations

According to the Law n° 216/92 of 13th October and to the Regulations of PhD by the University of Porto, we clarify that all the experiments and results presented, except if stated otherwise, as well as their interpretation and discussion are our own.

In this dissertation results were presented from the following publications:

De acordo com o disposto no Decreto-Lei n° 216/92 de 13 de Outubro e no Regulamento de Doutoramentos pela Universidade do Porto, esclarecem-se serem da nossa responsabilidade a execução das experiências que permitiram a obtenção dos resultados apresentados, excepto quando referido em contrário, assim como a sua interpretação e discussão.

Nesta dissertação foram apresentados os resultados contidos nos artigos publicados ou em vias de publicação seguidamente mencionados:

Gromelski, S., Saraiva, A. M., Krastev, R. and Brezesinski, G. (2009*) The formation of lipid bilayers on surfaces*. Colloids Surf. B **74**, 477-483.

Saraiva, A. M., Cardoso, I., Saraiva, M. J., Pereira, M. C., Coelho, M. A. N., Möhwald, H. and Brezesinski, G. (2010) *Controlling Amyloid-β Peptide(1-42) Oligomerization and Toxicity by Fluorinated Nanoparticles*. Accepted by Chembiochem.

Saraiva, A. M., Cardoso, I., Saraiva, M. J., Tauer, K., Pereira, M. C., Coelho, M. A. N., Möhwald, H. and Brezesinski, G. (2009) *Randomization of Amyloid-β Peptide(1-42) Conformation by Sulfonated and Sulfated Nanoparticles reduces Aggregation and Cytotoxicity*. DOI: 10.1002/mabi.200900448 (Macromolecular Bioscience).

Saraiva, A. M., Pereira, M. C. and Brezesinski, G. (2010) *Is the viscoelasticity of Alzheimer´s Aβ42 peptide oligomers a general property of protein oligomers related with their toxicity?* Submitted to Langmuir.